UNIVERSITY OF LATVIA

THE RELATIONSHIP OF SELF-RENEWAL AND ACCELERATED SENESCENCE IN RESPONSE TO DNA DAMAGE IN NORMAL AND TUMOUR CELLS

Doctoral thesis
Department of Molecular Biology and Biochemistry
FACULTY OF BIOLOGY

Author: Anda Hūna
Supervisor: Dr. hab.med. Jekaterīna Ērenpreisa

Riga 2015

University of Latvia

Promotion Council
Biology
Riga, Latvia

Opponents: **Prof., Dr. habil. biol. Nikolajs Sjakste**
(University of Latvia, Riga, Latvia)

Prof., Dr. biol.Alessandro Giuliani
(Istituto Superiore di Sanità, Rome, Italy)

Dr. biol. Inese Čakstiņa
(Riga Stradinš University, Riga, Latvia)

Summary

In the doses used in cancer chemo-radio-therapy of patients most cancer cells undergo accelerated senescence. Unfortunately, senescence induced by therapy may be reversible, the mechanisms of reverse needed exploration. For the first time we discovered activation of self-renewal in tetraploid presenescent normal human fibroblasts and TP53 dependent simultaneous activation of self-renewal and senescence regulators in etoposide treated teratocarcinoma cells. Together these results indicate the generality of coupling between senescence and stemness programs occuring in DNA damage response. Furthermore, we described importance of senescence acompanying autophagy for support of bi-potentiality and survival of DNA damaged tumour cells, as well as expansion of chromosome territories in polyploid cells which may favour transcription activation and reprograming.

Abbreviations

BrdU – bromodeoxyuridine
CIN – chromosomal instability
CSC - cancer stem cells
DDR – DNA damage response
EMT-epithelial-mesenhymal transition
ESC - embryonal stem cell
ETCs - endopolyploid tumour cells
ETO - etoposide
FBS – foetal bovine serum
FISH - Fluorescence *in situ* hybridisation
HR – homologous recombination
IF - immunofluorescence
IR – irradiation
MIN – microsatelite instability
mt – mutated
PDL - population doubling level
NT – non-treated
RT-PCR - reverse transcription polymerase chain reaction
PI - propidium iodide
SA-ß-gal - senescence associated ß galactosidase
SAHF – senescence associated heterochromatin foci
Wt – wild- type

Table of contents

Introduction

One of the major problems in cancer therapy is the formation of the secondary resistant tumour cells after initially successful genotoxic treatments, such as chemo- and radiotherapy, which cause relapse of the disease and metastases in up to 50% of cancer cases, which subsequently kill the patients. The cellular mechanisms of this resistance are not yet clear. Despite the recentdiscoveries made in the last decade in targeted therapy, which have helped making progress in overall treatment of cancer, the reductionist view fails to deal with cancer as it is in fact a moving target (Weinberg 2014). Therefore, new conceptual paradigms for explaining bigger picture are needed (Hanahan 2014; Weinberg 2014).

In the doses used in cancer chemo-radio-therapy of patients most of cancer cells undergo accelerated senescence, defined as a permanent arrest of proliferation (Roninson *et al.,* 2001). Unfortunately senescence induced by anticancer DNA damaging therapy may be insufficient or reversible (Wu *et al.,* 2012) with the mechanisms currently unknown.

Autophagy has for a long time been considered anear-death mechanism associated with senescence (Young *et al.,* 2009). However, recent findings show that moderate autophagy works as a pro-survival mechanism in tumour cells depending on context, therefore either this process should be promoted or suppressed in cancer treatments is under debate (Gewirtz 2013) and the paradoxical nature of autophagy has been widely discussed (Hanahan and Weinberg 2011).

One of the most intriguing facets that senescent cells share with cancer cells is polyploidy. Cells may enter polyploidy due to persistent damage during senescence and/or mitosis bypass (Davoli *et al.,* 2011; Castedo *et al.,* 2010). Highly malignant p53-mutated tumours under DNA damage may undergo mitotic slippage from G2/M arrest and re-enter G1 phase with doubled DNA amount, forming polyploidy (Erenpreisa *et al.,* 2008; Illidge *et al.,* 2000).

The previous studies in our and other laboratories showed that recovery of resistant tumour cells after genotoxins is associated with induced polyploidy and its reverse (Erenpreisa *et al.,* 2000, 2005, 2008) and that resultant diploid descendants are mitotically active (Illidge *et al.,* 2000; Puig *et al.,* 2008; Vitale *et al.,* 2011). It was shown that tumour cells can acquire embryonal stemness as a result of ionizing irradiation or genotoxic drugs. This occurs in reversibly polyploidised cells (Salmina *et al.,* 2010). These observations were confirmed and extended in several laboratories (Ghisolfi *et al.,* 2012; Lagadec and Pajonk 2012; Zhang *et al.,* 2013c). These studies showed changed transcription profiles with expression of stemness signature, the capability of sphere formation, the ability to undergo de-polyploidisation, and tumorigenicity at xenotransplantation of induced polyploid tumour stem cells, even just of one (Weihua *et al.,* 2011).

To sum up, genotoxic treatments cause activation of as if two opposite programms: senescence and stemness, both are paradoxically linked to induced polyploidy. Therefore it is important to study the relationship of regulators of these programs in individual cells and their cell cycles for explaining this paradox.

The aim and tasks of the study:

The aim of this study was to investigate the relationship of self-renewal and senescence in tumour cells after genotoxic treatment and in normal cells during aging, and the place and role of associated polyploidy.

For achieving the goal several tasks were set.

- To explore the role of tetraploidy induced by senescence and DNA damage in normal and tumour cells;
- To characterise co-expression of self-renewal and senescence regulators OCT4A and P21CIP1 after genotoxic damage in individual cells of embryonal carcinoma, the model of cancer stem cells;
- To explore the role of autophagy in survival of cancer cells after genotoxic therapy.
- To explore changes in the volumes of chromosome territories in irradiated cancer cells.

1. Literature overview

1.1. Cancer resistance to genotoxic treatments

"War against cancer" was declared in USA about 40 years ago and now the scientists all around the world have to recognize that. Despite the fact that some of the battles have been won, we are yet to approach this aim with the strategies currently in use. "Magical bullets", famous metaphor of targeted therapy turned out to be mostly ineffective and showing only transient effect for treating cancer (Hanahan 2014). The targets are in fact 'moving" and previous strategies based on reductionistic concepts such as mutational theory of cancer are insufficient (Weinberg 2014). Therefore, a new concept dealing with the complexity of cancer is needed (Hanahan 2014; Weinberg 2014).

Currently irradiation and chemotherapy are still used to treat most of the cancer types. The main problem with curing cancer is acquired resistance to genotoxic treatments. Several mechanisms of acquired resistance will be analyzed in further paragraphs.

1.2. DNA damage and its cell cycle checkpoint

"So, from the perspective of cancer, DNA damage causes the disease, it is used to treat the disease, and it is responsible for the toxicity of therapies for the disease" (Kastan and Bartek 2004).

Based on the "law of Bergonié and Tribondeau" formulated on 1906, cell sensivity against irradiation is proportional intensity of cell division (Haber and Rothstein 1969). Therefore agents used in traditional anti-cancer therapy are targeted against rapidly dividing cells and their acting mechanism is DNA damage that leads cells to a growth arrest, death and cellular senescence – the state when the cell stays alive, but is unable to further proliferate (Roninson *et al.*, 2001).

In proliferating somatic cells, the genome constancy is regulated through a cell cycle - DNA synthesis and following cell division. Cell cycle is regulated by several checkpoints, in which large enzyme complexes control physiological condition of a cell and decide whether cell may continue cycling or it has to stop for repairing the errors, or it is send to cell death or senescence in the case of irreparable damage (Elledge 1996). Defective cell cycle regulation can lead to unregulated cell division and cancer (Kops *et al.*, 2005; Kastan and Bartek 2004). In tumours checkpoint tresholds are often evaluated via genetic mutation or epigenetic inactivation of checkpoint activator proteins (Kinzler and Vogelstein 1997), like tumour suppressor protein P53, so called the "guardian of the genome", one of most commonly mutated gene in human cancers (Kastan 2007).

For safeguarding DNA integrity the most important is G2/M (DNA damage) checkpoint (Kastan and Bartek 2004). DNA damage response starts with ATM (Lee and Paull 2007) or ATR

(Smith *et al.,* 2010) signaling and the main axis is tumor suppressor P53 which activates cyclin kinase inhibitor P21CIP1 and halts the cell cycle, giving the time for cell to repair DNA and if it is impossible sending it to senescence or, in case of too large damage, to apoptosis (Roninson *et al.*, 2001; Seviour and Lin 2010). While apoptosis is well studied, the mechanisms of cellular senescence, in particular whether it can be reversed, are not clear.

1.3. Cellular senescence and cancer

1.3.1. Replicative senescence

Most commonly known type of senescence is replicative cellular senescence, basically defined as a final cell growth arrest, was firstly introduced by Leonard Hayflick (Hayflick 1965) when he noticed that human cells have a limited life span in the culture, dividing for about 40-60 times. This process is associated with asymmetrical nature of DNA replication on its two strands, with each division the telomeres become shorter (Harley *et al.,* 1990) and finally are recognized as DNA breaks (d'Adda di Fagagna *et al.,* 2003; Herbig *et al.,* 2004). Then ATM/CHK2/P53/P21CIP1 pathway is activated to inhibit G1/S transition and arrest the cell cycle. Senescent cells remain metabolically active, however further cell division is arrested (Gey and Seeger 2013).

Another parallel senescence pathway is P16INK4a-RB pathway (Beauséjour *et al.,* 2003), which is considered to be activated at deeper senescence than the state induced P21CIP1, the latter may be by some extent reversible (Atsumi *et al.,* 2011; Yoshioka *et al.,* 2012; Hayat 2013).

There are several markers for detection of cellular senescence besides P16INK4a and P21CIP1 expression, like lack of proliferative marking for Ki67 and mitotic activity due to cell cycle arrest, flattened cell form, positive SA-β-gal activity. At deep senescence stage forming of senescence-associated heterochromatin foci SAHFs epigenetically depress proliferation genes (Narita *et al.*, 2003). SAHFs can be detected by the preferential binding of DNA dyes (Funayama et al. 2006; Narita et al. 2003).

In the doses used in cancer chemo-radio-therapy of patients most of cancer cells undergo accelerated senescence (Roninson *et al.*, 2001; Gewirtz *et al.*, 2008; Schmitt 2007).

1.3.2. Premature (accelerated) senescence

Premature senescence can be triggered by certain stresses independently of the number of cell divisions or telomere length (Shay and Roninson 2004). There are three main kinds of such stresses: action of DNA damaging agents, oncogene activation like RAS or MYC, RAF (Serrano *et al.,* 1997; Bartkova *et al.,* 2006) or ROS (reactive oxygen species) (Vigneron and Vousden 2010). However, DNA damage is a mutual feature of accelerated senescence independent on the origin of stress (d'Adda di Fagagna 2008). This senescence starts at the DNA damage checkpoint in G2

arrest, when damaged cells become resistant against apoptosis and it is mediated by P53/P21CIP1 axis (Schmitt *et al.,* 2002; Campisi and d'Adda di Fagagna, 2007).

In general, in human cells, replicative senescence is usually dependent on P53/P21CIP1/pRb/E2F pathway, whereas accelerated senescence can be mediated through P53/P21CIP1/pRb/E2F or, P16INK4a/pRb/E2F pathway or both (Herbig *et al.,* 2004; Serrano *et al.,* 1997). Drug induced DNA damage causes senescence in tumour cells both, *in vitro* and *in vivo*, P21CIP1 playing a role at initiation and P16INK4a maintaining senescence (te Poele *et al.,* 2002).

1.3.3. Senescence induced by genotoxic cancer treatment

Senescence induced by anticancer DNA damaging therapy may be insufficient or reversible, likely most often due to inefficient P16INK4a or P53 pathway (Wu *et al.,* 2012). It has been shown that lack of P53 may be responsible for reversibility of senescence (Roberson *et al.,* 2005; Bond *et al.,* 1994) although P16INK4a can serve as a second barrier (Beauséjour *et al.,* 2003).

Cancer therapy based on deepening of senescence works by inhibiting telomerase activity, modulating cyclin dependent kinase activity such as P21CIP1 and P16INK4a, c-myc inhibition, reactivation of P53 function, statins and recently – manipulation with secretome activity (Acosta and Gil 2012; Wu *et al.,* 2012).

In general, cell senescence is a major barrier against tumour formation (Campisi 2001; Sharpless and DePinho 2005), supported by observations that transgenic mice expressing additional copies of senescence regulators p53 or Ink4/Arf have increased protection against cancer, without side effects (Serrano and Blasco 2007) but their antagonistically pleiotropic effects eventually lead to organism aging (Campisi 2005). Interestingly, cell senescence is a process not exclusive for ageing organism. Senescent cells can be found as early as embryonal development where they regulate organogenesis (Muñoz-Espín *et al.,* 2013), however the mechanisms are not clear.

Paradoxically it has been shown that senescence in tissue may promote cell proliferation, in particular, due to senescence associated enhanced metabolism, autophagy and secretory phenotype (SASP), which has been shown to contain many ingredients, like interleukines and chemokines, that may induce senescence in neighbor fibroblasts (Nelson *et al.,* 2012), proinflammatory cytokines such as IL-6, IL-8 and GROa may initiate an immune response required for tumor clearance (Xue *et al.,* 2007) unfortunately they may fuel tumour growth and stimulate EMT in tumours as well (Gorgoulis and Halazonetis 2010).

1.3.4. Autophagy and aging

Macroautophagy (further: autophagy) is the cellular process when autophagosome is formed around cargo that may carry different cellular structures, protein aggregates, nucleic acids, lipids, even entire organelles (Okamoto 2014) and later merge with a lysosome for digestion (Hurley and Schulman 2014). The end products of this process are amino and fatty acids, nucleotides, which are released back into the cytosol and recycled (Kuma and Mizushima 2010).

Autophagy was generally thought to affect cytoplasmic organelles, however release of DNA patches was found in yeasts, while degradation of the whole nuclei has been described, in unicellular organism *Tetrahymena* (Lu and Wolfe 2001) and filamentous fungi *Aspergillus oryzae* (Shoji *et al.,* 2010).

It has been found in polyploid tumour cells, induced after DNA damage, that a considerable amount of genetic material undergoes sequestration and extrusion as sub-nuclei and further autophagic digestion with possible role in genome sorting and stabilising effects (Erenpreisa *et al.*, 2000).

The autophagic pathway can be upregulated in response to a variety of stressful conditions and chemical triggers such as: starving, hypoxia, accumulation of misfolded proteins and typically by aging (Cuervo *et al.*, 2005). The activity of SA-ß-gal, showing in fact acidification of cytoplasm by acid lysosomal content and macroautophagy activation, are well correlated during oncogene (RAS) induced senescence, and it was found that, under depletion of the autophagy genes ATG5 or ATG7 SA-ß-gal activity is inhibited (Young and Narita 2010).

Autophagy has for a long time been considered as near-death mechanism associated with senescence (Capparelli *et al.,* 2012; Mosieniak *et al.,* 2012; Young *et al.,* 2009), however recent findings show that moderate autophagy works as a pro-survival mechanism in tumour cells depending on context, therefore either this process should be promoted or suppressed in cancer treatments is under debate (Gewirtz 2013; Kimmelman 2011) and the paradoxal nature of autophagy has been widely discussed (Hanahan and Weinberg 2011) Basically it is considered that autophagy, like cellular senescence, may serve as a barrier to tumour initiation, but once cancer is established, then autophagy plays a role in promotion of malignant progression and in subsequent tumour maintenance by supplying metabolic substrates, limiting oxidative stress of mitochondria, etc (Rosenfeldt and Ryan 2011; Kimmelman 2011).

One of the most intriguing facets that senescent cells share with cancer cells is polyploidy. Cells may enter polyploidy due to persistent telomere damage through prolonged G2 and mitosis bypass (Davoli *et al.,* 2011; Castedo *et al.,* 2010) and this eventually may lead to tumour formation (Davoli and de Lange 2011). Interestingly survivin, the protein which has been shown to have a role

in reverse of the therapy induced senescence, also promotes cell polyploidisation (Nagata *et al.*, 2005) and survivors also possess elevated survivin levels (Wang *et al.*, 2011).

1.4. Genetic instability and polyploidy of tumour cells

"The main rule for cancer cells is the absence of any rules" (Hanseman 1890).

1.4.1. Polyploidy in different normal cell types

Polyploidy - existence of more than two genome sets per one cell is a trait which is not common in mammals and embryonal polyploidy is lethal, as a matter of fact (Kaufman 1991). Two types of polyploidy can be distinguished – (I) generative or stable, where all cells in organism are polyploid, often found in cultivated plants; the only mammal with stable polyploidy is red vizcacha rat (*Tympanoctomys barrerae*) and its close relatives, which are tetraploid (Gallardo *et al.*, 1999) and (II) somatic polyploidy or endopolyploidy. The controlled somatic polyploidisation, occurring mostly through aborted mitosis has a clear genome doubling which can make it till to some extent reversible (Lee *et al.*, 2009). It is important that most cells undergoing endopolyploidisation do not exceed 32n/64C (normal cells in G1 – 2C) barrier, which provides cell with potential to return to diploidy. 32n is the largest ploidy size from which normal cells can still return to diploidy in very rare cases (Nagl 1978). Somatic polyploidisation is part of normal development, for example, terminally differentiated nurse cells in *Drosofila* ovaries (Weaver and Cleveland 2001) and mammalian trophoblast. Polyploid trophoblast support rapid developing of embryo by producing vast amounts of protein, because of decreased surface-to-volume ratio, thereby minimizing membrane requirements, however lowering the efficiency of transport makes polyploid cells unstable for long periods of time (Comai 2005). As a similar somatic polyploidy example in the adult human organism megakaryocytes can be mentioned (Lee *et al.*, 2009).

Somatic polyploidy in normal adult human cells can be seen in hepatocytes, vascular smooth muscle cells induced as reaction to stress, such as hypoxy. It was found, that in hepatocytes (Celton-Morizur *et al.*, 2010) and vascular smooth muscle cells (Hixon and Gualberto 2003) the frequency of polyploidy increases with age; also human fibroblasts and endothelial cells *in vitro* become tetraploid with replicative aging (Walen 2008; Davoli *et al.*, 2011). Therefore, polyploidy was for a long time considered as a senescence marker and was thought to be cell proliferation dead end, but in later years it was shown to be not, rodent hepatocytes has been shown to polyploidise and de-polyploidise and increase their genetic variability under stress conditions (Duncan *et al.*, 2010). It has been shown that senescent human fibroblasts *in vitro* undergo a similar process (Walen 2013).

Interestingly spindle checkpoint activation in somatic cells or in embryonal stem cell-derived early differentiated cells results in cell death, yet the same treatment does not trigger apoptosis in embryonal stem cells (ESC). It is therefore possible that such tolerance of ploidy changes by ESCs can contribute to their karyotypic instability (Mantel *et al.,* 2008).

In normal somatic polyploidy, the metabolism is changed to more energy saving pathways under stress conditions (Anatskaya and Vinogradov 2010). Polyploidy and glycolytic flux has been found associated in yeast (Conant and Wolfe 2007) and in endopolyploid mouse hepatocytes and human cardiomyocytes (Anatskaya and Vinogradov 2007).

Increased glycolytic flux is also a well-known trait in tumours (Kim and Dang 2006). Tumour cells also preferentially use glycolysis as an energy source, in aerobic condition and also used in anaerobic obstacles formed due to rapid growth and deficiency of blood supply, process called a Warburg effect and is known as one of main cancer hallmarks (Kim and Dang 2006; Ward and Thompson 2012). The increased glycolysis is coupled to increased nucleotide and lipid synthesis, therefore supporting rapid growth in different tumours (Hu *et al.*, 2013).

1.4.2. Stable polyploidy and genomic instability in tumours

Stable aneupolyploidy can be often found in epithelial and other types of cancers (Haroske *et al.*, 2001). Recently tetraploidy was found to have a role in colorectal cancer evolution through increase of genomic instability, where tetraploidization is an early event in the most colorectal cancers (Dewhurst *et al.,* 2014).

Two types of genetic instability can be discriminated – microsatellite instability (MIN) and chromosomal instability (CIN) Most of sporadic cancers have increased CIN (Ganem *et al.,* 2007). Two types of CIN have been defined – segmental – translocations, deletions and amplifications and whole genome CIN (Geigl *et al.,* 2008). CIN is mostly induced by breakage-fusion-bridge cycle, when chromosomes repeatedly fuse and then break in a following anaphase (McClintock 1942; Gisselsson *et al.,* 2000), caused by telomere shortening during the replicative senescence. Most noticeable features of CIN are chromosome bridges in anaphase, mitotic death, polyploidy and irregular nuclear shape (Gisselson *et al.,* 2001).

CIN has important role in carcinogenesis, as it increases genetic and epigenetic mutability up to 100-1000 times (Ganem *et al.,* 2007). Furthermore, 70% of mutations are due to chromosome translocations (Futreal *et al.,* 2004; Ye *et al.,* 2009), also mathematical modeling shows that CIN may be even an initiating step in colon cancer formation (Nowak *et al.,* 2002). CIN-caused aneuploidy in tumours correlates with poor clinical prognosis (Krämer *et al.*, 2002).

Although chromosomal instability (CIN) has capacity of increasing cell survival due to induced variability and clonal selection, tumor progression requires balanced aneuploidy which would not interfere with cell division (Duesbery and Woude 2002; Weaver and Cleveland 2007;

Gordon *et al.,* 2012). Among the most important advantages of polyploidy is capability of increasing genetic variability by unequal divisions of endopolyploid cells (Storchova and Kuffer 2008), by masking deleterious mutations between several genomes, and in recombination and exchanges between homologous chromosomes (Coward and Harding 2014).

1.4.3. Reversible polyploidy in tumours after DNA damage

Among other advantages, polyploidy can provide tumour cells with durability against genotoxic damage. Highly malignant TP53-mutated tumours under DNA damage can undergo mitotic slippage from G2/M arrest and re-enter G1 phase with doubled DNA amount, forming polyploidy (Erenpreisa *et al.,* 2008; 2000; Illidge *et al.,* 2000). After acquiring tetraploid state, cell with functional TP53 will enter apoptosis, senescence or cell cycle arrest, but mutation or inactivation of TP53 can lead to arrest escape and further polyploidisation (Aylon and Oren 2011). Several genomes in one cell increase capacity of DNA repair as it has several copies for performing homologic recombination (HR). It has been shown that after DNA damage the polyploid tumour cells increase expression of recombinase RAD51 , which is acting anti-apoptotically (Ivanov *et al.,* 2003).

It has been shown that small proportion of polyploid tumour cells induced by genotoxic treatments can return to diploidy (Illidge *et al.,* 2000; Puig *et al.,* 2008; Vitale *et al.,* 2011), possibly through meiosis-like reduction divisions (Erenpreisa *et al.,* 2009; Ianzini *et al.,* 2009) and that resultant diploid cells are mitoticaly active (Illidge *et al.,* 2000; Puig *et al.,* 2008; Vitale *et al.,* 2011). Interestingly, depolyploidisation can also decrease aneuploidy (Vitale *et al.,* 2010). As mentioned before, balancing of aneuploidy by getting just the right amount has important role in tumour cell propaation after therapy, as polyploidisation is always associated with increased chromosome instability and aneuploidy (Storchova and Kuffer 2008).

Nevertheless, these polyploid cells possessing persistent DNA damage still mostly undergo cell death (Illidge *et al.,* 2000). The reversible polyploidisation observed in tumour cells after DNA-damage can give clonogenic escape only in 10^4-10^6 of the treated cells (Puig *et al.,* 2008).

In summary, tetraploidy favours transformation towards cancer in four ways. First, inducing CIN and aneuploidy, second – buffering cells against deleterious effects of chromosomal loss, third – escape from genotoxic agent induced death or senescence, forth – changing metabolism towards hypoxy- and toxicity-resistant type; all this makes polyploidy a tumour gateway and important target for anticancer drugs (Coward and Harding 2014)

1.5. Stem-like features of tumour cells

1.5.1. Cancer stem cell concept

Cancer stem cells (CSC) as a concept of carcinogenesis and tumour growth appeared as an alternative for a traditional microevolution model (Nowell 1976), which stated that cells acquire random mutations while dividing and every cell has a potency to form cancer under a pressure of microevolution. It has helped to expand dimensions of how we see cancer and drive away from simply plain genetics and broken genes (Soto and Sonnenschein 2014; Tu 2013; Wang and Armstrong 2008). The model suggests that cancer has a similar hierarchy as an organism, with stem cells which are slowly dividing, progenitors – dividing usually rapidly, and less potent cells and differentiated cells which cannot form a cancer, if transplanted alone (Cabrera *et al.*, 2015). Cancer stem cells are defined through their ability to form new tumors upon inoculation into recipient host mice (Cho and Clarke 2008).

Starting with lymphoma, CSC where found in practically all cancer types. The presence of CSC in the tumour is considered as the main cause of malignancy which correlates with poor clinical outcome (Shekhani *et al.*, 2013). CSC hypothesis suggests that only these cells support self-renewal in tumours. The most used terms in literature are cancer stem cells (Jordan *et al.*, 2006), stem-like cancer cells (Liang *et al.*, 2010), tumour-initiating cells (Singh *et al.*, 2004) etc.

Cancer stem cell hypothesis made research society reconsider traditional therapies, as some tumour cells may have adult stem cell property to rest and not divide till receiving stimulus, therefore making anti-proliferative therapy ineffective against them (Blagosklonny 2007; Singh and Settleman 2010).

Further research showed that truth is not so simple and that these cancer stem cells do not have exclusive rights to form cancer but just have an increased capability to do so (Marjanovic *et al.*, 2013). Further experiments with cell sorting revealed that being a cancer stem cell is just a state of a tumour cell and not a perpetuating its property (Zhou *et al.*, 2013; Zapperi and La Porta 2012). In fact, this means that the microevolution and cancer stem cell models should be rather merged than opposed (Csermely *et al.*, 2014; Magee *et al.*, 2012; Beck and Blanpain 2013).

1.5.2. Embryonal core cassete expression in human tumours

The concept of cancer cell similarity to embryonal cells has been around since the 19th century (Erenpreiss 1993). As one of examples, one of the most powerful oncogenes c-myc has roles in cancer, embryonal development, and induction of pluripotency of normal cells (Kim *et al.*, 2010; Rothenberg *et al.*, 2010). Gene array analysis suggests that cancer stem cells resemble rather embryonal than adult stem cells (Wong *et al.*, 2008).

Embryonal stem cells (ECS) have a unique degree of autonomy, as being self-sufficient and self-replicating and this likely underlies their potential to form teratocarcinomas (Chambers and

Smith 2004). Self-renewal in ECS is closely associated with pluripotency (capacity to form three layers in embryogenesis). It is supported by three core ESC transcription factors OCT4, SOX2 and NANOG, which activate their target genes (and suppress silencing Polycomb protein genes) and also activate each other with a positive feedback loop (Boyer *et al.*, 2005) It is known that a certain threshold level of ESC factors is required to start the positive feed-back circuit of transcription activation (Hemberger *et al.*, 2009).

OCT4 *(POU5F*) is a POU domain transcription factor. Currently OCT4 has several splicing isoforms described, from which OCT4A has a role in target gene activation, OCT4B has cytoplasmatic localisation without transactictivation role (Cantz *et al.*, 2008) and OCT4B1 with an unknown role (Atlasi *et al.*, 2008). One of OCT4 main functions is to form in conjunction with SOX2 heterodimer active NANOG chromatin domain, a central factor in pluripotency network (Rodda *et al.*, 2005; Silva *et al.*, 2009). OCT4 expression in normal cells is not exclusive for embryonal and germline cells and has also been found in neural stem cells (Chin *et al.*, 2009).

OCT4 is required for survival of chemoresistent cancer stem cells in colorectal cancer and its supression reduces STAT and Survivin overexpression (Wen *et al.*, 2013; de Resende *et al.*, 2013; Peng *et al.*, 2010). Some researchers have determined SOX2 (Piva *et al.*, 2014; Tam and Ng 2014; Boumahdi *et al.*, 2014; Lee *et al.*, 2014; Leis *et al.*, 2012) or NANOG (Elsir *et al.*, 2014; Zhang *et al.*, 2013d; Lu *et al.*, 2014) as being a most critical factors for cancer stem cell survival.

1.5.3. Stemness of tumour cells increases after DNA damage

Cancer stem cells may be formed or increase in proportion through DNA damage and genetic instability (Liang *et al.*, 2010). The enrichment with cancer stem cells in tumour cell population after irradiation has been shown, which was initially explained by their positive selection after treatments (Phillips *et al.*, 2006).

It was shown in lymphoma and HeLa cells that shift to pluripotency by ionizing irradiation, treatments takes place, particularly in transiently induced polyploid cells, and it depends on deficiency of TP53 function (Salmina *et al.*, 2010). These observations were confirmed and extended in several laboratories (Ghisolfi *et al.*, 2012; Lagadec and Pajonk 2012; Zhang *et al.*, 2013c). These studies showed acquisition of stemness transcription profiles, capability of embryoid sphere formation, the ability to undergo de-polyploidisation and resume cell growth, the tumour arising activity at xenotransplantation of selected polyploidy tumour cells, even just of one (Weihua *et al.*, 2011).

In summary, genotoxic treatments cause activation of two opposite programms: senescence and stemness, on the bacground of induced polyploidy. Therefore it seems important to study regulators of both in individual cells for explaining this paradox.

2. Materials and methods

2.1. Cell culture and treatment.

The Burkitt's lymphoma cell lines Namalwa and Ramos was obtained from the American Type Culture Collection (ATCC), the human B-lymphoblastoid cell lines WI-L2-NS were obtained from Dr. P. Olive (Canada) and all cell lines are TP53 function deficient. Lymphoma cell-lines were maintained in RPMI-1640 containing 10% heat-inactivated 10% foetal bovine serum (FBS; Sigma) at 37 °C in a 5 % CO_2 humidified incubator.

The wild-type TP53 human embryo lung fibroblast cell line IMR90 was obtained from ATCC and also from Coriell collection kindly donated by Dr. A. Ivanov (Beatson Institute, Glasgow) after 21–23 population doublings (PDL). Cells were cultured in DMEM (Sigma) supplemented with 10% FBS (Sigma), without antibiotics, as monolayers in a humidified incubator in 5% CO2/95% air atmosphere. The early passage cells were split 1 : 3 (∼50× 104 of cells per flask (25cm^2) twice weekly. Mid-passage cells were split 1 : 2 weekly, and late-passage cultures were split 1 : 2 once cultures attained confluence. Culture medium was changed two or three times between subculture. This way, several subsequent passages were carried out until the cells failed to undergo > 0.8 population doublings in a 7-day culture period. Under the given conditions of cultivation, the cells typically reached this state after 40–50 PDL.

PA-1 is an ovarian teratocarcinoma (a germline tumour) cell-line, obtained from ATCC, with a stable near-diploid karyotype (Zeuthen *et al.,* 1980). It possesses functional TP53, despitepossible acquisition of one mutated allele reported at passages over 407 (Gao *et al.*, 1999). PA-1 and HEK- 293 (Human Embryonic Kidney 293) cells were cultured in Dulbecco's modified Eagle's media (DMEM) supplemented with 10% foetal bovine serum (FBS). Cells were grown without antibiotics in 5% CO2 incubators at 37 °C. For the sphere formation assay, PA1 cells were inoculated in DMEM/ F12 media supplemented with 20 ng/ml EGF (236-EG, R&D Systems), 10 ng/ml FGF (233-FB-025/CF, R&D Systems), 0.5 ng/ml hydrocortisone (H0888, Sigma), 10 ng/ml insulin (I9278, Sigma), 1× antibiotics/antimycotics (15240-062, Invitrogen), 1% L-glutamine (25030024, Invitrogen) and 20% methylcellulose (high viscosity, 4,000 cP; M0512, Sigma), and grown in 5% CO2 at 37 °C.

HeLa clone 3 cells of human cervix carcinoma were kindly provided by Fiorenza Ianzini (University of Iowa). The cells were grown on slides in Ham's F12 or HAM-1 medium (Sigma–Aldrich) medium supplied with 10% FCS (Biochrom) and penicillin/streptomycin (Life Technologies) at 37 °C in a 5% CO2 humidified incubator (Binder) on glass cover slides in medium supplied with 10% FCS Suspension culture were grown in suspension under constant rotation in Joklik's MEM containing 10% heat-inactivated calf serum (Hyclone) and antibiotics.

For experimental studies, cells were maintained in log phase of growth and treated with a single acute 10 Gy dose of gamma irradiation (1–2 Gy/min, Clinac 600 C, Varian Medical Systems or using a Gulmay D3 225 X-ray source at a dose rate of 0.77 Gy/min), ETO (etoposide; Sigma) – 8 mM for 20 h or PXT (paclitaxel, Ebewe Pharma) – 50 nM for 20 h. Following treatment, cell cultures were maintained by replenishing culture medium every 48h and sampled over a 2-week period posttreatment. In certain experiments Bafilomycin A (Baf A, Cayman Chemicals) 50 nM was added to the PA1 cell culture medium for 24h between day 3 to 4 after 20h treatment with 8 μM ETO.

To determine the capacity of cells to replicate DNA, BrdU was added at 5 mM to the cell culture for 24 h prior to fixation.

2.2. Silencing

Small interfering RNA (siRNA). TP53 protein Hs_TP53_9 FlexiTube siRNA (Qiagen) was used to silence TP53 expression and ON-TARGET plus non-targeting siRNA #1 (Dharmacon) was used as a negative control. PA-1 cells were transfected with siRNA using HiPerfect (Qiagen) according to the manufacturer's protocol.

Small interfering RNA (siRNA) silencing FlexiTube siRNA (SI04950274, SI04950267, SI04153835 and SI00690382; Qiagen) was used to silence OCT4A expression, and FlexiTube siRNA (SI00604905, SI00604898 and SI00299810; Qiagen) was used to silence p21Cip1 expression. ON-TARGET plus non-targeting siRNA #1 (Dharmacon) was used as a negative control. Cells were transfected with siRNA using HiPerfect (Qiagen) according to the manufacturer's protocol.

Small hairpin RNA (shRNA). The following plasmids were purchased from Addgene: pMKO.1 puro TP53 plasmid (Addgene plasmid 19119) deposited by Bob Weinberg and pMKO.1 puro (Addgene plasmid 8452) deposited by Bob Weinberg. PA-1 cells were transfected with plasmid using Fugene 6 (Promega) accord- ing to the manufacturer's protocol and then selected using puro- mycin (0.3 μg/ml). After 2 wk, growing colonies were sub-cloned, stable cell lines established and maintained in media containing puromycin. Selection was removed 3 d prior to experiments. Expression of HA-tagged forms of OCT4A and OCT4A- pseudogene-1. Expression vectors encoding HA-tagged forms of OCT4A or OCT4A-pseudogene-1 (OCT4A-PG1), a kind gift from Professor Aijun Hao, were transfected into HEK-293 cells using Fugene 6 (Promega) according to the manufacturer's protocol.

2.3. The senescence β-galactosidase

The senescence β-galactosidase (sa-β-gal) staining kit (Cell Signaling Technology, UK) was used to detect sa-β-gal activity in cells according to the manufacturer's protocol.

2.4. Cell cycle and ploidy analysis

DNA Image Cytometry. Cells grown on coverslips were rinsed in PBS and serum. Alternatively trypsinised cells were washed in warm PBS and suspended in FBS and cytospun onto glass slides. Both preparations were then fixed in ethanol/acetone (1 : 1, v/v) overnight at 4◦C and air dried. For stoichiometric DNA staining (Erenpreisa and Freivalds 1979), slides were hydrolysed with 5N HCl for 20min washed in distilled water (5 x 1 min) and stained for 10 min with 0.05% toluidine blue in 50% citrate-phosphate McIlvain buffer pH 4 for 10min at room temperature, rinsed, dehydrated in warm butanol, and passed through xylene prior to embedding in DPX (Sigma-Aldrich). DNA content was measured as the integral optical density in at least 200 cell nuclei in the green channel of the calibrated video camera, using Image Pro Plus 4.1 software (Media Cybernetics). In parallel, optical density and nuclear area were registered. The stoichiometry of DNA staining was verified using the values obtained for metaphases compared to anaphases and telophases (ratio 2.0). The estimated sum of device and measurement error was <5%. The 2C DNA content was determined by the modal value of the first G1 peak. Mitotic indices were counted per 1,000–2,000 cells in the same samples.

After shortened hydrolysis, interactive segmentation of mitotic figures was applied. Stoichiometry of DNA staining was verified using rat hepatocytes. With conventional 20-min acid hydrolysis, the 4C:2C ratio was 1.970; measurement error 1.5% (n5309); with 30-s hydrolysis, the 4C:2C ratio was 1.994; measurement error 0.3% n=182. Diploid DNA values for tumour cells determined after shortened hydrolysis were calculated by measuring metaphases and anaphase halves in 50 untreated cells, in which the variability coefficient was 7.7%

Cell cycle detection with flow cytometry. Cells (including those in media) were harvested at indicated time points, washed in PBS and re- suspended in hypotonic fluorochrome solution [50 µg/ml propidium iodide (PI), 0.1% (w/v) sodium citrate, 0.1% (v/v) Triton-X-100] and stored for at least 1 h in the dark at 4 °C. Flow cytometry was performed using a FACScan (BD Biosciences) or Accuri™ C6 Cytometer (BD Biosciences). Data was analyses using FlowJo analysis software.

2.5. Fluorescent in situ hybridisation (FISH)

FISH probes used for chromosome labelling in cell nuclei. Chromosome territories in five different specimens [non-irradiated control cells (NT); irradiated HeLa cells at day 2, 5, 6 and 7 (d2, d5, d6, d7) post radiation exposure] were hybridized with chromosome painting probes (MetaSystems). The slides of NT and d2 were hybridized with a combination of three chromosome painting probes (#1, #4 and #12). This combined probe set had the following spectral signatures: (a) Chromosome #1: Texas Red (red signature: $\lambda_{ex/em}$ = 586 nm/605 nm); (b) chromosome #4: FITC

(green signature: $\lambda_{ex/em}$ = 488 nm/518 nm); (c) chromosome #12: 1/1 mixture of Texas Red and FITC resulting in a yellow signature. The slides of d5, d6, and d7 were simultaneously hybridized with two probes for chromosome #1 (Texas Red) and chromosome #4 (FITC). Chromosome #12 was separately hybridized with a probe showing the same spectral signature as the chromosome #4 probe. Pericentric satellite probes (QBIOGENE – Molecular Cytogenetics/Diagnosticsfor chromosomes #6, #10, and #X were applied in addition to whole chromosome painting probes and hybridized according to the manufacturer's protocol. Slides of non-irradiated control cells (NT), and irradiated specimens at day 1 and 2 (d1, d2) were inspected visually for chromosome counting.

FISH (chromosome painting, centromere labelling) of cell nuclei. For quantitative microscopy, the cells fixed on SuperFrost Plus slides (Menzel Gläser) were treated according to the following protocol: For permeabilization of the membrane, the slides were incubated in 0.7 mL Triton-X100/99.3 mL 1× SSC for 30 min and washed with 2× SSC for 5 min. The specimens were incubated in RNase A (Sigma–Aldrich) for 30 min at 37 °C [2 µl stock solution (100 mg/mL) and 98 µL 2× SSC per slide]. After washing with 2× SCC for 3 min and 1× PBS for 5 min, proteins were digested in pepsin (Sigma–Aldrich) [21 µL stock solution (100 mg/mL) + 70 µL 0.01 M HCl in PBS] for 45 s. This was followed by a washing procedure in 1× PBS for 5 min, and in an ethanol series of 70%, 90%, and 100% for 3 min each. Denaturation was done in 70% formamide/2× SSC (at pH 7–7.2) for 5 min at 75◦C. Afterwards the slides were washed in 70%, 90%, and 100% ice-cold ethanol for 3 min each. As for the slides NT and d2, 2 µL of the probe mix combined with 2 µL of 60% formamide were dropped on the specimens. The in situ hybridization took place for 48 h at 37 °C. For the specimens d5, d6, and d7, the procedure was slightly different: 7 µL or 14 µL, respectively, of the probe mix were denatured during incubating at 75 °C for 5 min. The tubes were briefly cooled on ice. After that, the probes were incubated at 37 °C for 30 min and centrifuged for a short time. Then, the probe mix was pipetted onto the thermally denatured specimens and hybridized at 37 °C for 24 h. For post hybridization treatment, all slides were washed with 1× SSC at 75◦C and 2× SSC/0.01% Tween at room temperature. The cell nuclei were either counterstained with DAPI (Sigma–Aldrich) or with TO-PRO®-3 (Invitrogen) ($\lambda_{ex/em}$ = 642 nm/661 nm) 1:1000 in 1× PBS. The specimens NT, d1 and d2 were incubated with the antifade reagent ProLong® Gold (Invitrogen) at 37 °C for two days. The specimens were mounted in Immuno MountTM antifade solution (GeneTex Inc).

Chromosome preparation and FISH painting of metaphases. Half confluent HeLa clone 3 cultures were arrested at metaphase with 0.05 mg/mL Colcemid (GIBCO) for 3 h and then harvested by trypsin treatment. Chromosome spreads were obtained according to standard acetic acid:methanol (1:3) fixation protocols. Slides were stored at −20 °C until use. Three-colour chromosome painting (FISH) with a combination of chromosome #1, #4 and #12 paint probes

(MetaSystems) was performed. The hybridization mix was heated to 72 °C for 5 min and then incubated at 37 °C for 10 min prior to applying the mixture to the denatured chromosomes. Metaphase chromosomes were denatured on slides for 2 min at 72 °C in 70% formamide/2× SSC and then dehydrated in a series of 70%, 90% and 100% ethanol. Slides carrying denatured chromosomes were pre-warmed to 37 °C prior to the application of the denatured hybridization mixture, then covered by a 20 mm × 50 mm coverslip and sealed with rubber cement (Marabu). Hybridization was performed overnight at 37 °C in a moist chamber. The slides were then washed three times in 50% formamide/2× SSC, pH 7.0, at 42 °C for 15 min each followed by washes at 42 °C in 2× SSC, pH 7.0, for 15 min, in PN buffer (100 mM Na2HPO4, 50 mM NaH2PO4, 0.1% Triton X-100 (v/v))/0.1% Nonidet P40, pH 8.0, for 15 min, and in 3% bovine serum in 2× SCC for 30 min. At least 20 metaphases were analysed visually.

2.6. Reverse transcriptase(RT)-PCR, and sequencing

RT-PCR of NANOG. Total RNA was extracted from cells by using TRIZOL (Invitrogen) and treated with DNase I (Fermentas MBI). cDNA was synthesized using First Strand cDNA Synthesis Kit (Fermentas MBI) according to the protocols of the manufacturer. The absence of contamination with chromosomal DNA was verified by PCR using primers DQA-1 and KIR3DL2. Expression of Nanog was verified in comparison to embryonal stem cells cDNA (Millipore, SCR063). cDNA from peripheral blood lymphocytes (PBL) was kindly provided by Dr. HTC Chan, Southampton University, UK. Primers for PCR were designed using Primer 3 software (Rozen 2000) NANOG foreward primer sequence 5'→3' – CACCTACCTACCCCAGCCTT, reverse primer sequence 5'→3' CTCGCTGATTAGGCTCCAAC, lenght of fragment 585bp, GenBank accession number of the template used for design is: NM_024865. Amplification was carried out in a total volume of 50 µl with 1 – 4 µl cDNA in standard conditions using 0.5 units of Taq DNA polymerase (Fermentas MBI) with a BioCycler TC-S (BioSan). PCR conditions were as follows: 94 °C for 5min 94 °C for 30 s, 60 °C for 20 s, 72 °C for 1min; final extension step at 72 °C for 7 min. Amplified PCR products were resolved on 1.2 % agarose gels. The resulting PCR products fragments were analyzed by sequencing after ExoI/SAP treatment (Fermentas, MBI) using the fluorescent Big DyeTerminator v. 3.1 Cycle Sequencing protocol on a 3130xl Genetic Analyzer (Applied Biosystems).

RT-PCR analysis of Oct4-splicing forms. Total RNA was extracted from cells using TRIZOL (Invitrogen). cDNA was synthesized using First Strand cDNA Synthesis Kit (Fermentas MBI) according to the manufacturer's protocol and then diluted 10×. The absence of contamination with genomic DNA was verified by PCR using actin primers as described (Salmina *et al.,* 2010). cDNA from peripheral blood lymphocytes (PBL) as a control of somatic cells was kindly provided

by Dr Inta Vasiljeva. Amplification was performed with 1–4 μl of diluted cDNA and the following primers, β-actin F/R; Oct4A AF/AR; Oct4B/B1 BF1/BR2 under conditions previously described (Salmina *et al.*, 2010). Amplified PCR products were analyzed on an agarose gel after various PCR cycles and their identity determined by direct sequencing after ExoI/SAP treatment (Fermentas, MBI) using the fluorescent Big DyeTerminator v. 3.1 Cycle Sequencing protocol on a 3,130 xl Genetic Analyzer (Applied Biosystems).

Western blotting. Cells were harvested using trypsin digestion and lysed using RIPA buffer with protease inhibitor cocktail (Sigma P8340). Total protein was quantified using BCA protein assay kit (Pierce) or Bradford assay (Thermo Scientific), and equal quantities 10-30 μg of denatured protein verified by Ponceau S staining were subjected to electrophoresis on SDS polyacrylamide gels, blotted onto Immobilon-FC or BA85 nitrocellulose (Schleicher & Schuell GmbH) transfer membranes and probed with specific primary antibodies listed in Table 1 and secondary antibodies listed in Table 2 (Supplement). The signal was visualized using a LICOR Odyssey imaging system or ECL Western Blotting Substrate (Pierce, 32106).

For comparison of OCT4 isoforms protein was transferred onto immobilon-FC transfer membrane and probed with primary antibodies. Blots were then probed with fluorescent secondary antibodies and the signal was visualized using a LICOR Odyssey imaging system.

Subcellular fractionation. For cellular fractionation, the Subcellular Protein Fractionation Kit for Cultured Cells (Thermo Scientific) was used according to the manufacturer's instructions. Cytoplasmic, membrane, nuclear soluble, karyosol and chromatin-bound protein extracts were obtained. Protein concentrations were determined by Bio-Rad (Bio-Rad Inc.) protein assay, using a BSA standard set (Fermentas MBI) for quantitation. Proteins (10 or 15 μg) were separated on 10, 12, 5 or 20% SDS PAGE gels, followed by electrophoretic transfer onto BA85 nitro-cellulose membranes (Schleicher and Schuell GmbH) overnight.

2.7. Flow cytometry

Cells were harvested at relevant time points, washed in cold PBS and fixed with 70% ethanol for 20 min at room temperature. After two washes in tris buffered saline (TBS), cells were permeabilised with TBS/4% bovine serum albumin (BSA)/0.1% Triton X-100 for 10 min at room temperature. Samples were then incubated with primary antibodies (Table 1, supplement) in TBS/4% BSA/0.1% Triton X-100 for 1h at room temperature. Following two washes in TBS, cells were incubated with secundary antibodies (Table 2, supplement) in TBS/4% BSA/0.1% Triton X 100, for 30 min in the dark. DNA was counterstained with 10 μg/ml propidium iodide (PI) in PBS, and assessed by flow cytometry using a FACS Aria (BD Biosciences) using Cell Quest Pro Software). Data was analysed using FlowJo analysis software.

2.8. Immunofluorescence (IF)

Cells were trypsinized, pelleted, washed in warm PBS, resuspended in FBS and cytospun on to polylysine-coated slides. For detailed cytological studies, the cells were also grown on glass cover slips. Cells on coverslips were rinsed in PBS and FBS, then fixed in methanol at −20 °C for 7min (30min for γ-H2AX staining) followed by 10 short rinses in cold acetone at −20 °C. Slides were washed in TBS/0.01% Tween-20 (TBST) (0.05% Tween-20 for γ-H2AX staining) three times for 5min each, after which they were blocked with 1% bovine serum albumin in TBS/0.05% Tween-20 for 15min. Samples were covered with 50 μL of TBS, 0.025% Tween 20%, 1% BSA containing primary antibody and incubated overnight at 4 °C in a humidified chamber. Samples were washed thrice for 5min each time in TBST. The sources of the primary and secondary antibodies are listed in Tables 1 and 2 (supplement). Cells were conterstained with DAPI (0.25 μg/mL). Cells were finally embedded in Prolong Gold (Invitrogen). When staining for p-AMPKα1/2 (alone or in combination with the antibody for OCT4), fixation in 4% paraformaldehyde for 15 min was used, followed by washing thrice in PBS 0,1% glycine.

To detect protein disulfide isomerase, SelectFX Alexa Flour 488 Endoplasmic Reticulum Labeling Kit (S34200, Molecular Probes) was used according to the manufacturer's instructions.

2.9. Microscopy

Slides were evaluated using a Leitz Ergolux L03-10 microscope equipped with Sony DXC 390P colour video camera, for microscopic observations; in addition to separate optical filters, a three-band BRG (blue, red, green) optical filter (Leica) was used. Image cytometry was carried out by semi-automatic measuring fluorescence values for each cell nuclei in all three channels and analysed using Image-Pro Plus 4.1 software (Media Cybernetics). Apoptotic cells, determined by nuclear morphology, were omitted from measurements.

Phase contrast photography was performed using a light microscope (AxioImager A1, Carl Zeiss).

2.10. Other stainings

To reveal NORs (nucleolar organizers), prefixed cytospins were stained with a 50% aqueous solution of AgNO3 (Ural Factory of Chemical Reagents) diluted with 2% gelatin (2:1) at 60uC for 5–6 min and counterstained with 0.1% Methyl Green (Sigma–Aldrich) at room temperature for 1 min. This method is recognized as the universal indicator of NOR activity (Bancroft and Stevens 1996).

Lysosomal activity and autophagic vacuoles were detected by staining for cathepsin B (see below) and with MDC (monodansyl- cadaverin, Sigma). For MDC staining, cell cultures were incubated with 0.05 mM MDC at 37uC for 1 h followed by fixation in 4% paraformaldehyde and

two washes in PBS. The slides were counterstained with PI (propidium iodide; BD Biosciences Pharmingem), mounted into Permount (Thermo Fisher Scientific) and immediately imaged.

3D-Microscopy of FISH staining. Up to 50 cells of NT and d2 each were imaged with a Leica TCS NT confocal laser scanning microscope using a high numerical aperture lens (63×/NA 1.4 oil) and appropriate filter settings. Up to 50 cell nuclei each of the data sets d5, d6, and d7 were imaged with the Nikon TE2000-E Perkin Elmer UltraVIEW ERS Spinning Disc confocal microscope also using high numerical aperture lenses (63×/NA/1.2 water) and appropriate filter settings. For 3D-reconstructions the axial step size was 203 nm for all z-stacks.

3D Image evaluation. The numbers and positions of the chromosome territories #1, #4, and #12 in the irradiated specimens d2, d5, d6, and d7 were analysed and compared to data obtained from non-irradiated control cells (NT). 3D-microscopy image data stacks were evaluated by means of the freely available software 'Nemo', version 1.5 (https://www-lgc.toulouse.inra.fr/nemo/) implemented into the image analysis software package "ImageJ". For the different fluorescent objects within the cell nuclei, the shortest geometrical distances of the barycentres to the nuclear bor- der were calculated. For all chromosomes, a difference or change of ploidy did not influence the result since only the distances of the most peripherally (pCT) and the most centrally (cCT) located chromosome territories were always determined. These values were statistically compared over the course of time. The results were expressed as cumulative frequency histograms of distances.

2.11. Methods of statistical analysis.

Statistical analysis was performed by Minitab and GraphPad (GraphPad Software Ltd) systems. A paired t-test was used to calculate the statistical significance of difference of means where appropriate. Statistical significance was accepted when $p < 0.05$. Graphs were plotted by GraphPad Prism 5, IBM SPSS Statistics 22 and Statistica 6.

The Kolmogorov–Smirnov test was used for the statistical pairwise analysis of chromosome territory histogram curves. The null hypothesis of this test is that two samples are drawn from the same frequency distribution. On acceptance of the alternative hypothesis, namely that the two fre quency histograms belong to different distributions, the significance level of this test defines an error probability for the two distance distributions being equal, i.e. two distributions being of the same entity. In general, this error level was taken to be up to 5% or even less because the Kolmogorov–Smirnov test tends to be conservative. On the other hand, the test is robust and can be easily applied to distributions with rather large deviations in sample numbers. For volume calculations of the cell nuclei and chromosome territories, the voxels covered by the object were

counted and multiplied with the respective voxel volume of the image. Finally, the average volumes of all detected nuclei or chromosome territories were determined.

3. Results

The results are presented here as original publications.

The author's contribution to the enclosed original publications:

Original paper I

Huna, A., Salmina, K., Jascenko, E., Duburs, G., Inashkina, I., Erenpreisa, J. (2011). Self-Renewal Signalling in Presenescent Tetraploid IMR90 Cells. *Journal of Aging Research, 2011*, 103253. doi:10.4061/2011/103253

Performed DNA image cytometry, cultivated cells, participated in design and analysis of experiments and partly wrote the manuscript.

Original paper II

Jackson, T. R., Salmina, K., Huna, A., Inashkina, I., Jankevics, E., Riekstina, U., Kalnina Z., Ivanov A., Townsend P. A., Cragg M. S., Erenpreisa, J. (2013). DNA damage causes TP53-dependent coupling of self-renewal and senescence pathways in embryonal carcinoma cells. *Cell Cycle (Georgetown, Tex.)*, *12*(3), 430–41. doi:10.4161/cc.23285

Participated in experimental design, cultivated cells, performed cell treatments, part of the immunofluorescence and flow cytometry experiments, image analysis, prepared part of the graphical information and partially the manuscript.

Original paper III

Huna A, Salmina K, Erenpreisa J, Vazquez-Martin A, Krigerts J, Innashkina I, Gerashchenko BI, Towsend P, Cragg MS, Jackson TR Role of stress-activated OCT4A in the cell fate decisions of embryonal carcinoma cells treated with etoposide. Cell Cycle 2015 (in press)

Participated in experimental design, cultivated cells, performed cell treatments, did flow cytometry and part of immunofluorescence staining, fluorescence image analysis, prepared part of the graphical information and wrote the manuscript.

Original paper IV

Erenpreisa, J., Salmina, K., Huna, A., Kosmacek, E. A., Cragg, M. S., Ianzini, F., Anisimov, A. P. (2011). Polyploid tumour cells elicit paradiploid progeny through depolyploidizing divisions and regulated autophagic degradation. *Cell Biology Int*, *35*, 687–695. doi:10.1042/CBI20100762

Carried out DNA image cytometry of WI-L2-NS and analysis of results, and participated in the preparation of the manuscript draft.

Original paper V

Schwarz-Finsterle, J., Scherthan, H., Huna, A., González, P., Mueller, P., Schmitt, E., Erenpreisa, J., Hausmann, M. (2013). Volume increase and spatial shifts of chromosome territories

in nuclei of radiation-induced polyploidizing tumour cells. *Mutation Research*, 756 (1-2), 1–10. doi:10.1016/j.mrgentox.2013.05.004

Performed FISH experiments, participated in analysis of results, edited the manuscript.

Review article I

Erenpreisa, J., Salmina, K., Huna, A., Jackson, T. R., Vazquez-Martin, A., Cragg, M. S. (2015). The " virgin birth ", polyploidy , and the origin of cancer, *2*(1), 3–14.

Participated in the manuscript draft preparation, literature collection, edit, design of the figures.

3.1. Self renewal activation in normal ageing tetraploid human fibroblasts – Original paper I

SAGE-Hindawi Access to Research
Journal of Aging Research
Volume 2011, Article ID 103253, 14 pages
doi:10.4061/2011/103253

Research Article

Self-Renewal Signalling in Presenescent Tetraploid IMR90 Cells

Anda Huna,[1] Kristine Salmina,[1] Elina Jascenko,[2] Gunars Duburs,[2] Inna Inashkina,[1] and Jekaterina Erenpreisa[1]

[1] *Latvian Biomedical Research and Study Centre, Ratsupites 1, 1067 Riga, Latvia*
[2] *Latvian Institute of Organic Synthesis, Aizkraukles 21, 1006 Riga, Latvia*

Correspondence should be addressed to Jekaterina Erenpreisa, katrina@biomed.lu.lv

Received 15 December 2010; Revised 22 February 2011; Accepted 25 February 2011

Academic Editor: Noam Shomron

Endopolyploidy and genomic instability are shared features of both stress-induced cellular senescence and malignant growth. Here, we examined these facets in the widely used normal human fibroblast model of senescence, IMR90. At the presenescence stage, a small (2–7%) proportion of cells overcome the 4n-G1 checkpoint, simultaneously inducing self-renewal (NANOG-positivity), the DNA damage response (DDR; γ-H2AX-positive foci), and senescence (p16inka4a- and p21CIP1-positivity) signalling, some cells reach octoploid DNA content and divide. All of these markers initially appear and partially colocalise in the perinucleolar compartment. Further, with development of senescence and accumulation of p16inka4a and p21CIP1, NANOG is downregulated in most cells. The cells increasingly arrest in the 4n-G1 fraction, completely halt divisions and ultimately degenerate. A positive link between DDR, self-renewal, and senescence signalling is initiated in the cells overcoming the tetraploidy barrier, indicating that cellular and molecular context of induced tetraploidy during this period of presenescence is favourable for carcinogenesis.

1. Introduction

Cellular senescence is a condition in which the cells remain alive but are unable to proliferate. Premature senescence can be triggered by certain stresses independently of the number of cell divisions or telomere length [1], possibly as a result of protracted DNA damage signalling [2]. Oncogene-induced senescence is thought to behave similarly, driven at the very early stages of tumour development where it serves as a barrier to cancer progression [3]. Subsequent progression to full-blown malignancy is favoured when tumour stem cells acquire further mutations that impair the senescence pathway, for example, mutations in TP53 or CDKN2a [4, 5].

During *in vitro* culture, human fibroblast cells undergo a presenescence phenomenon whereby they display evidence of chromosome instability (CIN) within an apparently highly heterogenous population with signs of chromosomal damage, and the appearance of polyploid interphase cells and their divisions [4, 6–12]. Whereas the frequency of diploid mitotic cells at presenescence is declining, the number of polyploid mitoses increases to a peak before a sharp fall as the cells change to the characteristic flat morphology indicative of replicative senescence [13, 14]. These data stimulated the hypothesis that telomeric loss at senescence may represent a "genetic time bomb" causally involved in both cell senescence and malignant transformation [13, 15].

In is clear that CIN associated with polyploidy at the presenescence stage may substantially increase the mutability and risk of malignant transformation [16–18]. Moreover, there are reports from normal cell cultures of revertant cells escaping senescence by acquiring mutations [19] and their ability to depolyploidise and restart mitoses [9–12, 17]. The features of CIN, including polyploidy, are also characteristic of malignant tumors where the degree of CIN is correlated with aggression [20]. Induced endopolyploidy is a typical response of tumour cells with deficient p53 function to the action of DNA or spindle-damaging agents [21–24]. For a decade, it has been generally accepted that sublethal genotoxic damage to cancer cells associated with anticancer clinical modalities accelerates cellular senescence [1, 25], with concomitant induction of polyploidy as a component.

However, we and others have recently shown that the induction of endopolyploidy followed by arrest and subsequent slippage from a spindle checkpoint is accompanied

Table 1: Antibodies: source and use.

Primary antibodies	*Secondary antibodies* (dilution, if not stated otherwise, 1 : 400)
Mouse monoclonal anti-hNANOG (N3038, Sigma) 1 : 75	Goat anti-mouse IgG-Alexa Fluor 488 (A31619, Invitrogen) or 594 (A31623, Invitrogen)
Rabbit polyclonal anti-hOCT4 (ab19857, Abcam) 1 : 200	Goat anti-rabbit-IgG-Alexa Fluor 594 (A31631, Invitrogen)
Goat polyclonal anti-hOCT3/4 (N-20) (sc-8630X, Santa Cruz) 1 : 400	Rabbit anti-goat IgG-Cy3 (C2821, Sigma) 1 : 500
Rabbit polyclonal anti-hP21 C-19 (sc-397, Santa Cruz) IF 1 : 50	Goat anti-rabbit-IgG- .Alexa Fluor 594 (A31631, Invitrogen)
Rabbit polyclonal anti-hP16 N-20 (sc-467, Santa Cruz) IF 1 : 50	Goat anti-rabbit-IgG- .Alexa Fluor 594 (A31631, Invitrogen)
Mouse monoclonal anti-hPML (sc-966, Santa Cruz) 1 : 150	Goat anti-mouseIgG-Alexa Fluor 488 (A31627, Invitrogen)
Rabbit polyclonal anti-hAURORA B (ab2254, Abcam) 1 : 300	Goat anti-rabbit-IgG- .Alexa Fluor 594 (A31631, Invitrogen)
Rabbit polyclonal anti-h-γH2AX (4411-PC-100, R&D Systems) 1 : 200	Goat anti-rabbit-IgG- .Alexa Fluor 594 (A31631, Invitrogen)

in p53-mutant tumour cells by the activation of meiotic proteins [24, 26, 27] and key self-renewal transcription factors (OCT4, NANOG, and SOX2) [28]. The majority of these polyploid cells senesce. However, a minor fraction retains divisional activities (thus counteracts or reverses senescence), accumulate self-renewal factors in their subnuclei, and subsequently undergo depolyploidisation to paradiploid descendants that provide clonogenic regrowth [28, 29].

Cycling tetraploidy, an illicit deviation from the normal cell cycle, is considered to serve as a crucial step from diploidy to cancer-related aneuploidy and from senescence to malignancy [17, 30–32]. Together, these data highlight the need to more closely investigate the role of endopolyploidy in the relationship between self-renewal and senescence. These investigations will greatly assist the current endeavours being made to induce reprogramming of somatic cells that are free from genomic damage and provide further information regarding the use of senescence-induction as a potential anticancer strategy [33, 34].

Therefore, we chose to examine these phenomena using a well-established model of cell senescence, involving *in vitro* cultured normal human fibroblast IMR90 cells. We show here that a small proportion of cells undergoing senescence are able to overcome the tetraploidy barrier and that these cells appear to simultaneously upregulate self-renewal and senescent factors.

2. Materials and Methods

2.1. Cell Culture. The wild-type p53 human embryo lung fibroblast cell line IMR90 was obtained from ATCC and also from Coriell collection kindly donated by Dr. A. Ivanov (Beatson Institute, Glasgow) after 21–23 population doublings (PDL). Cells were cultured in DMEM (Sigma) supplemented with 10% FBS (Sigma), without antibiotics, as monolayers in a humidified incubator in 5% CO_2/95% air atmosphere. The early passage cells were split 1 : 3 ($\sim 50 \times 10^4$ of cells per flask (25 cm^2) twice weekly. Mid-passage cells were split 1 : 2 weekly, and late-passage cultures were split 1 : 2 once cultures attained confluence. Culture medium was changed two or three times between subculture. In this way, several subsequent passages were carried out until the cells failed to undergo >0.8 population doublings in a 7-day culture period. Under the given conditions of cultivation, the cells typically reached this state after 40–50 PDL.

2.2. Immunofluorescence (IF). Cells were trypsinized, pelleted, washed in warm PBS, resuspended in FBS and cytospun on to polylysine-coated slides. For detailed cytological studies, the cells were also grown on glass cover slips. Cells on coverslips were rinsed in PBS and FBS, then fixed in methanol at −20°C for 7 min (30 min for γ-H2AX staining) followed by 10 short rinses in cold acetone at −20°C. Slides were washed in TBS/0.01% Tween-20 (TBST) (0.05% Tween-20 for γ-H2AX staining) three times for 5 min each, after which they were blocked with 1% bovine serum albumin in TBS/0.05% Tween-20 for 15 min. Fifty microliters of the appropriate dilution of antibody was applied to each sample and the slides incubated overnight at 4°C. Samples were washed thrice for 5 min each time in TBST. The sources and dilutions of the primary and secondary antibodies are listed in Table 1. Poststaining was with DAPI (0.25 μg/mL). Cells were finally embedded in Prolong Gold (Invitrogen).

2.3. Microscopy. A fluorescence microscope (Leitz, Ergolux L03-10) equiped with a colour videocamera (Sony DX-S500) was used to examine cell preparations, record images, and perform image cytometry. For three-colour images and colocalisation studies, the BRG filter system (Leica) providing nonoverlapping excitation and transmission emission of blue, red, and green bands was used. In addition, confocal microscopy (Leica, DM 600) was used with the images scanned in the three different colour channels in sequence.

2.4. DNA Image Cytometry. Cells grown on coverslips were rinsed in PBS and serum. Alternatively trypsinised cells were washed in warm PBS and suspended in FBS and cytospun onto glass slides. Both preparations were then fixed in ethanol/acetone (1 : 1, v/v) overnight at 4°C and air dried. For stoichiometric DNA staining [35], slides were hydrolysed with 5 N HCl for 20 min and stained with 0.05% toluidine blue in McIlvain 50% buffer pH 4 for 10 min at room temperature, rinsed, dehydrated in warm butanol,

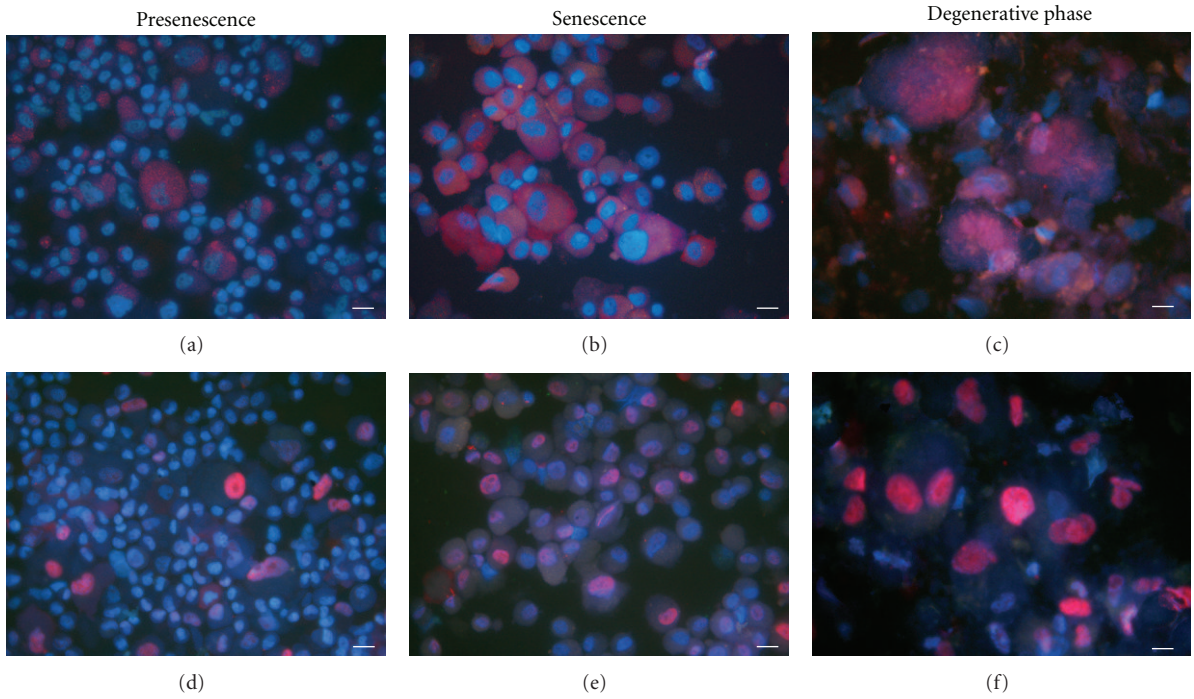

Figure 1: Phenotypic characteristics of IMR90 in the process of senescing showing cell enlargement and the accumulation of principal growth inhibitors involved in the regulation of senescence, p16 and p21, in three stages: ((a), (d)) presenescence, ((b), (e)) senescence, ((c), (f)) degeneration phase. ((a)–(c)) p16 (red) and DAPI (blue); ((d)–(f)) p21(red) and DAPI (blue). Scale bar = 20 μm.

and passed through xylene prior to embedding in DPX (Sigma-Aldrich). DNA content was measured as the integral optical density in 200 cell nuclei in the green channel of the calibrated video camera, using Image Pro Plus 4.1 software (Media Cybernetics; REO 2001, Latvia). In parallel, optical density and nuclear area were registered. The estimated sum of device and measurement error was <5%. The 2C DNA content was determined by the modal value of the first G1 peak. Mitotic indices were counted per 1,000–2,000 cells in the same samples.

2.5. RNA Extraction, RT-PCR, and DNA Sequencing of NANOG. These studies were performed on IMR90 cells in a logarithmic phase of growth as described before [28].

3. Results

3.1. Kinetics and Characteristics of Senescing Cells. Subcultivation of IMR90 cells invariably leads to diminishing growth after a number of passages. Under our experimental conditions, this was reached prematurely at passage 32–34 corresponding to 40–50 PDL. This was likely due to growing the cells in the air atmosphere shortening their lifespan [36]. During further passaging, full growth arrest was achieved, characterised by the mitotic index reaching zero and the cells attaining typical features of senescence such as cytoplasm enlargement and flattening and bi- and multinuclearity, as well as accumulation of senescence markers p16inka4a (p16) and p21inka4a (p21) as illustrated on Figures 1(a), 1(b), 1(d), and 1(e). Degenerative phase was characterised by nuclear swelling and cell lysis (Figures 1(c) and 1(f)).

3.2. DNA Cytometry Reveals a Minor Fraction of Cycling Tetraploid Cells. As the cells underwent this senescence phenomenon, they were analysed by DNA image cytometry in three independent experimental series. The following cytometric regularities were observed. In the stage of logarithmic growth (typified in Figure 2(a)), where the mitotic index was 4.5–3.0%, the cell population had a normal cell cycle, with typical DNA distribution of the major fractions between 2C and 4C. During presenescence, with the mitotic indices progressively lowering, the histogram of DNA distribution remained generally similar (exampled on Figure 2(b)), however the proportion of cells in the G1-2C phase increased and the S-phase decreased. At senescence, where no mitoses were observed, the proportion of interphase cells in the 4C-fraction was again increased (Figure 2(d)). This change was already noticeable at late presenescence, one-two passages earlier (Figure 2(c)). The average proportions of 4C cytometric fractions at the stages of logarithmic growth, presenescence and senescence, and corresponding proportions of the cells with p21-positive nuclei are presented on Figure 3.

In addition to the major DNA cytometric fractions, we also observed a small proportion (1–7%) of hypertetraploid cells, some of them reaching octoploidy. The number of hypertetraploid cells strongly inversely correlated with mitotic indices in each experimental series (Figure 4(a)). Furthermore, the number of octoploid cells was found

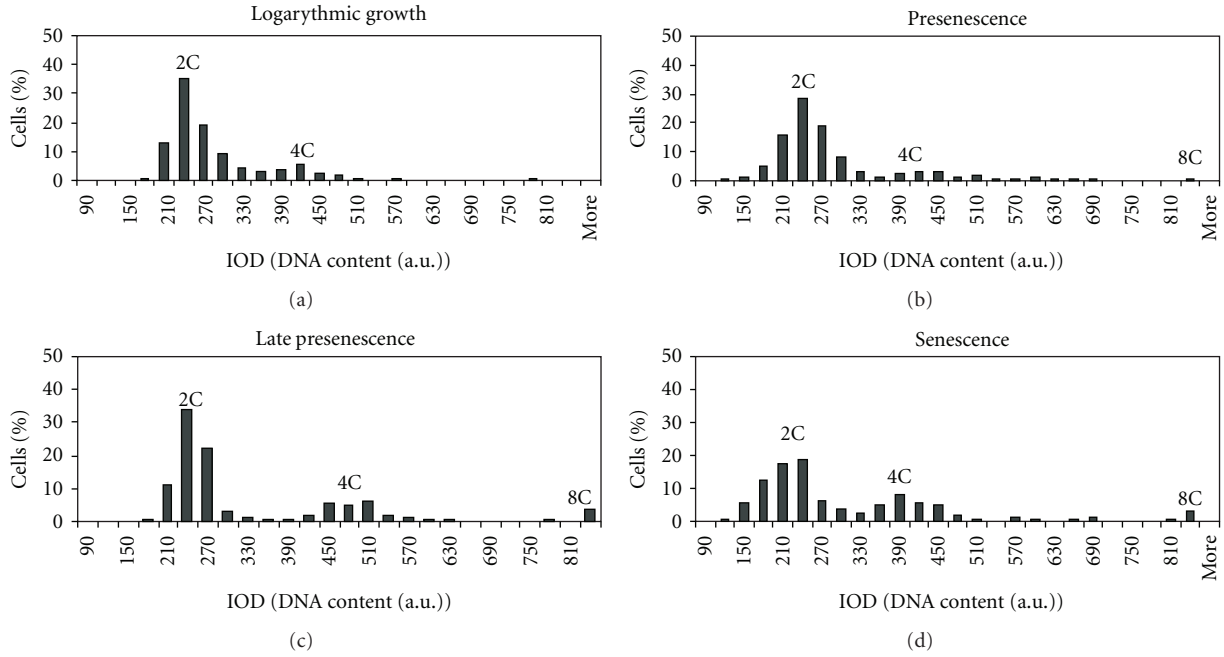

Figure 2: Histograms of IMR90 DNA content in several passages showing typical changes in the time course: (a) logarithmic growth, (b) presenescence, (c) late presenescence, and (d) senescence showing the accumulation of 4C cells and the increase of the proportion of hypertetraploid cells, some of which reach octoploidy.

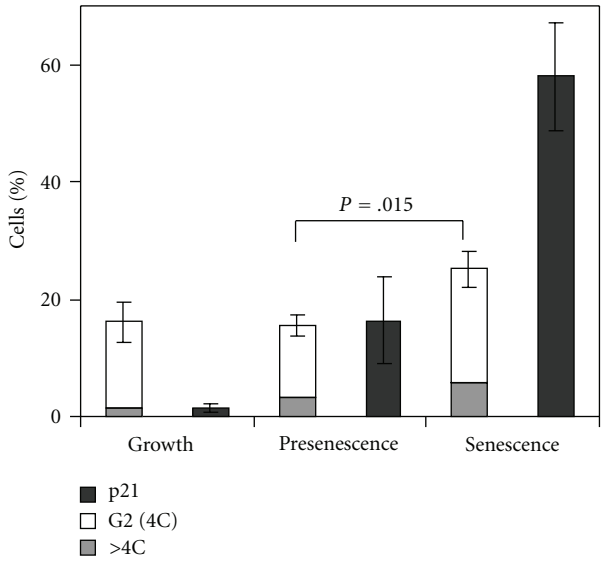

Figure 3: Quantitative data showing changes obtained from the DNA cytometry results, at the growth phase, presenescence, and senescence averaged from all experiments and the corresponding proportions of cells displaying nuclear positivity for p21. Significant increase of the 4C fraction accompany transition from presenescence to senescence ($P = .015$). Increase of the proportion of hypertetraploid cells, in parallel to considerable increase of the proportion of p21-positive cells, accompany the whole process.

increasing with hypertetraploidy (Figure 4(b) and can be seen from Figure 2). These data indicate that the process of (accelerated) senescence encourages the cells to leave the normal cell cycle favouring their cycling as tetraploids.

3.3. Self-Renewal Markers Appear at Presenescence in Tetraploid Cells Simultaneously with Senescence and DDR Markers. We were further interested to see the association of these polyploid features with DDR, self-renewal, and senescence markers. At presenescence, we found that the embryonal transcription factors of pluripotency and self-renewal OCT4 (mostly cytoplasmic) and NANOG (nuclear) were activated in parallel with the initial activation of senescence factors in the same cells. Notably, this occurred in the cells with larger nuclei and larger (often polygonal) p16-positive cytoplasm, suggesting that these were hypertetraploid cells which had initiated the process towards senescence (illustrated in Figure 5). In an effort to better characterise the position of these particular cells in the cell cycle, we undertook two kinds of analysis.

First, we stained samples stoichiometrically with Toluidine blue for DNA and recorded the integral optical density (DNA content), nuclear area, and subsequently optical density (OD, concentration of DNA) of 200 cells in each sample using Image Pro Plus software. Importantly, this imaging method is interactive and excludes any cell aggregates, which are either excluded or separated for single cells before the measurement by the operator. Using this approach, the concentration of DNA remained constant in all samples (the data are not shown), with dispersion of OD around the average within only 2-3%, up to the degeneration phase. The positive correlation between the DNA content per nucleus and its area counted for each sample is high ($r = 0.57$–0.76);

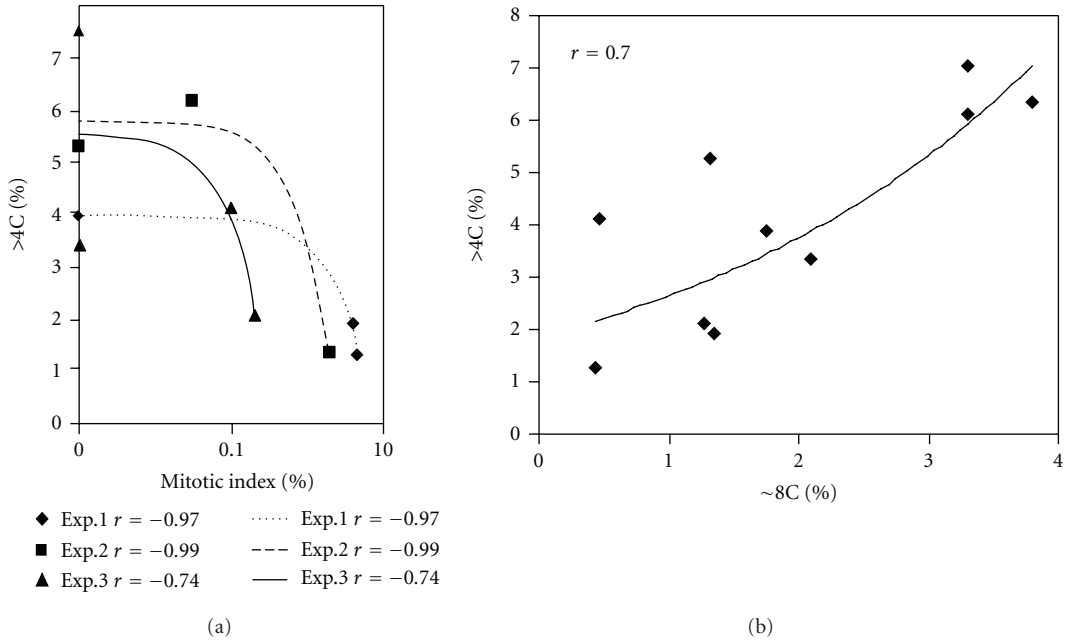

(a) (b)

Figure 4: Tetraploidy increases in the course of IMR90 senescence. (a) The number of hypertetraploid cells increases with senescence and strongly inversely correlates with mitotic indices in each experimental series; (b) the number of cells with octoploid DNA content increases with hypertetraploidy indicating to increase of tetraploid cycling (the united data from three experiments).

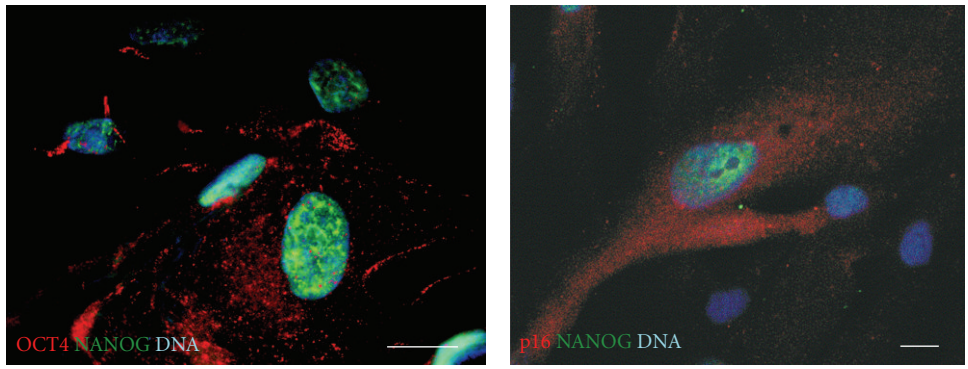

(a) (b)

Figure 5: Examples of pre-senescent IMR90 fibroblasts grown on the coverslip, which differ from the surrounding cells by enlarged nuclei, cytoplasm volume, and the tendency of flattening. These cells express: (a) enhanced OCT4 (mostly in cytoplasm) and nuclear NANOG and (b) paranucleolarly localized NANOG, which is combined with enhanced expression of the senescence regulator, p16. Both, self-renewal and senescence regulators are undetectable or at the background level in the neighbouring fibroblasts possessing small nuclei. Scale bars = 10 μm. On (a) OCT4 was stained with the antibody for both A and B isoforms (Abcam polyclonal antibody, see Table 1).

an example is shown in Figure 6(a). This confirms the accepted observation that nuclear area is proportional to DNA content; hence, its concentration remains constant [37, 38]. In Figure 6(a), sampled from presenescence phase, it is seen that the nuclear size of the 4C nuclei cluster is roughly twice as large as that of the 2C nuclei cluster, while the nuclear size of the cells with hypertetraploid DNA content exceeds that of the average 4C nuclei. It follows that the cells with a nuclear area visibly larger than that for G1 and G2 cells should contain the hypertetraploid DNA content.

Second, we stained samples for NANOG and one of the main senescence regulators (p16 or p21) in combination with DAPI. Using this approach, we identified cells possessing visibly larger nuclei as compared with G1- and G2-sized nuclei of surrounding fibroblasts which simultaneously expressed markers of both self-renewal (NANOG) and senescence. We subsequently applied DNA measurement of the integral nuclear fluorescence (INF) of these and neighbouring cell nuclei as exemplified on Figures 7(a) and 7(b), through 16 optical fields (total 242 cells); a selection of seven microscopic fields is also presented in supplemental

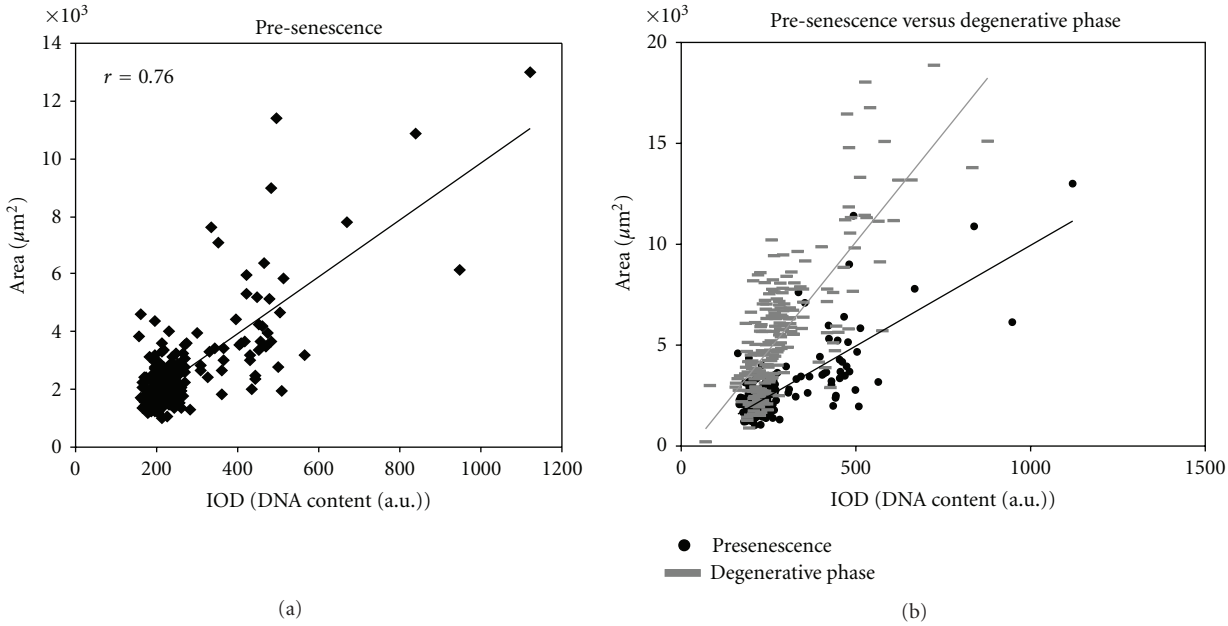

Figure 6: The relationship between the nuclear area and the DNA content (IOD) per each cell nucleus in: (a) a typical sample of presenescence phase and (b) the comparison of the latter and a sample in the degeneration phase. It is seen that the nuclear size is increasing roughly proportionally to the DNA content in the presenescence phase, while in the degeneration phase, the nuclear size is much larger indicating to nuclear swelling.

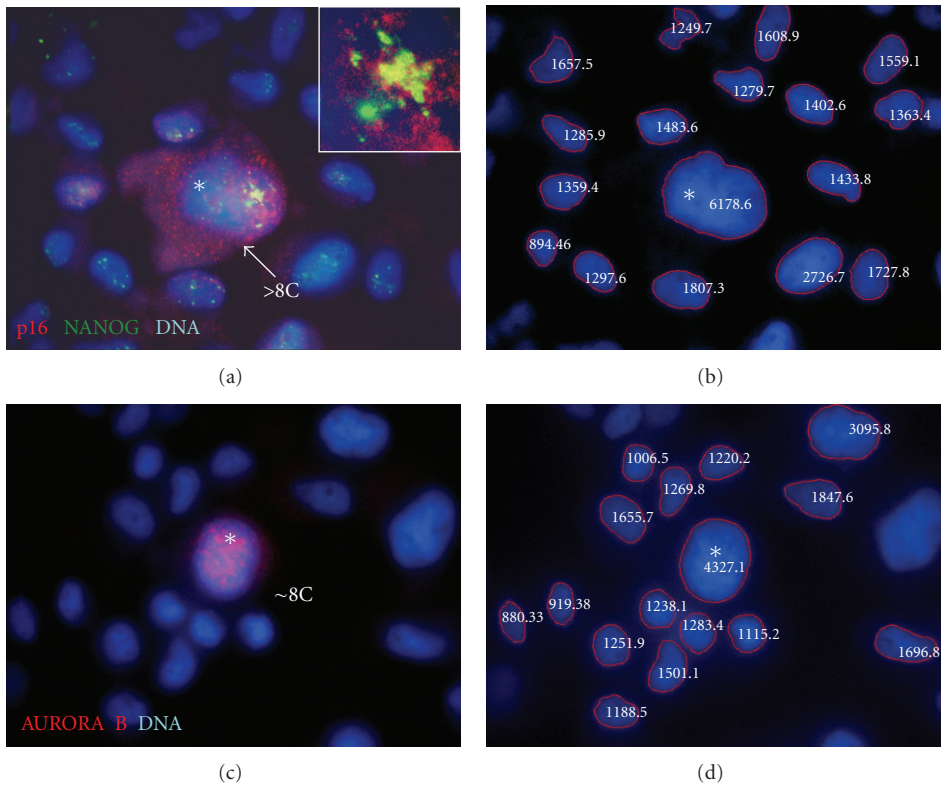

Figure 7: Examples of DNA content measurements by integral fluorescence in the DAPI channel using Image Pro Plus software in microscopic fields including cells with enlarged nuclei and stained for: ((a), (b)) NANOG, p16, and DNA by DAPI, ((c), (d)) Aurora B-kinase and DNA by DAPI. The selected hyperoctoploid cell (*) shown in (a) has an enlarged p16-positive cytoplasm and some amount of both NANOG and p16 in the nuclear region, and this region is magnified in the insertion; the paraoctoploid cell in (c) is positive for Aurora B-kinase.

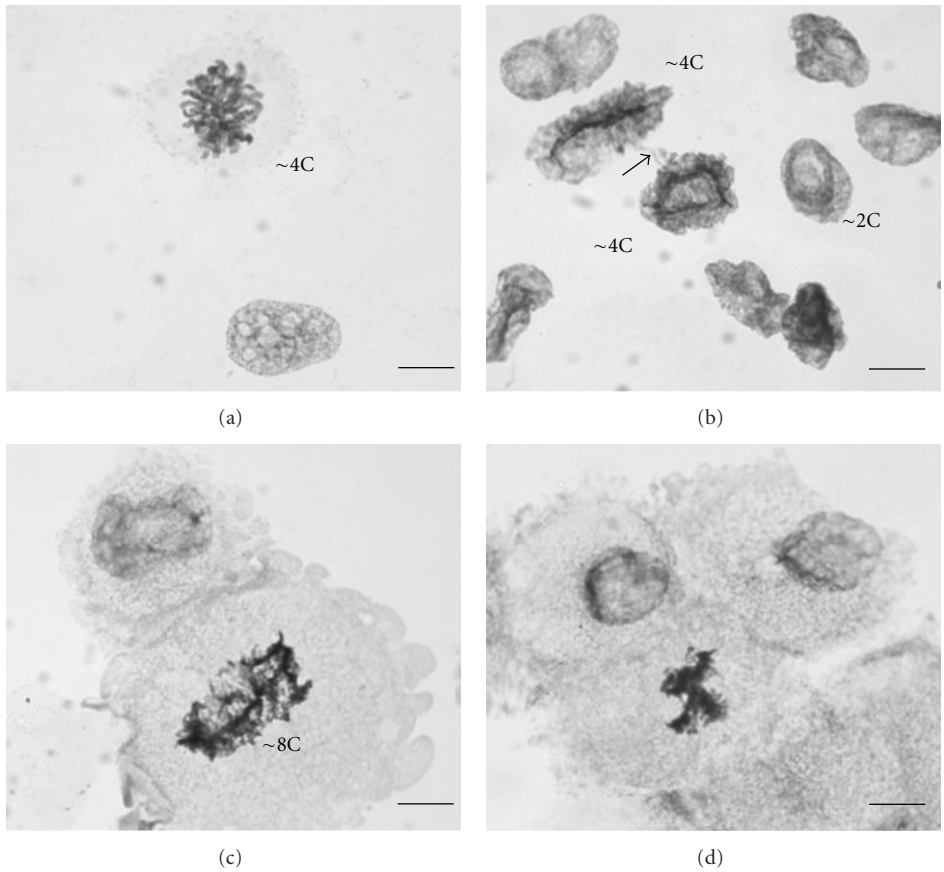

Figure 8: Mitoses of IMR90: (a) normal mitosis of a diploid cell in the growth stage, ((b)–(d)) mitoses in the presenescence stage. (b) Anaphase of the tetraploid cell, chromosome bridge (arrowhead) indicates to CIN. (c) Metaphase of the large tetraploid cell (~8C). (d) An attempt of the tetrapolar mitosis indicating to CIN. ((a),(b)) stoichiometric staining for DNA with Toluidine blue pH 4.0 after extraction of RNA. ((c),(d)) Similar staining after partial extraction of RNA. Scale bar = 10 μm.

Figures 1–6 in Supplementary Material available online at doi: 10.4061/2011/103253. The standard error of such nuclear measurements comparing the INF recorded on the smallest cell nuclei (2C-G1) was around 20%. The selected cells which expressed markers of self-renewal and senescence contained tetraploid, hypertetraploid, or octoploid amounts of DNA more frequently than surrounding cells.

We were interested subsequently if these cells retained proliferation capacity. Using immunostaining for Aurora B-kinase as a marker of cell division potential for endopolyploid cells [39], we often found that cells with enlarged nuclei containing the tetraploid or octoploid amounts of DNA (as also detected in DAPI channel), were Aurora B-positive (exemplified on Figures 7(c) and 7(d)). At presenescence, we also found mitoses of tetraploid cells. Although commonly aberrant or pycnotic, some proceed to anaphase with signs of CIN such as chromosome bridges or multipolar mitoses (Figure 8).

The enlarged nuclei were also often labelled by the DDR marker γ-H2AX coupled to the NANOG staining (Figures 9(a) and 9(f)). Thus, at the presenescence stage, the cells with enlarged nuclei possessing enlarged p16-positive cytoplasm, simultaneously expressing small amounts of self-renewal, senescence, and DDR markers in their nuclei were found to be tetraploid, had overcome the 4n-G1 barrier, were cycling to octoploidy, and possessed division potential.

3.4. Self-Renewal, DDR, and Senescence Markers Are Initially Localised in the Perinucleolar Compartment of Tetraploid Cells. Interestingly, manifestations of all three kinds of response (γ-H2AX, NANOG, and p16/p21) were seen to be partialy colocalised as foci detected by BRG three-band optical filter (with nonoverlapping excitation and emission bands); and confirmed by confocal microscopy (supplemental Figure 7). These concentrated in the perinucleolar compartment either to one side of the large central nucleolus or surrounding it (Figures 9(a)–9(c)). Initial signs of senescence-associated heterochromatin foci (SAHF) also appear to emerge from the perinucleolar chromatin in such cells (Figure 9(d)). The initially observed PML-bodies, partially colocalised with γ-H2AX -positive speckles, were also found in this area (Figure 9(e)). The IMR90 cells at the logarithmic stage of growth had very low background IF staining for NANOG confirmed by RT-PCR and DNA sequencing (data not shown). The amount of NANOG usually seen by IF in

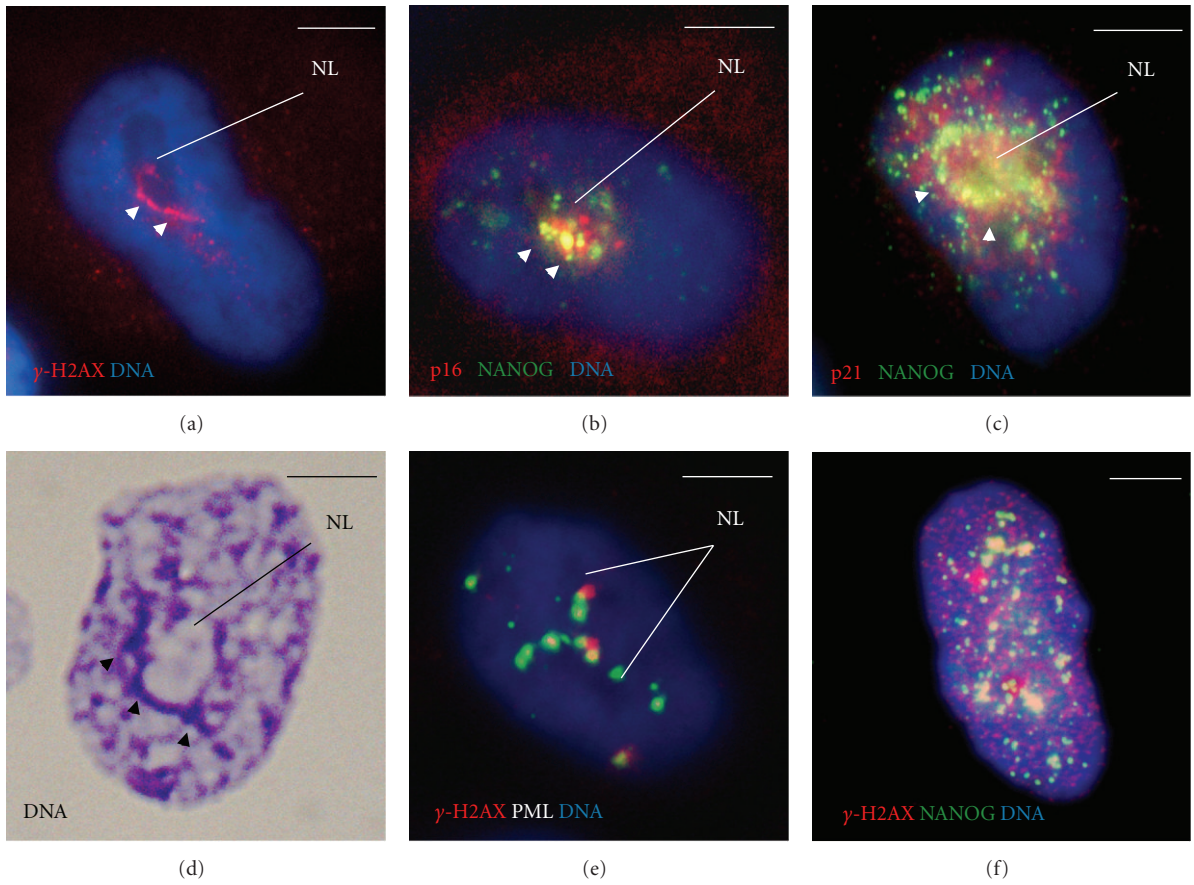

Figure 9: Characteristic cytological nuclear IF features of the tetraploid cells in the presenescence phase showing synergism of several labels located near the nucleoli. (a) Initial DDR in the perinucleolar chromatin indicated by the γ-H2AX-positive label (arrowheads), NL-nucleolus. (b) The accumulation of p16 and NANOG-positive, partly colocalising granules in the perinucleolar region (arrowheads). (c) The accumulation of p21 and NANOG—partial colocalisation around the central nucleolus (arrowheads). (d) The emergence of initial gentle SAHFs revealed by DNA-specific metachromatic staining with Toluidine-blue in the perinucleolar chromatin (arrowheads). (e) PML bodies in the vicinity of the central lobulated nucleolus, where they partly colocalise with γ-H2AX-foci. (f) The tetraploid cell from the mid-presenescence with the network of γ-H2AX and some amount of NANOG, partially colocalised. Images were obtained using BRG three-colour optical filters system. Scale bars =10 μm.

the enlarged cell nuclei at early presenescence exceeded the background of surrounding cells with normal nuclei by ~2–4-fold (supplemental Figure 7).

We compared the frequency of this coexisting self-renewal and senescence nuclear landmarks (mostly perinucleolar) in the cells with enlarged nuclei with that in the surrounding fibroblasts possessing normal 2C–4C-sized cell nuclei in one of early presenescence passages (Figure 11). From these counts, it can be seen that initial DDR and simultaneous senescence and self-renewal signalling were found in 84–96% of the cells with enlarged nuclei at far greater frequency (many-fold) than in the cells of the normal cell cycle. It should be stressed that it was practically impossible to find at this stage the cells where the nuclear enlargement and initial expression of DDR, NANOG, and senescence landmarks were dissociated. As such, also this approach confirmed that the expression of key markers of both senescence and pluripotency become selectively and simultaneously activated in tetraploid cells.

3.5. Through Intermediate Stage, NANOG Is Gradually Lost from Most Tetraploid Cell Nuclei, Correlating with an Accumulation of Senescence Markers during the Time Course of Senescence. Development of the tetraploid cells in subsequent passages of the culture as it progresses towards terminal senescence is characterised by the shaping of clear SAHFs, further increase of p16 in the enlarging cytoplasm, while smaller was this increase in the nuclei, and much stronger positivity of nuclear p21. p21 begins to extend from the perinucleolar region into the nucleoplasm (Figure 9(c)). Like p21, γ-H2AX also forms an elaborate network mostly in polyploid cells (Figure 9(f)). In these cells, NANOG can still be found, albeit in a more disseminated form, sometimes colocalised with regions of the p21 (Figure 9(c)) and γ-H2AX network (Figure 9(f)).

Figure 9(f) shows some intermediate state, when the both markers are still expressed. However, in mid-presenescence passages, γ-H2AX vanishes from the cells with the stronger expression of NANOG, and contrary to that, 2-3% of cells

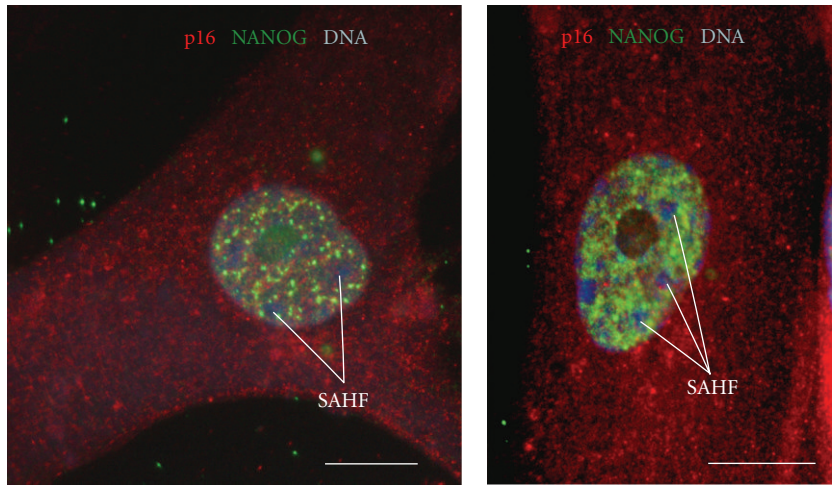

(a) (b)

Figure 10: Relatively rare flattening giant fibroblasts displaying at presenescence a considerable accumulation of NANOG filling the whole nucleus in parallel to clear DAPI-positive SAHFs; in addition, the cells contain p16-positive material in the cytoplasm. Images were obtained using BRG three-colour optical filters system. Scale bars = 10 μm.

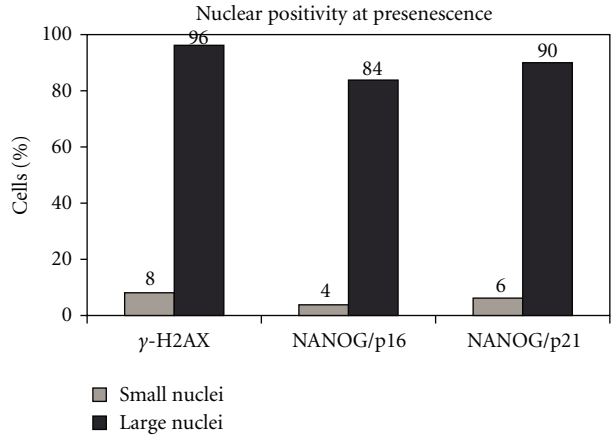

Figure 11: Proportions of the fibroblasts with enlarged (hypertetraploidy) nuclei and with conventional small nuclei in the early presenescence stage, estimated in one of the samples by the labelling frequency for γ-H2AX (n = 400 cells), NANOG/p16 positive (n = 300 cells), and NANOG/p21-positive nuclear granules (n = 300 cells). All nuclear labels were mostly present in this phase in the perinucleolar region. Evaluation reveals a many-fold prevailing signalling for DDR, self-renewal, and senescence regulators occurring simultaneously in the enlarged hypertetraploidy cells, which left normal cell cycle.

which develop very clear thick γ-H2AX foci do not contain NANOG (not shown). The cells with large nuclei and stronger expression of NANOG are more notable in the "midpassages" of the presenescence (2–5%), a few may accumulate it in their nuclei in the considerable amounts (Figure 10). However, the main tendency towards further senescing, contrary to the early phase of presenescence, when the initial expression of self-renewal and senescence markers appears positively linked, at more extended passages *the expression of NANOG in the giant nuclei generally decreases proportionally to the accumulation of cytoplasmic p16 and of the enhanced nuclear expression of p21*, as illustrated on Figure 12.

In the very last passages, approaching terminal senescence with the mitotic index tending to zero (<0.1%), this trend is further extended as illustrated in Figures 1(b), 1(c), 1(e), and 1(f), where the giant polyploid cells with large cytoplasm display considerable accumulation of p21 and p16. They are void of the NANOG expression or contain it at the background level. However, rare exceptions of the NANOG-positive cells with the only background expression of senescence factors were encountered (Figures 12(d)–12(e), arrowed). Further, the senescent cells appear to enter the terminal degeneration phase. Figures 1(c) and 1(f) show the appearance of cells at the terminal degeneration phase of the senescent culture, sampled from one typical experiment. These cells are characterised by the accumulation of p16 and p21 in the cell nuclei, absence of NANOG, lysis of the cytoplasm (Figures 1(c) and 1(f)), and by swelling of the nuclei as testified by DNA image cytometry presented in Figure 6(b).

4. Discussion

Here, we have documented the cellular behaviour of IMR90 cells as they undergo senescence after protracted *in vitro* culture. A notable observation in this process is the appearance of tetraploid cells. Clearly, tetraploid cells appearing in senescing cultures represent a deviation from normal cell cycle regulation. Such cells and their aberrant proliferative activities were reported from the very early studies of *in vitro* senescing cultures of normal fibroblasts occurring before terminal arrest of proliferation [6–8], and confirmed more recently [10]. Our results are entirely in accord with them.

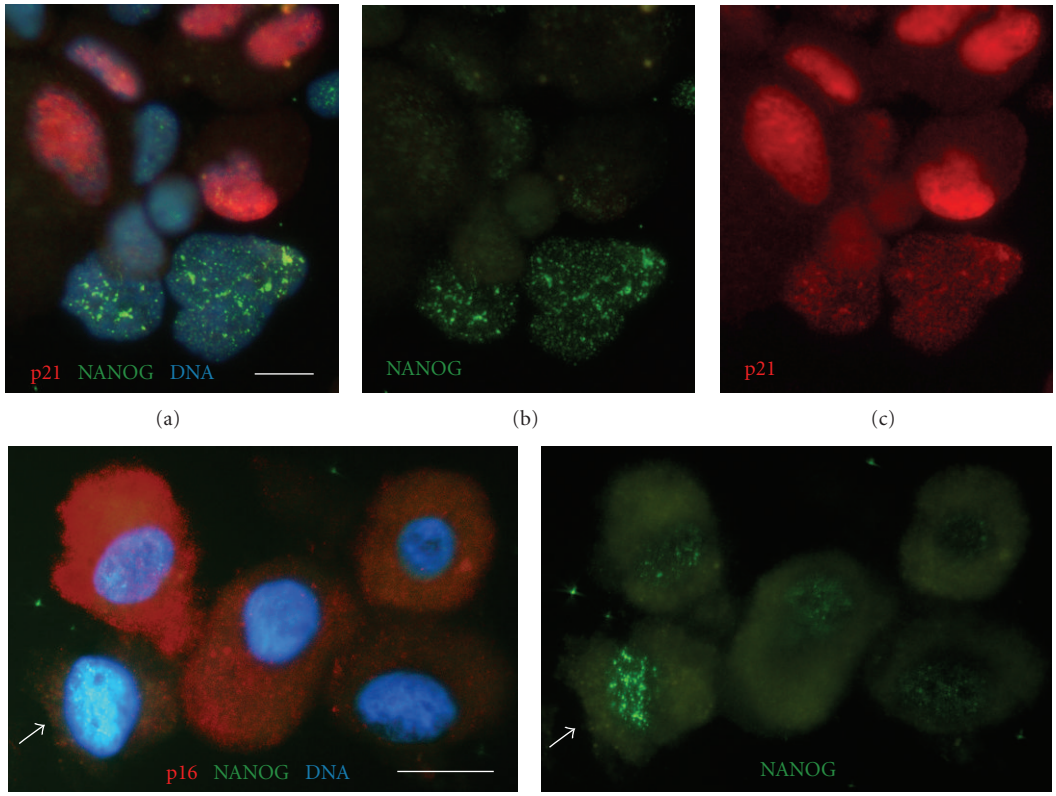

Figure 12: The antagonism between expression of NANOG and senescence regulators at the late presenescence and senescence phases: ((a)–(c)) late presenescence (MI = 0.1%): in the group of ten cells it is seen that nuclear staining of NANOG is found only in the cells with enlarged nuclei, where NANOG staining intensity is inverse to the staining for p21; ((d), (e)) senescence (MI = 0)—a rare NANOG-positive cell was encountered (arrowed), which has the weakest staining for p16 in its cytoplasm among five cells of the group. ((a), (d)) were imaged through the BRG filter; ((b), (e))—through blue, and (c)—through green filter. Scale bars = 10 μm.

These deviations, indicative of chromosomal instability during presenescence, were shown to be related to telomeric dysfunction [13–15, 40].

It is difficult to judge to what extent the induction of polyploidy is associated with the stress due to *in vitro* cultivation. Previously, more stressful conditions of passage were shown to have a slight increase in polyploidy induction, although the same results could have been obtained, if more laboriously, from unstressed cells [10]. On the whole, our present data and that generated previously show that in the senescing culture, there is a tendency for a small proportion of normal human fibroblasts to increasingly form tetraploid cells, to cycle to octoploidy, and then divide. Cycling tetraploidy is generally considered as a dangerous step towards carcinogenesis as it brings CIN and can result in aneuploidy [30, 32]. It is known that functional p53/p21CIP1 should prevent tetraploidy at the 4n-G1/S checkpoint [41, 42], the existence of which was also disputed [16]. Our DNA cytometric data showed that at presenescence, this barrier is leaky and is linked to accumulation of 4C cells during the senescence process as the cells approach full growth arrest. The same increase in the 4C cell fraction in senescing IMR90 cells, then interpreted as arrest at the 4n-G1 checkpoint, was previously reported by Sherwood and colleagues [43] following analysis by DNA flow cytometry and karyotyping and the same was found in an accelerated senescence model of Ras-oncogene transfected IMR90 cells [44].

In addition, we found here that illegitimate cycling of tetraploid cells at the early presenescence phase was associated with activation of the self-renewal response manifested by expression of the embryonal transcription factor NANOG. In our preliminary studies, we have also observed that the OCT4B splicing form (POU5F1_B) was activated; however, as its function is unknown, we concentrated here mostly on studies of NANOG expression.

The homeodomain gene, NANOG, is a key intrinsic determinant of self-renewal and pluripotency in embryonic stem cells. Beside its transactivation function, NANOG was also reported to directly propagate the G1-S transition by ativating cdk6 [45]. As the senescence regulator, p16 prevents endogenous Cdk6 and Cdk4 from associating with its catalytic unit cyclin D1 [46], NANOG should counteract this activity of p16. Moreover, normal embryonal stem cells in response to damage were shown to upregulate self-renewal transcription factors (Oct4 and Nanog) readily undergoing mitotic slippage and reversible tetraploidy [47]. Therefore, it remains possible that NANOG expression may force

the normal fibroblasts (or their stem cells) in stressed senescing cultures to bypass this tetraploidy limiting control.

Our IF observations showed directly that NANOG is expressed in tetraploid cells of pre-senescing cultures unless the cells accumulate considerable amounts of senescence regulators (which occurs increasing as the cultures approach terminal senescence); in particular, clear antagonism was found at late passages between NANOG and accumulation of nuclear p21. These observations are entirely in line with the suggestion that p16 represents a second barrier to senescence, which in the absence of the main barrier p53/p21 may be reversible [48]. Our observations on more accumulation of NANOG in some tetraploid cells, which lose the DDR signalling in the intermediate presenescence stage, may be cautiously interpreted as tendency to revert senescence. It follows that at the presenescence phase, the amount of the p53/p21 growth inhibitor appears insufficient to downregulate NANOG, which may to some extent neutralise p16 and that, therefore, more time (or activation of more p53 activators including for example, the p38 pathway [16, 49]) is needed for p53 to become an efficient enforcer of senescence barrier. This explanation of our observations is in line with the data that activated p53 suppresses the *NANOG* gene promoter [50].

Recently, Davoli and colleagues [40] showed that simultaneous elimination of telomerase and p53 causes chronic DDR resulting in the prolonged G2 arrest and tetraploidisation through licensing DNA rereplication origins. This data also well fit our observations as senescing is associated with telomere dysfunction (however, induction of self-renewal may counteract it by activating telomerase; this aspect needs further research), while found delay of p21 accumulation means relatively retarded activation of p53.

Although IMR90 are normal, nonmalignant cells containing wild-type p53, our observations importantly show for the first time that these normal cells can temporarily activate the self-renewal factor NANOG and enter "a window" when senescence regulators are as yet insufficiently active to irreversibly neutralise its activities. In line with this suggestion, upregulation of several embryonal pluripotency and self-renewal factors have also been reported by Riekstina and coauthors [51] in putative stem cells obtained from explanted adult human mesenchymal tissues during their first adaptive passages of *in vitro* cultivation. The step into tetraploidy is associated with DDR and genome instability, known to greatly increase the probability of chromosomal and genetic mutations and escape of revertants [30]. The same concern was formulated by Romanov et al. [19] and Walen [17], who showed that in presenescence the tetraploid cells display depolyploidisation activities and can ultimately escape senescence with a mutated genotype.

Although the IMR90 model is one of replicative or accelerated senescence *in vitro*, it has clear relevance to pathologic conditions *in vivo* where adult stem cells may be involved such as chronic inflammation and/or trauma.

However, a puzzle remains for the seemingly simultaneous initial induction of the opposing responses of DDR, self-renewal, and senescence in the early pre-senescent tetraploid cells. The site of convergence may be the RAS-RAF-MEK-ERK pathway priming both the mitogenic and accelerated senescence pathways [52]. It was shown that moderate activation of the wild-type *Ras* is mitogenic, while overexpression causes p38-MAPK-dependent senescence [49]. This trigger leads, in particular, to positive versus negative regulation of Cyclin D1 [53], the catalytic unit of cdk6 activated by Nanog [45]. In the negative loop, suppression of Nanog by MEK-ERK was shown through chemical inhibition of MEK [54]. Clearly, the impact of the MEK/ERK pathway on NANOG and its role in the signalling of senescence require further attention.

The data, somewhat supportive for our observations, were reported by Banito and colleagues [55] who showed upregulation of cellular senescence by transduction in IMR90 cells of the four pluripotency-inducing oncogenes.

Interestingly, all three kinds of the initial response, self-renewal, DDR and senescence, were found spatially confined to the perinucleolar compartment, and their partial or full colocalisation suggests a cross-talk between these pathways. Moreover, it is likely that the SAHFs which represent regions of epigenetically changed chromatin also start to form from the same region of the perinucleolar chromatin and are associated with the emergence of the DNA double-strand breaks. The question is why these various aspects are appearing in the nucleolus.

The nucleolus is involved in the regulation of senescence in several ways. Nucleostemnin, a nucleolar protein specifically involved in regulating the cell cycle in stem and tumour cells, can sequestrate MDM2 and MDM4 and, thus, favour accumulation of p53, the main player in senescence induction [56, 57]. Similarly nucleolar Arf will activate p53 in the senescence response [58]. In addition, relocation of hTERT to the nucleolus is associated with initiation of senescence [59]. Finally, PML binds MDM2 and sequesters it into the nucleolus [60], thus protecting p53 from proteosome-mediated degradation.

However, the most important aspect may be that, in eukaryotic systems, rDNA contains fragile sites that are extremely sensitive to replication-induced stress [61, 62]. This replication stress may be related to the p53 independent license of rereplication origins fired at prolonged G2 arrest [40]. The level of the DNA Polymerase I in IMR90 tetraploid cells may be insufficient at this time-point, causing stalling of replication forks and converting the underreplicated sites into rDNA strandbreaks [63]. This idea is compatible with cancer development from its earliest stages being associated with DNA replication stress, leading to DNA strandbreaks and subsequently to DDR [3, 64, 65].

In relation to p53-function-deficient tumours, our data [28, 29] also show that endopolyploid cells induced after genomic insult undertake sustainable activation of the pluripotency and self-renewal genes, and undergo a stage of competition between self-renewal and senescence with an improved chance for self-renewal to succeed. A proportion of these p53-mutated polyploid cells is capable of accumulating considerable amounts of self-renewal factors and subsequently depolyploidise into mitotic paradiploid descendants.

5. Conclusion

Our findings on senescing normal human IMR90 fibroblasts clearly provide us with insight into the risks of cancer development. Since it is assumed that a cancer clone develops from a single adult stem cell which receives a mutation(s), including those compromising the senescence barrier, our observations suggest that this may be favoured in the normal stressed tissue due to the unique cellular and molecular setting of the presenescence stage. It is hypothesised that telomere dysfunction causing DDR and temporary activation of self-renewal on a background of insufficient activity of senescence inducers may allow putative adult stem cells to overcome the G1 tetraploidy limit controlled by p53 leading to their replicative stress and aberrant divisions. This would favour acquisition of CIN, aneuploidy, and tumorigenic mutations, thereby driving tumorigenesis.

Conflict of Interests

The authors declare no conflict of interests.

Authors Contribution

A. Huna performed DNA image cytometry, participated in design and analysis of experiments and editing of the manuscript; K. Salmina performed immunofluorescence stainings, participated in design and analysis of experiments and editing of the MS; E. Jascenko carried out cell cultures, participated in design and analysis of experiments; G. Duburs participated in design and analysis of experiments; I. Inashkina performed RT-PCR with sequence analysis of NANOG expression, participated in design and analysis of experiments and editing of the MS; J. Erenpreisa designed experiments, performed microscopy and analysis of results and prepared the draft and editing of the manuscript, A. Huna and K. Salmina made an equal contribution.

Acknowledgments

The authors are thankful to Dr. Andrey Ivanov (Beatson Institute, Glazgow) for donating IMR90 cells, Dr. Talivaldis Freivalds for DAPI measurements, Professor Denys Wheatley for reading, to Professor Mark S Cragg and Dr. Karina Silina for English editing of the manuscript, and Pawel Zajakin for help in formatting the pictures. This study was supported by the ESF Grant no. 2009/0204/1DP/1.1.1.2.0/09/APIA/VIA/150, and by the European Social Fund within the project "Support for Doctoral Studies at University of Latvia".

References

[1] J. W. Shay and I. B. Roninson, "Hallmarks of senescence in carcinogenesis and cancer therapy," *Oncogene*, vol. 23, no. 16, pp. 2919–2933, 2004.

[2] F. D'Adda Di Fagagna, "Living on a break: cellular senescence as a DNA-damage response," *Nature Reviews Cancer*, vol. 8, no. 7, pp. 512–522, 2008.

[3] D. W. Meek, "Tumour suppression by p53: a role for the DNA damage response?" *Nature Reviews Cancer*, vol. 9, no. 10, pp. 714–723, 2009.

[4] T. Finkel, M. Serrano, and M. A. Blasco, "The common biology of cancer and ageing," *Nature*, vol. 448, no. 7155, pp. 767–774, 2007.

[5] M. Collado and M. Serrano, "Senescence in tumours: evidence from mice and humans," *Nature Reviews Cancer*, vol. 10, no. 1, pp. 51–57, 2010.

[6] L. Hayflick and P. S. Moorhead, "The serial cultivation of human diploid cell strains," *Experimental Cell Research*, vol. 25, no. 3, pp. 585–621, 1961.

[7] E. Saksela and P. S. Moorhead, "Aneuploidy in the degenerative phase of serial cultivation of human cell strains," *Proceedings of the National Academy of Sciences of the United States of America*, vol. 50, pp. 390–395, 1963.

[8] B. A. Houghton and G. H. Stidworthy, "A growth history comparison of the human diploid cells WI-38 and IMR-90: proliferative capacity and cell sizing analysis," *In Vitro*, vol. 15, no. 9, pp. 697–702, 1979.

[9] K. H. Walen, "Budded karyoplasts from multinucleated fibroblast cells contain centrosomes and change their morphology to mitotic cells," *Cell Biology International*, vol. 29, no. 12, pp. 1057–1065, 2005.

[10] K. H. Walen, "Human diploid fibroblast cells in senescence; cycling through polyploidy to mitotic cells," *In Vitro Cellular and Developmental Biology*, vol. 42, no. 7, pp. 216–224, 2006.

[11] K. H. Walen, "Origin of diplochromosomal polyploidy in near-senescent fibroblast cultures: heterochromatin, telomeres and chromosomal instability (CIN)," *Cell Biology International*, vol. 31, no. 12, pp. 1447–1455, 2007.

[12] K. H. Walen, "Bipolar genome reductional division of human near-senescent, polyploid fibroblast cells," *Cancer Genetics and Cytogenetics*, vol. 173, no. 1, pp. 43–50, 2007.

[13] C. B. Harley, "Telomere loss: mitotic clock or genetic time bomb?" *Mutation Research*, vol. 256, no. 2-6, pp. 271–282, 1991.

[14] J. R. Smith and O. M. Pereira-Smith, "Replicative senescence: implications for in vivo aging and tumor suppression," *Science*, vol. 273, no. 5271, pp. 63–67, 1996.

[15] R. A. DePinho, "The age of cancer," *Nature*, vol. 408, no. 6809, pp. 248–254, 2000.

[16] N. J. Ganem and D. Pellman, "Limiting the proliferation of polyploid cells," *Cell*, vol. 131, no. 3, pp. 437–440, 2007.

[17] K. H. Walen, "Genetic stability of senescence reverted cells: genome reduction division of polyploidy cells, aneuploidy and neoplasia," *Cell Cycle*, vol. 7, no. 11, pp. 1623–1629, 2008.

[18] E. M. Torres, N. Dephoure, A. Panneerselvam et al., "Identification of aneuploidy-tolerating mutations," *Cell*, vol. 143, no. 1, pp. 71–83, 2010.

[19] S. R. Romanov, B. K. Kozakiewicz, C. R. Holst, M. R. Stampfer, L. M. Haupt, and T. D. Tlsty, "Normal human mammary epithelial cells spontaneously escape senescence and acquire genomic changes," *Nature*, vol. 409, no. 6820, pp. 633–637, 2001.

[20] M. L. Friedlander, D. W. Hedley, and I. W. Taylor, "Clinical and biological significance of aneuploidy in human tumours," *Journal of Clinical Pathology*, vol. 37, no. 9, pp. 961–974, 1984.

[21] T. M. Illidge, M. S. Cragg, B. Fringes, P. Olive, and J. A. Erenpreisa, "Polyploid giant cells provide a survival mechanism for p53 mutant cells after DNA damage," *Cell Biology International*, vol. 24, no. 9, pp. 621–633, 2000.

[22] M. Sundaram, D. L. Guernsey, M. M. Rajaraman, and R. Rajaraman, "Neosis: a novel type of cell division in cancer," *Cancer Biology and Therapy*, vol. 3, no. 2, pp. 207–218, 2004.

[23] P. E. Puig, M. N. Guilly, A. Bouchot et al., "Tumor cells can escape DNA-damaging cisplatin through DNA endoreduplication and reversible polyploidy," *Cell Biology International*, vol. 32, no. 9, pp. 1031–1043, 2008.

[24] I. Vitale, L. Senovilla, M. Jema et al., "Multipolar mitosis of tetraploid cells: inhibition by p53 and dependency on Mos," *EMBO Journal*, vol. 29, no. 7, pp. 1272–1284, 2010.

[25] I. B. Roninson, "Tumor cell senescence in cancer treatment," *Cancer Research*, vol. 63, no. 11, pp. 2705–2715, 2003.

[26] J. Erenpreisa, M. S. Cragg, K. Salmina, M. Hausmann, and H. Scherthan, "The role of meiotic cohesin REC8 in chromosome segregation in γ irradiation-induced endopolyploid tumour cells," *Experimental Cell Research*, vol. 315, no. 15, pp. 2593–2603, 2009.

[27] F. Ianzini, E. A. Kosmacek, E. S. Nelson et al., "Activation of meiosis-specific genes is associated with depolyploidization of human tumor cells following radiation-induced mitotic catastrophe," *Cancer Research*, vol. 69, no. 6, pp. 2296–2304, 2009.

[28] K. Salmina, E. Jankevics, A. Huna et al., "Up-regulation of the embryonic self-renewal network through reversible polyploidy in irradiated p53-mutant tumour cells," *Experimental Cell Research*, vol. 316, no. 13, pp. 2099–2112, 2010.

[29] J. Erenpreisa, K. Salmina, A. Huna et al., "Polyploid tumour cells elicit para-diploid progeny through de-polyploidisation divisions and regulated autophagy," *Cell Biology International*, 2011.

[30] Z. Storchova and D. Pellman, "From polyploidy to aneuploidy, genome instability and cancer," *Nature Reviews Molecular Cell Biology*, vol. 5, no. 1, pp. 45–54, 2004.

[31] G. Mosieniak and E. Sikora, "Polyploidy: the link between senescence and cancer," *Current Pharmaceutical Design*, vol. 16, no. 6, pp. 734–740, 2010.

[32] M. Castedo, I. Vitale, and G. Kroemer, "A novel source of tetraploid cancer cell precursors: telomere insufficiency links aging to oncogenesis," *Oncogene*, vol. 29, no. 44, pp. 5869–5872, 2010.

[33] A. Carnero, "Targeting the cell cycle for cancer therapy," *British Journal of Cancer*, vol. 87, no. 2, pp. 129–133, 2002.

[34] M. Vergel, J. J. Marin, P. Estevez, and A. Carnero, "Cellular senescence as a target in cancer control," *Journal of Aging Research*, vol. 2011, Article ID 725365, 12 pages, 2011.

[35] J. Erenpreisa and T. Freivalds, "Anisotropic staining of apurinic acid with toluidine blue," *Histochemistry*, vol. 60, no. 3, pp. 321–325, 1979.

[36] Q. Chen, A. Fischer, J. D. Reagan, L. J. Yan, and B. N. Ames, "Oxidative DNA damage and senescence of human diploid fibroblast cells," *Proceedings of the National Academy of Sciences of the United States of America*, vol. 92, no. 10, pp. 4337–4341, 1995.

[37] E. Therman and M. Susman, *Human Chromosomes: Structure, Behaviour, and Effects*, Springer, New York, NY, USA, 1973.

[38] C. J. Epstein, "Cell size, nuclear content and the development of polyploidy in the mammalian liver," *Proceedings of the National Academy of Sciences of the United States of America*, vol. 57, pp. 327–334, 1967.

[39] J. Erenpreisa, A. Ivanov, S. P. Wheatley et al., "Endopolyploidy in irradiated p53-deficient tumour cell lines: persistence of cell division activity in giant cells expressing Aurora-B kinase," *Cell Biology International*, vol. 32, no. 9, pp. 1044–1056, 2008.

[40] T. Davoli, E. L. Denchi, and T. de Lange, "Persistent telomere damage induces bypass of mitosis and tetraploidy," *Cell*, vol. 141, no. 1, pp. 81–93, 2010.

[41] P. R. Andreassen, F. B. Lacroix, O. D. Lohez, and R. L. Margolis, "Neither p21 nor 14-3-3σ prevents G progression to mitotic catastrophe in human colon carcinoma cells after DNA damage, but p21 induces stable G arrest in resulting tetraploid cells," *Cancer Research*, vol. 61, no. 20, pp. 7660–7668, 2001.

[42] R. L. Margolis, "Tetraploidy and tumor development," *Cancer Cell*, vol. 8, no. 5, pp. 353–354, 2005.

[43] S. W. Sherwood, D. Rush, J. L. Ellsworth, and R. T. Schimke, "Defining cellular senescence in IMR-90 cells: a flow cytometric analysis," *Proceedings of the National Academy of Sciences of the United States of America*, vol. 85, no. 23, pp. 9086–9090, 1988.

[44] D. X. Mason, T. J. Jackson, and A. W. Lin, "Molecular signature of oncogenic ras-induced senescence," *Oncogene*, vol. 23, no. 57, pp. 9238–9246, 2004.

[45] X. Zhang, I. Neganova, S. Przyborski et al., "A role for NANOG in G1 to S transition in human embryonic stem cells through direct binding of CDK6 and CDC25A," *Journal of Cell Biology*, vol. 184, no. 1, pp. 67–82, 2009.

[46] R. Fåhraeus, S. Laín, K. L. Ball, and D. P. Lane, "Characterization of the cyclin-dependent kinase inhibitory domain of the INK4 family as a model for a synthetic tumour suppressor molecule," *Oncogene*, vol. 16, no. 5, pp. 587–596, 1998.

[47] C. Mantel, Y. Guo, R. L. Man et al., "Checkpoint-apoptosis uncoupling in human and mouse embryonic stem cells: a source of karyotpic instability," *Blood*, vol. 109, no. 10, pp. 4518–4527, 2007.

[48] C. M. Beauséjour, A. Krtolica, F. Galimi et al., "Reversal of human cellular senescence: roles of the p53 and p16 pathways," *EMBO Journal*, vol. 22, no. 16, pp. 4212–4222, 2003.

[49] Q. Deng, R. Liao, B. L. Wu, and P. Sun, "High intensity *ras* signaling induces premature senescence by activating p38 pathway in primary human fibroblasts," *Journal of Biological Chemistry*, vol. 279, no. 2, pp. 1050–1059, 2004.

[50] T. Lin, C. Chao, S. Saito et al., "p53 induces differentiation of mouse embryonic stem cells by suppressing Nanog expression," *Nature Cell Biology*, vol. 7, no. 2, pp. 165–171, 2005.

[51] U. Riekstina, I. Cakstina, V. Parfejevs et al., "Embryonic stem cell marker expression pattern in human mesenchymal stem cells derived from bone marrow, adipose tissue, heart and dermis," *Stem Cell Reviews and Reports*, vol. 5, no. 4, pp. 378–386, 2010.

[52] A. W. Lin, M. Barradas, J. C. Stone, L. Van Aelst, M. Serrano, and S. W. Lowe, "Premature senescence involving p53 and p16 is activated in response to constitutive MEK/MAPK mitogenic signaling," *Genes and Development*, vol. 12, no. 19, pp. 3008–3019, 1998.

[53] J. N. Lavoie, G. L'Allemain, A. Brunei, R. Müller, and J. Pouysségur, "Cyclin D1 expression is regulated positively by the p42/p44(MAPK) and negatively by the p38/HOG(MAPK) pathway," *Journal of Biological Chemistry*, vol. 271, no. 34, pp. 20608–20616, 1996.

[54] T. Hamazaki, S. M. Kehoe, T. Nakano, and N. Terada, "The Grb2/Mek pathway represses nanog in murine embryonic stem cells," *Molecular and Cellular Biology*, vol. 26, no. 20, pp. 7539–7549, 2006.

[55] A. Banito, S. T. Rashid, J. C. Acosta et al., "Senescence impairs successful reprogramming to pluripotent stem cells," *Genes and Development*, vol. 23, no. 18, pp. 2134–2139, 2009.

[56] R. Y. L. Tsai and R. D. G. McKay, "A nucleolar mechanism controlling cell proliferation in stem cells and cancer cells," *Genes and Development*, vol. 16, no. 23, pp. 2991–3003, 2002.

[57] H. Ma and T. Pederson, "Nucleophosmin is a binding partner of nucleostemin in human osteosarcoma cells," *Molecular Biology of the Cell*, vol. 19, no. 7, pp. 2870–2875, 2008.

[58] J. D. Weber, L. J. Taylor, M. F. Roussel, C. J. Sherr, and D. Bar-Sagi, "Nucleolar Arf sequesters Mdm2 and activates p53," *Nature Cell Biology*, vol. 1, no. 1, pp. 20–26, 1999.

[59] J. Huang, J. Lin, R. Jin et al., "Relocation of hTERT from nucleoplasm to nucleoli induces cancer cells senescence without affecting telomerase activity," *AACR Meeting Abstracts*, 2005, abstracts 1022.

[60] R. Bernardi, P. P. Scaglioni, S. Bergmann, H. F. Horn, K. H. Vousden, and P. P. Pandolfi, "PML regulates p53 stability by sequestering Mdm2 to the nucleolus," *Nature Cell Biology*, vol. 6, no. 7, pp. 665–672, 2004.

[61] T. W. Glover, C. Berger, J. Coyle, and B. Echo, "DNA polymerase α inhibition by aphidicolin induces gaps and breaks at common fragile sites in human chromosomes," *Human Genetics*, vol. 67, no. 2, pp. 136–142, 1984.

[62] J. Z. Torres, J. B. Bessler, and V. A. Zakian, "Local chromatin structure at the ribosomal DNA causes replication fork pausing and genome instability in the absence of the *S. cerevisiae* DNA helicase Rrm3p," *Genes and Development*, vol. 18, no. 5, pp. 498–503, 2004.

[63] A. M. Casper, P. A. Mieczkowski, M. Gawel, and T. D. Petes, "Low levels of DNA polymerase alpha induce mitotic and meiotic instability in the ribosomal DNA gene cluster of Saccharomyces cerevisiae," *PLoS Genetics*, vol. 4, no. 6, article e1000105, 2008.

[64] V. G. Gorgoulis, L. V. F. Vassiliou, P. Karakaidos et al., "Activation of the DNA damage checkpoint and genomic instability in human precancerous lesions," *Nature*, vol. 434, no. 7035, pp. 907–913, 2005.

[65] J. Bartkova, Z. Hořejší, K. Koed et al., "DNA damage response as a candidate anti-cancer barrier in early human tumorigenesis," *Nature*, vol. 434, no. 7035, pp. 864–870, 2005.

3.2. Self renewal and accelerated senescence crostalk in cancer cells after treatment – Original paper II

Cell Cycle 12:3, 430–441; February 1, 2013; © 2013 Landes Bioscience

DNA damage causes TP53-dependent coupling of self-renewal and senescence pathways in embryonal carcinoma cells

Thomas R. Jackson,[1] Kristine Salmina,[2] Anda Huna,[2] Inna Inashkina,[2] Eriks Jankevics,[2] Una Riekstina,[3] Zane Kalnina,[2] Andrey Ivanov,[4] Paul A. Townsend,[1,†] Mark S. Cragg[1,†,*] and Jekaterina Erenpreisa[2,†,*]

[1]Cancer Sciences Unit; Southampton University Faculty of Medicine; General Hospital; Southampton, UK; [2]Latvian Biomedical Research and Study Centre; Riga, Latvia; [3]The University of Latvia; Riga, Latvia; [4]Beatson Institute for Cancer Research; Glasgow, UK

[†]These senior authors contributed equally to this work.

Keywords: TP53, OCT4A/POU5F1, self-renewal, tumor cells, DNA damage, pluripotency, senescence

Abbreviations: EC, embryonal carcinoma; ES, embryonic stem; ETO, etoposide; IF, immunofluorescent; iPS, induced pluripotent stem; LC3, microtubule-associated protein 1 light chain 3; MI, mitotic index; NT, non-treated; ntg, non-target; pCHK2, phosphorylated CHK2; PI, propidium iodide; siRNA, small interfering RNA; shRNA, small hairpin RNA; Sa-β-gal, senescence-associated beta-galactosidase

Recent studies have highlighted an apparently paradoxical link between self-renewal and senescence triggered by DNA damage in certain cell types. In addition, the finding that TP53 can suppress senescence has caused a re-evaluation of its functional role in regulating these outcomes. To investigate these phenomena and their relationship to pluripotency and senescence, we examined the response of the TP53-competent embryonal carcinoma (EC) cell line PA-1 to etoposide-induced DNA damage. Nuclear POU5F1/OCT4A and P21CIP1 were upregulated in the same cells following etoposide-induced G_2M arrest. However, while accumulating in the karyosol, the amount of OCT4A was reduced in the chromatin fraction. Phosphorylated CHK2 and RAD51/γH2AX-positive nuclear foci, overexpression of AURORA B kinase and moderate macroautophagy were evident. Upon release from G_2M arrest, cells with repaired DNA entered mitoses, while the cells with persisting DNA damage remained at this checkpoint or underwent mitotic slippage and gradually senesced. Reduction of TP53 using sh- or si-RNA prevented the upregulation of OCT4A and P21CIP1 and increased DNA damage. Subsequently, mitoses, micronucleation and senescence were all enhanced after TP53 reduction with senescence confirmed by upregulation of CDKN2A/P16INK4A and increased sa-β-galactosidase positivity. Those mitoses enhanced by TP53 silencing were shown to be multicentrosomal and multi-polar, containing fragmented and highly deranged chromosomes, indicating a loss of genome integrity. Together, these data suggest that TP53-dependent coupling of self-renewal and senescence pathways through the DNA damage checkpoint provides a mechanism for how embryonal stem cell-like EC cells safeguard DNA integrity, genome stability and ultimately the fidelity of self-renewal.

Introduction

Aggressive somatic tumors possess a gene expression profile similar to embryonic stem (ES) cells, suggesting that key signaling pathways and biological links exist between them.[1] Importantly, both appear to display characteristics of self-renewal and differentiation potential, with current data implying that these properties underlie the resistance of cancer to genotoxic treatment modalities and help explain disease relapse.[2,3] The characteristic self-renewal, extensive proliferation and differentiation potential of ES cells is also evident in cancer stem cells, which are highly proliferative and phenotypically plastic.[4] The ability of cancer cells to utilize equivalent stem cell transcription networks is of great interest for the subsequent understanding and treatment of cancer.

Recent data shows that even normal somatic cells can be reprogrammed to become induced pluripotent stem (iPS) cells, and that upregulation of only a very small set of genes is sufficient to initiate de-differentiation to provide them with stem-like properties. OCT4A (POU5F1), SOX2 and NANOG are master transcription factors responsible for the maintenance and tight coordination of pluripotency and self-renewal in ES cells.[5] The first human iPS cells were created from somatic fibroblasts ectopically expressing two of these factors (OCT4A and SOX2) along with KLF4 and c-MYC.[6] Since then, expression of OCT4A and SOX2 alone has been shown to be sufficient to convert human somatic cells to iPS

*Correspondence to: Mark S. Cragg and Jekaterina Erenpreisa; Email: msc@soton.ac.uk and katrina@biomed.lu.lv
Submitted: 10/30/2012; Revised: 12/13/2012; Accepted: 12/14/2012
http://dx.doi.org/10.4161/cc.23285

cells.[7] These results suggest that cancer cells may be able to access ES cell properties through the upregulation of these genes alone. In keeping with this proposition, the prognostic significance of these two markers was recently reported for several kinds of cancer (lung, squamous cell carcinoma, colorectal and breast).[8-10]

We have previously reported the upregulation of OCT4A/SOX2/NANOG in TP53 mutant lymphoma cell lines as a response to DNA damage and highlighted the potential role of this ectopically upregulated embryonic self-renewal program as a survival strategy in TP53-deficient cells following genotoxic damage.[11]

Self-renewal and pluripotency factors have paradoxically also been linked to accelerated cellular senescence (termed senescense hereon). When Banito and colleagues transfected IMR90 human fibroblasts with the Yamanaka transcription factors (OCT4A, SOX2, c-MYC and KLF4), they found senescence was induced rather than pluripotency, which was associated with DNA damage.[12] A study of normal IMR90 fibroblasts showed that at pre-senescence, cells signaling DNA damage in the ≥ 4C compartment simultaneously express cyclin-dependent kinase inhibitors p16inka4a and p21cip1, as well as the self-renewal transcription factor NANOG,[13] further indicating that the properties of pluripotency, self-renewal and senescence are tightly coordinated by DNA damage.

The relationship between mitogenic activation of proliferation and cell senescence is also complex. For example, the concept of hyper-mitogenic arrest intimates that simultaneous stimulation of mitogen-activated pathways (integrated by mTOR) and downstream inhibition of cyclin-dependent kinases promotes senescence.[14] Similarly, DNA damage-induced senescence occurs in immortalized WI38 fibroblasts only when mitogenic growth factors are present.[15] In this context, the role of TP53 in regulating proliferation and senescence is critical, with evidence of its ability to both block and promote senescence. On one hand, TP53 signals to prevent cellular senescence, but conversely it can cause cell cycle arrest, thereby providing the cellular context from which the senescence program can start.[16] These data imply that senescence is not in fact a barrier to cancer but almost a prerequisite for it.[17] This concept and observations showing the complexity of the inter-regulation between these various cellular outcomes may help to understand how self-renewing (cancer) stem cells respond to DNA damage.

Together, these data indicate that intrinsic links exist between self-renewal, senescence and the DNA damage checkpoints of the cell. Further complexity arises from the fact that the regulation of the cell cycle in stem cells is evidently different from that in normal somatic cells and not yet fully understood. Current reports indicate that the cell cycle in stem cells lacks G_0, has a short G_1, absent G_1-S checkpoint[18] and a preferential activation of the G_2M DNA damage checkpoint, which is responsible for the augmented resistance of stem cells to genotoxic damage.[19] Presumably, these differences in cell cycle regulation are associated with the particular biological properties of ES cells, such as self-renewal (immortality).

EC cell lines, which are derived from germ cell tumors, can serve, to a certain extent, as a model of ES cells and express the key cassette of ES cell transcription factors, OCT4A, SOX2 and NANOG.[20,21] At the same time, these tumors are highly malignant and so may be used to closely model the features of aggressive tumors that show ES cell transcription profiles.[1,8-10] Therefore, in this current study, we chose to investigate the relationship between senescence and self-renewal regulation following DNA damage in the ovarian teratocarcinoma PA1 cell-line, which possesses functional TP53. For inducing DNA damage, we used the topoisomerase II inhibitor etoposide (ETO), which was previously used for studies of senescence in tumor and immortalized cells lines,[15,22,23] and which is also in clinical use for the treatment of various cancer types.

Results

Characterization of PA-1 cells. The PA-1 cell line used in this study was established from the metastases of a malignant ovarian teratocarcinoma. It possesses the features of embryonal carcinoma (EC), as testified by its ability to form OCT4A/NANOG-positive spheres in serum-free medium (**Fig. S1**).[24] It has a stable, near-diploid karyotype with a single chromosome translocation [t(15;20)(p11.2;q11.2)][25] and functional (although heterozygotic) TP53.[26] Several sources show that PA1 expresses the key self-renewal genes OCT4A, SOX2 and NANOG.[11,24,27]

Response of PA-1 cells to DNA damage. To determine the response of PA-1 cells to DNA damage, the cells were assessed following ETO treatment over time. Phosphorylated CHK2 (pCHK2) and γH2AX staining were used to report on the presence of DNA damage, and the cell cycle response of surviving cells was monitored using DNA cytometry. In response to ETO treatment, virtually all cells became arrested in G_2 within 2 days and displayed pCHK2 and γH2AX-positive nuclear foci as evidence of DNA damage and subsequently attempted DNA repair as judged by the presence of RAD51/γH2AX foci (**Fig. 1A and B**). The cells remained in G_2 for up to 4 days. Simultaneously, small G_1, 2C and polyploid (> 4C) cell fractions then appeared, increased for a few days before the polyploid fraction was overcome by the mitotic cycling fraction and disappeared by day 7 (**Fig. 1C**). Substantial apoptosis appeared from day 3, reached a maximum on day 5 and disappeared with the recovery of clonogenic growth after day 7 (data not shown and **Fig. 5A**).

In addition, the G_2-arrested cells showed enhanced nuclear staining of Aurora B kinase (**Fig. S2**), indicating the mitotic potential of these cells.

From day 3 onwards, pCHK2 nuclear staining disappeared in some cells, while persisting and even becoming enhanced in others (**Fig. 1A**). To elucidate which cells entered mitosis and which polyploidized, we examined them on day 5 using DAPI-integrated fluorescence to assess their DNA content and size as well as pCHK2 nuclear staining levels. Two distinct cell types were observed: those with small nuclei (G_1, 2C-sized) and those with large (G_2 and polyploid, 4C and > 4C) nuclei. As seen in **Figure 1D**, the majority of large cells (≥ 4C) were pCHK2-positive, and all pCHK2-positive cells were large cells. In contrast, all cells with small nuclei (G_1) were pCHK2-negative. These results indicate that ~30% of cells have repaired DNA and are returning

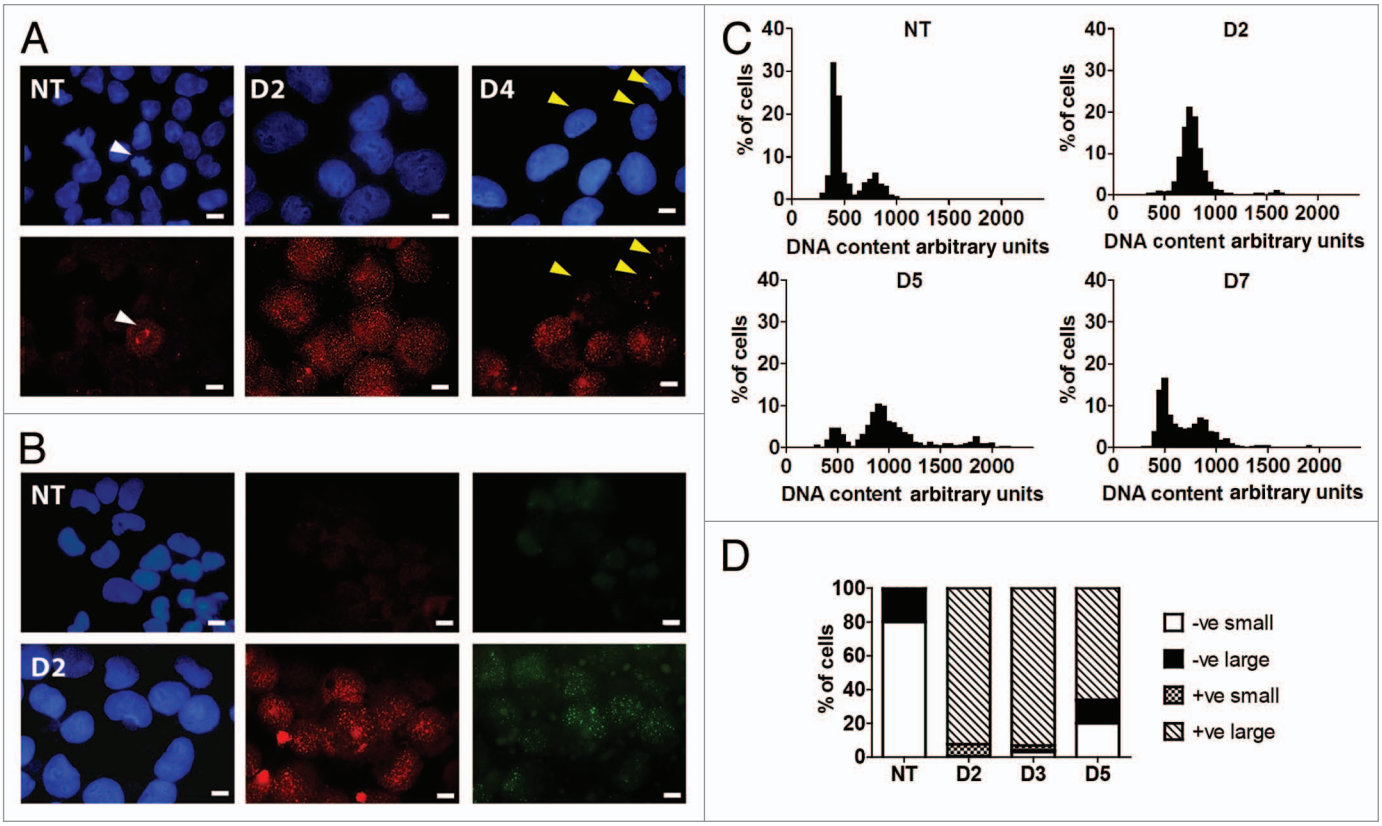

Figure 1. DNA damage response of PA-1 cells to ETO treatment. PA-1 cells were treated with 8 μM ETO for 20 h, then washed and assessed at the indicated time point. Cells were pelleted, cytospun, fixed and stained for (**A**) pCHK2 (red) or (**B**) γH2AX (red) and RAD51 (green) in combination with DAPI (blue). Bar = 10 μM. (**A**) NT PA-1 cells show very faint background pCHK2 staining in non-dividing cells and increased staining of centrosomes in dividing cells (white arrowheads). On day 2 post-ETO, small pCHK2-positive foci accumulate in the nuclei of all cells. By day 4, some small nuclei have lost pCHK2 staining (yellow arrowheads), while large cells remain pCHK2 positive. (**B**) NT PA-1 cells show no positive staining for γH2AX or RAD51. On day 2, the majority of cells show accumulation of γH2AX or RAD51 positive foci in the nuclei. (**C**) Cells were cytospun, fixed and stained for DNA image cytometry. DNA content was determined for at least 200 cells in each condition and represented as a percentage. Profound G_2 arrest on day 2 was observed followed by the simultaneous emergence of a polyploid (> 4C) and G_1 fraction on day 5 before the recovery of the normal cell cycle profile by day 7. (**D**) The proportion of pCHK2-positive cells was examined in the context of DNA content with cells sub-divided into small or large cells. In the NT control sample, all cells were pCHK2-negative with an expected nuclei size distribution (2C 80%; ≥ 4C 20%). On day 2, all cells were pCHK2-positive and the vast majority of nuclei were large (≥ 4C). By day 5, cells with small nuclei appear, all of which are pCHK2-negative. Data are representative of > three independent experiments.

to the mitotic cell cycle, while the remainder display persistent DNA damage and are either maintained in the 4C fraction or become polyploid.

During this period, macroautophagy was observed in response to ETO treatment as seen by LC3B and P62 lysosomal staining being compatible with the enhanced OCT4A staining (**Fig. S3A–D**) and gradually increasing from day 1 to 5. Macroautophagy returned to resting levels in cells as they re-entered mitotic cycling, but remained elevated in cells that persisted in G_2 and in most polyploid cells. TERT staining revealed nuclear foci in NT cells (not shown) and in the small cells re-entering the mitotic cycle following ETO treatment. Most large cells lacked nuclear foci and showed elimination of TERT in perinuclear LC3B-lined vacuoles; however, in parallel, large amounts of TERT also appeared in their cytoplasm (**Fig. S3E and F**), possibly due to the stress-protecting binding of TERT to mitochondria.[28] Most PA-1 cells displayed low NANOG expression, which was more evident around chromosomes in recovering mitotic cells and clones (**Fig. S4A**). In contrast, rare cells expressed high levels of NANOG in both control and ETO-treated conditions (**Fig. S4B**). The NANOG-overexpressing cells observed after ETO treatment were large and presumably polyploid. We hypothesize that they arose by overcoming the G_1–4N checkpoint and avoiding senescence. These cells have the potential to reach 8–16C and then de-polyploidize. Such a response is typical of mutant TP53 lymphoma cells after DNA damage,[11,29] but is a rare event with PA-1.

Upregulation of OCT4A and P21CIP1 in response to DNA damage. We next assessed key molecular regulators of the DNA damage response by immunofluorescence (IF). As expected, TP53 and, subsequently, P21CIP1 (CDKN1A), were upregulated in response to ETO treatment. However, the pluripotency self-renewal transcription factor OCT4A was also upregulated (**Fig. 2A–C**). In fact, paradoxically, OCT4A and P21CIP1 were shown by IF to be both expressed in the same cells (**Fig. 2B and C**). Expression of high levels of both proteins

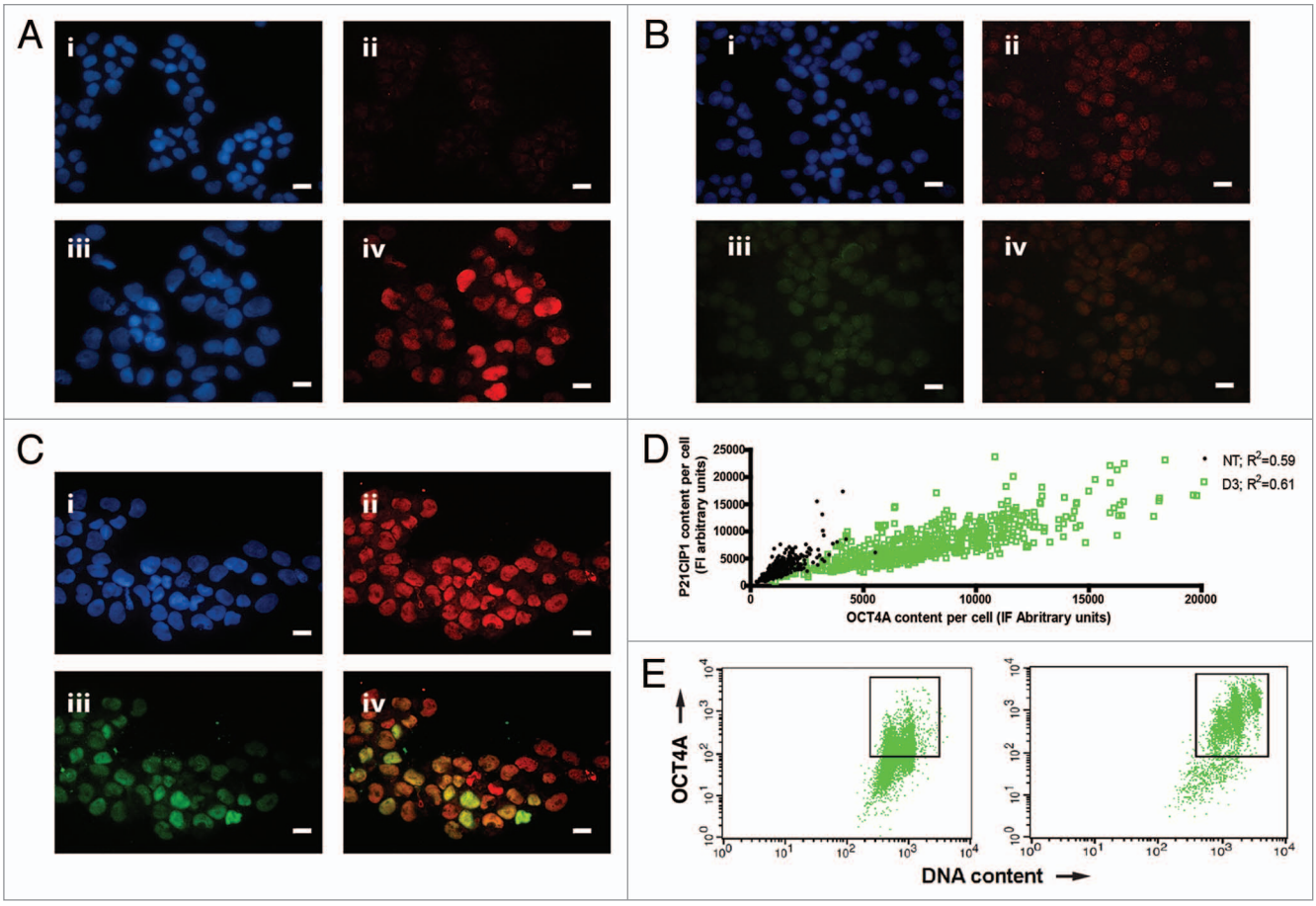

Figure 2. Regulation of TP53, P21CIP1 and OCT4A in PA-1 cells after ETO treatment. PA-1 cells were treated with 8 μM ETO for 20 h, then washed and assessed at the indicated time point. Cells were pelleted, cytospun, fixed and stained for (**A**) TP53 (red) (**B**) P21CIP1 (red) or (**C**) P21CIP1 (red) and OCT4A (green) in combination with DAPI (blue); Bar = 10 μM. Results representative of nine separate experiments. (**A**) NT cells showed very faint background staining for TP53. On day 3 post-ETO treatment, TP53 accumulated in the majority of nuclei. (**B and C**) NT cells had faint background staining for P21CIP1 and weak staining of OCT4A. On day 3 post-ETO treatment, P21CIP1 and OCT4A accumulated in the majority of cell nuclei. (**D**) Using image analysis on fixed cytospins, the fluorescence intensity of P21CIP1 and OCT4A during the first 3 d post-ETO treatment was determined and plotted for 500 cells in four independent experiments. There was substantial increase and a clear positive correlation between the fluorescent intensity of staining for OCT4A and P21CIP1 after ETO treatment. At the same time, the amplitude of the expression of both factors greatly increased: Non-treated OCT4A expression mean = 2,448, SD = 1,236; OCT4A expression on day 3 mean = 12,641, SD = 6,189; non-treated P21CIP1 expression mean = 2,875, SD = 1,594; P21CIP1 expression on day 3 mean = 10,291, SD = 5,795. (**E**) Two-channel flow cytometry was used to measure DNA content (PI fluorescence) and OCT4A expression. In NT samples, the OCT4A expression was similar in the 2C and 4C fractions. After ETO treatment, OCT4A was highly elevated in the 4C and 8C fractions and to a lesser extent in the G_1–2C fraction. These data indicate that OCT4A accumulation was mostly induced in the DNA damage checkpoint and persisted in the polyploid cells.

displayed a strong positive correlation (**Fig. 2D**) in the first 3 days post-treatment in the G_2 (4C by DNA content) and polyploid (> 4C) fractions described above (**Fig. 2E**; **Fig. S5A**). However, individual cells were shown to vary greatly in their expression of both of these factors after treatment as indicated by their mean expression levels, standard deviations and extended outliers (**Fig. 2D**; **Fig. S5B**).

The TP53 dependency of the OCT4A response. To further investigate the link between increased OCT4A expression and TP53 induction after DNA damage in PA-1 cells, siRNA directed against TP53 was used. Western analysis of whole-cell lysates confirmed that ETO treatment strongly upregulated TP53, OCT4A and P21CIP1 (CDKN1A), confirming our IF results (**Fig. 3**). In the post-G_2 period, from day 4 after ETO treatment, both TP53 and OCT4A levels partially decreased, while P21CIP1 continued to increase. Transfection of PA-1 cells with TP53-siRNA successfully silenced TP53 expression throughout the time-course and, as expected, inhibited the increase in P21CIP1 in response to ETO treatment. However, unexpectedly, silencing of TP53 also largely inhibited the upregulation of OCT4A. Thus, the increase in OCT4A in response to ETO is largely TP53-dependent. To confirm this surprising finding, we repeated these experiments using PA-1 cells stably transfected with a shRNA vector directed against a different region of TP53 and saw the same results (**Fig. S6**) with diminished OCT4A upregulation.

Previous studies have indicated that the expression of OCT4A in cancer cell lines may have been misreported due to the presence

Table 1. Primary antibodies

Target	Description	Specifity/immunogen	Product nr and manufacturer	Use*
TP53	Rabbit polyclonal	Against full-length human p53 fusion protein	#9282 Cell Signalling Technology	W, IF
OCT	Mouse mAb	Peptide raised against amino acids 1–134 of OCT-3/4 of human origin non-cross-reactive with OCT-3/4 isoforms B and B1.	sc-5279, Santa Cruz	W, IF, F
OCT4A/B	Rabbit polyclonal, ChIP grade	Peptide derived from within residues 300 to the C terminus of human OCT4.	ab19857, Abcam	W, IF, F
NANOG	Mouse mAb, clone NNG-811	Against human NANOG.	N3038, Sigma	IF
P16INK4A	Rabbit polyclonal	Human P16, C-terminal.	ab7962, Abcam	IF
P16INK4A	Rabbit polyclonal	Raised against a peptide mapping at the N terminus of p16 of human origin.	sc-467, Santa Cruz	W, IF
AURORA B kinase	Rabbit polyclonal	Peptide derived from within residues 1–100 of human AURORA B.	ab2254, Abcam	IF
Telomerase reverse transcriptase (TERT)	Mouse mAb	Against human TERT.	ab5181, Abcam	IF
P62 (SQSTM1)	Rabbit polyclonal	Epitope corresponding to amino acids 151–440 of SQSTM1 of human origin.	sc-25575, Santa Cruz	IF
pCHK2 (phosphorylated T68)	Rabbit polyclonal	Epitope around the phosphorylation site of Threonine 68 (VST pQE) of human CHK2.	ab38461, Abcam	W, IF
α-tubulin	Mouse mAb	Recognizes an epitope located at the C-terminal end of the α-tubulin isoform in a variety of organisms.	T5168, Sigma	IF
γ-H2AX	Rabbit polyclonal	Recognizes mammalian, yeast, D. melanogaster and *X. laevis* γ-H2AX.	4411-PC-100, Trevigen	IF
RAD51	Mouse mAb	Targeted to amino acids 1–138 of human RAD51.	ab213, Abcam	IF
LC3B	Rabbit polyclonal	Peptide derived from within residues 1–100 of human LC3B.	ab63817, Abcam	IF
P21CIP1	Rabbit polyclonal	Raised against a peptide mapping at the C terminus of P21 of human origin.	sc-397, Santa Cruz	W, IF
GAPDH	Mouse mAb, clone 6C5	Rabbit muscle GAPDH.	ab8245, Abcam	W
β-actin	Rabbit polyclonal	Synthetic peptide derived from within residues 1–100 of human β-actin.	ab8227, Abcam	W

*W, western; IF, immunofluorescent staining; F, flow cytometry.

of other OCT4 isoforms (OCT4 B, B1 and/or transcribable pseudogenes-1, -3 and -4). To address this issue here, we performed RT-PCR and revealed that OCT4A transcription was present but not particularly enhanced after ETO treatment (**Fig. 4A**), whereas isoform B was entirely absent. The splicing isoform OCT4 B1 (characteristic for ES/EC cells and poorly differentiated cancer)[30,31] was induced after ETO treatment (**Fig. 4A**). In addition, our results indicated that pseudogene-1 was transcribed, whereas pseudogenes-3 and -4 were not (not shown). The OCT4B1 splicing form is appreciably smaller in size in comparison to OCT4A, and was not detected in our immunoblotting analysis with either OCT4A or OCT4A/B antibodies and so can be disregarded. However, to evaluate our IF and immunoblotting findings in relation to pseudogene-1, expression vectors encoding HA-tagged forms of OCT4A or OCT4-pseudogene 1 were produced, transfected into HEK-293 cells and the ability of OCT4 antibodies to detect them examined. It was revealed that although both proteins were equivalently expressed as judged by detection with anti-HA antibodies, only the OCT4A form was detected with the anti-OCT4A monoclonal antibody reagent (**Fig. S7**). Together, these data confirm that the increase in OCT4A described here was attributed to bona fide OCT4A and not alternative splicing or pseudogene forms. However, it should be noted that an additional smaller protein species of OCT4A was also observed in our experiments, which increased in intensity in response to ETO treatment. As discussed above, the size of this protein does not correspond to OCT4B1, nor does this antibody detect other isoforms of OCT4. It therefore may reflect a

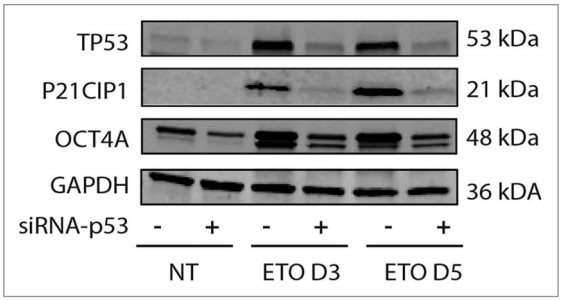

Figure 3. Immunoblot analysis of TP53, OCT4A and P21CIP1 in PA-1 cells after ETO treatment. PA-1 cells were treated with non-target (ntg) siRNA (–) or siRNA-Tp53 (+) for 24 h before treatment with 8 μM ETO, washing after 20 h and cell lysates made and assessed by immunoblotting for Tp53, P21CIP1, OCT4A or GAPDH as a loading control at the indicated time points (day 3 and day 5). TP53 was upregulated in response to ETO treatment and suppressed by siRNA-TP53. P21CIP1 and OCT4A were also upregulated by ETO treatment, and the upregulation was restricted by treatment with siRNA-Tp53. Data are representative of three independent experiments.

post-translational change in OCT4A that increases in response to DNA damage.

OCT4A does not bind chromatin during the DNA damage response. Subcellular fractionation was subsequently used to establish the location of the OCT4A within the cell. Cytoplasm, membrane-bound, nuclear (karyosolic) and chromatin-bound fractions were obtained, and OCT4A presence was assessed by immunoblotting. This analysis revealed a considerable increase of OCT4A in response to ETO treatment in the nuclear (karyosolic) fraction as attested to by two different antibodies, directed to the N or C terminus of OCT4. However, OCT4A was shown to be depleted after ETO treatment from the chromatin-bound fraction as compared with non-treated cells (**Fig. 4B**), indicating that although it is elevated, it may lack the ability to bind its own promoter or the promoters of its cooperative partners (SOX2 and Nanog) and influence the downstream transactivation targets.

Effect of TP53 on the cell cycle response. We next sought to examine the effect of TP53 on the cell cycle response of PA-1 cells after ETO treatment using flow cytometry and DNA image analysis (**Fig. 5A–C**). As indicated above using DNA image cytometry, ETO treatment of TP53-competent PA-1 cells resulted in a pronounced G_2 arrest by day 1–2, followed by its release from day 3–4 and a degree of polyploidy and apoptosis. When TP53 was silenced by shRNA in transfected cell lines, a larger proportion of cells accumulated in the 4C and polyploid fractions. Subsequently, less cells recovered in the G_1-2C fraction (**Fig. 5A and B**). These relationships were more evident upon DNA image analysis that omitted apoptotic cells (**Fig. 5C**; **Fig. S8**). Surprisingly, despite an apparent delay in proliferation, mitotic counts revealed a significant increase in the mitotic index (MI) of TP53-silenced samples compared with TP53-sufficient controls. (**Fig. 5D**; and shown for an individual experiment in **Fig. 5C**). To address the nature of this response further, pCHK2 and α-tubulin staining was performed on adherent cells on day 4 after ETO treatment. Using this approach, bipolar and bicentrosomal mitotic cells and aberrant multipolar mitotic cells were distinguished and enumerated (for examples of normal and abnormal patterns, see **Fig. S9**). The results of this analysis showed that all mitoses in TP53-silenced samples were multicentrosomal and most of them multipolar, with a smaller proportion showing coalescence of multiple centrosomes at two poles, indicating a high degree of chromosome and centrosome instability (**Fig. 6A**). Conversely, the mitoses in control cells after ETO treatment were mostly bipolar and bicentrosomal, with a smaller proportion of multicentriolar multipolarity. Inspection of metaphases by DNA staining after TP53 silencing revealed that they were highly aberrant with deranged plates, partly uninemic, fragmented and clumped chromosomes and no anaphases, while only rare aberrant mitoses were seen in the control sample (characteristic patterns are shown in **Fig. S10A and B**). Some of these aberrant metaphase plates in ETO-treated controls had chromosomes separated from the mitotic spindle and, when stained for γH2AX, displayed DNA damage (**Fig. S10C**). Intense DNA damage was also observed in the polyploid cells with micronuclei, while cells with small nuclei were free of γH2AX staining or contained only residual damage (**Fig. S10D**). Presumably, these observations explain the link between damaged DNA, aberrant mitoses, spindle checkpoint arrest and the induction of polyploidy by mitotic slippage. Therefore, we conclude that in spite of increased entrance into mitosis after TP53 silencing, these cells are arrested in metaphase and delay proliferation, enhancing their propensity to undergo mitotic slippage, and become tetraploid. However, the eventual recovery of the cell population from small clones re-entering mitosis was comparable in both TP53-silenced and control cells, suggesting that TP53-silenced cells compensate for their initial delay in proliferation.

Effect of TP53-silencing on micronucleation. Next, we examined the effect of TP53-silencing on chromosome stability using the presence of micronuclei as a marker (**Fig. 6B**). As expected, treatment with ETO caused an increase in micronucleation and, thus, nuclear instability. Chromosome instability was substantially increased by silencing of TP53 as judged by the ~4-fold increase in micronucleation index.

Effect of TP53-silencing on senescence. Subsequently, we addressed how TP53 affected the induction of senescence after ETO treatment, initially by assessing the expression of P16INKA4A. We found that an increase in P16INKA4A expression was detected from days 4–5 post-treatment in TP53-silenced cells (**Fig. 7A**), corresponding with the partial release from G_2 arrest and increase in (aberrant) mitoses. In contrast, mock-transfected control cells had only marginal expression of P16INKA4A during this time. To confirm whether the increase in P16INKA4A expression corresponded with other indicators of senescence, senescence-associated β-galactosidase (sa-β-gal) staining and morphological analysis were performed. In control cells, ETO treatment evoked a modest but measurable increase in cell size (hypertrophy) and weak sa-β-gal staining at later time points. However, this was greatly accelerated by the silencing of TP53 with strong sa-β-gal staining in a significantly ($p < 0.05$, $n = 3$) higher proportion of cells in TP53-silenced (mean = 70.7%) vs. control (mean = 38.7%) samples at day 5 post-treatment, corresponding with the accelerated increase of DNA damage marked

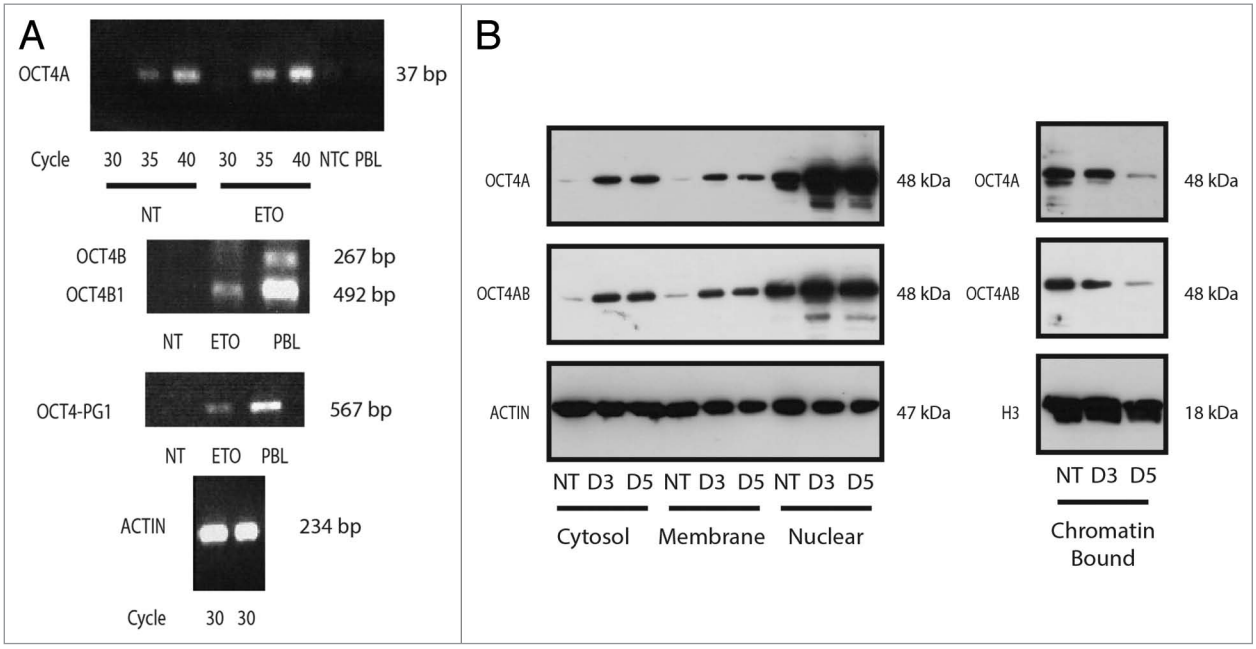

Figure 4. Analysis of OCT4 regulation in PA-1 cells after ETO treatment. PA-1 cells were treated with 8 μM ETO for 20 h, then washed and examined at the indicated time points by (**A**) semi-quantitative PCR or (**B**) cell fractionation and immunoblotting using antibodies against OCT4A or OCT4A and B, actin or histone H3 (H3), the latter two as loading controls. (**A**) OCT4A transcription was shown to be modestly upregulated in response to ETO after 3 d (upper panel). OCT4B was not substantially detected (middle panel). OCT4B1 was upregulated in response to ETO. OCT4-PG-1 was also upregulated in response to ETO (lower panel). Controls were NTC, non-template control; PBL, peripheral blood lymphocytes. Equivalent amplification of actin after 30 cycles was used as a control for cDNA input (bottom panel). Data representative of three independent experiments. (**B**) OCT4A protein was upregulated in response to ETO treatment in the cytosol, membrane and nuclear fractions. OCT4A was downregulated in the chromatin-bound fraction. No additional bands were detected with the OCT4A/B dual specificity (C-terminal) antibody compared with the mono-specific OCT4A antibody (N-terminal), indicating only OCT4A species are expressed. Data representative of two independent experiments.

by pCHK2 (**Fig. S6**) and the senescence marker P16INKA4A (**Fig. 7A**) seen above.

Discussion

In this study, we investigated the DNA damage response of the ovarian teratocarcinoma cell line PA-1, with particular focus on the relationship between self-renewal and senescence and the role of TP53 in regulating these different cell fates. Despite expressing functional TP53, PA-1 cells showed a preferential G_2M arrest following ETO-induced DNA damage, a characteristic feature and cause of genotoxic resistance of ES cells.[19] We also observed equivalent results with other forms of DNA damage such as X-ray irradiation (data not shown).

This arrest was typically characterized by extensive DNA damage signaling (indicated by the upregulation pCHK2 and γH2AX) and by attempted repair through homologous recombination (as shown by the induction of RAD51/γH2AX foci). The subsequent cellular response varied: while most cells died, some cells successfully repaired, halted DNA damage signaling and returned to mitotic cycling, whereas others displayed persistent DNA damage, remained in the 4C fraction or became polyploid. These latter cells underwent upregulated macroautophagy, indicative of a move toward senescence. However, these cells were also OCT4A and AURORA B kinase-positive, contained a large amount of cytoplasmic TERT and were therefore potentially able to enter mitosis, so retained a clear plasticity of response, not yet terminally committed to senescence.

The DNA damage response in the PA-1 cells appears to couple the upregulation of the pluripotency and self-renewal-promoting master molecule, OCT4A, with cell cycle arrest and senescence-promoting molecules (TP53 and P21CIP1) in the same cells, providing them with bipotentiality in the DNA damage checkpoint. Furthermore, the expression levels of these proteins in individual cells after treatment was highly varied. Although heterogeneous expression of NANOG within ES cell cultures has been observed,[32] and this, in turn, has been attributed to fluctuation of NANOG levels,[33] it is generally accepted that OCT4A expression is tightly regulated and expressed relatively uniformly in ES cell populations and does not fluctuate.[34] In the context of TP53-dependent upregulation of OCT4A, the heterogeneity observed here may be due to fluctuation in TP53 expression itself, which is well-documented in cell stress responses.[35,36]

Artificially reducing the level of TP53 using si- or shRNA resulted in precocious mitosis and, subsequently, an increase in chromosome and centrosome instability in response to ETO treatment. In addition, TP53 silencing caused an increase in DNA damage and enhanced senescence. This is in agreement with previous studies that demonstrated TP53 can suppress cellular senescence.[16] We therefore propose that unrepaired DNA damage and the increase in chromosome instability may link TP53 suppression to senescence.

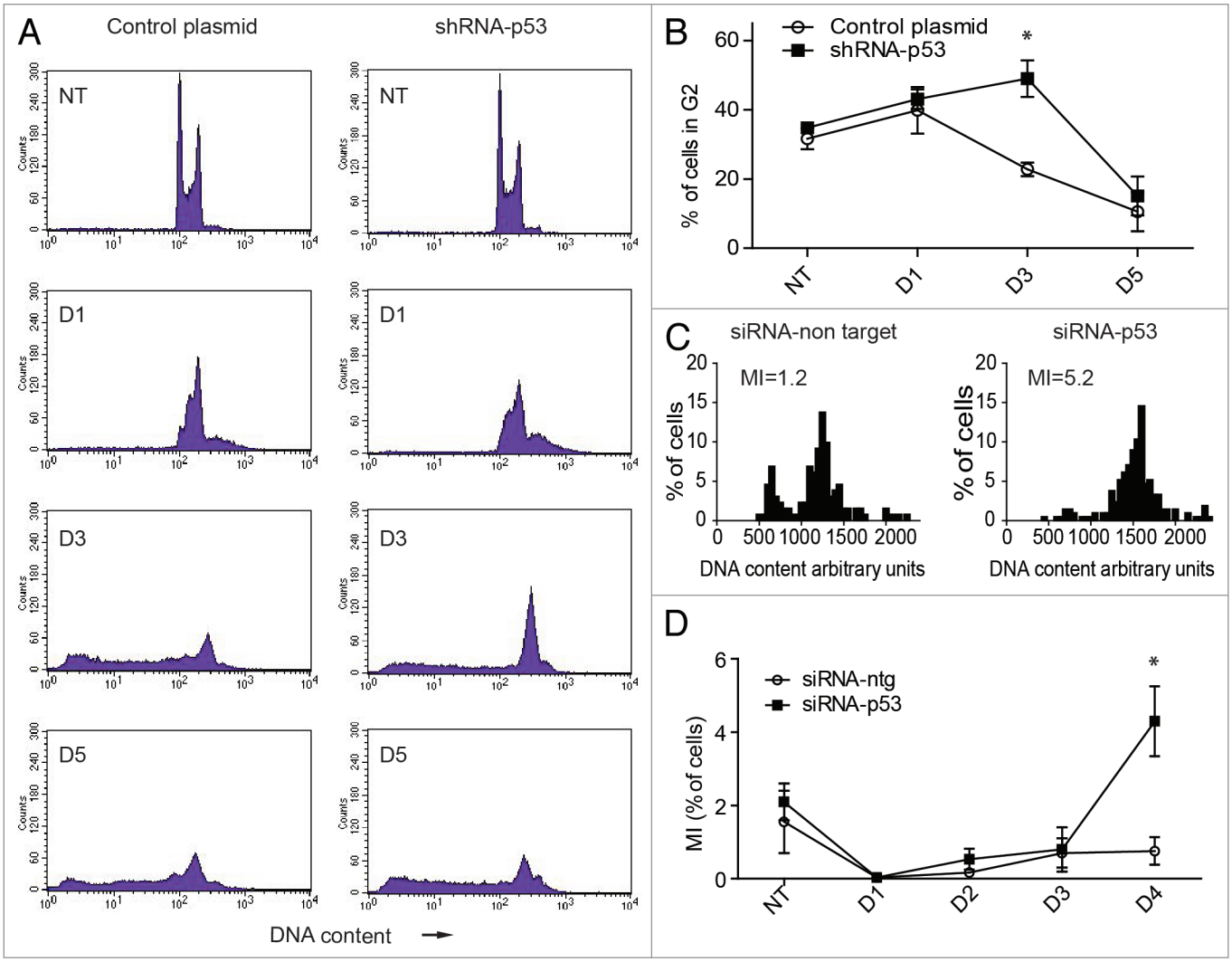

Figure 5. Effect of silencing TP53 on the cell cycle response of PA-1 cells after ETO treatment. PA-1 cells were treated with 8 μM ETO for 20 h, then washed and examined at the indicated time points by (**A and B**) flow cytometry, (**C**) DNA image cytometry and (**D**) mitotic counts. (**A**) Both control plasmid and shRNA p53-silenced cells undergo a G_2M arrest after ETO treatment, which is, however, more profound from day 3 in TP53-silenced cells. The TP53-silenced cells also show a larger increase in the ≥ 4C cell fraction in response to ETO treatment. Conversely, the recovering G_1–2C fraction is reduced. By day 5, the relative proportion of the G_2 fraction is diminished in both samples, due to the increase in apoptosis. (**B**) The proportion of cells in G_2 was enumerated over the time course in three independent experiments with the mean and SEM plotted (* $p < 0.05$). (**C**) DNA image cytometry analysis was also performed on day 4 after ETO treatment. Apoptotic cells were excluded from the measurements, and highlighted more clearly the relationship between the increased 4C fraction and relative delay in recovery of the proliferating G_1–2C fraction (reduced 2.5-fold) after TP53-silencing. The corresponding mitotic index (MI) at this time point is also shown. For full cell cycle dynamics over the time course in this experiment, please see **Figure S6**. Data representative of two similar experiments. (**D**) Mitotic counts were performed on control plasmid or shRNA p53-silenced cells over time after ETO treatment. The results from three independent experiments show a significant increase in the proportion of mitoses after TP53 silencing (* $p < 0.05$).

The question then becomes how. Precocious aberrant mitoses containing DNA damage readily undergo mitotic slippage (to become G_1-4N cells with micronuclei), which may undergo apoptosis or alternatively trigger terminal senescence through TP53-independent P21CIP1 and P16INKA4A targeting of the cyclin kinases governing the G_1–S transition. Weaver and Cleveland also suggested adaptation of the spindle checkpoint as a pathway to cell survival vs. senescence through tetraploidy.[37] Based upon our observations, we suggest that coupling the expression of self-renewal and senescence regulators through TP53 at the DNA damage checkpoint favors DNA damage repair, reduces chromosome and centrosome instability and, thus, safeguards the fidelity of self-renewal in the damage-resistant EC cells.

The question again follows, how are these opposing processes coordinated at the molecular level? The explanation may be provided by the observation that the OCT4A induced by TP53 at the DNA damage checkpoint is unable to bind chromatin. Presumably then, OCT4A is unable to execute its transactivation role in binding to the NANOG promoter regulatory element essential for the pluripotency function.[34,38] Conversely, the NANOG promoter should be directly blocked by activated TP53.[39] However, importantly, in ETO-treated PA-1 cells,

OCT4A accumulates in the cell nucleus, and this should be a prerequisite for its effective upregulation of NANOG through a positive feedback loop, when the NANOG promoter becomes free from inhibition by TP53 after DNA damage repair. Therefore, accumulation of OCT4A can be considered as a precursor for self-renewal potential. Simultaneously, the cell is primed for senescence through the accumulation of P21CIP1, again in a TP53-dependent manner, but is prevented from its full execution, possibly by the pre-mitotic molecular environment of the G_2 cell. It follows that the PA-1 cells in the G_2M damage checkpoint are in a state of bi-potential metastability between self-renewal and senescence, akin to the situation of bi-potentiality between self-renewal and differentiation in stem cells.

This interpretation fits well with the extensive heterogeneity in OCT4A and P21CIP1 levels observed in the individual cells held at the G_2 arrest, potentially suggesting that their expression levels are dynamically fluctuating.[40] To our knowledge, this notion of bi-potential metastability has not previously been considered as a key result of DNA damage, and we believe our data support further study of this area.

In conclusion, our studies have described two previously unknown phenomena relating to the intrinsic link between self-renewal and senescence in DNA damaged cells expressing stem cell-like transcriptional networks and revealed the role of TP53 in this process. This knowledge may be of use in improving our understanding of normal stem cells and also in designing better strategies to eliminate cancer stem cells.

Materials and Methods

Cell culture and ETO treatment. PA-1 (ATCC) and HEK-293 cells were cultured in Dulbecco's modified Eagle's media (DMEM) supplemented with 10% fetal calf serum. Cells were grown without antibiotics in 5% CO_2 incubators at 37°C. For the sphere formation assay, PA1 cells were inoculated in DMEM/F12 media supplemented with 20 ng/ml EGF (236-EG, R&D Systems), 10 ng/ml FGF (233-FB-025/CF, R&D Systems), 0.5 ng/ml hydrocortisone (H0888, Sigma), 10 ng/ml insulin (I9278, Sigma), 1× antibiotics/antimycotics (15240-062, Invitrogen), 1% L-glutamine (25030024, Invitrogen) and 20% methylcellulose (high viscosity, 4,000 cP; M0512, Sigma), and grown in 5% CO_2 at 37°C. Exponentially growing PA-1 cells were incubated with an 8 μM dose of ETO for 20 h.

Small interfering RNA (siRNA). TP53 protein Hs_TP53_9 FlexiTube siRNA (Qiagen) was used to silence TP53 expression and ON-TARGET plus non-targetting siRNA #1 (Dharmacon) was used as a negative control. PA-1 cells were transfected with siRNA using HiPerfect (Qiagen) according to the manufacturer's protocol.

Small hairpin RNA (shRNA). The following plasmids were purchased from Addgene: pMKO.1 puro TP53 plasmid (Addgene plasmid 19119) deposited by Bob Weinberg;[41] and pMKO.1 puro (Addgene plasmid 8452) deposited by Bob Weinberg.[42] PA-1 cells were transfected with plasmid using Fugene 6 (Promega) according to the manufacturer's protocol and then selected using puromycin (0.3 μg/ml). After 2 wk, growing colonies were sub-cloned, stable cell lines established and maintained in media containing puromycin. Selection was removed 3 d prior to experiments.

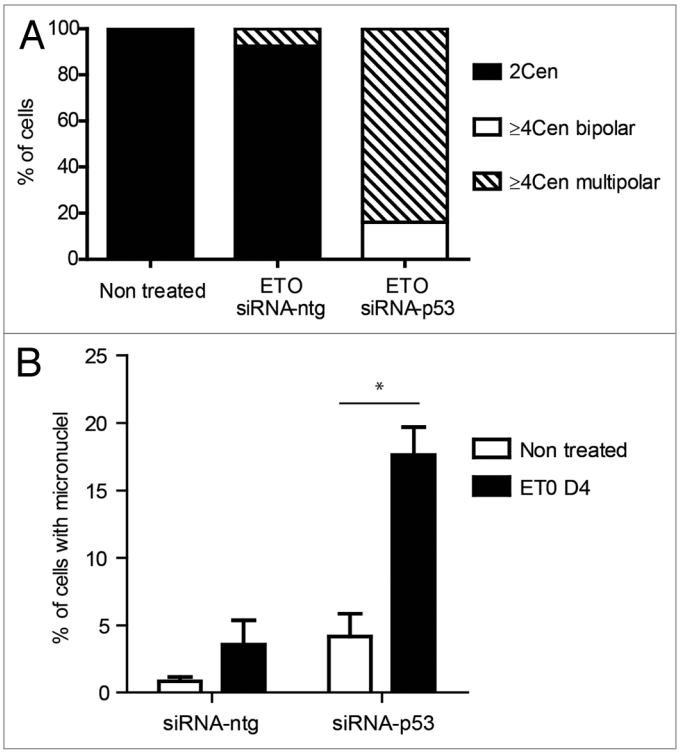

Figure 6. Effect of silencing TP53 on genome instability in PA-1 cells after ETO treatment. PA-1 cells were treated with 8 μM ETO for 20 h, then washed and examined at the indicated time points for the (**A**) the proportion of normal (2 centrosomal; 2 cen), ≥ 4 cen bipolar and ≥ 4 cen multipolar mitoses and (**B**) micronucleation. (**A**) Cells were treated as before and then examined by IF staining for pCHK2 and α-tubulin. Silencing of TP53 caused multi-centrosomal mitoses (≥ 4 cen) that were mostly multi-polar or showed coalescence of centrosomes in two poles. (**B**) Cells were treated as before and then assessed for the extent of micronucleation following DNA in situ staining. An increase in the proportion of interphase cells with micronuclei was observed in response to ETO treatment. Silencing of TP53 significantly increased the amount of micronucleation, which was further enhanced in response to ETO ($p < 0.05$). Data are representative of three independent experiments.

Expression of HA-tagged forms of OCT4A and OCT4A-pseudogene-1. Expression vectors encoding HA-tagged forms of OCT4A or OCT4A-pseudogene-1 (OCT4A-PG1), a kind gift from Professor Aijun Hao,[43] were transfected into HEK-293 cells using Fugene 6 (Promega) according to the manufacturer's protocol.

DNA image cytometry. Cytospins were prepared and fixed in ethanol:acetone (1:1) for > 30 min at 4°C and air-dried. Slides were then treated with 5N HCl for 20 min at room temperature, washed in distilled water (5 × 1 min) and stained for 10 min with 0.05% toluidine blue in 50% citrate-phosphate McIlvain buffer pH 4. Slides were rinsed with distilled water, blotted dry and dehydrated by incubating twice in butanol for 3 min each at 37°C. Samples were then incubated twice in xylene for 3 min each at room temperature before being embedded in DPX. Slides were then evaluated using a Leitz Ergolux L03-10 microscope equipped with a calibrated Sony DXC 390P color video camera.

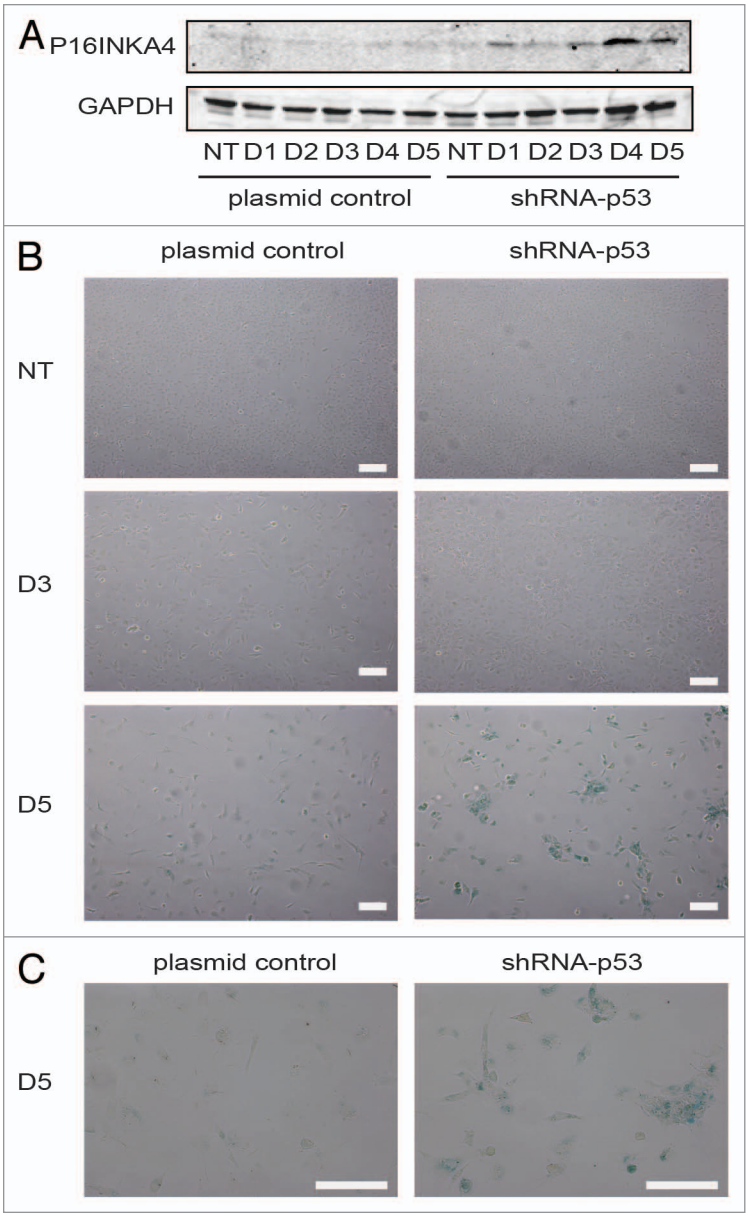

Figure 7. Senescence response of PA-1 cells to ETO treatment. PA-1 cells stably transfected with shRNA-p53 or plasmid control were treated with 8 μM ETO for 20 h, then washed and assessed at the indicated time point by (**A**) immunoblotting or (**B**) for sa-β-gal expression and cellular morphology. (**A**) Cell lysates were made and assessed by immunoblotting for P16INKA4 and GAPDH as a loading control. An accumulation of P16INKA4 was detected in TP53-silenced cells after ETO treatment. (**B**) sa-β-gal staining was used to detect sa-β-gal activity in response to ETO treatment at indicated time points. Detection of sa-β-gal activity was increased by TP53-silencing and largely mirrored the induction of P16INKA4 seen above. (**C**) Higher power image of the cells seen on day 5. Bar = 20 μM. Data are representative of > three independent experiments.

DNA content was measured as the integral optical density in the green channel, using Image-Pro Plus 4.1 software (Media Cybernetics). Apoptotic cells were omitted from measurements. The stoichiometry of DNA staining was verified using the values obtained for metaphases compared with anaphases and telophases (ratio 2.0); the method error was estimated to be less than 5%.

DNA flow cytometry. Cells were trypsinized, harvested at indicated time points, washed in PBS and suspended in hypotonic fluorochrome solution [50 μg/ml propidium iodide (PI), 0.1% (w/v) sodium citrate, 0.1% (v/v) Triton X-100] and stored for at least 1 h in the dark at 4°C. Flow cytometry was performed using a FACScan (BD Biosciences) using Cell Quest Pro Software.

Two-channel flow cytometry. Cells were harvested at relevant time points, washed in cold PBS and fixed with 70% ethanol for 20 min at room temperature. After two washes in TBS, cells were permeabilized with TBS/4% bovine serum albumin (BSA)/0.1% Triton X-100 for 10 min at room temperature. Samples were then incubated with rabbit polyclonal anti-OCT4 antibody solution (ab19857, Abcam) (5 μg/ml) in TBS/4% BSA/0.1% Triton X-100 for 1 h at room temperature. Following two washes in TBS, cells were incubated with goat anti-rabbit Alexa Fluor 488 solution (1:200) in TBS/4% BSA/0.1% Triton X 100, for 30 min in the dark. DNA was counterstained with 10 μg/ml PI solution in PBS, containing 200 μg/ml RNase (Sigma) and assessed by flow cytometry using a FACS Calibur (BD Biosciences) using Cell Quest Pro Software.

Immunofluorescent (IF) staining. IF was performed as described previously.[44] Cytospins were fixed in methanol for 7 min at –20°C and dipped 10 times in ice-cold acetone. Slides were then washed three times in TBS 0.01% Tween 20 (TBST) for 5 min. Slides were subsequently blocked for 15 min in TBS, 0.05% Tween 20%, 1% BSA at room temperature. Samples were covered with 50 μL of TBS, 0.025% Tween 20%, 1% BSA containing primary antibody and incubated overnight at 4°C in a humidified chamber. Samples were then washed three times in TBST and covered with 50 μL of TBST containing the appropriate secondary antibody before incubation for 40 min at room temperature in the dark. Slides were washed three times for 5 min with PBST and once for 2 min in PBS. Samples were then counterstained with 0.25 μg/ml DAPI for 1 min, mounted using ProLong Gold antifade reagent (Invitrogen) and evaluated using a Leitz Ergolux L03-10 microscope equipped with a Sony DXC 390P color video camera. Antibodies and their source are listed in **Tables 1 and 2**. Note: when staining for tubulin, the fixation step using acetone was omitted and detergent was absent from all buffers. For TERT staining alone, the fixed cells were pre-treated with 2N HCl for 20 min at room temperature.

Detection of sa-β-galactosidase activity. The senescence β-galactosidase (sa-β-gal) staining kit (Cell Signaling, 9860) was used to detect sa-β-gal activity in cultured cells at indicated time points according to the manufacturer's protocol.

Western blotting (whole-cell lysate). Cells were harvested using trypsin digestion and lysed using RIPA buffer with protease inhibitor cocktail (Sigma P8340). Total protein was quantified using BCA protein assay kit (Pierce) and equal quantities

Table 2. Secondary antibodies

Antibody	Conjugate	Product nr and manufacturer	Use*
Goat anti-mouse IgG	Alexa Fluor 488	A31619, Invitrogen	IF, F
Goat anti-rabbit- IgG	Alexa Fluor 594	A31631, Invitrogen	IF
Goat anti-rabbit IgG	HRP	32460, Thermo Fisher Scientific	W
Rabbit anti-mouse IgG	HRP	61-6520, Invitrogen	W
Goat anti-rabbit IgG	IRDye 800CW	926-32211, IRDye Antibodies	W
Goat anti-mouse IgG	IRDye 800CW	926-32210, IRDye Antibodies	W
Goat anti-rabbit IgG	IRDye 680LT	926-68021, IRDye Antibodies	W

of denatured protein were subjected to electrophoresis on SDS-polyacrylamide gels, blotted onto Immobilon-FC transfer membrane and probed with specific primary antibodies listed in **Table 1** and secondary antibodies listed in **Table 2**. The signal was visualized using a LICOR Odyssey imaging system.

Subcellular fractionation. For cellular fractionation, the Subcellular Protein Fractionation Kit for Cultured Cells (Thermo Scientific) was used according to the manufacturer's instructions. Cytoplasmic, membrane, nuclear soluble, karyosol and chromatin-bound protein extracts were obtained. Protein concentrations were determined by Bio-Rad (Bio-Rad Inc.) protein assay, using a BSA standard set (Fermentas MBI) for quantitation. Proteins (10 or 15 μg) were separated on 10, 12, 5 or 20% SDS PAGE gels, followed by electrophoretic transfer onto BA85 nitro-cellulose membranes (Schleicher and Schuell GmbH) overnight. Equal protein loading in each lane was verified by Ponceau S staining. Blots were probed with specific primary antibodies listed in **Table 1** and secondary antibodies listed in **Table 2**. The signal was visualized using the Chemiluminescent Nucleic Acid Detection Module (Thermo Scientific).

RT-PCR analysis of Oct4-splicing forms. Total RNA was extracted from cells using TRIZOL (Invitrogen). cDNA was synthesized using First Strand cDNA Synthesis Kit (Fermentas MBI) according to the manufacturer's protocol and then diluted 10×. The absence of contamination with genomic DNA was verified by PCR using actin primers as described.[11] cDNA from peripheral blood lymphocytes (PBL) as a control of somatic cells was kindly provided by Dr Inta Vasiljeva. Amplification was performed with 1–4 μl of diluted cDNA and the following primers, β-actin F/R; Oct4A AF/AR; Oct4B/B1 BF1/BR2 under conditions previously described.[11] Amplified PCR products were analyzed on an agarose gel after various PCR cycles and their identity determined by direct sequencing after ExoI/SAP treatment (Fermentas, MBI) using the fluorescent Big DyeTerminator v. 3.1 Cycle Sequencing protocol on a 3,130 xl Genetic Analyzer (Applied Biosystems).

Methods of statistical analysis. Statistical analysis was performed in Minitab. A paired t-test was used to calculate the statistical significance of difference of means where appropriate. Statistical significance was accepted when $p < 0.05$. Graphs were plotted in GraphPad Prism 5 and Statistica 6.

Disclosure of Potential Conflicts of Interest

No potential conflicts of interest were disclosed.

Acknowledgments

The authors would like to thank Professor Hao and Dr Zhao, Dept. of Histology and Embryology, Shandong University School of Medicine for the kind gift of the OCT4A and OCT4A-Psg-1 vector constructs and Dr Pawel Zayakin (Latvian Biomedical Centre) for insightful discussions. T.R.J. was funded through an MRC PhD studentship and the Gerald Kerkut Charitable Trust awarded to P.A.T. and M.S.C.; J.E. was funded by the Latvian National Research Programme 2010–2013 "BIOMEDICINE" and AH by European Social Fund within the project "Support for Doctoral Studies at University of Latvia." Exchange visits between Riga and Southampton were supported by the Royal Society of London. The publishing costs associated with this article are in part provided by the ERDF project no. 2DP/2.1.1.2.0/10/ APIA/VIAA/004.

Supplemental Materials

Supplemental materials may be found here:
www.landesbioscience.com/journals/cc/article/23285

References

1. Ben-Porath I, Thomson MW, Carey VJ, Ge R, Bell GW, Regev A, et al. An embryonic stem cell-like gene expression signature in poorly differentiated aggressive human tumors. Nat Genet 2008; 40:499-507; PMID:18443585; http://dx.doi.org/10.1038/ng.127
2. Dean M, Fojo T, Bates S. Tumour stem cells and drug resistance. Nat Rev Cancer 2005; 5:275-84; PMID:15803154; http://dx.doi.org/10.1038/nrc1590
3. Jordan CT, Guzman ML, Noble M. Cancer stem cells. N Engl J Med 2006; 355:1253-61; PMID:16990388; http://dx.doi.org/10.1056/NEJMra061808
4. Reya T, Morrison SJ, Clarke MF, Weissman IL. Stem cells, cancer, and cancer stem cells. Nature 2001; 414:105-11; PMID:11689955; http://dx.doi.org/10.1038/35102167
5. Boyer LA, Lee TI, Cole MF, Johnstone SE, Levine SS, Zucker JP, et al. Core transcriptional regulatory circuitry in human embryonic stem cells. Cell 2005; 122:947-56; PMID:16153702; http://dx.doi.org/10.1016/j.cell.2005.08.020
6. Takahashi K, Tanabe K, Ohnuki M, Narita M, Ichisaka T, Tomoda K, et al. Induction of pluripotent stem cells from adult human fibroblasts by defined factors. Cell 2007; 131:861-72; PMID:18035408; http://dx.doi.org/10.1016/j.cell.2007.11.019
7. Huangfu DW, Osafune K, Maehr R, Guo W, Eijkelenboom A, Chen S, et al. Induction of pluripotent stem cells from primary human fibroblasts with only Oct4 and Sox2. Nat Biotechnol 2008; 26:1269-75; PMID:18849973; http://dx.doi.org/10.1038/nbt.1502
8. Ge N, Lin HX, Xiao XS, Guo L, Xu HM, Wang X, et al. Prognostic significance of Oct4 and Sox2 expression in hypopharyngeal squamous cell carcinoma. J Transl Med 2010; 8:94; http://dx.doi.org/10.1186/1479-5876-8-94; PMID:20937145
9. Saigusa S, Tanaka K, Toiyama Y, Yokoe T, Okugawa Y, Ioue Y, et al. Correlation of CD133, OCT4, and SOX2 in rectal cancer and their association with distant recurrence after chemoradiotherapy. Ann Surg Oncol 2009; 16:3488-98; PMID:19657699; http://dx.doi.org/10.1245/s10434-009-0617-z
10. Xiang R, Liao D, Cheng T, Zhou H, Shi Q, Chuang TS, et al. Downregulation of transcription factor SOX2 in cancer stem cells suppresses growth and metastasis of lung cancer. Br J Cancer 2011; 104:1410-7; PMID:21468047; http://dx.doi.org/10.1038/bjc.2011.94

11. Salmina K, Jankevics E, Huna A, Perminov D, Radovica I, Klymenko T, et al. Up-regulation of the embryonic self-renewal network through reversible polyploidy in irradiated p53-mutant tumour cells. Exp Cell Res 2010; 316:2099-112; PMID:20457152; http://dx.doi.org/10.1016/j.yexcr.2010.04.030
12. Banito A, Rashid ST, Acosta JC, Li S, Pereira CF, Geti I, et al. Senescence impairs successful reprogramming to pluripotent stem cells. Genes Dev 2009; 23:2134-9; PMID:19696146; http://dx.doi.org/10.1101/gad.1811609
13. Huna A, Salmina K, Jascenko E, Duburs G, Inashkina I, Erenpreisa J. Self-Renewal signalling in presenescent tetraploid IMR90 cells. J Aging Res 2011; 2011:103253; PMID:21629737; http://dx.doi.org/10.4061/2011/103253
14. Blagosklonny MV. Cell senescence and hypermitogenic arrest. EMBO Rep 2003; 4:358-62; PMID:12671679; http://dx.doi.org/10.1038/sj.embor.embor806
15. Leontieva OV, Blagosklonny MV. DNA damaging agents and p53 do not cause senescence in quiescent cells, while consecutive re-activation of mTOR is associated with conversion to senescence. Aging (Albany NY) 2010; 2:924-35; PMID:21212465
16. Demidenko ZN, Korotchkina LG, Gudkov AV, Blagosklonny MV. Paradoxical suppression of cellular senescence by p53. Proc Natl Acad Sci USA 2010; 107:9660-4; PMID:20457898; http://dx.doi.org/10.1073/pnas.1002298107
17. Blagosklonny MV. Cell cycle arrest is not senescence. Aging (Albany NY) 2011; 3:94-101; PMID:21297220
18. Boheler KR. Stem cell pluripotency: a cellular trait that depends on transcription factors, chromatin state and a checkpoint deficient cell cycle. J Cell Physiol 2009; 221:10-7; PMID:19562686; http://dx.doi.org/10.1002/jcp.21866
19. Rich JN. Cancer stem cells in radiation resistance. Cancer Res 2007; 67:8980-4; PMID:17908997; http://dx.doi.org/10.1158/0008-5472.CAN-07-0895
20. Sperger JM, Chen X, Draper JS, Antosiewicz JE, Chon CH, Jones SB, et al. Gene expression patterns in human embryonic stem cells and human pluripotent germ cell tumors. Proc Natl Acad Sci USA 2003; 100:13350-5; PMID:14595015; http://dx.doi.org/10.1073/pnas.2235735100
21. Josephson R, Ording CJ, Liu Y, Shin S, Lakshmipathy U, Toumadje A, et al. Qualification of embryonal carcinoma 2102Ep as a reference for human embryonic stem cell research. Stem Cells 2007; 25:437-46; PMID:17284651; http://dx.doi.org/10.1634/stemcells.2006-0236
22. te Poele RH, Okorokov AL, Jardine L, Cummings J, Joel SP. DNA damage is able to induce senescence in tumor cells in vitro and in vivo. Cancer Res 2002; 62:1876-83; PMID:11912168
23. Sabisz M, Skladanowski A. Cancer stem cells and escape from drug-induced premature senescence in human lung tumor cells: implications for drug resistance and in vitro drug screening models. Cell Cycle 2009; 8:3208-17; PMID:19738435; http://dx.doi.org/10.4161/cc.8.19.9758
24. Lifantseva N, Koltsova A, Krylova T, Yakovleva T, Poljanskaya G, Gordeeva O. Expression patterns of cancer-testis antigens in human embryonic stem cells and their cell derivatives indicate lineage tracks. Stem Cells Int 2011; 2011:795239; PMID:21785609; http://dx.doi.org/10.4061/2011/795239
25. Sarraf S, Tejada R, Abawi M, Oberst M, Dennis T, Simon KC, et al. The human ovarian teratocarcinoma cell line PA-1 demonstrates a single translocation: analysis with fluorescence in situ hybridization, spectral karyotyping, and bacterial artificial chromosome microarray. Cancer Genet Cytogenet 2005; 161:63-9; PMID:16080959; http://dx.doi.org/10.1016/j.cancergencyto.2005.01.003
26. Gao C, Miyazaki M, Li JW, Tsuji T, Inoue Y, Namba M. Cytogenetic characteristics and p53 gene status of human teratocarcinoma PA-1 cells in 407-445 passages. Int J Mol Med 1999; 4:597-600; PMID:10567668
27. Zhang XN, Jaramillo M, Singh S, Kumta P, Banerjee I. Analysis of regulatory network involved in mechanical induction of embryonic stem cell differentiation. PLoS One 2012; 7:e35700; PMID:22558203; http://dx.doi.org/10.1371/journal.pone.0035700
28. Chiodi I, Mondello C. Telomere-independent functions of telomerase in nuclei, cytoplasm, and mitochondria. Front Oncol 2012; 2:133; http://dx.doi.org/10.3389/fonc.2012.00133; PMID:23061047
29. Erenpreisa J, Salmina K, Huna A, Kosmacek EA, Cragg MS, Ianzini F, et al. Polyploid tumour cells elicit paradiploid progeny through depolyploidizing divisions and regulated autophagic degradation. Cell Biol Int 2011; 35:687-95; PMID:21250945; http://dx.doi.org/10.1042/CBI20100762
30. Atlasi Y, Mowla SJ, Ziaee SAM, Gokhale PJ, Andrews PW. OCT4 spliced variants are differentially expressed in human pluripotent and nonpluripotent cells. Stem Cells 2008; 26:3068-74; PMID:18787205; http://dx.doi.org/10.1634/stemcells.2008-0530
31. Asadi MH, Mowla SJ, Fathi F, Aleyasin A, Asadzadeh J, Atlasi Y. OCT4B1, a novel spliced variant of OCT4, is highly expressed in gastric cancer and acts as an antiapoptotic factor. Int J Cancer 2011; 128:2645-52; PMID:20824712; http://dx.doi.org/10.1002/ijc.25643
32. Singh AM, Hamazaki T, Hankowski KE, Terada N. A heterogeneous expression pattern for Nanog in embryonic stem cells. Stem Cells 2007; 25:2534-42; PMID:17615266; http://dx.doi.org/10.1634/stemcells.2007-0126
33. Kalmar T, Lim C, Hayward P, Muñoz-Descalzo S, Nichols J, Garcia-Ojalvo J, et al. Regulated fluctuations in nanog expression mediate cell fate decisions in embryonic stem cells. PLoS Biol 2009; 7:e1000149; PMID:19582141; http://dx.doi.org/10.1371/journal.pbio.1000149
34. Chambers I, Silva J, Colby D, Nichols J, Nijmeijer B, Robertson M, et al. Nanog safeguards pluripotency and mediates germline development. Nature 2007; 450:1230-4; PMID:18097409; http://dx.doi.org/10.1038/nature06403
35. Lev Bar-Or R, Maya R, Segel LA, Alon U, Levine AJ, Oren M. Generation of oscillations by the p53-Mdm2 feedback loop: a theoretical and experimental study. Proc Natl Acad Sci USA 2000; 97:11250-5; PMID:11016968; http://dx.doi.org/10.1073/pnas.210171597
36. Lahav G, Rosenfeld N, Sigal A, Geva-Zatorsky N, Levine AJ, Elowitz MB, et al. Dynamics of the p53-Mdm2 feedback loop in individual cells. Nat Genet 2004; 36:147-50; PMID:14730303; http://dx.doi.org/10.1038/ng1293
37. Weaver BAA, Cleveland DW. Decoding the links between mitosis, cancer, and chemotherapy: The mitotic checkpoint, adaptation, and cell death. Cancer Cell 2005; 8:7-12; PMID:16023594; http://dx.doi.org/10.1016/j.ccr.2005.06.011
38. Levasseur DN, Wang J, Dorschner MO, Stamatoyannopoulos JA, Orkin SH. Oct4 dependence of chromatin structure within the extended Nanog locus in ES cells. Genes Dev 2008; 22:575-80; PMID:18283123; http://dx.doi.org/10.1101/gad.1606308
39. Lin T, Chao C, Saito S, Mazur SJ, Murphy ME, Appella E, et al. p53 induces differentiation of mouse embryonic stem cells by suppressing Nanog expression. Nat Cell Biol 2005; 7:165-71; PMID:15619621; http://dx.doi.org/10.1038/ncb1211
40. Huang S. Non-genetic heterogeneity of cells in development: more than just noise. Development 2009; 136:3853-62; PMID:19906852; http://dx.doi.org/10.1242/dev.035139
41. Godar S, Ince TA, Bell GW, Feldser D, Donaher JL, Bergh J, et al. Growth-inhibitory and tumor- suppressive functions of p53 depend on its repression of CD44 expression. Cell 2008; 134:62-73; PMID:18614011; http://dx.doi.org/10.1016/j.cell.2008.06.006
42. Stewart SA, Dykxhoorn DM, Palliser D, Mizuno H, Yu EY, An DS, et al. Lentivirus-delivered stable gene silencing by RNAi in primary cells. RNA 2003; 9:493-501; PMID:12649500; http://dx.doi.org/10.1261/rna.2192803
43. Zhao SD, Yuan QH, Hao HB, Guo YJ, Liu SM, Zhang YM, et al. Expression of OCT4 pseudogenes in human tumours: lessons from glioma and breast carcinoma. J Pathol 2011; 223:672-82; PMID:21341266; http://dx.doi.org/10.1002/path.2827
44. Erenpreisa J, Cragg MS, Salmina K, Hausmann M, Scherthan H. The role of meiotic cohesin REC8 in chromosome segregation in gamma irradiation-induced endopolyploid tumour cells. Exp Cell Res 2009; 315:2593-603; PMID:19463812; http://dx.doi.org/10.1016/j.yexcr.2009.05.011

3.3.DNA damage stress-activated OCT4A role in tumour cell survival – Original paper III

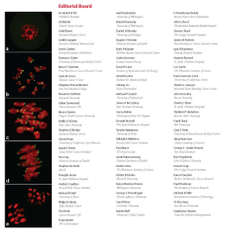

Cell Cycle

ISSN: 1538-4101 (Print) 1551-4005 (Online) Journal homepage: http://www.tandfonline.com/loi/kccy20

Role of stress-activated OCT4A in the cell fate decisions of embryonal carcinoma cells treated with etoposide

Anda Huna, Kristine Salmina, Jekaterina Erenpreisa, Alejandro Vazquez-Martin, Jekabs Krigerts, Inna Inashkina, Bogdan I Gerashchenko, Paul A Townsend, Mark S Cragg & Thomas R Jackson

To cite this article: Anda Huna, Kristine Salmina, Jekaterina Erenpreisa, Alejandro Vazquez-Martin, Jekabs Krigerts, Inna Inashkina, Bogdan I Gerashchenko, Paul A Townsend, Mark S Cragg & Thomas R Jackson (2015): Role of stress-activated OCT4A in the cell fate decisions of embryonal carcinoma cells treated with etoposide , Cell Cycle, DOI: 10.1080/15384101.2015.1056948

To link to this article: http://dx.doi.org/10.1080/15384101.2015.1056948

Accepted online: 23 Jun 2015.Published online: 23 Jun 2015.

Cell Cycle 14:15, 1–16; August 1, 2015; © 2015 Taylor & Francis Group, LLC

Role of stress-activated OCT4A in the cell fate decisions of embryonal carcinoma cells treated with etoposide

Anda Huna[1], Kristine Salmina[1], Jekaterina Erenpreisa[1], Alejandro Vazquez-Martin[1], Jekabs Krigerts[1], Inna Inashkina[1], Bogdan I Gerashchenko[1,4], Paul A Townsend[2], Mark S Cragg[3], and Thomas R Jackson[2,*]

[1]Latvian Biomedical Research and Study Center; Riga, Latvia; [2]Institute of Cancer Sciences; Manchester Cancer Research Center; University of Manchester; Manchester Academic Health Science Center; Manchester, UK; [3]Cancer Sciences Unit; University of Southampton; Faculty of Medicine; General Hospital; Southampton, UK; [4]R. E. Kavetsky Institute of Experimental Pathology; Oncology and Radiobiology; National Academy of Sciences of Ukraine; Kyiv, Ukraine

Keywords: cell-fate, DNA damage, OCT4A/POU5F1, p53, p21Cip1, p16ink4a, p62, pluripotency, senescence, self-renewal, tumor cells

Abbreviations: AMPK, AMP-activated protein kinase; Baf, bafilomycin; EC, embryonal carcinoma; ES, embryonic stem; ETO, Etoposide; IF, immunofluorescent; LC3, microtubule associated protein 1 light chain 3; NT, non-treated; NT2, NTera 2; ntg, non-target; pCHK2, phosphorylated CHK2; PI, propidium iodide; siRNA, small interfering RNA; shRNA, small hairpin RNA; Sa-b-gal, senescence associated β-galactosidase.

Tumor cellular senescence induced by genotoxic treatments has recently been found to be paradoxically linked to the induction of "stemness." This observation is critical as it directly impinges upon the response of tumors to current chemo-radio-therapy treatment regimens. Previously, we showed that following etoposide (ETO) treatment embryonal carcinoma PA-1 cells undergo a p53-dependent upregulation of OCT4A and p21Cip1 (governing self-renewal and regulating cell cycle inhibition and senescence, respectively). Here we report further detail on the relationship between these and other critical cell-fate regulators. PA-1 cells treated with ETO display highly heterogeneous increases in OCT4A and p21Cip1 indicative of dis-adaptation catastrophe. Silencing OCT4A suppresses p21Cip1, changes cell cycle regulation and subsequently suppresses terminal senescence; p21Cip1-silencing did not affect OCT4A expression or cellular phenotype. SOX2 and NANOG expression did not change following ETO treatment suggesting a dissociation of OCT4A from its pluripotency function. Instead, ETO-induced OCT4A was concomitant with activation of AMPK, a key component of metabolic stress and autophagy regulation. p16ink4a, the inducer of terminal senescence, underwent autophagic sequestration in the cytoplasm of ETO-treated cells, allowing alternative cell fates. Accordingly, failure of autophagy was accompanied by an accumulation of p16ink4a, nuclear disintegration, and loss of cell recovery. Together, these findings imply that OCT4A induction following DNA damage in PA-1 cells, performs a cell stress, rather than self-renewal, function by moderating the expression of p21Cip1, which alongside AMPK helps to then regulate autophagy. Moreover, this data indicates that exhaustion of autophagy, through persistent DNA damage, is the cause of terminal cellular senescence.

Introduction

The relationship between cancer cells, normal stem cells, and cancer stem cells represents a question of substantial current interest.[1] It has been proposed that transcription networks that confer stem cell properties such as self-renewal, plasticity, or an increased resistance to genotoxic stimuli in normal stem cells may perform a similar function in cancer cells.[2] This hypothesis is supported by the growing clinical evidence that expression of key embryonal stem cell (ESC) transcription factors POU1F5 (OCT4A), NANOG and SOX2, are associated with poorer prognosis through tumor resistance, recurrence and progression in a wide variety of cancers.[3-9] Furthermore, it has been demonstrated by several groups that ESC transcription factors can be upregulated in response to DNA damage where they likely play a role in regulating survival.[10-12]

Conversely, accelerated cellular senescence is a phenomenon that has also been shown to be induced by genotoxic treatments of cancer cells.[13] Cellular senescence has traditionally been considered a terminal cell fate.[13,14] However, more recently it has been shown to be reversible at early stages, at least in tumor cells.[15-18] Furthermore, a direct link between senescence and "stemness," essential cytological characteristics of a stem cell that distinguishes it from ordinary somatic cells, emerged in experiments where pluripotency is induced in normal cells.[19,20]

*Correspondence to: Thomas Robert Jackson; Email: tom.jackson-2@manchester.ac.uk
Submitted: 04/17/2015; Revised: 05/22/2015; Accepted: 05/27/2015
http://dx.doi.org/10.1080/15384101.2015.1056948

The molecular regulators of these processes in normal embryonal development, such as p21Cip1, are slowly becoming discerned.[21] One intriguing observation is that embryonal cellular senescence is associated with upregulation of the same pathways which govern the epithelial-mesenchymal transition (EMT).[22] This, apparently paradoxical, link between opposites in cell fate provides a challenge for scientific reasoning.

We have previously observed in IMR90 fibroblasts that a pre-senescent phenotype is associated with the appearance of self-renewal and senescence markers coupled to DNA damage.[23] We also demonstrated co-incident p53-dependent upregulation of 2 opposing cell fate regulators, p21Cip1 and OCT4A in embryonal carcinoma PA-1 cells treated with Etoposide (ETO).[24] We hypothesized that this bi-potential state favors DNA damage repair (DDR) while preventing full commitment to either senescence or self-renewal. In this system, p53 silencing promoted terminal senescence and premature mitosis. Together these data support the presence of a pre-senescent cell state which can arise in response to both senescence and stemness programmes being coactivated in response to genotoxic damage.

In the present study, we asked how key regulators of stemness (OCT4A, SOX2 and NANOG) and senescence (p16inka4a) behave in individual PA-1 cells during the response of ETO-induced DNA damage. Using siRNA silencing approaches we addressed the effect of OCT4A and p21Cip1 expression on each other and subsequent cell fates, determining the role of autophagy and how OCT4A activation impacts on the energy and genomic stress sensor and master metabolic regulator and activator of autophagy AMP-activated protein kinase (AMPK).

Results

Etoposide-treatment elicits a senescence-like phenotype in PA-1 cells

Following ETO treatment many PA-1 cells undergo gradual cell apoptosis and anoikis, while the remainder arrest in G2M and upregulate p53 and p21Cip.[24] G2M arrest and nuclear swelling were evident on day 3 after ETO treatment, with restoration of normal cell cycle and nuclear size 4 d later (**Fig. 1A and B**). Concurrent nuclear area assessments and DNA content measurements demonstrate that the nuclei of ETO treated cells increased in size irrespective of the stage of the cell cycle, but was most evident in G2M and polyploid cells (**Fig. 1C and D**). Increased nuclear area and DNA content were also accompanied by an increase in cellular granularity, as determined by an increase in side scatter detected by flow cytometry analysis (**Fig. 1E**), and autophagy (see below). The majority of cells displayed flattened morphology (**Fig. 1F**), but only a proportion displayed p16Ink4a nuclear positivity (**Fig. 1 G, H**). Furthermore, p16Ink4a expression was largely confined to the cytoplasm (**Fig. 1 G**). All of these features are indicative of senescence.

Heterogeneous expression of OCT4A and p21Cip1 following Etoposide treatment

We previously showed that the senescence marker p21Cip1 and the stemness marker OCT4A simultaneously increase and co-exist in the same cells following ETO treatment.[24] After confirming the pre-senescent phenotype of these cells, we next wished to explore how these critical factors for cell fate were dynamically regulated, integrated and diversified. As judged by flow cytometry ~60% of the cells become positive for both markers at the peak of the response (day 5), thereafter the expression of both markers and the proportion of double positive cells gradually decreases (**Fig. 2A**) as clonogenic, mitotic division ensues. To exclude the possible impact of the senescence-associated cytoplasmic and nuclear area changes on the flow cytometry measurements, semi-automatic image cytometry was undertaken, measuring the expression of both factors in the cell nucleus (apoptotic cells possessing very high p21Cip1 positivity lacking OCT4A were deliberately excluded from this analysis as distorting stoichiometry of measurements). Both the expression and variation of expression of OCT4A and p21Cip1 increased on day 3 after ETO treatment; and increased further on day 5 (**Fig2B and C**, **Fig. S1**) and a high number of double-positive cells confirmed (**Fig. 2B**).

OCT4A upregulation is not accompanied by changes in SOX2 or NANOG

In its function as a master regulator of pluripotency and self-renewal, OCT4A cooperates with SOX2 and NANOG whose expression are therefore required for maintaining the embryonic stem cell phenotype.[25] We thus explored the expression of these transcription factors in the DNA damage response of PA-1 cells. Immunoblotting confirmed that p53 increased in response to ETO from day 1, resulting in the induction of p21Cip1, which reached its maximum on day 5 (**Fig 3A**). As documented previously, OCT4A expression was present in control cells and increased following ETO treatment, coincident with p53 upregulation.[24] Weak expression of SOX2 was found in untreated cells but did not alter following ETO-treatment (**Fig. 3A**); a result confirmed by image cytometry measurements in individual cells (**Fig3B**, **Fig. S1**). NANOG was not detected in PA-1 cells by immunoblotting (**Fig 3A**) although rare NANOG positive cells (less than 5%) were found in control and ETO-treated samples by 3 different antibodies (Supplementary **Fig. 1**). Intriguingly, SOX2 failed to show unambiguous antagonism with p21Cip1, which has previously been reported as directly inhibiting SOX2 in neurodifferentiation.[26] Furthermore, SOX2 expression did not show significant correlation with its self-renewal partner OCT4A (data not shown). Together, these data suggest a dissociation of OCT4A from its self-renewal capacity when it is induced by p53 (in the presence of p21Cip1) in response to DNA damage.

OCT4A suppresses p21Cip1 and promotes an enhanced senescence phenotype

Given its potential lack of self-renewal capacity, we next investigated the role of OCT4A in PA-1 cells following ETO

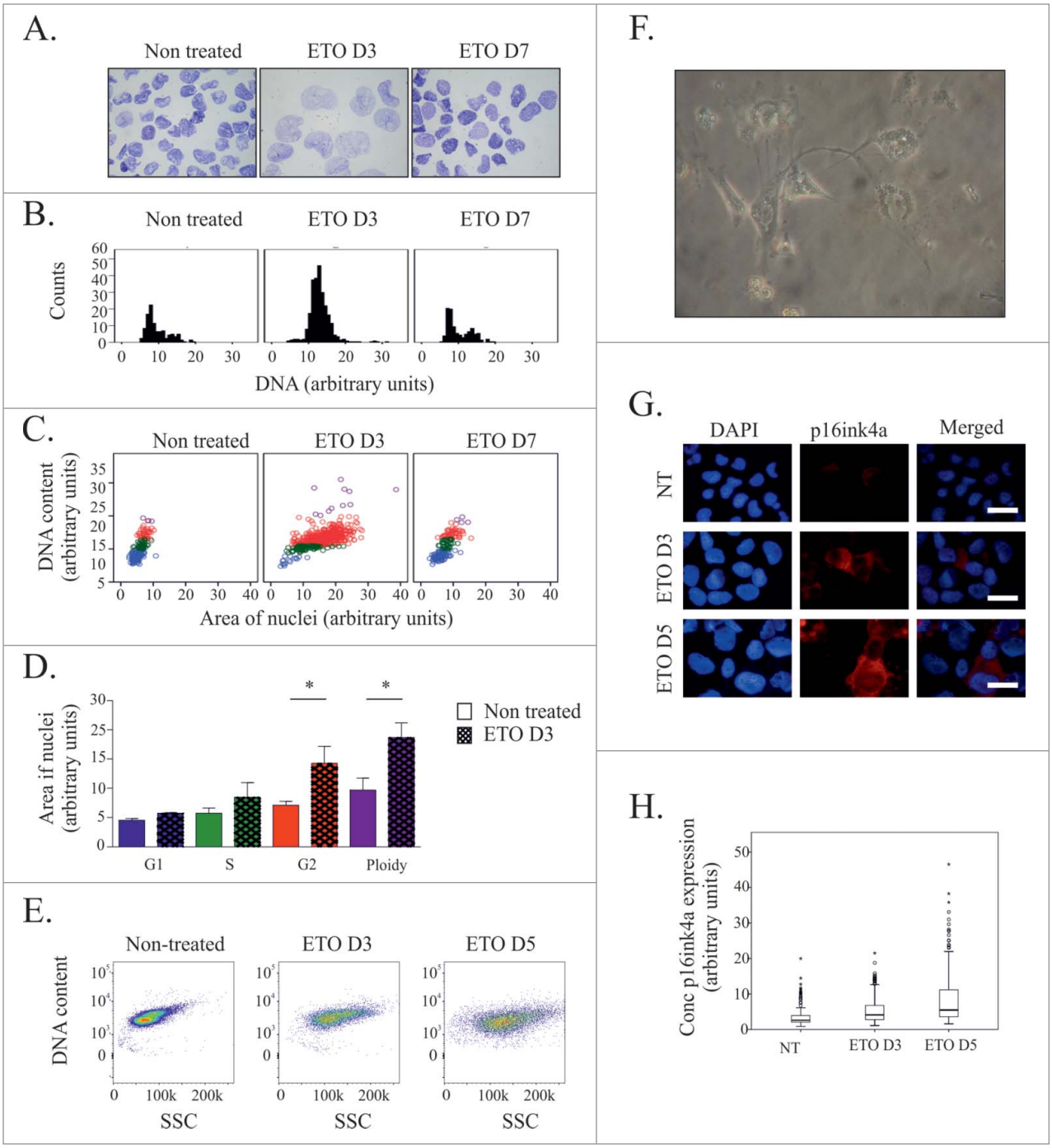

Figure 1. Senescent-like phenotype of ETO-treated PA-1 cells. PA-1 cells were treated with 8 μM ETO for 20 h before being replaced with fresh media. (**A-D**) DNA content and nuclear area were assessed using toluidine blue staining at indicated time points. (**A**) Images of toluidine blue stained nuclei at indicated time points. (**B**) Histograms of DNA content were produced and used to determine the cell cycle stage of individual cells. (**C**) Dot-plots of DNA content versus nuclei area with each cell colored according to cell cycle stage as determined by DNA content histograms: G1 (blue); S phase (green); G2 (red); purple (polyploid). A statistically significant difference in nuclear size between treated and non-treated cells was observed in G2 and polyploid fractions (*$p < 0.05$, $n = 3$). (**E**) Granularity of cells (SSC) was measured at indicated time points by flow cytometry. (**F**) Phase contrast microscopy of PA-1 cells displaying a flattened morphology. (**G**) Immunofluorescence staining for p16ink4a (red) and counterstained with DAPI at indicated time points demonstrating an increase in p16ink4a following ETO treatment. (**H**) Quantification of p16ink4a expression determined in individual cells by image cytometry displayed as a box plot showing its increase after ETO treatment. Images are representative for at least 3 individual experiments.

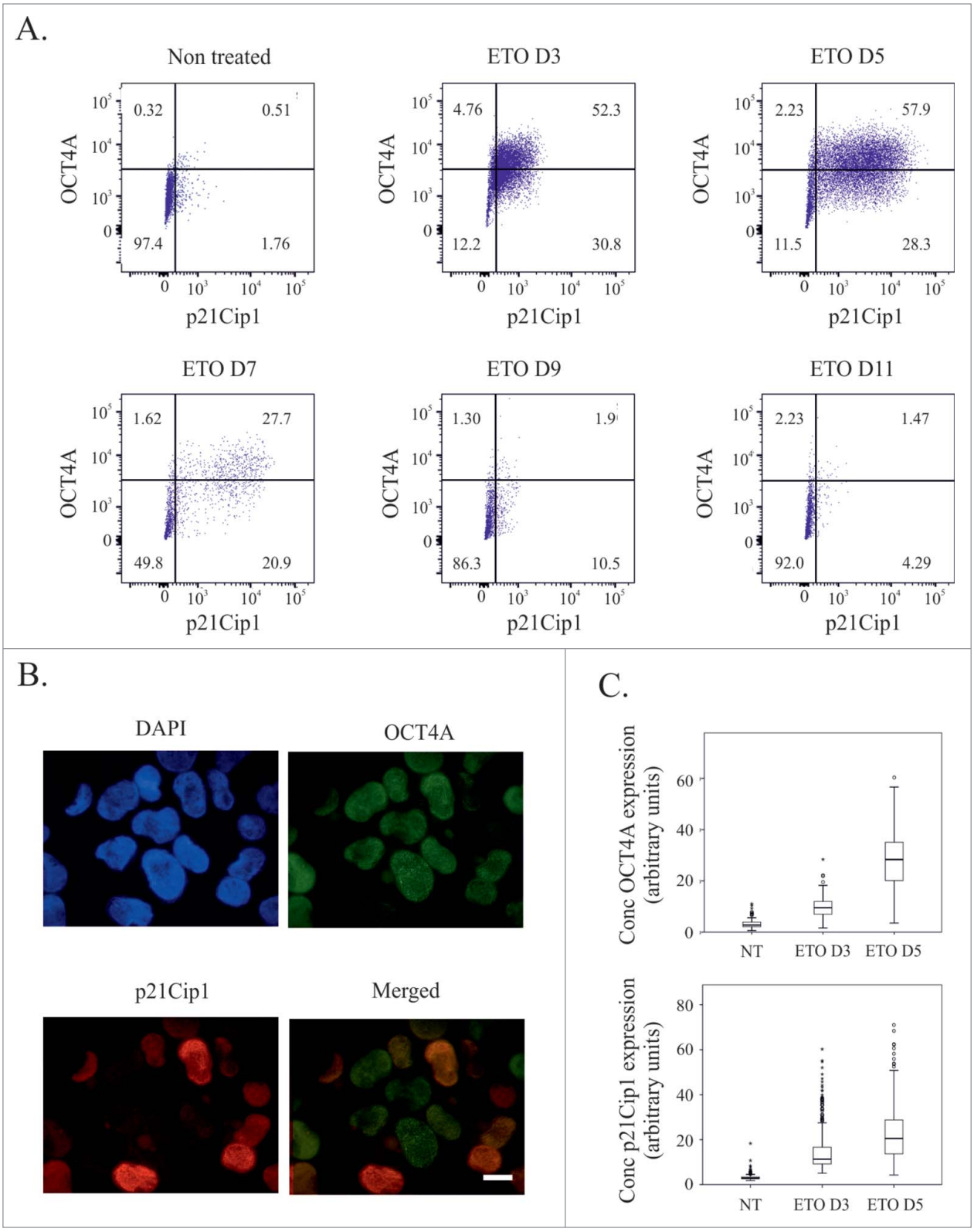

Figure 2. Expression of OCT4A and p21Cip1 following ETO treatment of PA-1 cells. (**A**) Dual staining for OCT4A and p21cip1 by immunofluorescence 3 d after ETO treatment. (**B**) Quantitation of OCT4A and p21Cip1 expression on day 3 and day 5 after ETO treatment as measured by image cytometry. (**C**) Detection of OCT4A and p21Cip1 by flow cytometry after ETO treatment. Data collected over 11 d indicate an increasing expression and heterogeneity, with numerous double positive cells at the time of maximal increase (day 5). Starting from day 7 their expression, double-positive population and degree of heterogeneity gradually decreases during the recovery of clonogenic growth.

treatment using siRNA. Prior to this analysis, we first established which OCT4 isoforms were expressed in PA-1 cells. Using a panel of specific mAb, immunoblotting revealed that OCT4B was undetectable in these cells both before and after ETO treatment (**Fig. S2**), consistent with published previously RT-PCR data.[24]

Having established that OCT4B was not expressed in PA-1 cells, siRNA silencing was used to assess the role of OCT4A in their response to ETO treatment. Efficient (80–95%) knock-down of OCT4A was confirmed with 3 different siRNA, in addition to a 3 siRNA pool (**Fig. S3**) and the molecular response to ETO was then examined by immunoblotting (**Fig 4A**) for key regulators of DNA damage, (pCHK2, p53, p21Cip1, and RAD51). These experiments revealed p53, RAD51 and pCHK2 were all upregulated from day 1 independently of OCT4A expression. p21Cip1 expression rose gradually from day 1 throughout the course of experiment as seen in previous experiments. Silencing of OCT4A resulted in a marked increase in p21Cip1 expression from day 1. These results imply that the presence of OCT4A induced by DNA damage suppresses p21Cip1 expression despite comparable levels of p53 expression and equivalent DNA damage as judged by RAD51 and pCHK2 expression.

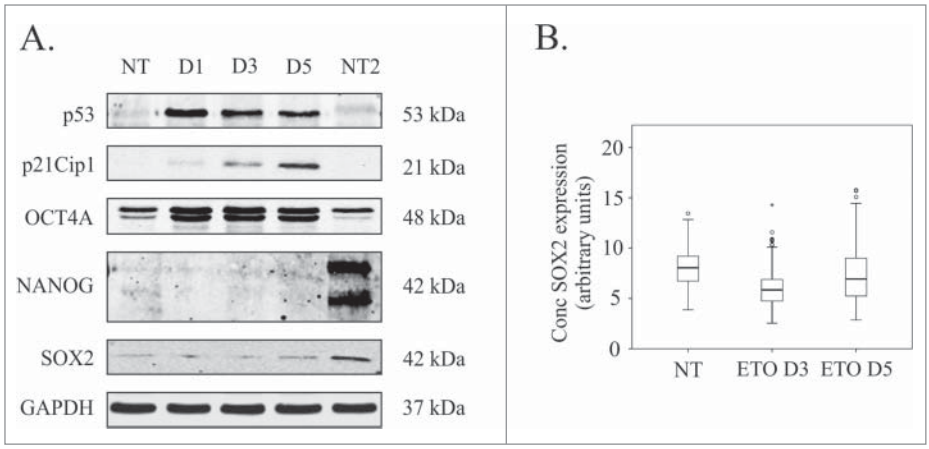

Figure 3. Analysis of pluripotency transcription factors in response to ETO treatment in PA-1 cells. (**A**) Protein expression of p53, p21Cip1, OCT4A, SOX2 and NANOG were analyzed by immunoblotting at indicated time points after ETO-treatment. GAPDH was used as a loading control NT2 cells were used as a positive control for pluripotency genes OCT4A, SOX2 and NANOG. p53 and p2Cip1 protein expression was upregulated in the DNA damage response. An upregulation of the OCT4A protein was detected from day 1 post ETO treatment, while SOX2 remained low and unchanged post ETO expression. NANOG was not detected in NT or ETO treated PA-1 cells. Results are representative of 3 independent experiments. (**B**) Semi-automatic image cytometry of SOX2 expression was performed on the nuclei of individual cells. Box-plots indicate the heterogeneity and expression levels measured. The data show that SOX2 remains unresponsive to ETO-treatment.

When investigating the cell cycle response, loss of OCT4A caused an almost identical phenotype to that previously reported with p53 silencing[24] i.e. OCT4A-silenced cells underwent a profound G2M arrest with apoptosis being greatly reduced (**Fig. 4B and C**). The cells displayed the large, flattened morphology and Sa-β-gal staining associated with senescence on day 5 (**Fig. 4D**), identical to that previously reported when silencing p53. Thus, the increase in G2M arrest and increased accelerated senescence previously observed with p53 silencing appears to be entirely due to the loss of the induction of OCT4A. Prolonged loss of OCT4A lead to the polyploidisation of these senescent cells and a reduction in clonal recovery (**Fig. 5**). The absence of off target effects was confirmed by repeating silencing and cell cycle analysis experiments with 3 separate siRNA molecules targeting different sequences of OCT4A mRNA (Supplementary **Fig. 4**).

p21Cip1 silencing does not affect OCT4A expression or cell cycle arrest

Having established that OCT4A suppresses p21Cip1 and a senescent phenotype we sought to investigate the possibility of a reciprocal suppression of OCT4A by p21Cip1. To do this p21Cip1 was silenced using siRNA. Silencing of p21Cip1 was efficient as judged by immunoblotting but was not found to affect the expression of OCT4A in the presence or absence of ETO treatment (**Fig. 6**). Furthermore, we detected no difference in the cell cycle profiles of p21Cip1-silenced cells compared to control siRNA treated cells following ETO treatment.

In summary, we found that OCT4A tempers p21Cip1 upregulation, restricting entry into senescence, indicating that co-expression defines the pre-senescent state. While p21Cip1 did not regulate OCT4A expression or change the cell cycle, depletion of OCT4A profoundly impacted it. We also found that p53-activated OCT4A does not support the pluripotency network in pre-senescent cells (owing to the lack of SOX2/NANOG co-ordination), leaving its biological role unclear. We, therefore, interrogated its possible role as a stress responder where one of these stresses may be metabolic. AMPK is a key sensor of metabolism and energy status.[27] Therefore, we next explored the activation of AMPK by virtue of its phosphorylation at Threonine 172 ($pAMPK^{Thr172}$), in relation to OCT4A expression.

AMPK and OCT4A are coordinately activated in response to ETO-treatment

The results of this comparative study are shown in **Fig. 7**. Microscopy of control, untreated, cells revealed heterogeneous $pAMPK^{Thr172}$ activation with expression in some cell nuclei and also in centrosomes, central spindle and mid-bodies of mitotic cells as described previously,[28] and rarely (<1% cells), in the cytoplasm (**Fig. 7A**, upper row). In ETO-treated cells the staining for AMPK increased and strikingly coincided with the localization and intensity of staining for OCT4A in most cells (**Fig. 7A**, second row) as also confirmed by IF measurements, where clear correlation was shown (**Fig. 7B**). However, while OCT4A is seen homogenously throughout the nucleus

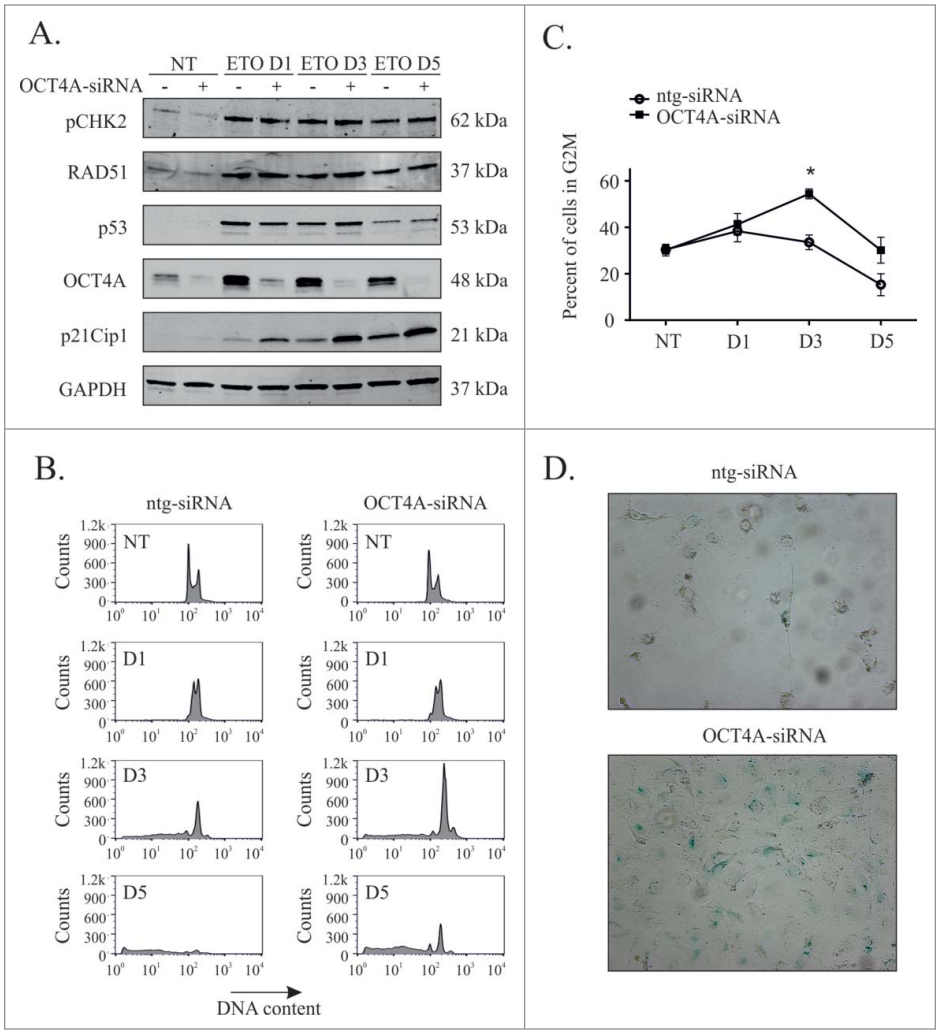

Figure 4. OCT4A suppresses p21, G2 arrest and induces senescence. PA-1 cells were treated with ntg-siRNA or OCT4-siRNA for 24 h before treatment with 8 μM ETO for 20 h and replacement with fresh media. (**A**) Protein expression was assessed at the indicated time points by immunoblotting. Cell lysates were made and assessed by immunoblotting for pCHK2, RAD51, p53, p21Cip1, OCT4A and GAPDH as a loading control. (**B**) Cells were fixed, stained with PtdIns and analyzed by flow cytometry. Both ntg-siRNA treated and OCT4-siRNA treated cells underwent a G2M arrest followibg ETO treatment, which is more profound at day 3 and 5 in OCT4A-siRNA-treated cells. There is subsequently a much lower extent of cell death (sub G1) in OCT4A-siRNA treated cells. (**C**) The G2M arrest was calculated from the DNA histograms shown in (**B**) and demonstrate significantly higher levels in OCT4A-silenced cells (*$p < 0.05$, $n = 3$). (**D**) PA-1 cells were treated with ETO as above and assessed for Sa-β-gal activity after 5 d Senescence, as monitored by Sa-β-gal activity, was increased by OCT4A-silencing. Both ntg-siRNA and OCT4A-siRNA treated cells became large following ETO treatment but non-silenced cells lacked Sa-β-gal activity.

pAMPK^{Thr172} staining revealed a fine (euchromatic) nuclear pattern, which indicates binding to chromatin, unlike OCT4A.

Intense staining of pAMPK^{Thr172} was also found in apoptotic cell nuclei and bodies, while OCT4A was not (**Fig. 7C**). In arrested metaphases appearing after ETO on day 4, pAMPK^{Thr172} was localized to multiple centrosomes, while OCT4A was not (**Fig. 7A**, second row). This difference in staining was confirmed by co-staining for γ-tubulin and AURORA B kinase (not shown). Together, these data indicate that OCT4A is co-ordinately regulated alongside pAMPK^{Thr172} in interphase cells but that in apoptotic cells their functions may differ. Moreover, the concordant expression of OCT4A and pAMPK^{Thr172} in interphase cells suggests that the p53-dependent OCT4A induction is a result of a stress response following ETO treatment.

As a part of its role as a central metabolic regulator, AMPK is directly involved in the regulation of autophagy.[29] In this regard, previous studies have shown that autophagy is implicated in the chemo-resistance to ETO and this effect is reversed by inhibition of AMPK, which led to cell death by apoptosis.[30]

Conversely, cellular senescence is also associated with autophagy[30] representing another potential cell fate phenotype following ETO-treatment.[24] p16ink4a is believed to drive irreversible senescence. [31] Therefore, we next decided to explore the relationship of p16ink4a and macroautophagy.

p16ink4a is sequestered by autophagy in ETO-treated cells

Autophagy was verified using immunofluorescence for p62 as a marker of autophagy. Post ETO treatment, an increase in the number of p62 foci/cell was observed by immunofluorescence (**Fig. 8A and B**) and mean number of p62 foci/cell in 3 independent experiments was shown to increase > fold5- (**Fig 8C**). Bafilomycin A (Baf) halted autophagic flux in ETO-treated cells (shown as an accumulation of LC3B in relation to LC3A), confirming functional autophagy and its suppression (**Fig. 8D**). Baf treatment also enhanced cell death preventing clonogenic recovery only in ETO-treated cells (**Fig. S5**), which indicates the importance of autophagy for cell survival after DNA damage.

We then assessed immunostaining for p16ink4a and LAMP2 in the presence and absence of Baf post ETO treatment. LAMP2 is an important regulator of lysosomal biogenesis, required for the maturation of functional autophagosomes. In control, untreated cells, p16ink4a was observed in ~5% of cells as small aggresomes, surrounded by LAMP2-positive foci (data not shown). In ETO-treated cells (day 4), the cytoplasm was highly enriched with LAMP2, while p16ink4a-positive aggresomes (larger and more numerous than in control) were sequestered in

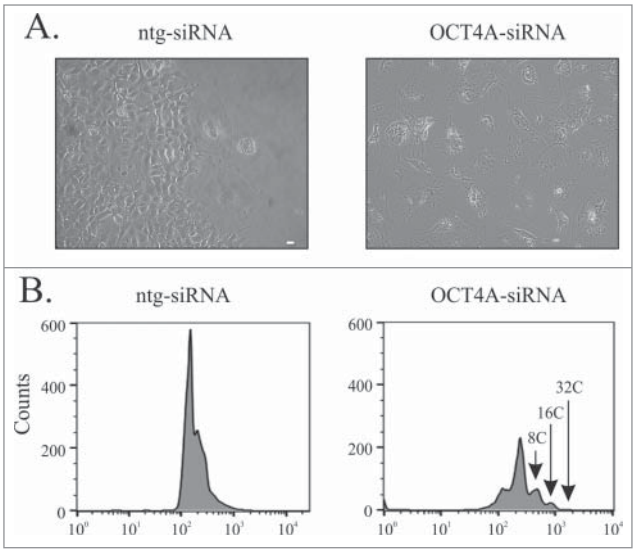

Figure 5. OCT4A silencing inhibits clonal recovery of ETO-treated PA-1 cells. PA-1 cells were treated with ntg-siRNA or OCT4A-siRNA for 24 h before treatment with 8 μM ETO for 20 h and replacement with fresh media. Cells were maintained until day 11. Clonal recovery was observed in non-silenced cells but not in OCT4A-silenced cells, which maintained a flat senescent like morphology. (**B**) Cells were fixed, stained with PI and analyzed by flow cytometry. A return of the G1 peak was observed in non-silenced ntg cells whereas OCT4A-silenced cells maintained a profound G2 arrest. OCT4A-silenced cells entered rounds of endoreduplication with genomes as large as 32C observed.

autophago-lysosomes (**Fig. 9 A and B**). Approximately 30% of cells were seen to accumulate large amounts of p16ink4a in multiple aggresomes, as measure by >3 aggresomes and/or diffusely detected within cytoplasm, or in large vacuoles (**Fig. 9A-C**), and often showed DNA in cytoplasm (**Fig. 9C**). The proportion of such cells, with high levels of p16ink4a, increased fold2- (29 ± 6 .5 and 58 ± 3 .5, +/− Baf, respectively) as measured on day 4. These observations indicate the important role of autophagy in sequestering and degrading p16ink4a in ETO-treated PA-1 cells, thus preventing senescence. They also show that a considerable proportion of ETO-treated cells suffer from exhaustion of autophagy.

Failure of autophagy to sequester p16ink4a in the cytoplasm is accompanied by drastic nuclear changes and loss of DNA

In ETO-treated samples counterstained with DAPI, we noted that the failure of macroautophagy to control and sequester p16ink4a in the cytoplasm coincided with prominent changes in cell nuclei, particularly following Baf treatment. Nuclei became thinner, less intensely DAPI-stained (e.g. **Fig. 9C**), or, more frequently, displaced to one of the cell poles by large autophagic vacuoles (**Fig. 9B**). Twisting, thinning, and disintegrating cell nuclei were the main phenotypes of ETO+Baf-treated cells. As detailed above, in their extreme distortions, the cell nuclei were displaced and squeezed by large autophagic vacuoles and attained a sickle-like shape (**Fig. 9D**). It remains possible that the loss of sequestration of p16ink4a, distortion of cell nuclei and loss of DNA are all linked, belonging to a related series of processes associated with exhausted autophagy, which is further exaggerated by Baf where full disintegration of the cell nucleus and alveolar LC3-positive cytoplasm are evident (**Fig. 10 A**).

Trying to understand how the penetrability of the cell nuclei was related to DNA damage we stained with an antibody (PL2–6) which detects a unique epitope involving a ternary complex of histones H2A and H2B and DNA at the site of the chromatin attachment to lamin B1.[32] We applied it to ETO-treated cell nuclei (day 4) combining it with a label for DNA damage (pCHK2). The result shows (**Fig. 10B**) bright nuclear staining with PL2–6 in cell nuclei without DNA damage and its reduction in cell nuclei containing DNA damage, possibly suggesting that binding to lamin B receptors in compromised.

In view of this data, we decided to use detailed stoichiometric DNA image cytometry following ETO treatment in the presence or absence of Baf. Typical histograms from one representative experiment are shown in **Fig. 10C**, while in **Fig. S6** comparative DNA histograms of selected normal- and sickle-shaped cell nuclei from ETO+Baf treatment are presented. Measurements from ETO-treated cells revealed a peak of delay in late S-phase, which was augmented after Baf treatment showing apparent redistribution from G2 (4C) into <4C, which was exaggerated in selected sickle-type nuclei of ETO+Baf-treated cells (**Fig. S6**). These data support our microscopic observations that DNA is preferentially lost from the sickle-like shape nuclei in the cells as a result of failed autophagic processing with the proportion of sickle-like nuclei cells with sickle-like nuclei in ETO-treated samples increased more than 2-fold (2.38 ± 0.2) following Baf treatment (n = 3).

Discussion

In this study, we expanded our investigation of the response of PA-1 embryonal carcinoma cells to DNA damaging chemotherapy. We previously observed,[24] a concurrent p53-dependent increase in OCT4A and p21Cip1 protein expression after ETO-treatment, with the resulting cells transiting through an apparently bi-potential state with hallmarks of both premature multicentriolar mitoses and senescence. Herein, we extended our analysis and highlight a hitherto unobserved DNA damage response (DDR) function of OCT4A following ETO treatment, which is different from its established pluripotency and self-renewal functions. This p53-dependant DDR-induced OCT4A is not coordinated with SOX2 or NANOG activity, but does serve to suppress p21Cip1. This finding is in accord with the previously shown observation that OCT4A can directly repress p21Cip1 expression by binding its promoter in the absence of SOX2 and NANOG. [33] Although not yet confirmed in other cell types or following different stimuli, this phenomenon likely relates to properties evidenced during embryonal 'stemness', as similar nuclear accumulation of OCT4A was similarly recently reported following laser beam damage of live ESC cells.[34]

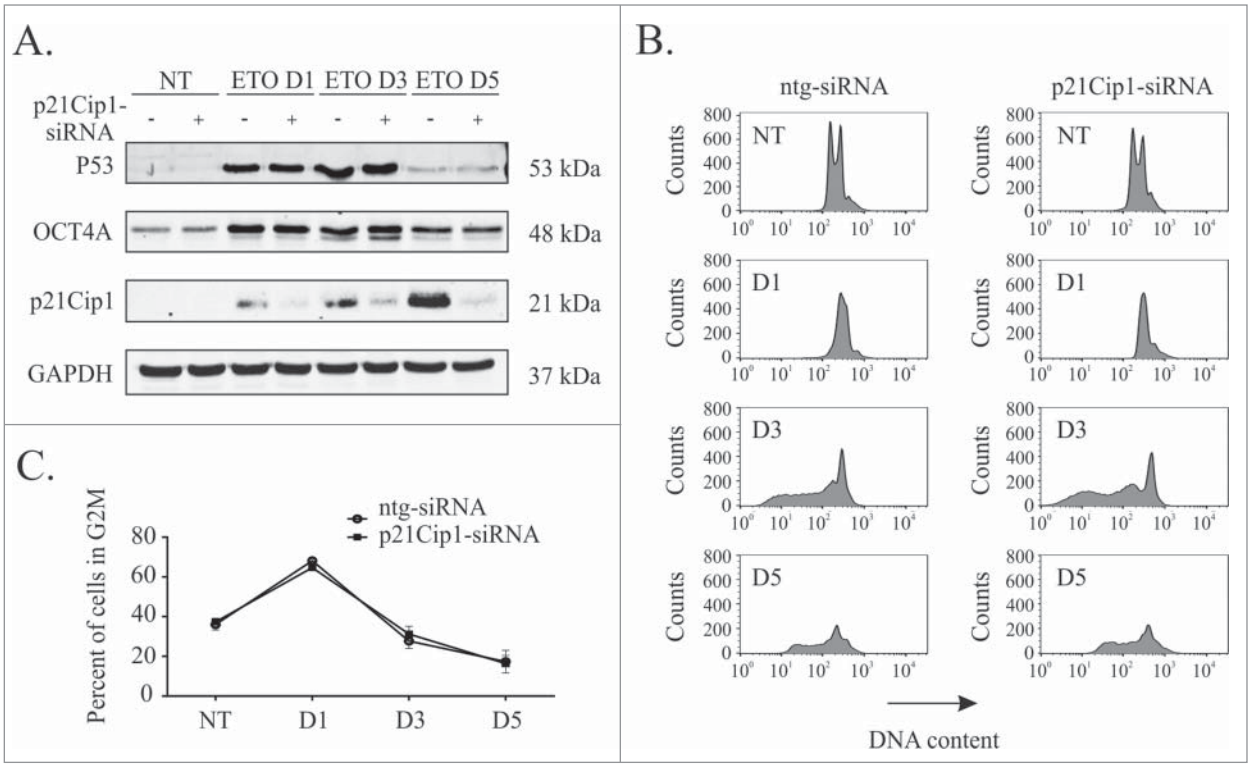

Figure 6. p21Cip1 expression does not affect G2M arrest in response to ETO treatment of PA-1 cells. PA-1 cells were treated with ntg-siRNA or p21Cip1-siRNA for 24 h before treatment with 8 μM ETO for 20 h and replacement with fresh media. (**A**) Expression of OCT4A, p21Cip1 and p53 were assessed at the indicated time points by immunoblotting. GAPDH was used as a loading control. (**B**) Cells were fixed, stained with PtdIns and analyzed by flow cytomtery. Both ntg-siRNA treated and p21Cip1-siRNA treated cells underwent a comparable G2M arrest after ETO treatment. (**C**) There was no significant difference in G2M arrest between p21Cip1 silenced and non-silenced cells.

Our measurements of OCT4A and p21Cip1 expression in individual cells revealed that cell fate, in response to extensive DNA damage, occurs with high levels of heterogeneity. Both factors increase coordinately with huge variations in expression, covering (at day 5) a wide spectrum of p21Cip1 and OCT4A expression.[35] These observations demonstrate a typical characteristic of self-organizing, adapting systems, using heterogeneity over time to provide bifurcations of cell fate choice.[36,37] The increased variance in both factors – from day 3 until day 7 – corresponds to the period with most prominent cell death (99% cells will die and only <1% has the chance to survive, likely representing the degree of challenge that they must overcome).[24] When OCT4A is silenced the level of p21Cip1 increases, more cells enter senescence and mitotic recovery is reduced, abrogating fragile balance in bifurcation point and removing the possibility for rare cells to choose survival as their fate. It is worth noting that this response was phenotypically identical to that seen when silencing p53.[24] We hypothesize that the loss of p53 or OCT4A in silencing experiments causes the loss of the embryonal G2M checkpoint leading to increased mitotic slippage, ultimately ending in terminal senescence rather than executing the G2M checkpoint function via apoptosis. Continued silencing of OCT4A inhibited clonogenic recovery post ETO treatment highlighting the importance of the pre-senescent G2M arrest for clonogenic recovery of the small percentage of cells that are able to repair their DNA damage. Silencing of OCT4A also leads to endoreplication in senescent cells further eluding to the presence of mitotic slippage.[38] p21Cip1 silencing experiments demonstrated that the observed G2M arrest was independent of p21Cip1 expression.

Mitotic survival of the ETO-treated cells ultimately originates from metastable pre-senescence. Theoretically, this means that the self-renewal function of OCT4A is finally restored. The attractor of self-renewal fate in individual cells is high NANOG,[39] released from direct suppression by p53[40] and activated by OCT4A-SOX2 heterodimer. Although NANOG is only found in a very small number of PA-1 cells, its role requires further exploration.

This moderator function of DDR-induced OCT4A occurs alongside activation of AMPK. AMPK is an evolutionary conserved low-energy checkpoint that operates as a master regulator of cellular metabolism and activator of autophagy. AMPK also acts as a genomic stress sensor that is required for the adaptation of metabolism switches and the DDR for efficient repair of DNA.[41] We previously observed a bidirectional relationship between AMPK and ATM/CHK2 pathways that integrates both the metabolic and DNA damage stress signaling.[42] AMPK activation was previously shown as necessary for maximal stress-induced transcription of p53-dependent genes that promote cell

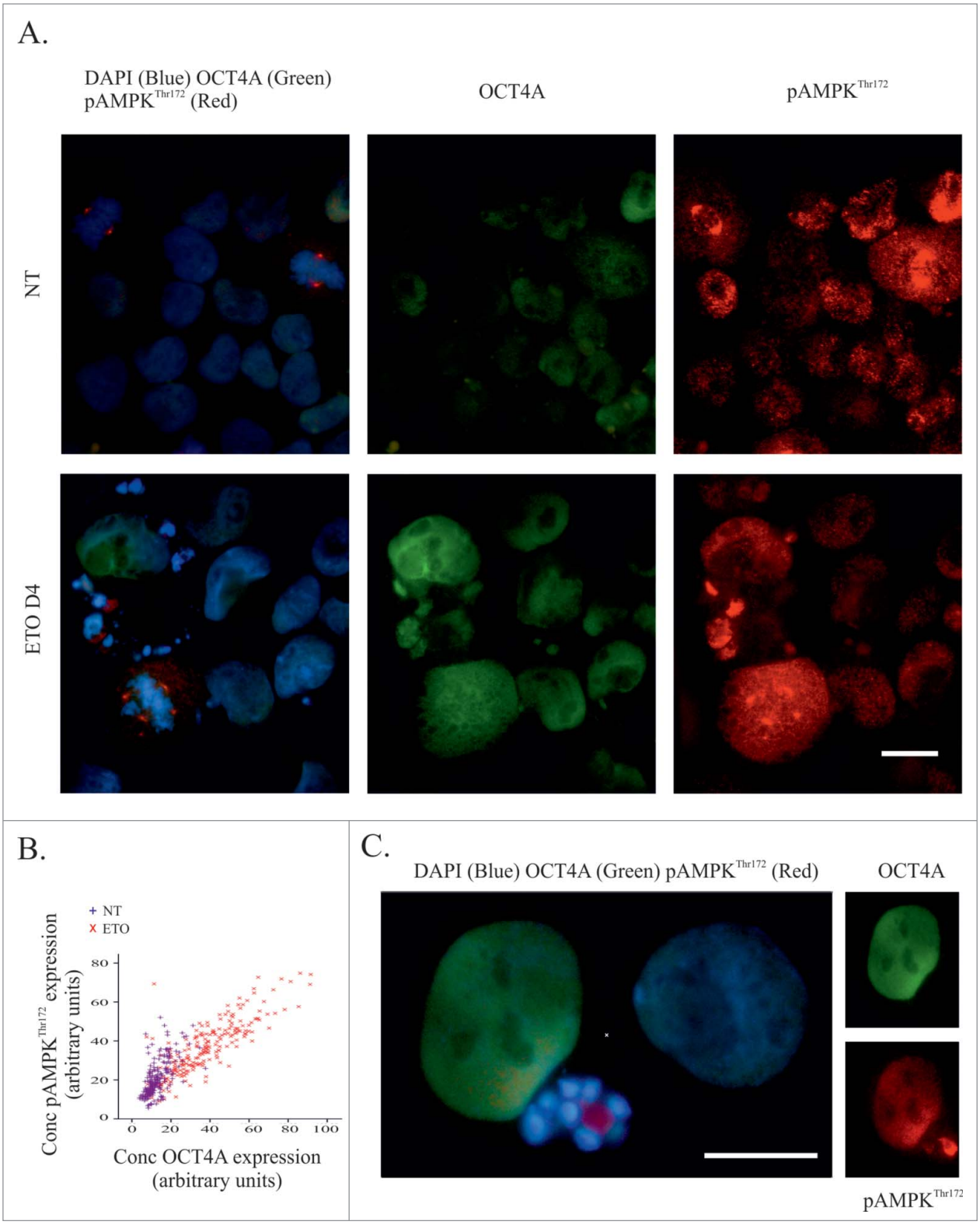

Figure 7. Activation of AMPK and OCT4A in response to ETO-treatment. PA-1 cells were treated with 8 μM ETO for 20 h and replacement with fresh media. Cells were harvested after 4 d before immunofluorescent staining for OCT4A, pAMPK^{Thr172} and DAPI. (**A**) Non-treated (upper panel) and ETO-treated (lower panel) samples were compared. AMPK and OCT4 are both activated by ETO (day 4) in interphase cells, however pAMPK is located in multiple centrosomes of arrested metaphases, while OCT4A does not; (**B**) scatterplot of image cytometry of OCT4A and pAMPK in individual cells assessed on day 4. There is a clear correlation between enhanced expression of OCT4A and pAMPK^{Thr172} of ETO-treated cells; (**C**) OCT4A and pAMPK^{Thr172} immunofluorescence in PA-1 cells 4 d after ETO-treatment. OCT4A and pAMPK^{Thr172} are mostly expressed in the same interphase nuclei, but an extremely high signal of pAMPK but not OCT4A is found within apoptotic cells. Staining of pAMPK^{Thr172} is associated with euchromatin, while the pattern of OCT4A staining is karyoplasmic (not bound to the chromatin). BRG – a 3-band optical filter. Bars =20 μm.

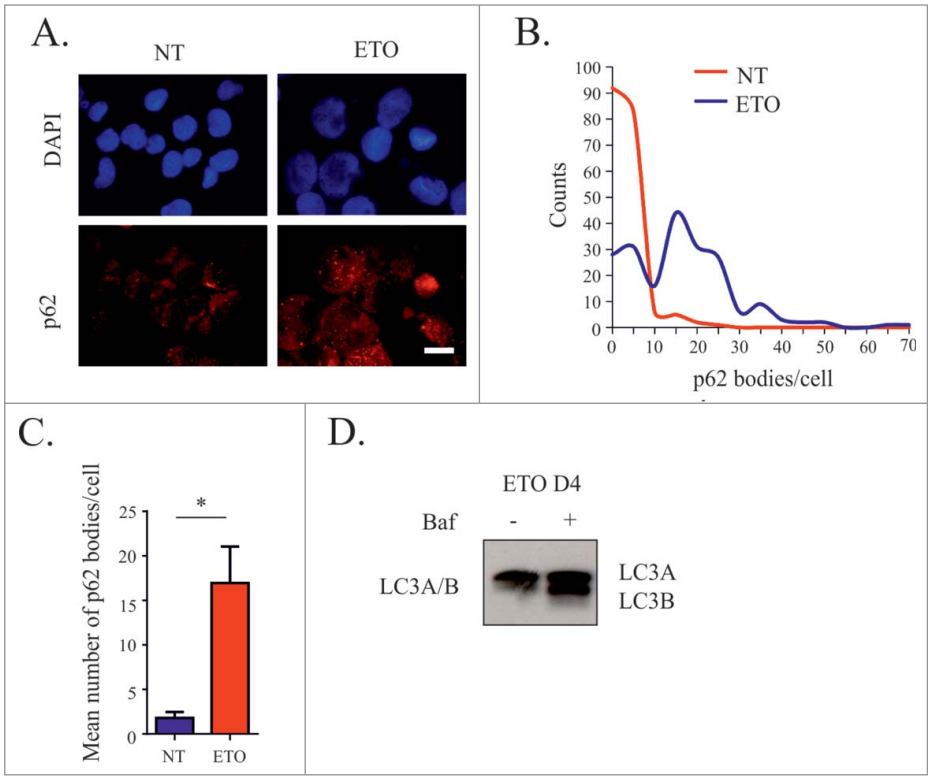

Figure 8. Assessment of macroautophagy following ETO treatment (day 4). PA-1 cells were treated with 8 μM ETO for 20 h and replacement with fresh media in the presence or absence of Baf. Cells were then stained for p62 and the number of p62 positive bodies per cell counted. (**A**) Immunofluorescent examples of staining for p62 showing foci (p62 bodies) in control and ETO-treated cells. (**B**) Representative histograms of p62 bodies/cell. (**C**) The average number of p62 bodies per cell was compared for NT and ETO treated cells from 3 independent experiments (* $p < 0.05$, $n = 3$) indicating activation by autophagy. (**D**) Immunoblotting analysis of the ratio of LC3A and LC3B with and without Baf treatment post ETO treatment. Enhanced levels of LC3B in relation to LC3A as a result of Baf treatment indicates interruption of autophagic flux in ETO treated cells. Bars = 20μm.

survival.[43] Interestingly, AMPK has also been shown to activate and stabilize p53.[44,45] Thus, the energetic stress-response of AMPK is tightly linked to the DDR of p53. The role of AMPK in the autophagy and cell death response after ETO has previously been reported.[30]

We previously revealed the p53-dependant DDR-induced elevation in OCT4A in PA-1 cells following ETO treatment. Therefore, it was not unexpected that DDR-induced OCT4A and AMPK activation should be coordinately regulated by ETO as we observed here. We found that while autophagy apparently remains functional, cells retaining both AMPK and DDR-induced OCT4A in cell nuclei are capable of preventing terminal senescence. This data are in accordance with the report by Chitikova and colleagues, [46] who demonstrated that silencing mTOR (the antagonist of AMPK suppressing autophagy) in irradiated, apoptosis-resistant cells caused a reversal of senescence. Thus OCT4A moderating p21Cip1 in collaboration with $pAMPK^{Thr172}$, supporting cells with metabolites and energy through autophagy and other means, channel cells through disadaptation chaos caused by high DNA damage toward a survival phenotype. ETO-treated PA-1 cells struggle against terminal senescence in particular by autophagic sequestration and removal of its regulator p16ink4a.

There is much controversy regarding markers of terminal senescence and even what the process really is. It has become recently apparent that terminal senescence is not only growth arrest,[47] moreover, it is intrinsically associated with the origin of EMT[22] and predicts poor clinical outcome after cancer treatment.[48]

In our previous and current article we have partly unravelled a mechanism showing that in response to DNA damage p53 induces 2 regulators of opposite cell fates. The setting is interesting: although they both are positively regulated by the same up-stream inducer, OCT4A suppresses p21Cip1, while the latter does not directly suppress OCT4A. Nevertheless, the scattering of the cells in expression of both through the phase space ending up in one of 2 cell fates presumes their reciprocity. The observation of cell-to-cell variability can also be a result from biological oscillations in time.[49] The best documented example of this is the p53-mdm2 oscillating system in which p53 oscillations are, indeed, crucial for cell recovery after DNA damage.[50] It is, therefore, possible that heterogeneity in p53 due to oscillations results in downstream heterogeneity of both OCT4A and p21Cip1 in PA-1 cells.

Senescence is intrinsically associated with macroautophagy induction (regulated by AMPK and persistent DNA damage). [51] Here, we found that persistent DNA damage was associated with destruction of the ternary complex of histones (H2A and H2B) and DNA in their attachment to nuclear lamin B1 using a unique antibody reagent.[32] This observation is in keeping with data of the thinning and disassembly of lamin B1 and leakage of DNA from cells as a feature of terminal senescence.[52]

Our DNA cytometric observations revealed a delay in late S-phase after ETO, augmented by BafA1. The consequence of this delay would be under-replication of heterochromatin,[53] appearance of single strand DNA breaks, demethylation and activation of the transposable elements (TE) ALU/LINE 1, whose mobility after ETO has already been described.[54] As sequestering ALU mRNA and LINE 1 by autophagy in the cytoplasm has been reported as a mechanism for protecting against transposition,[55] it therefore remains possible, (although purely speculative) that functional autophagy prevents terminal senescence in this manner also. The model with the scenario of terminal senescence

occurring due to activation of TE as discussed in several other studies.[56-58] It follows then that terminal senescence may in fact be mainly triggered by several mechanisms, which potentiate each other and result from failure of autophagy. Thus, autophagy should be a key target for preventing resistance of cancer stem cells to genotoxic therapies, a supposition supported by others.[59,60]

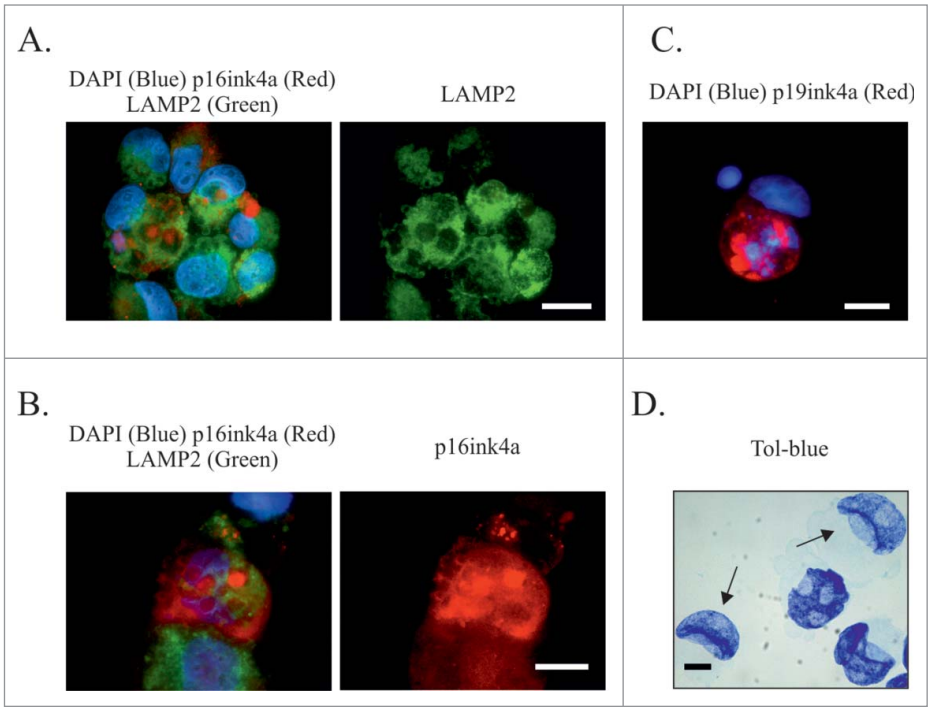

Figure 9. The relationship between autophagy functionality and senescence marker p16ink4ain ETO-treated PA-1 cells. PA-1 cells were treated with 8 μM ETO for 20 h without or with Baf, prior to media being removed and replaced with fresh media; cells were harvested 48h later (day 4). (**A, B**) imunofluorescent staining for p16ink4a (red), LAMP2 (green) or DAPI (blue). (**A**) As shown via the BRG optical filter, (**B**) only the green filter for LAMP2 demonstrating high level of functional autophagy sequestrating p16ink4a- containing aggresomes. (**B, C**) show examples of autophagic failure, where on (**B**) sequestration of p16ink4a is partly lost, diffusing in to the cytoplasm, while on (**C**) the dysfunction of autophagy is evidenced by a large vacuole overloaded with undigested p16ink4a. In all 3 cases, the nuclei are impaired: (**B**) 'laced'; (**C**) displaced and twisted by a large autophagic vacuole with some DNA lost from cell nucleus observed. These processes were observed both in ETO-treated (**B**) and more commonly in ETO+BAF(c) treated cells. (**D**) An image showing cell nuclei of normal and sickle-type shape as stained specifically for DNA with Toluidine bluein the ETO-teated specimen (sickle-like shaped nuclei are shown with arrows).

Materials and Methods

Cells

PA-1 is an ovarian teratocarcinoma (a germline tumor) cell-line, obtained from ATCC, with a stable near-diploid karyotype.[61] It possesses functional p53, in spite of possible acquisition of one mutated allele reported at passages over 407.[62] Importantly it retains the ability to differentiate into all 3 tissue types, thus possessing the features of embryonal carcinoma.[61] The NTera 2 (NT2) cell line, obtained from ATCC and used as a positive control for pluruipotency genes OCT4A, SOX2 and NANOG.

Antibodies

Primary antibodies and their uses are detailed in **Table 1**. Secondary antibodies and their uses are detailed in **Table 2**.

Cell culture and treatment

PA-1 cells were cultured in Dulbecco's modified Eagle's media (DMEM) supplemented with 10% foetal bovine serum (FBS) if not otherwise stated. NT2 cells were cultured in Dulbecco's modified Eagle's media (DMEM) supplemented with 10% foetal bovine serum (FBS). Cells were grown without antibiotics in 5% CO_2 at 37°C. Exponentially growing PA-1 cells were incubated with 4–8 μM ETO for 20 h. Following ETO treatment, cells were maintained by replenishing culture medium every 48h. Bafilomycin A (Baf A, Cayman Chemicals) 50 nM was added to the culture medium for 24h between day 3 to 4 after 20h treatment with 8 μM ETO.

Flow cytometry

Cells were harvested at relevant time points, washed in cold PBS and fixed with 70% ethanol for 20 min at room temperature. After two washes in tris buffered saline (TBS), cells were permeabilised with TBS/4% bovine serum albumin (BSA)/0.1% Triton X-100 for 10 min at room temperature. Samples were then incubated with mouse monoclonal anti-OCT4 antibody solution (Santa Cruz) and rabbit polyclonal p21Cip1 (Pierce) in TBS/4% BSA/0.1% Triton X-100 for 1h at room temperature. Following two washes in TBS, cells were incubated with goat anti-rabbit- IgG-Alexa Fluor 488 (A31627, Invitrogen) and Chicken anti-mouse IgG-Alexa Fluor 647 (A21463, Invitrogen) (1:200) in TBS/4% BSA/0.1% Triton × 100, for 30 min in the dark. DNA was counterstained with 10 μg/ml propidium iodide (PtdIns) in PBS, and assessed by flow cytometry using a FACS Aria (BD Biosciences) using Cell Quest Pro Software). Data was analyses using FlowJo analysis software.

Immunofluorescence

Cells were suspended in warm FBS and cytospun onto glass slides. Cytospins were fixed in methanol for 7 min at −20°C and dipped 10 times in ice cold acetone. Slides were then washed thrice in TBS 0.01% Tween 20 (TBST) for 5 min. Slides were subsequently blocked for 15 min in TBS, 0.05% Tween 20%, 1% BSA at room temperature. Samples were covered with TBS, 0.025% Tween 20%, 1% BSA containing primary antibody and incubated overnight at 4°C in a humidified chamber. Samples

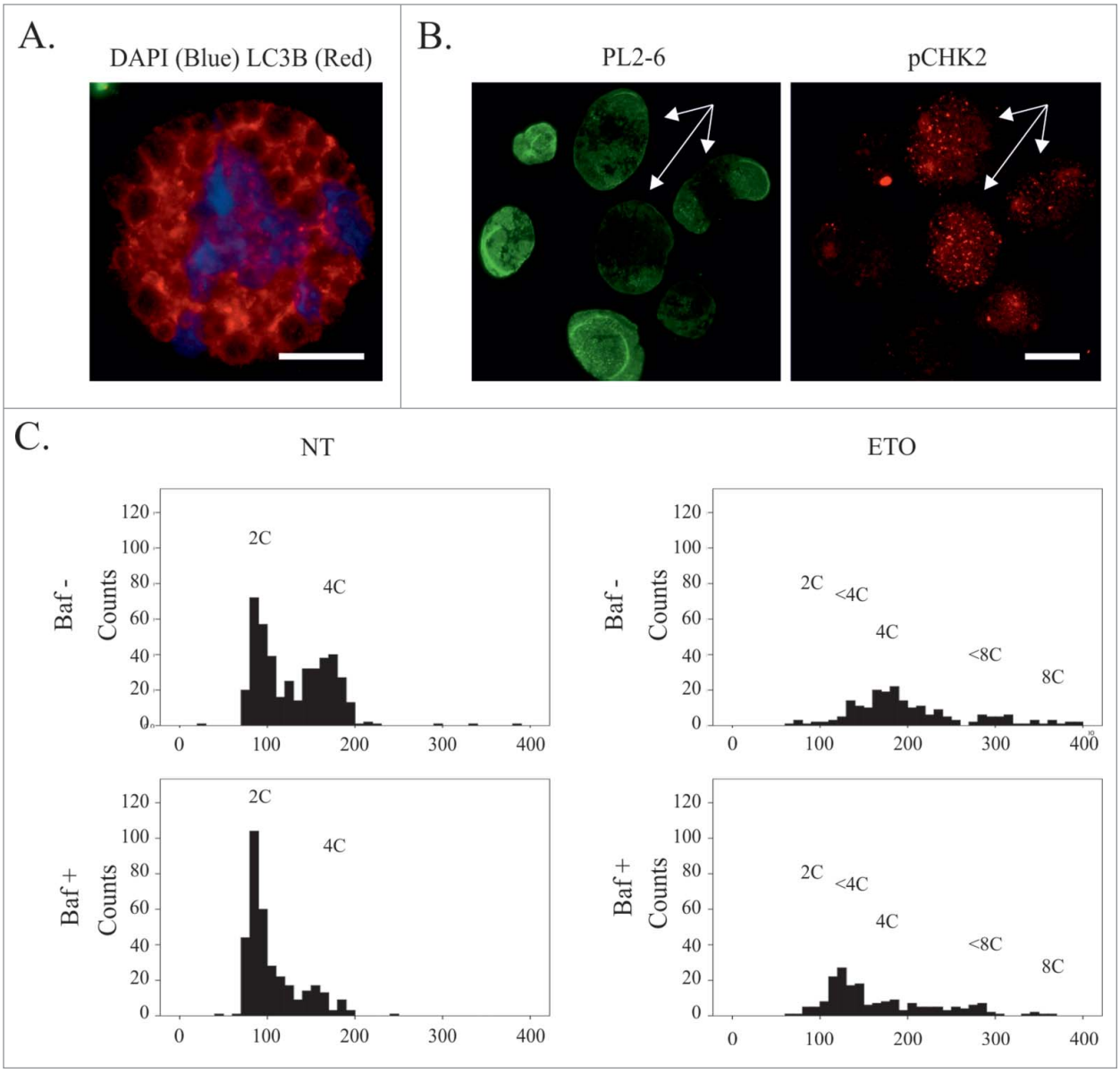

Figure 10. ETO and ETO+Baf impair cell nuclear integrity causing a delay in late S-phase in a proportion of cells with persistent DNA damage. (**A**) Disintegration of the nucleus is observed in ETO treated cells following prolonged Baf exposure (72h), where impaired autophagic flux is confirmed by alveolar structure of LC3B-positive cytoplasm in the absence of LC3 foci; Bars = 20 μm. (**B**) Persistent DNA damage leads to destruction of the epichromatin ternary complex (a specific conformation of nucleosomes attached to lamin B1) seen by a decrease in staining by the PI2–6 antibody where Chk2-positive foci is detected in ETO-treated PA1 cells at day 4. (**C**) Representative DNA histograms obtained by image cytometry of ETO-treated and ETO+BAF-treated cells samples (day 4 after treatment); one of 3 independent experiments. BafA alone causes partial arrest in G1 in control (NT)cells and a subsequent decrease of the G2 fraction; ETO-treatment induces G2-arrest, however, a proportion of cells remain delayed in late S-phase (<4C). Cells with the DNA content <4C and 4C(G2) still reach peaks of corresponding doubling, <8C and 8C. Suppression of autophagy by Baf in ETO-treated cells favors an increase of the proportion of cells in the <4C fraction and reduces the number of cells.

were then washed thrice in TBST and covered with TBST containing the appropriate secondary antibodies (Goat anti-mouse IgG Alexa Fluor 488 (A31619, Invitrogen) and Goat anti-rabbit-IgG Alexa Fluor 594 (A31631, Invitrogen)) and incubated for 40 min at room temperature in the dark. Slides were washed thrice for 5 min with TBST and once for 2 min in PBS. Samples were then counterstained with 0.25 μg/ml DAPI for 2 min, and finally embedded in Prolong Gold (Invitrogen). When staining for p-AMPKα1/2 (alone or in combination with the antibody for OCT4), fixation in 4% paraformaldehyde for 15 min was used, followed by washing thrice in PBS 0,1% glycine. Primary antibodies and their source are listed in **Table 1**.

Microscopy and immunofluorescence image cytometry

Slides were evaluated using a Leitz Ergolux L03–10 microscope equipped with Sony DXC 390P color video camera, for

Table 1. Primary antibodies

Antibody against	Description	Specificity/immunogen	Product nr and Manufacturer	Use*
AURORA B	Rabbit polyclonal	Peptide derived from within residues 1 – 100 of Human Aurora B	ab2254, Abcam	IF
p16INK4a	Rabbit polyclonal	C-terminus of human p16	ab7962, Abcam	IF
pCHK2 (phospho T68)	Rabbit polyclonal	Epitope around the phosphorylation site of Threonine 68 (VSTpQE) of human Chk2	ab38461, Abcam	IF, W
GAPDH	Mouse monoclonal, clone 6C5	Rabbit muscle GAPDH	ab8245, Abcam	W
LAMP-2	Mouse monoclonal	The details of the immunogen for this antibody are not available.	ab25631, Abcam	IF
LC3A/B	Rabbit polyclonal	Synthetic peptide between amino acids 1–100 of the human LC3 protein	PA1–16930, Pierce	IF
LC3B	Rabbit polyclonal	Peptide derived from within residues 1 – 100 of Human LC3B	ab63817, Abcam	IF
NANOG	Mouse monoclonal, clone NNG-811	Against human Nanog.	N3038, Sigma	IF
NANOG (23D2–3C6)	Mouse monoclonal	Full-length human recombinant protein expressed in bacteria	MA-1–017, Pierce	IF
NANOG H-155	Rabbit polyclonal	epitope corresponding to amino acids 151–305 mapping at the C-terminus of Nanog of human origin	sc-33759, Santa Cruz	IF
OCT3/4	Mouse monoclonal	Peptide raised against amino acids 1–134 of Oct-3/4 of human origin non cross-reactive with Oct-3/4 isoforms B and B1	sc-5279, Santa Cruz	IF, F, W
OCT4	Rabbit polyclonal, ChIP Grade	Peptide derived from within residues 300 to the C-terminus of Human Oct4	ab19857, Abcam	IF, W
p21Cip1	Rabbit polyclonal	Raised against a peptide mapping at the C-terminusof p21 of human origin	sc-397, Santa Cruz	IF
p21Cip1	Rabbit monoclonal	Synthetic peptide corresponding to residues near the carboxy-terminus of human p21	MA5–14949, Pierce	IF, F, W
p-AMPKα1/2 (Thr183/172)	Rabbit polyclonal	Epitope corresponding to phosphorylated Thr 172 of AMPKα1 of human origin	sc-101630, Santa Cruz	IF
PL2–6	Mouse monoclonal	autoimmune anti-nucleosome antibody specifically recognizes the peripheral surface of interphase chromatin and mitotic chromosomes, epichromatin epitope	A kind gift from Olins.[32]	IF
SOX2	Mouse monoclonal	Full-length human recombinant protein expressed in bacteria	MA1–014, Pierce	IF, W
SOX2	Rabbit polyclonal	Epitope corresponding to amino acids 131–195 of Sox-2 of human origin	sc-20088x, Santa Cruz	IF
SQSTM1 (p62)	Rabbit polyclonal	Epitope corresponding to amino acids 151–440 of SQSTM1 of human origin.	sc-25575, Santa Cruz	IF

*W, western; IF, immunofluorescent staining; F, flow cytometry.

microscopic observations; in addition to separate optical filters, a 3-band BRG (blue, red, green) optical filter (Leica) was used. Image cytometry was carried out by semi-automatic measuring fluorescence values for each cell nuclei in all 3 channels and analyzed using Image-Pro Plus 4.1 software (Media Cybernetics). Apoptotic cells, determined by nuclear morphology, were omitted from measurements.

DNA image cytometry

For DNA cytometry measurements, stoichiometric toluidine blue DNA staining was performed as previously.[63] In brief, cytospins were fixed in ethanol:acetone (1:1) for >30 min at 4°C and air dried. Slides were then treated with 5N HCl for 20 min at room temperature, washed in distilled water (5 × 1 min) and stained for 10 min with 0.05% toluidine blue in

Table 2. Secondary antibodies

Antibody	Conjugate	Product No.and Manufacturer	Use*
Goat anti-mouse IgG	Alexa Fluor 488	A31619, Invitrogen	IF
Chicken anti-mouse IgG	Alexa Fluor 647	A21463, Invitrogen	F
Goat anti-rabbit- IgG	Alexa Fluor 488	A11008, Invitrogen	F
Goat anti-rabbit- IgG	Alexa Fluor 594	A31631, Invitrogen	IF
Goat anti-rabbit IgG	HRP	32460,Thermo Fisher Scientific	W
Rabbit anti-mouse IgG	HRP	61–6520, Invitrogen	W
Goat anti-rabbit IgG	IRDye 800CW	926–32211, IRDye Antibodies	W
Goat anti-mouse IgG	IRDye 800CW	926–32210, IRDye Antibodies	W
Goat anti-rabbit IgG	Goat anti-rabbit IgG	926–68021, IRDye Antibodies	W

*W, western; IF, immunofluorescent staining; F, flow cytometry.

50% citrate-phosphate McIlvain buffer pH 4. Slides were rinsed with distilled water, blotted dry and dehydrated in butanol for 2×3 min at 37°C. Samples were then incubated twice in xylene for 3 min each at room temperature and embedded in DPX (Sigma). DNA content was measured as the integral optical density with a calibrated Sony DXC 390P video camera in the green channel. Nuclear area was calculated using Image-Pro Plus 4.1 software (Media Cybernetics). Apoptotic cells were omitted from measurements. The stoichiometry of DNA staining was verified using the values obtained for metaphases compared to anaphases and telophases (ratio 2.0); the summary error of the method and device was estimated to be less than 5%.

DNA flow cytometry

Cells (including those in media) were harvested at indicated time points, washed in PBS and re-suspended in hypotonic fluorochrome solution [50 μg/ml propidium iodide (PI), 0.1% (w/v) sodium citrate, 0.1% (v/v) Triton-X-100] and stored for at least 1 h in the dark at 4°C. Flow cytometry was performed using a FACScan (BD Biosciences) or Accuri™ C6 Cytometer (BD Biosciences). Data was analyses using FlowJo analysis software.

Detection of sa-β-galactosidase activity

The senescence β-galactosidase (sa-β-gal) staining kit (Cell Signaling Technology, UK) was used to detect sa-β-gal activity in cells according to the manufacturer's protocol.

Immunoblotting

For whole-cell lysates, cells were harvested, washed once with PBS and lysed using RIPA buffer containing protease inhibitor cocktail (Sigma P8340). Protein concentrations were determined by Bradford assay (Thermo Scientific), with 10–30 μg of total protein separated on 20% SDS polyacrylamide gels followed by electrophoretic transfer onto BA85 nitrocellulose membranes (Schleicher & Schuell GmbH) overnight. Equal protein loading in each lane was confirmed by Ponceau S staining. Blots were probed with appropriate antibodies primary and secondary detected using ECL Western Blotting Substrate (Pierce™, 32106).

For comparison of OCT4 isoforms protein was transferred onto immobilon-FC transfer membrane and probed with primary antibodies. Blots were then probed with fluorescent secondary antibodies and the signal was visualized using a LICOR Odyssey imaging system.

Small interfering RNA (siRNA) silencing

FlexiTube siRNA (SI04950274, SI04950267, SI04153835 and SI00690382; Qiagen) was used to silence OCT4A expression, and FlexiTube siRNA (SI00604905, SI00604898 and SI00299810; Qiagen) was used to silence p21Cip1 expression. ON-TARGET plus non-targeting siRNA #1 (Dharmacon) was used as a negative control. Cells were transfected with siRNA using HiPerfect (Qiagen) according to the manufacturer's protocol.

Methods of statistical analysis

Statistical analysis was performed in GraphPad (GraphPad Software Ltd). Student t-test was used to calculate the statistical significance of difference of means where appropriate. Statistical significance was accepted when $p < 0.05$. Graphs were plotted in GraphPad Prism 5 and IBM SPSS statistics 22.

Disclosure of Potential Conflicts of Interest

No potential conflicts of interest were disclosed.

Acknowledgments

The authors would like to thank Professor Hao and Dr Zhao, Dept of Histology and Embryology, Shandong University School of Medicine for the kind gift of the OCT4A and OCT4A-Psg-1 vector constructs and Ada and Donald Olins for providing the antibody for epichromatin.

Funding

The project was funded through an MRC PhD studentship and the Gerald Kerkut Charitable Trust, the University of Manchester Project Diamond and the Manchester Cancer Research Center and by the Europe Social Fund Project, project No.

2013/0023/1DP/1.1.1.2.0/13/APIA/VIAA/037. The publishing costs associated with this article are in part provided by the Manchester Project Diamond and by the Europe Social Fund Project, project No. 2013/0023/1DP/1.1.1.2.0/13/APIA/VIAA/037.

Supplemental Material

Supplemental data for this article can be accessed on the pub lisher's website publisher's website.

References

1. Ben-Porath I, Thomson MW, Carey VJ, Ge R, Bell GW, Regev A, Weinberg RA. An embryonic stem cell-like gene expression signature in poorly differentiated aggressive human tumors. Nat Genet 2008; 40(5): 499-507; PMID:18443585; http://dx.doi.org/10.1038/ng.127
2. Reya T, Morrison SJ, Clarke MF, Weissman IL. Stem cells, cancer, and cancer stem cells. Nature 2001; 414 (6859): 105-111; PMID:11689955; http://dx.doi.org/10.1038/35102167
3. Chiou SH, Yu CC, Huang CY, Lin SC, Liu CJ, Tsai TH, Chou SH, Chien CS, Ku HH, Lo JF. Positive correlations of Oct-4 and Nanog in oral cancer stem-like cells and high-grade oral squamous cell carcinoma. Clin Cancer Res 2008; 14(13): 4085-4095; PMID:18593985; http://dx.doi.org/10.1158/1078-0432.CCR-07-4404
4. Meng HM, Zheng P, Wang XY, Liu C, Sui HM, Wu SJ, Zhou J, Ding YQ, Li JM. Overexpression of nanog predicts tumor progression and poor prognosis in colorectal cancer. Cancer Biol Ther 2010; 9(4): 295-302; PMID:20026903; http://dx.doi.org/10.4161/cbt.9.4.10666
5. Du LT, Yang YM, Xiao XY, Wang CX, Zhang XH, Wang LL, Zhang X, Li W, Zheng GX, Wang S. others. Sox2 nuclear expression is closely associated with poor prognosis in patients with histologically node-negative oral tongue squamous cell carcinoma. Oral Oncol 2011; 47(8): 709-713; PMID:21689966; http://dx.doi.org/10.1016/j.oraloncology.2011.05.017
6. Lengerke C, Fehm T, Kurth R, Neubauer H, Scheble V, Muller F, Schneider F, Petersen K, Wallwiener D, Kanz L. others. Expression of the embryonic stem cell marker SOX2 in early-stage breast carcinoma. Bmc Cancer 2011; 11:42; PMID:21276239; http://dx.doi.org/10.1186/1471-2407-11-42
7. He W, Li K, Wang F, Qin YR, Fan QX. Expression of OCT4 in human esophageal squamous cell carcinoma is significantly associated with poorer prognosis. World J Gastroenterol 2012; 18(7): 712-719; PMID:22363145; http://dx.doi.org/10.3748/wjg.v18.i7.712
8. Huang P, Chen J, Wang L, Na YQ, Kaku H, Ueki H, Sasaki K, Yamaguchi K, Zhang K, Saika T. others. Implications of transcriptional factor, OCT-4, in human bladder malignancy and tumor recurrence. Med Oncol 2012; 29(2): 829-834; PMID:21533858; http://dx.doi.org/10.1007/s12032-011-9962-4
9. Lin T, Ding YQ, Li JM. Overexpression of Nanog protein is associated with poor prognosis in gastric adenocarcinoma. Med Oncol 2012; 29(2): 878-885; PMID:21336986; http://dx.doi.org/10.1007/s12032-011-9860-9
10. Lagadec C, Vlashi E, Della Donna L, Dekmezian C, Pajonk F. Radiation-Induced Reprogramming of Breast Cancer Cells. Stem Cells 2012; 30(5): 833-844; PMID:22489015; http://dx.doi.org/10.1002/stem.1058
11. Abubaker K, Latifi A, Luwor R, Nazaretian S, Zhu HJ, Quinn MA, Thompson EW, Findlay JK, Ahmed N. Short-term single treatment of chemotherapy results in the enrichment of ovarian cancer stem cell-like cells leading to an increased tumor burden. Mol Cancer 2013; 12; PMID:23537295; http://dx.doi.org/10.1186/1476-4598-12-24
12. Salmina K, Jankevics E, Huna A, Perminov D, Radovica I, Klymenko T, Ivanov A, Jascenko E, Scherthan H, Cragg M. others. Up-regulation of the embryonic self-renewal network through reversible polyploidy in irradiated p53-mutant tumour cells. Exp Cell Res 2010; 316(13): 2099-2112
13. Roninson IB. Tumor cell senescence in cancer treatment. Cancer Res 2003; 63(11): 2705-2715; PMID:12782571
14. Roninson IB, Broude EV, Chang BD. If not apoptosis, then what? - Treatment-induced senescence and mitotic catastrophe in tumor cells. Drug Resistance Updates 2001; 4(5): 303-313; PMID:11991684; http://dx.doi.org/10.1054/drup.2001.0213
15. Sherman MY, Meng L, Stampfer M, Gabai VL, Yaglom JA. Oncogenes induce senescence with incomplete growth arrest and suppress the DNA damage response in immortalized cells. Aging Cell 2011; 10(6): 949-961; PMID:21824272; http://dx.doi.org/10.1111/j.1474-9726.2011.00736.x
16. Puig PE, Guilly MN, Bouchot A, Droin N, Cathelin D, Bouyer F, Favier L, Ghiringhelli F, Kroemer G, Solary E. others. Tumor cells can escape DNA-damaging cisplatin through DNA endoreduplication and reversible polyploidy. Cell Biol Int 2008; 32(9): 1031-1043.
17. Roberson RS, Kussick SJ, Vallieres E, Chen SYJ, Wu DY. Escape from therapy-induced accelerated cellular senescence in p53-null lung cancer cells and in human lung cancers. Cancer Res 2005; 65(7): 2795-2803; PMID:15805280; http://dx.doi.org/10.1158/0008-5472.CAN-04-1270
18. Sabisz M. Skladanowski A. Cancer stem cells and escape from drug-induced premature senescence in human lung tumor cells Implications for drug resistance and in vitro drug screening models. Cell Cycle 2009; 8(19): 3208-3217; PMID:19738435; http://dx.doi.org/10.4161/cc.8.19.9758
19. Banito A, Rashid ST, Acosta JC, Li S, Pereira CF, Geti I, Pinho S, Silva JC, Azuara V, Walsh M. others. Senescence impairs successful reprogramming to pluripotent stem cells. Genes Dev 2009; 23(18): 2134-2139; PMID:19696146; http://dx.doi.org/10.1101/gad.1811609
20. Jaenisch R. Nuclear cloning and direct reprogramming: the long and the short path to Stockholm. Cell Stem Cell 2012; 11(6): 744-747; PMID:23217419; http://dx.doi.org/10.1016/j.stem.2012.11.005
21. Storer M, Mas A, Robert-Moreno A, Pecoraro M, Ortells MC, Di Giacomo V, Yosef R, Pilpel N, Krizhanovsky V, Sharpe J. others. Senescence is a developmental mechanism that contributes to embryonic growth and patterning. Cell 2013; 155(5): 1119-1130; PMID:24238961; http://dx.doi.org/10.1016/j.cell.2013.10.041
22. Kishi S, Bayliss PE, Hanai JI. A prospective epigenetic paradigm between cellular senescence and epithelial-mesenchymal transition in organismal development and aging. Transl Res 2015; 165(1): 241-249; PMID:24924348; http://dx.doi.org/10.1016/j.trsl.2014.05.007
23. Huna A, Salmina K, Jascenko E, Duburs G, Inashkina I, Erenpreisa J. Self-Renewal Signalling in Presenescent Tetraploid IMR90 Cells. J Aging Res 2011; 2011: 103253; PMID:21629737; http://dx.doi.org/10.4061/2011/103253
24. Jackson TR, Salmina K, Huna A, Inashkina I, Jankevics E, Riekstina U, Kalnina Z, Ivanov A, Townsend PA, Cragg MS. others. DNA damage causes TP53-dependent coupling of self-renewal and senescence pathways in embryonal carcinoma cells. Cell Cycle 2013; 12(3): 430-441; PMID:23287532; http://dx.doi.org/10.4161/cc.23285
25. Boyer LA, Lee TI, Cole MF, Johnstone SE, Levine SS, Zucker JR, Guenther MG, Kumar RM, Murray HL, Jenner RG. others. Core transcriptional regulatory circuitry in human embryonic stem cells. Cell 2005; 122 (6): 947-956; PMID:16153702; http://dx.doi.org/10.1016/j.cell.2005.08.020
26. Marques-Torrejon MA, Porlan E, Banito A, Gomez-Ibarlucea E, Lopez-Contreras AJ, Fernandez-Capetillo O, Vidal A, Gil J, Torres J, Farinas I. Cyclin-Dependent Kinase Inhibitor p21 Controls Adult Neural Stem Cell Expansion by Regulating Sox2 Gene Expression. Cell Stem Cell 2013; 12(1): 88-100; PMID:23260487; http://dx.doi.org/10.1016/j.stem.2012.12.001
27. Sun Y, Connors KE, Yang DQ. AICAR induces phosphorylation of AMPK in an ATM-dependent, LKB1-independent manner. Mol Cell Biochem 2007; 306(1-2): 239-245; PMID:17786544; http://dx.doi.org/10.1007/s11010-007-9575-6
28. Vazquez-Martin A, Lopez-Bonet E, Oliveras-Ferraros C, Perez-Martinez MC, Bernado L, Menendez JA. Mitotic kinase dynamics of the active form of AMPK (phospho-AMPK α(Thr172)) in human cancer cells. Cell Cycle 2009; 8(5): 788-791; PMID:19221486; http://dx.doi.org/10.4161/cc.8.5.7787
29. Kim J, Kundu M, Viollet B, Guan KL. AMPK and mTOR regulate autophagy through direct phosphorylation of Ulk1. Nat Cell Biol 2011; 13(2): 132-U71; PMID:21258367; http://dx.doi.org/10.1038/ncb2152
30. Xie BS, Zhao HC, Yao SK, Zhuo DX, Jin B, Lv DC, Wu CL, Ma DL, Gao C, Shu XM. others. Autophagy inhibition enhances etoposide-induced cell death in human hepatoma G2 cells. Int J Mol Med 2011; 27 (4): 599-606; PMID:21274505
31. Rayess H, Wang MB, Srivatsan ES. Cellular senescence and tumor suppressor gene p16. Int J Cancer 2012; 130(8): 1715-1725; http://dx.doi.org/10.1002/ijc.27316
32. Olins AL, Langhans M, Monestier M, Schlotterer A, Robinson DG, Viotti C, Zentgraf H, Zwerger M, Olins DE. An epichromatin epitope Persistence in the cell cycle and conservation in evolution. Nucleus-Austin 2011; 2(1): 47-60; http://dx.doi.org/10.4161/nucl.13655
33. Lee J, Go Y, Kang I, Han YM, Kim J. Oct-4 controls cell-cycle progression of embryonic stem cells. Biochem J 2010; 426: 171-181; PMID:19968627; http://dx.doi.org/10.1042/BJ20091439
34. Bartova E, Sustackova G, Stixova L, Kozubek S, Legartova S, Foltankova V. Recruitment of Oct4 Protein to UV-Damaged Chromatin in Embryonic Stem Cells. Plos One 2011; 6(12); PMID:22164208; http://dx.doi.org/10.1371/journal.pone.0027281
35. Gorban AN, Smirnova EV, Tyukina TA. Correlations, risk and crisis: From physiology to finance. Physica A-Statistical Mechanics Its Applications 2010; 389(16): 3193-3217: http://dx.doi.org/10.1016/j.physa.2010.03.035
36. Stuart A. Kauffman, "The origins of order: Self-organization and selection in evolution.,"in (Oxford university press, 2013)
37. Huang S. Non-genetic heterogeneity of cells in development: more than just noise. Development 2009; 136 (23): 3853-3862; PMID:19906852; http://dx.doi.org/10.1242/dev.035139
38. Edgar BA, Orr-Weaver TL. Endoreplication cell cycles: More for less. Cell 2001; 105(3): 297-306; PMID:11348589; http://dx.doi.org/10.1016/S0092-8674(01)00334-8
39. Kalmar T, Lim C, Hayward P, Munoz-Descalzo S, Nichols J, Garcia-Ojalvo J, Arias AM. Regulated Fluctuations in Nanog Expression Mediate Cell Fate Decisions in Embryonic Stem Cells. Plos Biol 2009; 7(7); PMID:19582141; http://dx.doi.org/10.1371/journal.pbio.1000149

40. Lin TX, Chao C, Saito S, Mazur SJ, Murphy ME, Appella E, Xu Y. P53 induces differentiation of mouse embryonic stem cells by suppressing Nanog expression. Nat Cell Biol 2005; 7(2): 165-U80; PMID:15619621; http://dx.doi.org/10.1038/ncb1211
41. Sanli T, Steinberg GR, Singh G, Tsakiridis T. AMP-activated protein kinase (AMPK) beyond metabolism A novel genomic stress sensor participating in the DNA damage response pathway. Cancer Biol Ther 2014; 15 (2): 156-169; PMID:24100703; http://dx.doi.org/10.4161/cbt.26726
42. Vazquez-Martin A, Oliveras-Ferraros C, Cufi S, Martin-Castillo B, Menendez JA. Metformin activates an Ataxia Telangiectasia Mutated (ATM)/Chk2-regulated DNA damage-like response. Cell Cycle 2011; 10(9): 1499-1501; PMID:21566461; http://dx.doi.org/10.4161/cc.10.9.15423
43. Bungard D, Fuerth BJ, Zeng PY, Faubert B, Maas NL, Viollet B, Carling D, Thompson CB, Jones RG, Berger SL. Signaling Kinase AMPK Activates Stress-Promoted Transcription via Histone H2B Phosphorylation. Science 2010; 329(5996): 1201-1205; PMID:20647423; http://dx.doi.org/10.1126/science.1191241
44. Jones RG, Plas DR, Kubek S, Buzzai M, Mu J, Xu Y, Birnbaum MJ, Thompson CB. AMP-activated protein kinase induces a p53-dependent metabolic checkpoint. Mol Cell 2005; 18(3): 283-293; PMID:15866171; http://dx.doi.org/10.1016/j.molcel.2005.03.027
45. Lee CW, Wong LLY, Tse EYT, Liu HF, Leong VYL, Lee JMF, Hardie DG, Ng IOL, Ching YP. AMPK Promotes p53 Acetylation via Phosphorylation and Inactivation of SIRT1 in Liver Cancer Cells. Cancer Res 2012; 72(17): 4394-4404; PMID:22728651; http://dx.doi.org/10.1158/0008-5472.CAN-12-0429
46. Chitikova ZV, Gordeev SA, Bykova TV, Zubova SG, Pospelov VA, Pospelova TV. Sustained activation of DNA damage response in irradiated apoptosis-resistant cells induces reversible senescence associated with mTOR downregulation and expression of stem cell markers. Cell Cycle 2014; 13(9): 1424-1439; PMID:24626185; http://dx.doi.org/10.4161/cc.28402
47. Blagosklonny MV. Cell cycle arrest is not senescence. Aging-Us 2011; 3(2): 94-101.
48. Wang Q, Wu PC, Dong DZ, Ivanova I, Chu E, Zeliadt S, Vesselle H, Wu DY. Polyploidy road to therapy-induced cellular senescence and escape. Int J Cancer 2013; 132(7): 1505-1515; http://dx.doi.org/10.1002/ijc.27810
49. Brock A, Chang H, Huang S. OPINION Non-genetic heterogeneity - a mutation-independent driving force for the somatic evolution of tumours. Nat Rev Genet 2009; 10(5): 336-342; PMID:19337290; http://dx.doi.org/10.1038/nrg2556
50. Purvis JE, Karhohs KW, Mock C, Batchelor E, Loewer A, Lahav G. p53 Dynamics Control Cell Fate. Science 2012; 336(6087): 1440-1444; PMID:22700930; http://dx.doi.org/10.1126/science.1218351
51. Capparelli C, Chiavarina B, Whitaker-Menezes D, Pestell TG, Pestell RG, Hulit J, Ando S, Howell A, Martinez-Outschoorn UE, Sotgia F, others. CDK inhibitors (p16/p19/p21) induce senescence and autophagy in cancer-associated fibroblasts, "fueling" tumor growth via paracrine interactions, without an increase in neo-angiogenesis. Cell Cycle 2012; 11(19): 3599-3610; PMID:22935696; http://dx.doi.org/10.4161/cc.21884
52. Ivanov A, Pawlikowski J, Manoharan I, van Tuyn J, Nelson DM, Rai TS, Shah PP, Hewitt G, Korolchuk VI, Passos JF, others. Lysosome-mediated processing of chromatin in senescence. J Cell Biol. 2013; 202(1): 129-143; PMID:23816621; http://dx.doi.org/10.1083/jcb.201212110
53. Nagl Walter. Endopolyploidy and polyteny in differentiation and evolution. 1978
54. Hagan CR, Sheffield RF, Rudin CM. Human Alu element retrotransposition induced by genotoxic stress. Nat Genet 2003; 35(3): 219-220; PMID:14578886; http://dx.doi.org/10.1038/ng1259
55. Guo HS, Chitiprolu M, Gagnon D, Meng LR, Perez-Iratxeta C, Lagace D, Gibbings D. Autophagy supports genomic stability by degrading retrotransposon RNA. Nat Commun 2014; 5:5276
56. Wang JR, Geesman GJ, Hostikka SL, Atallah M, Blackwell B, Lee E, Cook PJ, Pasaniuc B, Shariat G, Halperin E, others. Inhibition of activated pericentromeric SINE/Alu repeat transcription in senescent human adult stem cells reinstates self-renewal. Cell Cycle 2011; 10(17): 3016-3030; PMID:21862875; http://dx.doi.org/10.4161/cc.10.17.17543
57. Baker DJ, Sedivy JM. Probing the depths of cellular senescence. J Cell Biol 2013; 202(1): 11-13; PMID:23816622; http://dx.doi.org/10.1083/jcb.201305155
58. Cecco M, Criscione SW, Peckham EJ, Hillenmeyer S, Hamm EA, Manivannan J, Peterson AL, Kreiling JA, Neretti N, Sedivy JM. Genomes of replicatively senescent cells undergo global epigenetic changes leading to gene silencing and activation of transposable elements. Aging Cell 2013; 12(2): 247-256; PMID:23360310; http://dx.doi.org/10.1111/acel.12047
59. Sui X, Chen R, Wang Z, Huang Z, Kong N, Zhang M, Han W, Lou F, Yang J, Zhang Q, others. Autophagy and chemotherapy resistance: a promising therapeutic target for cancer treatment. Cell Death Dis 2013; 4: e838
60. Dorr JR, Yu Y, Milanovic M, Beuster G, Zasada C, Dabritz JHM, Lisec J, Lenze D, Gerhardt A, Schleicher K, others. Synthetic lethal metabolic targeting of cellular senescence in cancer therapy. Nature 2013; 501 (7467):421-5; PMID:23945590; http://dx.doi.org/10.1038/nature12437
61. Zeuthen J, Norgaard JOR, Avner P, Fellous M, Wartiovaara J, Vaheri A, Rosen A, Giovanella BC. Characterization of A Human Ovarian Teratocarcinoma-Derived Cell-Line. Int J Cancer 1980; 25(1): 19-32; http://dx.doi.org/10.1002/ijc.2910250104
62. Gao C, Miyazaki M, Li JW, Tsuji T, Inoue Y, Namba M. Cytogenetic characteristics and p53 gene status of human teratocarcinoma PA-1 cells in 407–445 passages. Int J Mol Med 1999; 4(6): 597-600; PMID:10567668
63. Erenpreisa J, Freivalds T. Anisotropic staining of apurinic acid with toluidine blue. Histochemistry 1979; 60 (3): 321-325; PMID:89109; http://dx.doi.org/10.1007/BF00500660

3.4. Autophay eliminates chromatin in depolyploidising therapy-induced giant tumour cells – Original paper IV

Cell Biology International

Cell Biol. Int. (2011) 35, 687–695 (Printed in Great Britain)

online data

Research Article

Polyploid tumour cells elicit paradiploid progeny through depolyploidizing divisions and regulated autophagic degradation

Jekaterina Erenpreisa[1]*, Kristine Salmina*, Anda Huna*, Elizabeth A. Kosmacek[†], Mark S. Cragg[‡], Fiorenza Ianzini[†,§,‖] and Alim P. Anisimov[¶]

* Latvian Biomedical Centre, Ratsupites 1, Riga LV-1067, Latvia
† Department of Pathology, University of Iowa, Iowa City, IA, U.S.A.
‡ Cancer Sciences Division, Southampton University School of Medicine, General Hospital, Southampton SO16 6YD, U.K.
§ Department of Radiation Oncology, University of Iowa, Iowa City, IA, U.S.A.
‖ Department of Biomedical Engineering, University of Iowa, Iowa City, IA, U.S.A.
¶ Far-Eastern Federal University, Vladivostok, Russian Federation

Abstract

'Neosis' describes the process whereby p53 function-deficient tumour cells undergo self-renewal after genotoxic damage apparently via senescing ETCs (endopolyploid tumour cells). We previously reported that autophagic digestion and extrusion of DNA occurs in ETC and subsequently revealed that self-renewal transcription factors are also activated under these conditions. Here, we further studied this phenomenon in a range of cell lines after genotoxic damage induced by gamma irradiation, ETO (etoposide) or PXT (paclitaxel) treatment. These experiments revealed that chromatin degradation by autophagy was compatible with continuing mitotic activity in ETC. While the actively polyploidizing primary ETC produced early after genotoxic insult activated self-renewal factors throughout the polygenome, the secondary ETC restored after failed multipolar mitosis underwent subnuclei differentiation. As such, only a subset of subnuclei continued to express OCT4 and NANOG, while those lacking these factors stopped DNA replication and underwent degradation and elimination through autophagy. The surviving subnuclei sequestered nascent cytoplasm to form subcells, while being retained within the confines of the old ETC. Finally, the preformed paradiploid subcells became released from their linking chromosome bridges through autophagy and subsequently began cell divisions. These data show that 'neotic' ETC resulting from genotoxically damaged p53 function-deficient tumour cells develop through a heteronuclear system differentiating the polyploid genome into rejuvenated 'viable' subcells (which provide mitotically propagating paradiploid descendents) and subnuclei, which become degraded and eliminated by autophagy. The whole process reduces aneuploidy in descendants of ETC.

Keywords: autophagy; neosis; p53 mutant tumour; polyploidy; self-renewal; senescence

1. Introduction

Somatic polyploidy (endopolyploidy) and autophagy are paradoxically involved in execution of the opposing effects on tumour growth. While most ETC (endopolyploid tumour cells) induced after genotoxic or spindle damage of tumour cells lacking wild-type p53 function are lost for reproduction through mitotic death, apoptosis, necrosis or accelerated senescence (Ianzini and Mackey, 1997; Mackey and Ianzini, 2000; Shay and Roninson, 2004; Vakifahmetoglu et al., 2008), the capability of a small fraction of ETC to depolyploidize and provide clonogenic descendants has been repeatedly demonstrated (Baroja et al., 1998; Illidge et al., 2000; Sundaram et al., 2004; Puig et al., 2008; Ianzini et al. 2009; Vitale et al., 2010). In turn, although autophagy is a hallmark of cellular senescence (Kondo and Kondo, 2006; Vellai, 2009), it is activated upon acute induction of senescence (Galluzzi et al., 2009; Young et al., 2009) and may be oncosuppressive in certain contexts (Morselli et al., 2009; Galluzzi et al., 2010) or, when excessive, may accompany cell death (Scarlatti et al., 2009); both chemotherapy- and metabolic stress-induced activation of the autophagic pathway reportedly contributes to the survival of tumour cells (Edinger and Thompson, 2004; Debnath et al., 2005; Morselli et al., 2009; Galluzzi et al., 2010). In addition, autophagy extends organismal lifespan (Madeo et al., 2010).

Several years ago Sundaram, Rajaraman and colleagues (Sundaram et al., 2004; Rajaraman et al., 2006; Rajaraman et al., 2007) proposed the 'neosis' hypothesis to explain the rejuvenation and restoration of immortality through the descendents of supposedly senescing ETC based upon their interpretations of live cell imaging experiments. Subsequently, Tam et al. (2007) suggested that the reverse of cellular senescence may be associated with the capability of aging somatic cells to reactivate key embryonal proteins. Blagosklonny (2007) suggested that proliferating progenitors of cancer stem cells can be activated to become 'stemloids'. There are many indications in literature that cancer cells

[1] To whom correspondence should be addressed (email katrina@biomed.lu.lv).

Abbreviations: ELCS, envelope-limited chromatin sheet; ETCs, endopolyploid tumour cells; ETO, etoposide; FCS, fetal calf serum; FMM, failed multipolar mitosis; IF, immunofluorescence; MDC, monodansylcadaverin; PXT, paclitaxel.

can overcome senescence (for example, Elmore et al., 2005; Roberson et al., 2005; Sabisz and Skladanowski, 2009). We recently (Salmina et al., 2010) found that up-regulation of embryonal self-renewal factors occurs in ETC induced after genotoxic insult and that this up-regulation is transmitted to the daughter cells upon depolyploidization. On the whole, up-regulation of pluripotency and self-renewal transcriptional factor NANOG was shown to antagonize activation of senescence regulator p16, and the latter further takes over only in a proportion of ETC (Salmina et al., 2010). These observations supported our previous finding that while a proportion of p53-deficient ETC activate senescence-associated β-galactosidase and down-regulate Aurora B-kinase, the other ETC continue its expression and division activities into the second week post-irradiation (Erenpreisa et al., 2008). Moreover, we and others also demonstrated (Erenpreisa et al., 2005; Kalejs et al., 2006; Ianzini et al., 2009; Erenpreisa et al., 2009; Vitale et al., 2010) that meiosis-specific genes and proteins are activated by stress-induced mitotic catastrophe and in resulting ETC, which are capable to undergo reduction divisions. Through live cell imaging, we further demonstrated that the progeny originated via depolyploidization retain proliferative capacity evidenced by their ability to produce colonies of mitotically dividing cells (Ianzini et al., 2009)

The central issue in this process of neosis is how depolyploidization and survival can be executed in a potentially mortal ETC, at the cellular and molecular level. Our first insight into the facet of this problem came over a decade ago where we demonstrated the dual activities of ETC in producing mitotic descendents and simultaneously undergoing partial chromatin degradation. In this latter process, a considerable portion of genetic material in viable ETC undergoes autophagic digestion and extrusion, indicating some form of sorting (Erenpreisa et al., 2000; commented by Wheatley, 2006). Further EM (electron microscopy) analysis showed that autolysosomes degrading the DNA are frequently induced in the cytoplasmic pockets of the nuclear ELCSs (envelope-limited chromatin sheets) (Erenpreisa et al., 2002), the structures whose role may be right in settling the chromosomes in the cell nuclei (Olins and Olins, 2009; Olins et al., 2011). Here, we extend our initial observations by revealing that different parts within the same multigenomic ETC can undergo degradation or self-renewal in order to give rise to viable clonogenic paradiploid survivors.

2. Materials and methods

2.1. Cell lines

Namalwa, Ramos and HeLa cell lines were obtained from the ATCC. The lymphoblastoma WI-L2-NS was obtained from Dr P. Olive (Canada). All cell lines are p53 function deficient. Lymphoma cell lines (Namalwa, Ramos, WI-L2-NS) were maintained in RPMI-1640 containing 10% heat-inactivated FCS (fetal calf serum; Sigma) at 37°C in a 5% CO_2 humidified incubator. HeLa S3 cells were grown in suspension under constant rotation in Joklik's MEM containing 10% heat-inactivated calf serum (Hyclone) and antibiotics. The adherent HeLa cells were cultured on glass cover slides in HAM-1 (Sigma) medium supplied with 10% FCS.

2.2. Cell treatments

For experimental studies, cells were maintained in log phase of growth and treated with a single acute 10 Gy dose of gamma irradiation (1–2 Gy/min, Clinac 600 C, Varian Medical Systems or using a Gulmay D3 225 X-ray source at a dose rate of 0.77 Gy/min), ETO (etoposide; Sigma) – 8 μM for 20 h or PXT (paclitaxel, Ebewe Pharma) – 50 nM for 20 h. Cell cultures were further fed every 2–3 days and sampled over a 2-week period posttreatment. To determine the capacity of cells to replicate DNA, BrdU was added at 5 μM to the cell culture for $\sim$24 h prior to fixation of cytospins with methanol as described previously (Erenpreisa et al., 2009).

2.3. Microscopy

A fluorescence light microscope (Leitz Ergolux L03-10) equipped with a colour videocamera (Sony DXC 390P) and a confocal laser microscope (Leica DM600) were used to capture fluorescent images. Phase contrast photography was performed using a light microscope (AxioImager A1, Carl Zeiss).

2.4. Cytological staining and DNA cytometry

For cytological studies, the cells were suspended in warm FCS and cytospun onto glass slides, fixed in cold ethanol/acetone (1:1) and air dried. Slides were hydrolysed with 5 N HCl for 30–60 s and stained with 0.05% Toluidine Blue in McIlvain 50% buffer pH 4–5 for 10 min, rinsed, dehydrated in warm butanol and xylene prior to embedding in DPX (Sigma–Aldrich).

To reveal NORs (nucleolar organizers), prefixed cytospins were stained with a 50% aqueous solution of $AgNO_3$ (Ural Factory of Chemical Reagents) diluted with 2% gelatin (2:1) at 60°C for 5–6 min and counterstained with 0.1% Methyl Green (Sigma–Aldrich) at room temperature for 1 min. This method is recognized as the universal indicator of NOR activity (Bancroft and Stevens, 1996).

Lysosomal activity and autophagic vacuoles were detected by staining for cathepsin B (see below) and with MDC (monodansylcadaverin, Sigma). For MDC staining, cell cultures were incubated with 0.05 mM MDC at 37°C for 1 h followed by fixation in 4% paraformaldehyde and two washes in PBS. The slides were counterstained with PI (propidium iodide; BD Biosciences Pharmingem), mounted into Permount (Thermo Fisher Scientific) and immediately imaged.

For conventional DNA staining, prefixed cytospins were hydrolysed with 5 N HCl at room temperature for 20 min and stained for 10 min with Toluidine Blue (pH 4.0). For DNA image analysis of mitotic cells where vacuoles were visualized in the cytoplasm, the hydrolysis with 5 N HCl was shortened to 30 s. DNA content was measured as the integral optical density in the green channel of the calibrated video camera using Image Pro Plus 4.1 software (Media Cybernetics; REO 2001). After shortened hydrolysis, interactive segmentation of mitotic figures was applied. Stoichiometry of DNA staining was verified using rat hepatocytes. With conventional 20-min acid hydrolysis, the 4C:2C ratio was 1.970; measurement error 1.5% (n=309); with 30-s hydrolysis, the 4C:2C ratio was 1.994; measurement error 0.3%

Table 1 **Antibodies: source and usage**

Primary antibodies:	Secondary antibodies (dilution, if not stated otherwise, 1:400)
Rabbit polyclonal anti-hOCT4 (ab19857, Abcam) 1:75–400 Blocking peptide (ab20650, Abcam)	Goat anti-rabbit-IgG Alexa Fluor 594 (A31631, Invitrogen)
Mouse monoclonal anti-hNANOG (N3038, Sigma) 1:50–75	Goat anti-mouse IgG-Alexa Fluor 488 (A31619, Invitrogen)
Rabbit polyclonal anti-hAurora B-kinase (Abcam, ab2254), 1:300	Goat anti-rabbit-IgG-Alexa Fluor 594 (A31631, Invitrogen)
Mouse monoclonal anti-hRAD51(ab213, Abcam) 1:100	Goat anti-mouse-IgG-Alexa Fluor 488 (A31619, Invitrogen)
Mouse monoclonal anti-h-β-TUBULIN (Neomarkers; clone DM1B) 1:100	Goat anti-mouse IgG-biotin antibody (1:100) (Vector Labs, UK) and by streptavidin-FITC antibody (1:150) (Vector Labs, UK
Mouse monoclonal anti-α-tubulin mouse (Sigma, B-512) 1:2000	Goat anti-mouse IgG-Alexa Fluor 488 (A31619, Invitrogen)
Rabbit polyclonal anti-g-H2AX (Trevigen; AMS Biotechnology, U.K. or 4411-PC-100, R&D Systems) 1:50	Goat anti-rabbit-IgG-Alexa Fluor 594 (A31631, Invitrogen)
Mouse monoclonal anti-bromodeoxyuridine (BdU) (A21300, Invitrogen) 1:200	Goat anti-mouse-IgG-Alexa Fluor 488 (A31619, Invitrogen)
Goat polyclonal anti-hRAD52 (C-17) (sc-7674, Santa Cruz) 1:50	Donkey anti-goat IgG-Alexa Fluor 488 (A11055, Invitrogen)
Rabbit polyclonal anti-hCATHEPSIN B (ab30443, Abcam) 1:100	Goat anti-rabbit-IgG-Alexa Fluor 594 (A31631, Invitrogen)

(n=182). Diploid DNA values for tumour cells determined after shortened hydrolysis were calculated by measuring metaphases and anaphase halves in 50 untreated cells, in which the variability coefficient was 7.7%.

2.5. IF (immunofluorescence)

Standard IF staining was performed according to procedures detailed previously (Erenpreisa et al., 2008). The primary and secondary antibodies used are given (Table 1). To detect protein disulfide isomerase, SelectFX Alexa Flour 488 Endoplasmic Reticulum Labeling Kit (S34200, Molecular Probes) was used according to the manufacturer's instructions.

3. Results

3.1. DNA-digesting autolysosomes appear in ETC late on after genotoxic and spindle damage

Following genotoxic insult, Ramos, Namalwa, and WI-L2-NS cells all undergo extensive polyploidization (Illidge et al., 2000; Ivanov et al., 2003), form ETC and subsequently begin chromatin extrusion coincident with the appearance of autolysosomes at the nucleo-cytoplasmic border as previously described (Erenpreisa et al., 2000, 2002). Many autophagic vacuoles could be stained for both DNA and for the lysosomal activation marker cathepsin B (Figure 1a) as well as for MDC, a marker of autophagic vacuoles (Figure 1b; for control, see Supplementary Figure S1 at http://www.cellbiolint.org/cbi/035/cbi0350687add.htm). The chromatin eliminated by autolysosomes was shown to be both TUNEL- (Erenpreisa et al., 2000) and γ-H2AX-positive (Figure 1c) indicating its selective nucleolytic degradation. The degradation and extrusion of large amounts of DNA from viable ETC was observed in lymphoma cell cultures after extensive cell loss through apoptosis or necrosis from the end of the first week postirradiation. In the control, untreated cells, polyploidy remained at low levels ($<$4%), and chromatin extrusion was extremely rare. These experiments were repeated on each lymphoma cell line at least six times with similar results.

A similar phenomenon was observed in HeLa cells at 6–14 days postirradiation (Figures 1d, 1e; data from one of four similar experiments) and at 4–6 days in WI-L2-NS and Namalwa cells after ETO and PXT treatments (exemplified in Figure 1f; data from one of three similar experiments). These data demonstrate that in these surviving ETCs, chromatin is sorted into two categories – one for preservation and the other for autodigestion and

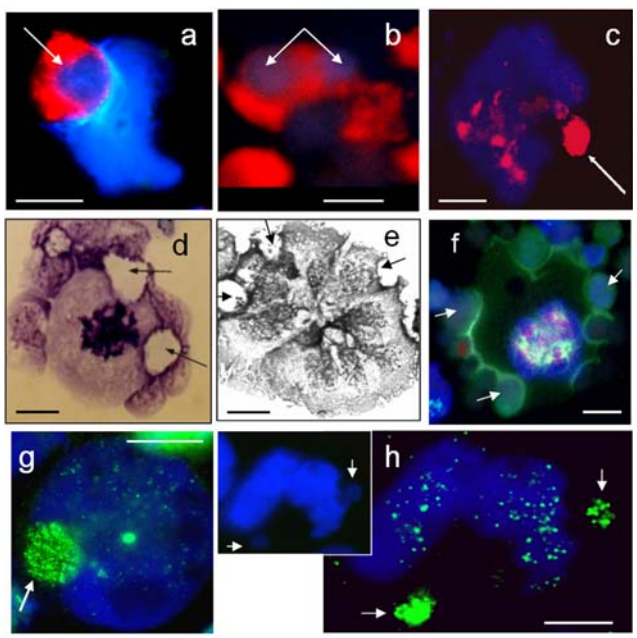

Figure 1 **Chromatin extrusion, mitotic activity and DNA repair in ETCs**
WIL-L2-NS ETC generated after irradiation (**a**) or ETO treatment (**b**) stained on day 8 with either DAPI (blue on '**a**') or propidium iodide (red on '**b**') to detect DNA and either cathepsin B (red on '**a**') or monodansylcadaverin (blue on '**b**'), as markers of autophagy. These data indicate that autolysosomes contain DNA. (**c**) Namalwa ETC induced by irradiation stained on day 5 for γ-H2AX (red) and DAPI, indicating the degradation of extruded chromatin (arrow); (**d**) HeLa ETC induced by irradiation stained on day 14 with Toluidine Blue (pH 5) after short acid hydrolysis, displays mitotic features and autophagic vacuoles (arrowed); (**e**) HeLa ETC stained with Toluidine Blue (pH 5) after short acid hydrolysis on day 9 after irradiation, reveals multipolar bridged anaphase and autophagic vacuoles (arrows); (**f**) WI-L2-NS ETC undergoing multipolar mitosis on day 5 after paclitaxel treatment, α-tubulin (green), Aurora B-kinase (red) and DNA (blue); multiple cytoplasmic 'bubbles' can be seen with destructured tubulin containing the DAPI-positive DNA remnants (arrows); (**g–h**) Namalwa ETC stained 6 days after irradiation for Rad 51 or Rad 52 (labelled in green) repair foci and extrusion of these recombinases are shown (arrows). In the inset to (**h**) only, the DAPI channel of the same cell is showed to indicate the location of DNA in the marginal vacuoles at the nucleo-cytoplasmic border (arrowed). The extruded chromatin is enriched with inactive DNA repair factors; DNA repair foci are evident in the other ETC depicted in the figure. Bars=10 μm.

elimination. Furthermore, it should be noted that the amounts of chromatin degraded can be considerable, for example, greater than 50% of a 16C ETC DNA content can be lost, and the whole subnuclei may be extruded in this way (Figure 1e, see also in Erenpreisa et al., 2000). As these cells possess the hallmarks of lysosomal and autophagic activity, often used as markers of senescence (Vellai, 2009), the question arises: are these cells senescing and entering irreversible growth arrest?

3.2. Compatibility of chromatin extrusion and mitotic activity in ETC

To address this question, we further analysed the ETC for signs of mitosis and chromatin extrusion. As shown, it is clear that ETCs are able to undertake mitotic activity (metaphase features in panel d; multipolar mitosis in panel e) (in Figures 1d–1e). This appearance was observed for all four cell lines. The question remains, however, as to whether these cells are also actively engaging in chromatin extrusion. Because of the proximity of what appears to be autophagic vacuoles (arrowed bodies in Figures 1d and 1e), it is tempting to speculate that the latter were extruded by the former. Although this conclusion can only be inferred; nevertheless, the features present (Figure 4e) would account for such interpretation. Thus, it is possible that chromatin extrusion may be compatible with mitotic activity in ETC and that the latter are not *bone fide* senescent cells (growth arrested by definition).

3.3. Chromatin extrusion in ETC is compatible with DNA repair and may participate in chromatin sorting

To address whether ETCs undergoing chromatin extrusion/degradation were capable of undergoing DNA repair, we stained ETC of Namalwa, HeLa and WI-L2-NS for the presence of DNA repair foci as labelled by the twin recombinases RAD 51 and RAD 52. These experiments were repeated for each cell line at least twice with similar results in each case. Again, because of the vicinity of the features present (Figures 1g, 1h), it is tempting to speculate that a portion of the ETC exerts both DNA repair and autophagic activities. Rad 51 staining appears in autolysosomal vacuoles as bundles of linearly arranged polymeric fibres (Figure 1g), possibly due to the loss of its proper association with Rad52 and DNA in the rejected chromatin (West, 2003). These observations imply a prior chromatin sorting process, which may occur during attempted DNA repair. It has been shown (Ivanov et al., 2003) that this repair occurs extensively in 40–80% of ETC before depolyploidization proceeds and requires suppression of p53 function; thus, we were further interested as to how these processes might relate to our recent findings regarding ETC and stem cell gene transcription (Salmina et al., 2010).

3.4. Diverse fate of sub-nuclei in late ETC

Most (~90%) ETC, which are formed by mitotic slippage from p53 function-deficient lymphoma cells after gamma irradiation begin to up-regulate the key germline transcription factors OCT4 and NANOG on days 3–5 postirradiation. These findings were observed in WI-L2-NS and Namalwa cells in greater than six experiments. In a similar fashion, HeLa cells displayed an up-regulation of these transcription factors (from a very low background level in untreated controls cells; data not shown), with an enhanced cytoplasmic expression (mostly in the centrosome) seen on days 4–5 postirradiation in most cells (Supplementary Figure S2a at http://www.cellbiolint.org/cbi/035/cbi0350687add.htm). However, nuclear up-regulation of OCT4/NANOG as exemplified (Supplementary Figure 2b) was found in only 5–10% of endopolyploid HeLa cells in three similar experiments.

Up-regulation was also found after treatment of WI-L2-NS cells with the radiomimetic ETO (not shown) and the stabilizer of microtubules PXT, where 98 and 85% of ETC, respectively, demonstrated a 2- to 3-fold increase of these germline transcription factors (typical staining is shown in Supplementary Figures 2c, 2d; representative of greater than three experiments). From day 5 to day 6 after these treatments, the surviving ETC of all cell lines initiated depolyploidization such that ETCs were found in bipolar and multipolar divisions, some after skipping S-phase (Erenpreisa et al., 2005, 2008, 2009; Ianzini et al., 2009). At these times, chromatin extrusion became observed. However, late on, large ETC displaying radial cleavage furrows during multipolar anaphase often do not complete cytotomy, and the restituted daughter nuclei assume a radial or horseshoe-like position in the ETC, while the furrows partly or completely regress (Figures 1e, 2; see also Erenpreisa et al., 2008, Figures 1d, 1e). This is a previously reported phenomenon, which is due to the hindrance of abscission by the chromosome bridges that exist between

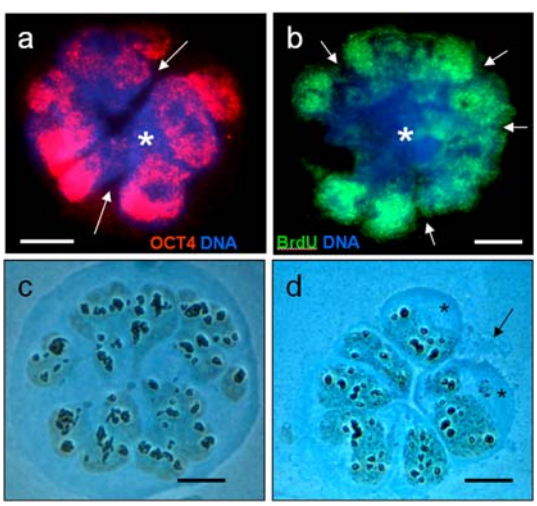

Figure 2 Differential rejuvenation and senescence of subnuclei in ETC after FMM

(**a**) Namalwa ETC stained on day 8 after irradiation for OCT4; the OCT4-positive subnuclei are found at the periphery of the ETC, while the OCT4-negative subnuclei occupy the centre (*); (**b**) BrdU uptake in Namalwa cells (following a 24 h pulse from day 7 to 8 after irradiation) revealed by immunofluorescence shows both replicatively active (green) and inert (*) chromatin within the ETC; (**c**, **d**) HeLa ETC observed on day 13 after irradiation stained for Ag-NORs, counterstained with Methyl Green and imaged in phase contrast. (**c**) Multinuclear ETC after FMM with five to seven subnuclei and still intact cytoplasm; (**d**) post-FMM ETC presenting degradation of the outer (old) cytoplasm and distribution of the inner cytoplasm enclosing the individual subnuclei (*); the remnant of the old cytoplasm is indicated by the arrow. Bars=10 μm.

subnuclei (Steigemann et al., 2009). In these ETC subnuclei, we see multiple Ag-positive NORs (Figures 2c, 2d), implying that these cells have recently passed mitosis and that the subnuclei have the capacity for further formation of ribosomes and ergastoplasm (see below). In late ~16C–32C ETC days 8–14 postirradiation, which, as judged by the radial cytoplasmic clefts and/or triangular-shaped nuclei, have undergone similar FMM (failed multipolar mitosis), we observed signs of the chromatin differentiation. Some subnuclei become rounded and separate from the remainder. They display markers of reproductive potential such as nuclear OCT4 (Figure 2a) and NANOG (data not shown) and replicate DNA (incorporating BrdU, Figure 2b). However, not all of the subnuclei stain positively for OCT4, and a region of (usually close to the centre) or even entire subnuclei are commonly OCT4 negative (Figure 2a, asterisk) and fail to include BrdU even in a 24-h incubation period (Figure 2b, asterisk). In our earlier pulse-chase experiments with ^{3}H-thymidine, we noted that the DNA in the extruded chromatin had been previously replicated in the ETC but had stopped replication prior to its expulsion from the cell (Erenpreisa et al., 2000). In practically all of the late ETC, derived from each cell line, we observed chromatin extrusion and the remaining vacuoles invaginating into the cell nuclei.

3.5. Diverse fate of cytoplasm parts in ETC

Next, we studied the fate of the ETC cytoplasm. We found that not only subnuclei but also the associated cytoplasm undergoes differentiation and separation in ETC undergoing FMM, whereby the external layer of cytoplasm becomes discarded, as the inner cytoplasm sequesters its territory around rejuvenated rounded subnuclei (compare Figures 2c and 2d). Furthermore, during the segregation of the cytoplasm, the nucleoli of rejuvenated cells become highly active, enriching the inner cytoplasm with ribosomes (Figures 3a, 3b); the rejuvenated subnuclei activate their surrounding ergastoplasm (Figure 3c) and organize the cytoskeleton with its own centrosome (Figure 3d). Thus, rejuvenated daughter subcells arise and become preformed within an old mother ETC prior to their release. This same phenomenon was observed in lymphoma cell lines and the HeLa cells.

3.6. Autophagy releases ETC daughter subcells from their constraining chromosome bridges

Depolyploidization of ETC is a poorly understood multistep process, where the multipolar divisions are suggested to play a role (Gisselsson et al., 2008; Vitale et al., 2010). As described before, ETCs undergo meiosis-like bi- and multipolar divisions (Erenpreisa et al., 2005, 2008, 2009; Ianzini et al., 2009); however the sequence, relationships and contribution of the various types of ETC divisions in the clonogenicity are currently far from clarity (Erenpreisa and Cragg, 2010). Here, we describe a particular facet of this complex process showing that after failed multipolar divisions, ETC sort and extrude some subnuclei, discard the original cytoplasm and preform rejuvenated daughter subcells with their own nascent cytoplasm. However, after failed multipolar mitosis, the chromosome bridges between daughter subcells are linked by the Aurora B-aided radial cleavage furrows into one or more knots (Figure 1e; 4a; also illustrated by Erenpreisa et al., 2005, Figures 1a, 1e, 1d; 2008, Figure 8a), preventing final abscission. As these structures do not persist, it appears that autophagolysosomes can engulf and digest not only the inert chromatin but also these knots. The formation of the autolysosome in the cell centre between preformed subcells is commonly observed during the disintegration of these ETC in all studied cell lines (Figure 4b). The process likely releases free energy leading to repulsion of daughter subcells (Figure 4c) and possibly even a flare of lysosomic autofluorescence (Figure 4d). The repulsion of the daughter subcells is reminiscent of budding (see also in Erenpreisa et al., 2005, Figure 1f). Importantly, the budding subcells are enriched with the self-renewal factors OCT4 and NANOG (Figures 4c, 4d) and resume cell divisions (Figures 4d–4f). The mitotic cells released from ETC mostly contain a paradiploid amount of DNA reducing aneuploidy characteristic for ETC as determined by interactive image cytometry on WI-L2-NS after ETO treatment (Figure 5). Broadly similar things happen in HeLa cells (data not shown).

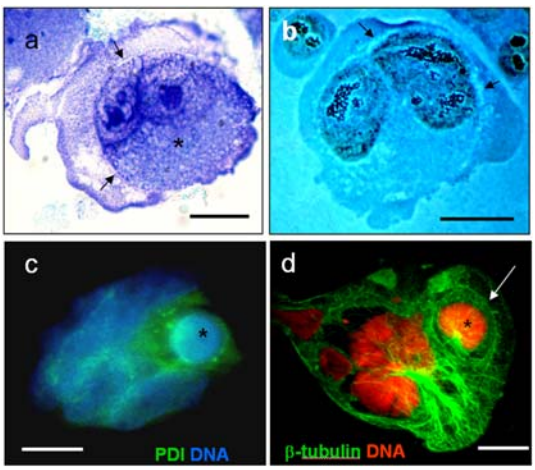

Figure 3 Differential rejuvenation and senescence of cytoplasm in ETC
(**a**) HeLa ETC on day 8 after irradiation stained with Toluidine Blue, pH 5, after a short acid hydrolysis; splitting off the outer layer of cytoplasm (the fissure is arrowed) from the inner area enriched in ribosomal RNA is visible (*); (**b**) HeLa ETC on day 8 after irradiation stained as on Figures 2c, 2d; nuclei are actively engaged in ribosomal synthesis (Ag-NOR positivity of the developed nucleolonema), while the outer cytoplasm is splitting from the inner (the fissure is arrowed); (**c**) WI-L2-NS ETC observed 8 days after ETO treatment, immunostained for the ergastoplasmic marker protein disulfide isomerase (PDI); the high activity of PDI (green) around single rounded subnuclei (asterisk) is evident. (**d**) Confocal microscopy image of Namalwa ETC observed 6 days after irradiation and stained for β-tubulin and DNA using propidium iodide; a separating subcell (*) can be seen within its own cytoskeletal network (arrow) distinct from the linked network containing several other subnuclei. The latter displays converging microtubular branches – possibly the result of incomplete multipolar mitosis. Bars=10 μm.

4. Discussion

There is a view that polyploidy may serve as a link between quite opposite biological processes as cellular senescence and self-renewal, thereby paving the road to cancer or its progression (Rajaraman et al., 2006; Mosieniak and Sikora, 2010). Here, we

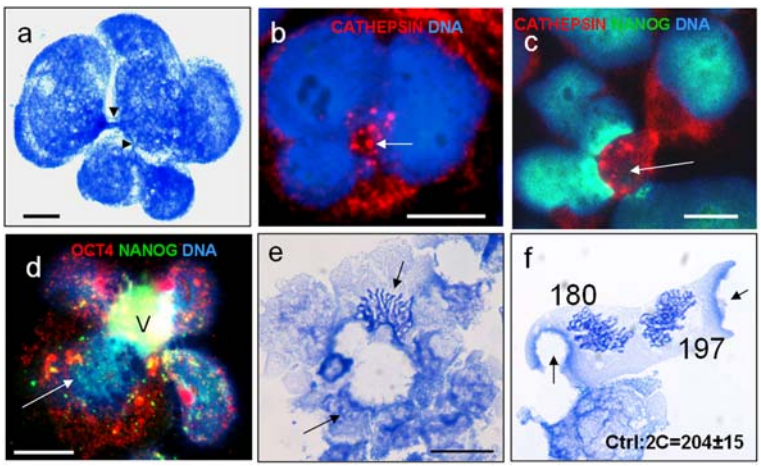

Figure 4 Potential role of autolysosomes in the final disintegration of ETC

(**a**) HeLa ETC on day 5 after irradiation stained with Toluidine Blue pH 5 after short acid hydrolysis; after incomplete multipolar mitosis, daughter subcells remain linked by a series of chromosome bridges (arrowheads). (**b**) Cells on day 9 after irradiation stained for cathepsin B and DNA; distinct cathepsin-positive foci can be seen in the central cytoplasmic area between subnuclei (arrow). (**c**) WI-L2-NS ETC on day 8 after irradiation stained for cathepsin B, DNA and NANOG; cathepsin-positive autolysosome (arrow) is apparently dissociating NANOG-positive subcells. (**d**) WI-L2-NS ETC stained on day 9 after irradiation for OCT4, NANOG and DNA (DAPI); a flare of autofluorescence is observed in the central autolysosome (V) possibly repulsing the OCT4/NANOG-positive subcells, one of which is in metaphase (arrow). (**e**) Namalwa cells on day 14 post-ETO treatment stained with Toluidine Blue pH 4 after shortened acid hydrolysis; separation of subcells by a central autophagic vacuole; the arrows indicate two separated anaphase halves. (**f**) WI-L2-NS cells on day 14 post-ETO treatment stained with Toluidine Blue pH 4 after shortened acid hydrolysis; a distinct ETC daughter cell in anaphase with the remnants of autophagic vacuoles (arrowed) is shown; the DNA content (IOD) is indicated and reveals paradiploidy. Bars=10 μm.

have addressed this conundrum in p53-deficient ETCs induced after genotoxic and spindle damage. Our observations indicate that a proportion of the multinucleated ETCs induced after such damage through mitotic catastrophe do not undergo growth arrest even though they possess such hallmark features of senescence as polyploidy and autophagy. These ETCs, in fact, seem to be able to provide paradiploid mitotic survivors. In particular, the autophagy observed during this process (which is coupled with the chromatin extrusion) is non-senescent in nature, as it is compatible with the mitotic activities of these cells. So, *stricto sensu* senescence is not induced in these cells. Rather, our data suggest that the genomically unstable ETC use this process to rid themselves of excessive and/or irreparable genetic material following a DNA repair and sorting processes that precede polygenomic separation. Furthermore, it appears likely that autophagy is also directly involved in the final stages of depolyploidization when the chromosome bridges linking sub-nuclei are dissolved. These autophagic functions may favour survival of tumour cells after genotoxic damage and are in keeping with reports on the cytoprotective function of autophagy and its contribution to tumour cell survival after chemotherapy (Morselli et al., 2009; Galluzzi et al., 2010).

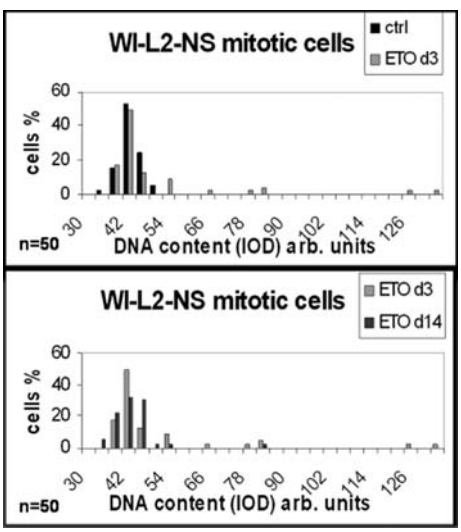

Figure 5 Reduction of aneuploidy in late ETC and their descendents, in the time-course after genotoxic damage

Mitotic DNA content of WI-L2-NS cells at three time points: in non-treated cells, on day 3 after ETO treatment and recovering on day 14 after ETO treatment. WI-L2-NS cells were treated with ETO, and then, the mitotic content of dividing cells was examined 3 and 14 days later and compared with control (Ctl) untreated cells. All day 14 post-ETO mitotic cells bore the remnants of autophagic vacuoles as shown (Figure 4f). Mitotically active paradiploid cells are present in the cell population at this time posttreatment. The graphs show an increase of aneuploidy on day 3 and its decrease on day 14, returning most dividing cells to the paradiploid DNA content. NB: 20% of the mitotic cells on day 14 ETO-treated group displayed deranged disseminated chromosomes and were omitted from these measurements for technical reasons.

Coexistence of this partial chromatin elimination with activation of an embryonal self-renewal programme in ETC is interesting from the ontophylogenic point of view. Partial elimination of chromatin ('chromatin diminution') was first described over 100 years ago by Theodor Boveri in *Ascaris lumbricoides* (Boveri, 1887). It represents one way in which somatic cells in the embryo can undergo differentiation, while the full DNA/chromosome complement remains preserved in the cells of the germline. Diminution has been found in more than 200 families of invertebrates. During this process, whole or selected portions of chromosomes, comprising up to 25–85% of the total DNA, become eliminated from somatic cell precursors (Akifyev et al., 2002; Burt and Trivers, 2006; Kloc and Zagrodzinska, 2008; Gilbert, 2010). In plant hybrids, a

potentially analogous process occurs, whereby a complement of uniparental chromosomes can become assembled, degraded and eliminated (Gernand et al., 2005). In *Tetrahymena pyriformis*, the genomically rearranged chromatin of macronuclei disrupting DNA replication, becomes extruded (reviewed by Raikov, 1995) combining with features of autophagy (Levy and Elliott, 1968) and nucleolysis (Mpoke and Wolf, 1996, 1997). Elimination of mitotic chromosomes through autophagy has been described in human Chang liver cells after a burst of free radicals (Sit et al., 1996). Crucially, in all known cases of chromatin diminution, there is a dependence on cell division (Gilbert, 2010) much as we have seen here in ETCs produced after genomic insult.

As alluded to previously, this particular autophagy may also play a key role in the chromatin-sorting process. DNA sorting in ETC has been suggested previously based upon the presence of micronuclei enriched with Rad 51 (Haaf et al., 1999) and the elimination of amplified DNA sequences by this process (Shimizu et al., 1998). Although not reported as such, these events may be related to the autophagic chromatin extrusion detailed here. Other related important results are experimental observations (Kalejs et al., 2006; Ianzini et al., 2009; Erenpreisa et al., 2009; Vitale et al., 2010) that demonstrate the ability of cancer cells to escape from genotoxin- or spindle-damage-induced mitotic death by activating a depolyploidization programme facilitated by the action of meiosis-specific genes that results in the production of proliferating progenies. In keeping with our findings, Walen (2008, 2010) recently reported cytological observations in pre-senescent cultures of human embryonal fibroblasts, showing both degrading and mitotic subnuclei in the same, albeit rare (1–4%), endopolyploid cells. In addition, chromatin sorting and extrusion might also favour the decrease of aneupolyploidy and genomic stabilization during ETC depolyploidization. Decrease of aneuploidy was described in ETCs of colorectal cancer after nocodazole treatment by Vitale et al. (2010, commented by Erenpreisa and Cragg, 2010) and shown here in lymphoblastoma by DNA image cytometry after ETO irradiation treatments. It may further be aided by the activity of dynamic ELCS moving along the perinuclear space and forming autophagy-inducing loops and pockets enrolling extrachromatin (Erenpreisa et al., 2002); the latest data show that ELCS are engaged in the balanced docking of chromosomes to the nuclear envelope (Olins et al., 2011). Conversely, compromised autophagy was shown to promote DNA damage and aneupolyploidy of tumour cells in response to metabolic stress (Mathew et al., 2009).

Following the chromatin-sorting process in the ETCs, individual subcells become separated and released. Sundaram, Rajaraman and colleagues (Sundaram et al., 2004; Rajaraman et al., 2006) previously interpreted the final budding of subnuclei from disintegrating giant mother cells to be amitotic fragmentation. That interpretation is partially true as autophagic release of daughter nuclei/cells from the chromosome bridges is indeed amitotic. However, our observations (Erenpreisa et al., 2005, 2008, 2009, and here) show that prior to budding, the genetic material has already been segregated in a more regulated manner involving multipolar and bipolar divisions that use meiotic/mitotic machinery (Ianzini et al., 2009; Erenpreisa et al., 2009). Moreover, our observations revealed that chromatin extrusion is compatible with activation of the embryonal self-renewal program and the transfer of its key constituents (OCT4 and NANOG) into the depolyploidized descendents. As we demonstrated through live cell imaging experiments (Ianzini et al., 2009), some of these subcells re-enter normal mitosis and are capable of further propagation ensuring clonogenic survival. However, further studies are needed to clarify the exact role of chromatin extrusion and the sequence of events occurring during ETC divisions.

Importantly, we report here that differentiation of subnuclei is accompanied by a re-synthesis of fresh cytoplasm and the formation of rejuvenated individual subcells, while they still reside within the cytoplasm or detritus of the original ETCs. Presumably, this diversification of subnuclear fate in these ETC can occur by two pathways: (i) by the second FMM, which follows the first and involves only part of the chromatin after its re-sorting between the two events; (ii) by asymmetric bipolar divisions of the subnuclei identifying them as either immortal (extending self-renewal) and mortal through features characteristic of stem cells. Formation of individual cytoplasm territory around the 'stemloid' daughters allows the compartmentalization of the self-renewal/mitotic activators into the individual rejuvenated subcells within the deteriorating mother ETC facilitating the rejection of the excluded subnuclei and old cytoplasm. In this respect, a single ETC at this stage behaves like a developing multicellular system, which may be due to the prolonged activity of embryonal factors. As a result, the new generation is born from, and comes to substitute for, the previous generation of tumour cells. This is the essence of both 'neosis' (Sundaram et al., 2004; Rajaraman et al., 2006) and the 'cancer life cycle' (Erenpreisa and Cragg, 2007, 2010) and reveals how these processes occur cytologically. However, although we have demonstrated this process in several p53 non-functional cell lines, the question remains as to whether primary tumours are capable of developing in this way.

In conclusion, the data presented here further outline the complex cytological processes which occur when ETC undergo depolyploidization and rejuvenation of their descendents through a coupled sorting and autophagic elimination of superfluous genetic material revealing the way (or at least one of the ways) in which these cells are able to return to the clonogenic paradiploidy.

Author contribution

Jekaterina Erenpreisa designed the experiments, carried out microscopical analysis of the material and drafted the manuscript. Kristine Salmina participated in experimental design, carried out immunocytochemistry and analysis of results. Anda Huna carried out DNA image cytometry of WI-L2-NS and analysis of results, and participated in the preparation of the draft manuscript. Elizabeth Kosmacek carried out the experiments and DNA image cytometry on HeLa cells and analysed results. Mark Cragg participated in the design and analysis of experiments and edited the draft manuscript. Fiorenza Ianzini participated in the design of experiments on HeLa cells and edited the draft manuscript. Alim Anisimov carried out mocroscopical analysis of the experiments of HeLa cells, and participated in drafting and editing the manuscript.

Acknowledgements

We thank the expert assistance of Roger Alston (Southampton) for help in confocal imaging.

Funding

This work was partially supported by the ESF [grant number 1DP/1.1.1.2.0/09/ APIA/VIAA/150], the Latvian state programme VPP4.5, the Royal Society of London enabling exchange visits between Riga and Southampton, the National Institutes of Health [grant numbers CA/GM94801 and CA86862] and by the Latvian–U.S.A. Governmental Exchange Grant enabling visits between Riga and Iowa City and vice versa.

References

Akifyev AP, Grishanin AK, Degtyarev SV. Chromatin diminution is a key process explaining the eucaryotic genome size paradox and some mechanisms of genetic isolation. Genetika 2002;38:486–95.

Bancroft JD, Stevens A. Theory and practice of histological techniques, 4th ed. New York: Churchill Livingstone; 1996.

Baroja A, de la Hoz C, Alvarez A, Vielba R, Sarrat R, Arechaga J, de Gandarias JM. Polyploidization and exit from cell cycle as mechanisms of cultured melanoma cell resistance to methotrexate. Life Sci 1998;62:2275–82.

Blagosklonny M. Cancer stem cell and cancer stemloids: from biology to therapy. Cancer Biol Ther 2007;6:1684–90.

Boveri T. Ueber Differenzierung der Zellkerne während der Furchung des Eies von *Ascaris megalocephala*. Anat Anz 1887;2:688–93.

Burt A, Trivers R. Genes in conflict: the biology of selfish genetic elements, chapter 11. Harvard: Belknap Press; 2006.

Debnath J, Baehrecke EH, Kroemer G. Does autophagy contribute to cell death? Autophagy 2005;1:66–74.

Edinger AL, Thompson CB. Death by design: apoptosis, necrosis and autophagy. Curr Opin Cell Biol 2004;16:663–9.

Elmore LW, Di X, Dumur C, Holt SE, Gewirtz DA. Evasion of a single-step, chemotherapy-induced senescence in breast cancer cells: implications for treatment response. Clin Cancer Res 2005;11:2637–43.

Erenpreisa JA, Cragg MS, Fringes B, Sharakhov I, Illidge TM. Release of mitotic descendants by giant cells from irradiated Burkitt's lymphoma cell line. Cell Biol Int 2000;24:635–48.

Erenpreisa J, Ivanov A, Cragg M, Selivanova G, Illidge T. Nuclear envelope-limited chromatin sheets are part of mitotic death. Histochem Cell Biol 2002;117:243–55.

Erenpreisa J, Kalejs M, Ianzini F, Kosmacek EA, Mackey MA, Emzinsh D, Cragg MS, Ivanov A, Illidge T. Segregation of genomes in polyploid tumour cells following mitotic catastrophe. Cell Biol Int 2005;29:1005–11.

Erenpreisa J, Cragg MS. Cancer: a matter of life cycle? Cell Biol Int 2007;31:1507–10.

Erenpreisa J, Ivanov A, Wheatley SP, Kosmacek EA, Ianzini F, Anisimov AP, MacKey MA, Davis PJ, Plakhins G, Illidge TM. Endopolyploidy in irradiated p53-deficient tumour cell lines: persistence of cell division activity in giant cells expressing Aurora-B kinase. Cell Biol Int 2008;32:1044–56.

Erenpreisa J, Cragg MS, Salmina K, Hausmann M, Scherthan H. The role of meiotic cohesin REC8 in chromosome segregation in gamma irradiation-induced endopolyploid tumour cells. Exp Cell Res 2009;315:2593–603.

Erenpreisa J, Cragg MS. MOS, aneuploidy and the ploidy cycle of cancer cells. Oncogene 2010;29:5447–51.

Galluzzi L, Aaronson SA, Abrams J, Alnemri ES, Andrews DW, Baehrecke EH et al. Guidelines for the use and interpretation of assays for monitoring cell death in higher eukaryotes. Cell Death Differ 2009;16:1093–107.

Galluzzi L, Morselli E, Kepp O, Mariño G, Michaud M, Vitale I, Maiuri MC, Kroemer G. Oncosuppressive functions of autophagy. Antioxid Redox Signal 2010; doi: abs/10.1089/ars.2010.3478.

Gernand D, Varshne A, Rubtsov M, Prodanov S, Brüβ C, Kumlehn J, Matzk F, Houben A. Uniparental chromosome elimination at mitosis and interphase in wheat and pearl millet crosses involves micronucleus formation, progressive heterochromatinization, and DNA fragmentation. Plant Cell 2005;17:2431–8.

Gilbert SF. Mechanisms of chromosome diminution. Developmental biology, 9th ed, Chapter 16, Sinauer Associates. 2010; http://9e.devbio.com/article.php?ch=16&id=253

Gisselsson D, Håkanson U, Stoller P, Marti D, Jin Y, Rosengren AH, Stewenius Y, Kahl F, Panagopoulos I. When the genome plays dice: circumvention of the spindle assembly checkpoint and near-random chromosome segregation in multipolar cancer cell mitoses. PLoS One 2008;3:e1871.

Haaf T, Raderschall E, Reddy G, Ward DC, Radding CM, Golub EI. Sequestration of mammalian Rad51-recombination protein into micronuclei. J Cell Biol 1999;144:11–20.

Ianzini F, Kosmacek EA, Nelson ES, Napoli E, Erenpreisa J, Kalejs M, Mackey MA. Activation of meiosis-specific genes is associated with depolyploidization of human tumour cells following radiation-induced mitotic catastrophe. Cancer Res 2009;69:2296–304.

Ianzini F, Mackey MA. Spontaneous premature chromosome condensation and mitotic catastrophe following irradiation of HeLa S3 cells. Int J Radiat Biol 1997;72:409–21.

Illidge T, Cragg M, Fringe B, Olive P, Erenpreisa JA. Polyploid giant cells provide survival mechanism for p53 mutant cells after DNA damage. Cell Biol Int 2000;24:621–33.

Ivanov A, Cragg MS, Erenpreisa J, Emzinsh D, Lukman H, Illidge TM. Endopolyploid cells produced after severe genotoxic damage have the potential to repair DNA double strand breaks. J Cell Sci 2003;116:4095–106.

Kalejs M, Ivanov A, Plakhins G, Cragg MS, Emzinsh D, Illidge T, Erenpreisa J. Upregulation of meiosis-specific genes in lymphoma cell lines following genotoxic insult and induction of mitotic catastrophe. BMC Cancer 2006;6:6.

Kloc M, Zagrodzinska B. Chromatin elimination – an oddity or a common mechanism in differentiation and development? Differentiation 2008;68:84–91.

Kondo Y, Kondo S. Autophagy and cancer therapy. Autophagy 2006;2:85–90.

Levy MR, Elliott AM. Biochemical and ultrastructural changes in *Tetrahymena pyriformis* during starvation. J Protozool 1968;15:208–22.

Mackey MA, Ianzini F. Enhancement of radiation-induced mitotic catastrophe by moderate hyperthermia. Int J Radiat Biol 2000;76:273–80.

Madeo F, Tavernakis N, Kroemer G. Can autophagy promote longevity? Nat Cell Biol 2010;12:842–6.

Mathew R, Karp CM, Beaudoin B, Vuong N, Chen G, Chen HY, Bray K, Reddy A, Bhanot G, Gelinas C, DiPaola RS, Karantza-Wadsworth V, White E. Autophagy suppresses tumourigenesis through elimination of p62. Cell 2009;137:1062–75.

Morselli E, Galluzzi L, Kepp O, Vicencio JM, Criollo A, Maiuri MC, Kroemer G. Anti- and pro-tumour functions of autophagy. Biochim Biophys Acta 2009;1793:1524–32.

Mosieniak G, Sikora E. Polyploidy: the link between senescence and cancer. Curr Pharm Des 2010;16:734–40.

Mpoke S, Wolf J. DNA digestion and chromatin condensation during nuclear death in *Tetrahymena*. Exp Cell Res 1996;225:357–65.

Mpoke SS, Wolf J. Differential staining of apoptotic nuclei in living cells: application to macronuclear elimination in *Tetrahymena*. J Histochem Cytochem 1997;45:675–83.

Olins DE, Olins A. Nuclear envelope-limited chromatin sheets (ELCS) and heterochromatin higher order structure. Chromosoma 2009;118:537–48.

Olins AL, Langhans M, Monestier M, Schlotterer A, Robinson DG, Viotti C, Zentgraf H, Zwerger M, Olins DE. An epichromatin epitope. Persistence in the cell cycle and conservation in evolution. Nucleus 2011;2:1–14.

Puig PE, Guilly MN, Bouchot A, Droin N, Cathelin D, Bouyer F, Favier L, Ghiringhelli F, Kroemer G, Solari E, Martin F, Chauffert B. Tumour cells can escape DNA-damaging cisplatin through DNA endoreduplication and reversible polyploidy. Cell Biol Int 2008;32:1031–43.

Raikov IB. Structure and genetic organisation of the polyploidy macronucleus of ciliates: a comparative review. Acta Protozool 1995;34:151–71.

Rajaraman R, Guernsey DL, Rajaraman MM, Rajaraman SR. Stem cells, senescence, neosis and self-renewal in cancer. Cancer Cell Int 2006;6:25.

Rajaraman R, Guernsey DL, Rajaraman MM and Rajaraman SR. Neosis – a parasexual somatic reduction division in cancer. Int J Hum Genet 2007;7:29–48.

Roberson RS, Kussick SJ, Vallieres E, Chen SY, Wu DY. Escape from therapy-induced accelerated cellular senescence in p53-null lung cancer cells and in human lung cancers. Cancer Res 2005;65:2795–803.

Sabisz M, Skladanowski A. Cancer stem cells and escape from drug-induced premature senescence in human lung tumour cells. Implications for drug resistance and *in vitro* drug screening models. Cell Cycle 2009;8:3208–17.

Salmina K, Jankevics E, Huna A, Perminov D, Radovica I, Klymenko T, Ivanov A, Jascenko E, Scherthan H, Cragg M, Erenpreisa J. Up-regulation of the embryonic self-renewal network through reversible polyploidy in irradiated p53-mutant tumour cells. Exp Cell Res 2010;316:2099–112.

Scarlatti F, Granata R, Meijer AJ, Codogno P. Does autophagy have a license to kill mammalian cells? Cell Death Differ 2009;16:12–20.

Shay JW, Roninson IB. Hallmarks of senescence in carcinogenesis and cancer therapy. Oncogene 2004;23:2919–33.

Shimizu N, Itoh N, Utiyama H, Wahl GM. Selective entrapment of extrachromosomally amplified DNA by nuclear budding and micronucleation during S-phase. J Cell Biol 1998;140:1307–20.

Sit KH, Paramanantham R, Bay BH, Chan HL, Wong KP, Thong P, Watt F. Sequestration of mitotic (M-phase) chromosomes in autophagosomes: mitotic programmed cell death in human Chang liver cells induced by an OH* burst from vanadyl(4). Anat Rec 1996;245:1–8.

Steigemann P, Wurzenberger C, Schmitz MH, Held M, Guizetti J, Maar S, Gerlich DW. Aurora B-mediated abscission checkpoint protects against tetraploidization. Cell 2009;136:473–84.

Sundaram M, Guernsey DL, Rajaraman MM, Rajaraman R. Neosis: a novel type of cell division in cancer. Cancer Biol Ther 2004;3:207–18.

Tam WL, Ang YS, Lim B. The molecular basis of ageing in stem cells. Mech Ageing Dev 2007;128:137–48.

Vakifahmetoglu H, Olsson M, Zhivotovsky B. Death through a tragedy: mitotic catastrophe. Cell Death Differ 2008;15:1153–62.

Vellai T. Autophagy genes and ageing. Cell Death Differ 2009;16:94–102.

Vitale I, Senovilla L, Jemaa M, Michaud M, Galluzzi L, Kepp O, Nanty L, Criollo A, Rello-Varona S, Manic G, Métivier D, Vivet S, Tajeddine N, Joza N, Valent A, Castedo M, Kroemer G. Multipolar mitosis of tetraploid cells: inhibition by p53 and dependency on Mos. EMBO J 2010;29:1272–84.

Walen KH. Genetic stability of senescence reverted cells: genome reduction division of polyploidy cells, aneuploidy and neoplasia. Cell Cycle 2008;7:1623–9.

Walen KH. Mitosis is not the only distributor of mutated cells: non-mitotic endopolyploid cells produce reproductive genome-reduced cells. Cell Biol Int 2010;34:867–72.

West SC. Molecular views of recombination proteins and their control. Nat Rev Mol Cell Biol 2003;4:435–45

Wheatley D. Regrowth of tumour cells from supposedly terminal giant cells. Oncology News 2006;1:3.

Young AR, Narita M, Ferreira M, Kirschner K, Sadaie M, Darot JF, Tavaré S, Arakawa S, Shimizu S, Watt FM, Narita M. Autophagy mediates the mitotic senescence transition. Genes Dev 2009;23:798–803.

Received 18 October 2010/11 January 2011; accepted 21 January 2011

Published as Immediate Publication 21 January 2011, doi 10.1042/CBI20100762

3.5. Therapy-induced polyploid tumour cells undergo nuclear architecture changes – Original paper V

Mutation Research xxx (2013) xxx–xxx

Contents lists available at SciVerse ScienceDirect

Mutation Research/Genetic Toxicology and Environmental Mutagenesis

journal homepage: www.elsevier.com/locate/gentox
Community address: www.elsevier.com/locate/mutres

Volume increase and spatial shifts of chromosome territories in nuclei of radiation-induced polyploidizing tumour cells

Jutta Schwarz-Finsterle[a], Harry Scherthan[b], Anda Huna[c], Paula González[a], Patrick Mueller[a], Eberhard Schmitt[a,d], Jekaterina Erenpreisa[c], Michael Hausmann[a,*]

[a] Kirchhoff-Institute for Physics, University of Heidelberg, Im Neuenheimer Feld 227, 69120 Heidelberg, Germany
[b] Bundeswehr Institute of Radiobiology affiliated to the University of Ulm, Neuherbergstr. 11, 80937 Munich, Germany
[c] Latvian Biomedical Research and Study Centre, Ratsupites 1, Riga LV-1067, Latvia
[d] Institute for Numerical and Applied Mathematics, Georg-August-University of Göttingen, Lotzestr, 16-18 37083 Göttingen, Germany

ARTICLE INFO

Article history:
Received 6 May 2013
Accepted 7 May 2013
Available online xxx

Keywords:
High dose X-irradiation
Endopolyploid tumour cells
FISH
Quantitative image analysis
Chromosome number
Nuclear architecture

ABSTRACT

The exposure of tumour cells to high doses of ionizing radiation can induce endopolyploidization as an escape route from cell death. This strategy generally results in mitotic catastrophe during the first few days after irradiation. However, some cells escape mitotic catastrophe, polyploidize and attempt to undergo genome reduction and de-polyploidization in order to create new, viable para-diploid tumour cell subclones. In search for the consequences of ionizing radiation induced endopolyploidization, genome and chromosome architecture in nuclei of polyploid tumour cells, and sub-nuclei after division of bi- or multi-nucleated cells were investigated during 7 days following irradiation. Polyploidization was induced in p53-function deficient HeLa cells by exposure to 10 Gy of X-irradiation. Chromosome territories #1, #4, #12 and centromeres of chromosomes #6, #10, #X were labelled by FISH and analysed for chromosome numbers, volumes and spatial distribution during 7 days post irradiation. The numbers of interphase chromosome territories or centromeres, respectively, the positions of the most peripherally and centrally located chromosome territories, and the territory volumes were compared to non-irradiated controls over this time course. Nuclei with three copies of several chromosomes (#1, #6, #10, #12, #X) were found in the irradiated as well as non-irradiated specimens. From day 2 to day 5 post irradiation, chromosome territories (#1, #4, #12) shifted towards the nuclear periphery and their volumes increased 16- to 25-fold. Consequently, chromosome territories returned towards the nuclear centre during day 6 and 7 post irradiation. In comparison to non-irradiated cells (~500 μm^3), the nuclear volume of irradiated cells was increased 8-fold (to ~4000 μm^3) at day 7 post irradiation. Additionally, smaller cell nuclei with an average volume of about ~255 μm^3 were detected on day 7. The data suggest a radiation-induced generation of large intra-nuclear chromosome territories and their repositioning prior to genome reduction.

1. Introduction

Somatic mammalian cells possess a diploid genome, whose propagation is regulated by a tightly controlled cell cycle. Cell cycle control involves several checkpoints that ensure genomic integrity and an ordered cell division. The tumour suppressor protein p53 plays a key role in the regulation of the cell cycle and activation of apoptotic pathways [1]. Furthermore, p53 is involved in cell differentiation [2], senescence, and DNA repair processes [3].

When exposed to high doses of ionizing radiation, tumour cells show different escape routes that bypass cell cycle checkpoints and apoptosis, especially when p53 is dysfunctional [4]. Tumour cells can escape cell death by endopolyploidization [5]. Although most of these endopolyploid tumour cells (ETC) run into mitotic catastrophe [6] and cell death, some can activate survival strategies that include genome reduction and the generation of viable para-diploid tumour cells. These cells resume mitotic cell cycle and are often more resistant to ionizing radiation [7–9].

Erenpreisa et al. [10,11] have described profound cell cycle changes in HeLa cells after 10 Gy of X-irradiation:

- On day 1–2 post irradiation, the cells undergo mitosis followed by the cleavage furrow regression and reunion of sister nuclei into bi-nucleated cells.

Abbreviations: ETC, endopolyploid tumour cell; MNGC, multi-nucleated giant cells; NT, non-irradiated; FISH, fluorescence in situ hybridization; SSC, saline sodium citrate buffer; PBS, phosphate buffered saline; pCT, most peripherally located chromosome territory; cCT, most centrally located chromosome territory.

* Corresponding author. Tel.: +49 6221 549824; fax: +49 6221 549112.
E-mail address: hausmann@kip.uni-heidelberg.de (M. Hausmann).

1383-5718/$ – see front matter © 2013 Elsevier B.V. All rights reserved.
http://dx.doi.org/10.1016/j.mrgentox.2013.05.004

- On day 2–3 post irradiation, the individual sub-nuclei in bi-nucleated cells start to undergo intra-cellular asynchronous a-cytotomic bi-polar mitosis forming multi-nucleated giant cells (MNGC). At that time, the cell population consists of 70% MNGC, which may contain individual sub-nuclei with 1C, 2C, 3C, 4C, and 6C DNA content. In addition a smaller proportion of mononuclear giant cells emerge at that time point.
- On day 3–5 post irradiation, there is an increase of polyploidy due to endoreduplication cycles reaching in sum up to 24–32C in giant cells; from day 5 onwards, a wave of bi-polar and a-cytotomic multi-polar mitoses occurs; the latter forms secondary MNGCs.
- From day 6 to 9 post irradiation, the majority of giant cells stop endoreduplication and undergo senescence, while some release para-diploid mitotic sub-cells, starting clonogenic regrowth [10,11].

These complex changes in irradiated polyploidizing tumour cells are accompanied by increased expression of Aurora B-kinase, a core component of the chromosomal passenger complex. The up-regulation of Aurora B-kinase occurs between day 3 and day 6 post irradiation and may play a significant role in late mitotic activity of ETCs which may lead to genome reduction [10]. Aurora B has been shown to play a role in sister chromatid cohesion and homologue segregation in meiosis [12,13]. Likewise, there was an up-regulation of the meiotic REC8 cohesin in ETCs and MNGCs during day 3 to day 6 [14]. REC8 mediates sister chromatid cohesion and thereby the correct chromosome disjunction in meiosis [14]. Beyond these findings, the activation of other meiosis specific genes was noted during de-polyploidization phase of ETCs [15].

Ionizing radiation exposure elicits DNA damage response up-regulating different repair processes which are known to be correlated with changes in chromatin compaction states (e.g., heterochromatin or euchromatin) [16], chromosome association [17,18], and nuclear architecture [19–22]. In irradiated p53-deficient endopolyploidizing cells, additive rounds of the DNA double strand break repair by homologous recombination were occurring during replication cycles [23]. Thus, the genome architecture of acutely irradiated ETCs may also be influenced in a certain way by DNA repair mechanisms.

It is well established that in the interphase nucleus of diploid somatic cells chromosomes and sub-chromosomal units occupy non-randomly positioned distinct, largely mutually exclusive territories and sub-domains [24–27] which are arranged dynamically depending on gene expression [28]. The intra-nuclear position of chromosome territories is described by the relative radial distance to the nuclear centre or border, respectively. Positioning of chromosome territories and sub-chromosomal domains is generally non-random, and seems to follow special functionally correlated constraints; for instance, a correlation of a chromosome territory's radial position with its gene density [29] or gene activity [30] has been observed. Relative chromosome positioning and inter-chromosome compartment form an intra-nuclear network [31] that is well preserved within a particular cell type [30,32]. It has also been shown that radiation-induced translocations seem to depend on the neighbourhood of the involved chromosome territories [33,34], so that larger chromosomes may participate more frequently in exchanges than smaller ones [19].

Changes in the spatial chromosomal organization in irradiation-induced polyploidizing tumour cells have so far not been systematically investigated. Several findings indicate that DNA damage at larger doses may induce local re-positioning that leads to clustering of damaged sites [17,18,35] and increasing of mis-repair rates at larger doses [36]. However, little is known about the spatial events and constraints that chromosomes undergo during polyploidization of irradiated tumour cells. Here, we exposed p53-deficient HeLa cells to 10 Gy of X-radiation and analysed the numbers, sizes, and positions of chromosome territories (#1, #4, #12) during 7 days for radiation-induced changes.

2. Materials and methods

2.1. Cell culture

HeLa clone 3 cells of human cervix carcinoma were kindly provided by Ianzini [37]. The cells were grown on slides in Ham's F12 medium (Sigma–Aldrich, Steinheim, Germany) medium supplied with 10% FCS (Biochrom, Berlin, Germany) and penicillin/streptomycin (Life Technologies, Darmstadt, Germany) at 37 °C in a 5% CO_2 humidified incubator (Binder, Tuttlingen, Germany). For experimental studies the cells were maintained in log phase of growth for at least 24 h prior to irradiation. At ~60% sub-confluence, the cell cultures were irradiated at room temperature, and further cultured for 1–7 days post irradiation.

2.2. Irradiation

The cells grown on sterilized glass slides (Menzel Gläser, Braunschweig, Germany) were irradiated in medium in Quadriperm culture dishes (Nunc, Roskilde, Denmark) at room temperature. The cells were exposed to 10 Gy of 240 kV X-rays at a dose rate of 1 Gy/min. The Roentgen tube was filtered with 3 mm beryllium and driven at 13 mA current (Isovolt 320/10; Seifert, Ahrensberg, Germany), and the delivered dose was measured with a Duplex dosimeter (PTW, Freiburg, Germany). After irradiation the cells were further cultured for the time indicated and subsequently fixed with ice-cold acetic acid:methanol (1:3) (Merck, Darmstat, Germany; J.T. Baker, Deventer, Netherlands).

2.3. Chromosome preparation and FISH painting of metaphases

Half confluent HeLa clone 3 cultures were arrested at metaphase with 0.05 mg/mL Colcemid (GIBCO, Carlsbad, CA) for 3 h and then harvested by Trypsin (Invitrogen, Karlsruhe, Germany) treatment. Chromosome spreads were obtained according to standard acetic acid:methanol (1:3) fixation protocols. Slides were stored at −20 °C until use. Three-colour chromosome painting (FISH) with a combination of chromosome #1, #4 and #12 paint probes (MetaSystems, Altlussheim, Germany) was done as published [38,39]. Briefly: The hybridization mix was heated to 72 °C for 5 min and then incubated at 37 °C for 10 min prior to applying the mixture to the denatured chromosomes. Metaphase chromosomes were denatured on slides for 2 min at 72 °C in 70% formamide/2× SSC (Sigma–Aldrich, Steinheim, Germany; Invitrogen, Karlsruhe, Germany) and then dehydrated in a series of 70%, 90% and 100% ethanol (J.T. Baker, Deventer, Netherlands). Slides carrying denatured chromosomes were pre-warmed to 37 °C prior to the application of the denatured hybridization mixture, then covered by a 20 mm × 50 mm coverslip (Menzel Gläser, Braunschweig, Germany) and sealed with rubber cement (Marabu, Tamm, Germany). Hybridization was performed overnight at 37 °C in a moist chamber. The slides were then washed three times in 50% formamide/2× SSC, pH 7.0, at 42 °C for 15 min each followed by washes at 42 °C in 2× SSC, pH 7.0, for 15 min, in PN buffer (100 mM Na_2HPO_4, 50 mM NaH_2PO_4, 0.1% Triton X-100 (v/v))/0.1% Nonidet P40 (Sigma–Aldrich, Steinheim, Germany) pH 8.0, for 15 min, and in 3% bovine serum albumin (Sigma–Aldrich, Steinheim, Germany) in 2× SCC for 30 min. At least 20 metaphases were analysed visually.

2.4. FISH probes used for chromosome labelling in cell nuclei

Chromosome territories in five different specimens [non-irradiated control cells (NT); irradiated HeLa cells at day 2, 5, 6 and 7 (d2, d5, d6, d7) post radiation exposure] were hybridized with chromosome painting probes (MetaSystems, Altlussheim, Germany). The slides of NT and d2 were hybridized with a combination of three chromosome painting probes (#1, #4 and #12). This combined probe set had the following spectral signatures: (a) Chromosome #1: Texas Red (red signature: $\lambda_{ex/em}$ = 586 nm/605 nm); (b) chromosome #4: FITC (green signature: $\lambda_{ex/em}$ = 488 nm/518 nm); (c) chromosome #12: 1/1 mixture of Texas Red and FITC resulting in a yellow signature (Fig. 1a).

The slides of d5, d6, and d7 were simultaneously hybridized with two probes for chromosome #1 (Texas Red) and chromosome #4 (FITC). Chromosome #12 was separately hybridized with a probe showing the same spectral signature as the chromosome #4 probe.

In addition to whole chromosome painting probes also pericentric satellite probes (QBIOGENE – Molecular Cytogenetics/Diagnostics, Illkirch Graffenstaden, France) for chromosomes #6, #10, and #X were applied and hybridized according to the manufacturer's protocol. Slides of non-irradiated control cells (NT), and irradiated specimens at day 1 and 2 (d1, d2) were inspected visually for chromosome counting.

2.5. FISH (chromosome painting, centromere labelling) of cell nuclei

For quantitative microscopy, the cells fixed on SuperFrost Plus slides (Menzel Gläser, Braunschweig, Germany) were treated according to the following protocol: For permeabilization of the membrane, the slides were incubated in 0.7 mL

Please cite this article in press as: J. Schwarz-Finsterle, et al., Volume increase and spatial shifts of chromosome territories in nuclei of radiation-induced polyploidizing tumour cells, Mutat. Res.: Genet. Toxicol. Environ. Mutagen. (2013), http://dx.doi.org/10.1016/j.mrgentox.2013.05.004

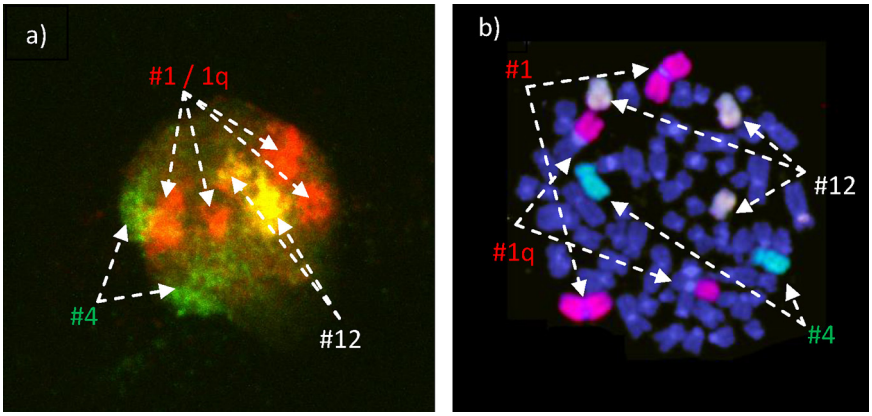

Fig. 1. (a) Microscopic image of a typical cell nucleus (NT) after chromosome painting with a triple probe for the CTs #1 (red), #4 (green), and #12 (yellow). (b) Microscopic image of a typical metaphase spread after chromosome painting with a triple probe for chromosomes #1 (red), #4 (green), and #12 (yellow).

Triton-X100/99.3 mL 1× SSC (Merck, Darmstat, Germany; Invitrogen, Karlsruhe, Germany) for 30 min and washed with 2× SSC for 5 min. The specimens were incubated in RNase A (Sigma–Aldrich, Steinheim, Germany) for 30 min at 37 °C [2 μl stock solution (100 mg/mL) and 98 μL 2× SSC per slide]. After washing with 2× SCC for 3 min and 1× PBS (Invitrogen, Karlsruhe, Germany) for 5 min, proteins were digested in pepsin (Sigma–Aldrich, Steinheim, Germany) [21 μL stock solution (100 mg/mL) + 70 μL 0.01 M HCl in PBS] for 45 s. This was followed by a washing procedure in 1× PBS for 5 min, and in an ethanol series of 70%, 90%, and 100% for 3 min each. Denaturation was done in 70% formamide/2× SSC (at pH 7–7.2) for 5 min at 75 °C. Afterwards the slides were washed in 70%, 90%, and 100% ice-cold ethanol for 3 min each. In the case of the slides NT and d2, 2 μL of the probe mix combined with 2 μL of 60% formamide were dropped on the specimens. The in situ hybridization took place for 48 h at 37 °C. For the specimens d5, d6, and d7, the procedure was slightly different: 7 μL or 14 μL, respectively, of the probe mix were denatured during incubating at 75 °C for 5 min. The tubes were shortly cooled on ice. After that, the probes were incubated at 37 °C for 30 min and centrifuged for a short time. Then, the probe mix was pipetted onto the thermally denatured specimens and hybridized at 37 °C for 24 h.

For post hybridization treatment, all slides were washed with 1× SSC at 75 °C and 2× SSC/0.01% Tween at room temperature.

The cell nuclei were either counterstained with DAPI (Sigma–Aldrich, Steinheim, Germany) or with TO-PRO®-3 (Invitrogen, Karlsruhe, Germany) ($\lambda_{ex/em}$ = 642 nm/661 nm) 1:1000 in 1× PBS. The specimens NT, d1 and d2 were incubated with the antifade reagent ProLong® Gold (Invitrogen, Karlsruhe, Germany) at 37 °C for two days. The specimens d5, d6, and d7 were mounted in Immuno Mount™ antifade solution (GeneTex Inc., Irvine, USA).

2.6. 3D-Microscopy

Up to 50 cells of NT and d2 each were imaged with a Leica TCS NT confocal laser scanning microscope using a high numerical aperture lens (63×/NA 1.4 oil) and appropriate filter settings. Up to 50 cell nuclei each of the data sets d5, d6, und d7 were imaged with the Nikon TE2000-E Perkin Elmer UltraVIEW ERS Spinning Disc confocal microscope also using high numerical aperture lenses (63×/NA/1.2 water) and appropriate filter settings. For 3D-reconstructions the axial step size was 203 nm for all z-stacks.

2.7. Image evaluation and statistical analysis

The numbers and positions of the chromosome territories #1, #4, and #12 in the irradiated specimens d2, d5, d6, and d7 were analysed and compared to data obtained from non-irradiated control cells (NT). 3D-microscopy image data stacks were evaluated by means of the freely available software 'Nemo', version 1.5 (https://www-lgc.toulouse.inra.fr/nemo/) implemented into the image analysis software package "ImageJ". For the different fluorescent objects within the cell nuclei, the shortest geometrical distances of the barycentres to the nuclear border were calculated. For all chromosomes, a difference or change of ploidy did not influence the result since only the distances of the most peripherally (pCT) and the most centrally (cCT) located chromosome territories were always determined. These values were statistically compared over the time course.

The results were expressed as cumulative frequency histograms of distances. For the statistical pairwise analysis of these histogram curves, which show different shapes, the most appropriate test was the Kolmogorov–Smirnov test [40]. The null hypothesis of this test is that two samples are drawn from the same frequency distribution. On acceptance of the alternative hypothesis, namely that two frequency histograms belong to different distributions, the significance level of this test defines an error probability for the two distance distributions being equal, i.e. two distributions being of the same entity [41]. In general, this error level was taken to be up to 5% or even less because the Kolmogorov–Smirnov test tends to be conservative. On the other hand, the test is robust and can be easily applied to distributions with rather large deviations in sample numbers. Its applicability and usefulness in histochemistry and cytochemistry has been widely demonstrated (e.g. [42,43]).

For the volume calculations of the cell nuclei and chromosome territories, the voxels covered by the object were counted and multiplied with the respective voxel volume of the image (for details see e.g. [44]). Finally, the average volumes of all detected nuclei or chromosome territories were determined.

3. Results

3.1. Metaphase karyotyping using whole chromosome painting

The numerical karyotype of non-irradiated HeLa clone 3 cells was studied in more than 100 DAPI stained cells. A modal number of 65 chromosomes per cell were observed, verifying its hypotriploid nature without radiation treatment (non-irradiated control). The metaphase analysis of 126 metaphase spreads shows the occurrence of two chromosomes #1, two translocated chromosome arms #1q, two chromosomes #4 and three chromosomes #12 per metaphase (Fig. 1b).

3.2. Interphase FISH and chromosome numbers

Chromosome painting experiments on interphase cell nuclei of NT cells corroborate the metaphase analysis data for chromosome #1 (2 or 3 FISH labelled territories/cell) and #4 (mostly 2 FISH labelled territories/cell). For chromosome #12, two labelled

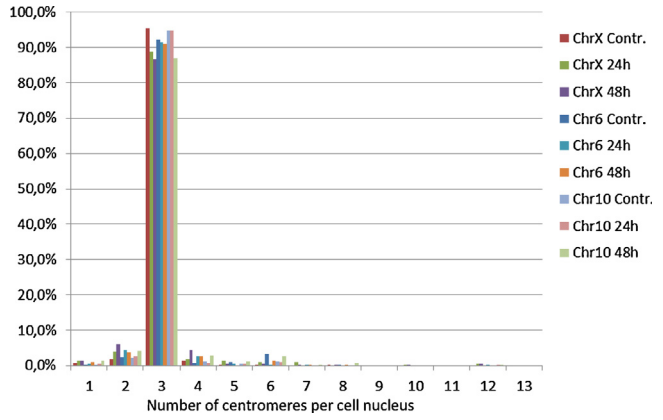

Fig. 2. Frequency (%) of cell nuclei vs. number of chromosomes #6, #10 and #X counted by visual inspection of centromere labels. The columns refer to the specimens NT (Contr.), d1 (24 h), and d2 (48 h) for each chromosome.

Please cite this article in press as: J. Schwarz-Finsterle, et al., Volume increase and spatial shifts of chromosome territories in nuclei of radiation-induced polyploidizing tumour cells, Mutat. Res.: Genet. Toxicol. Environ. Mutagen. (2013), http://dx.doi.org/10.1016/j.mrgentox.2013.05.004

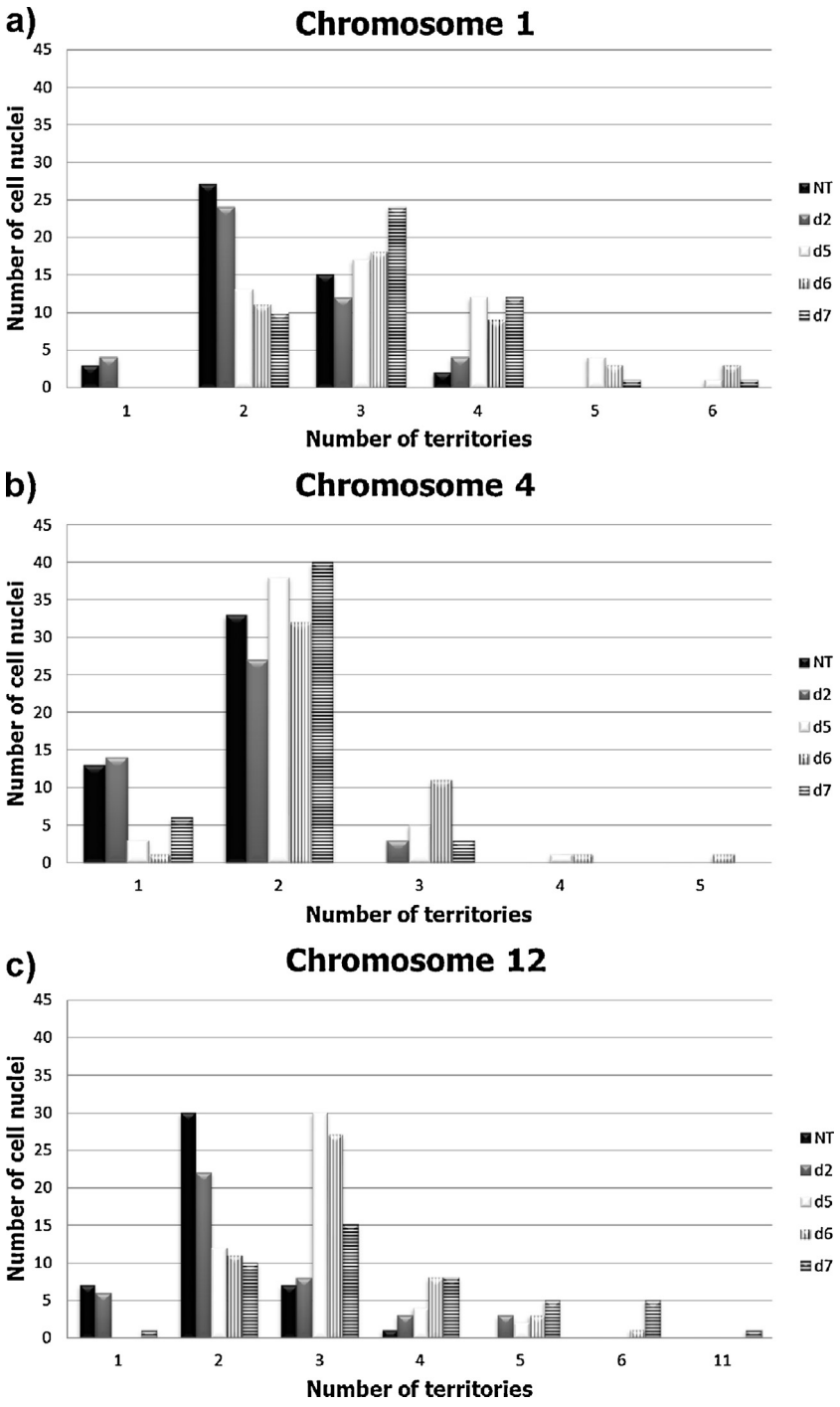

Fig. 3. Frequency of cell nuclei vs. number of automatically segmented painting territories referring to chromosome #1 (a), #4 (b), and #12 (c). The different columns represent the data at the respective day post IR. Note that the most notable shift of the number of chromosome territories is observed on day 5.

territories were mostly observed in the NT specimen. Since metaphase analysis suggests three chromosomes #12 in HeLa clone 3 cells, it cannot be excluded that two chromosome territories were spatially associated into one detectable territory.

In order to further study the hypotriploid nature of the HeLa clone 3 cells in use, 440–850 interphase cell nuclei were analysed each after centromere-specific FISH of chromosome #6, # 10, and #X. For all three chromosomes, more than 92% of the cell nuclei showed three signals in the NT specimens. The hypotriploid karyotype for chromosomes #6, #10, and #X was maintained on day 1 and 2 (Fig. 2: 24 h, 48 h) post irradiation, which was displayed by more than 86% of the cells with three centromere-specific signals (Fig. 2).

Automated image analysis of the chromosome painting experiments revealed an increase of cells with higher numbers of chromosome territory #1 with advancement of time post irradiation. The most notable shift was observed up to day 5. From day 5 to day 7 the majority of the cells showed 3 or 4 distinctly labelled territories #1. In contrast, the number of chromosome territories #4 was found to be constant over the complete time course and revealed two clearly labelled territories in most nuclei (Fig. 3a and b). For chromosome #12, mostly two painted territories were observed

Please cite this article in press as: J. Schwarz-Finsterle, et al., Volume increase and spatial shifts of chromosome territories in nuclei of radiation-induced polyploidizing tumour cells, Mutat. Res.: Genet. Toxicol. Environ. Mutagen. (2013), http://dx.doi.org/10.1016/j.mrgentox.2013.05.004

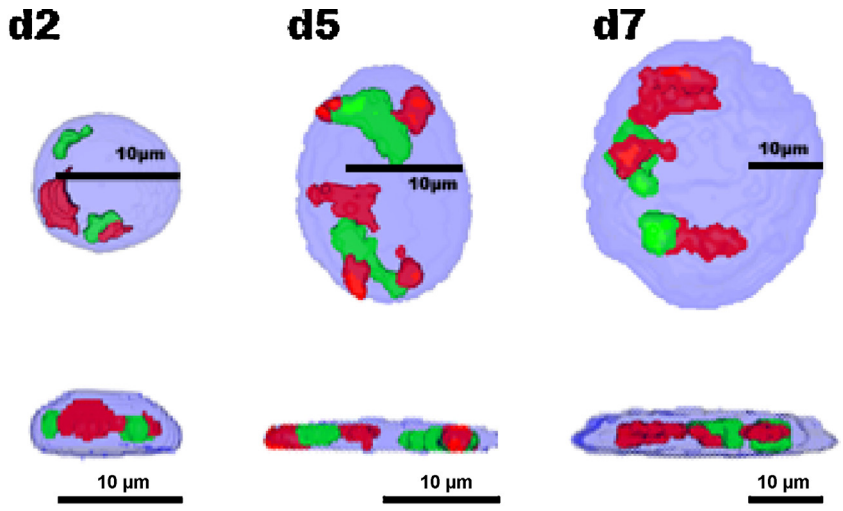

Fig. 4. Examples of segmented images of hybridized and DAPI-stained cell nuclei at d2, d5, and d7. Territories of chromosome #1 are labelled in red; territories in green represent chromosome #4. Upper row: maximum projection of the lateral (*xy*) image sections through a cell nucleus. Lower row: maximum projection of the axial (*yz*) image sections through a cell nucleus. Note the differently scaled bar for comparison of the cell nuclei.

in d2. With increasing nuclear and chromosome territory volumes from day 5 to day 7, the average number of the detected chromosomes #12 shifted to three copies. This, however, could be the result of a better image segmentation of the highly jagged staining pattern of this chromosome in larger cell nuclei (Fig. 3c). Thus, this data confirmed the previous observations [9,10] that polyploidization of irradiated HeLa cells was mostly occurring by multi-nucleation (through a-cytotomic mitoses) and in a smaller proportion of giant cells by multiplication of the chromosome numbers at the peak of polyploidy (day 5).

3.3. Volumes of chromosome territories and cell nuclei

Nuclear and chromosome territory volumes were determined from the segmented 3D images. In Fig. 4 typical examples for d2, d5 and d7 are shown. Size and shape for non-irradiated control (NT; data not shown) and d2 cell nuclei appeared to be similar, whereas d5, d6, and d7 nuclei appeared to be much larger and in many cases also flattened. This means that the z-dimension was not considerably increased in d5, d6, and d7 compared to d2, which might be due to the morphology of the adherently growing HeLa clone 3 cells. The frequency distributions of the nuclear volumes showed a more pronounced bimodal distribution for NT and d2 than for d5, d6 and d7, indicating the status of the cell nuclei before or after DNA duplication (Fig. 5a–e), when most cells became arrested at G2 and polyploidized by mitotic slippage. The range of nuclear volumes increased with advancement of time post irradiation. The average volume of non-irradiated cell nuclei (NT) was about 500 μm^3, which was still maintained 2 days post irradiation (d2). Thereafter, the average nuclear volume increased with advancing time. At day 7 post irradiation it reached an 8-fold volume of about 4200 μm^3 (Fig. 5f). Aside from the larger nuclei at d7, smaller cell nuclei with an average volume of 255 μm^3 were detected, which seem to have no small progenitors from day 3 to day 6 post irradiation. Most of these small cell nuclei were found to be adjacent to a large cell nucleus and often to be bridged to it (Fig. 6). This indicates that they result from the selective de-polyploidization of the mother cell. The occurrence of such asymmetric cell divisions was very typical for HeLa clone 3 cells after high dose IR exposure [10]. The smaller cell nucleus might be interpreted as a daughter nucleus of a senescing mother cell [11].

The most significant findings, however, are presented in Fig. 7: Chromosome territory volumes increased up to 25-fold in case of chromosome #12 (Fig. 7a), 21-fold for chromosome #4 (Fig. 7b), and 16-fold for chromosome #1 (Fig. 7c). The average nuclear volume increased from d2 to d7 only by a factor of about 10. These findings indicate a differential loss of compaction and/or enlarged entanglement of the chromosome territories, which may reflect the extensive DNA repair processes during that time. In particular, a sharp increase of chromosome territory volumes was observed at the peak of polyploidization at day 5 (5- to 9-fold), while the nuclear volumes increased only 3-fold. On the further days the nuclear volumes increased more significantly.

3.4. 3D radial positions of painted chromosome territories #1, #4, and #12

The absolute distances of the barycentres of the painted territories to the nuclear edges were determined and compared for NT (control), d2, d5, d6, and d7. The results are summarized by normalized cumulative frequency distributions (Fig. 8). The most peripheral (pCT) and the most central (cCT) chromosome territories were compared because all other territories were located in between. A shift of a frequency distribution curve to the left indicated a territory position closer towards the nuclear periphery; a shift to the right a position closer towards the nuclear centre. Compared to NT, all tested chromosome territories changed their 3D-positions during the time course post irradiation (d2–d7). In Table 1 the statistical results for the Kolmogorov–Smirnov test are summarized:

- Chromosome #1: the positions of the pCTs in d5 were significantly different ($p = 0.0001$) to their positions in NT and d2. A similar result was obtained for the cCTs in d5 compared to NT ($p = 0.001$) and to d2 ($p = 0.013$). The distance distributions of the cCTs of d6 and d7 compared to NT and d2 did not show any statistically significant difference.
- Chromosome #4: from d2 to d6 the distance frequency distribution of pCTs significantly shifted to the periphery of the cell nucleus ($p = 0.0001$); the positions in d7 appeared to be compatible with NT. The distance frequency distributions of cCTs in d2 and d5 were significantly different ($p = 0.0001$) compared to the distance frequency distributions of cCTs in d6 and d7. Again for d6 and d7 no significant difference was found in comparison to the distribution of NT.

Please cite this article in press as: J. Schwarz-Finsterle, et al., Volume increase and spatial shifts of chromosome territories in nuclei of radiation-induced polyploidizing tumour cells, Mutat. Res.: Genet. Toxicol. Environ. Mutagen. (2013), http://dx.doi.org/10.1016/j.mrgentox.2013.05.004

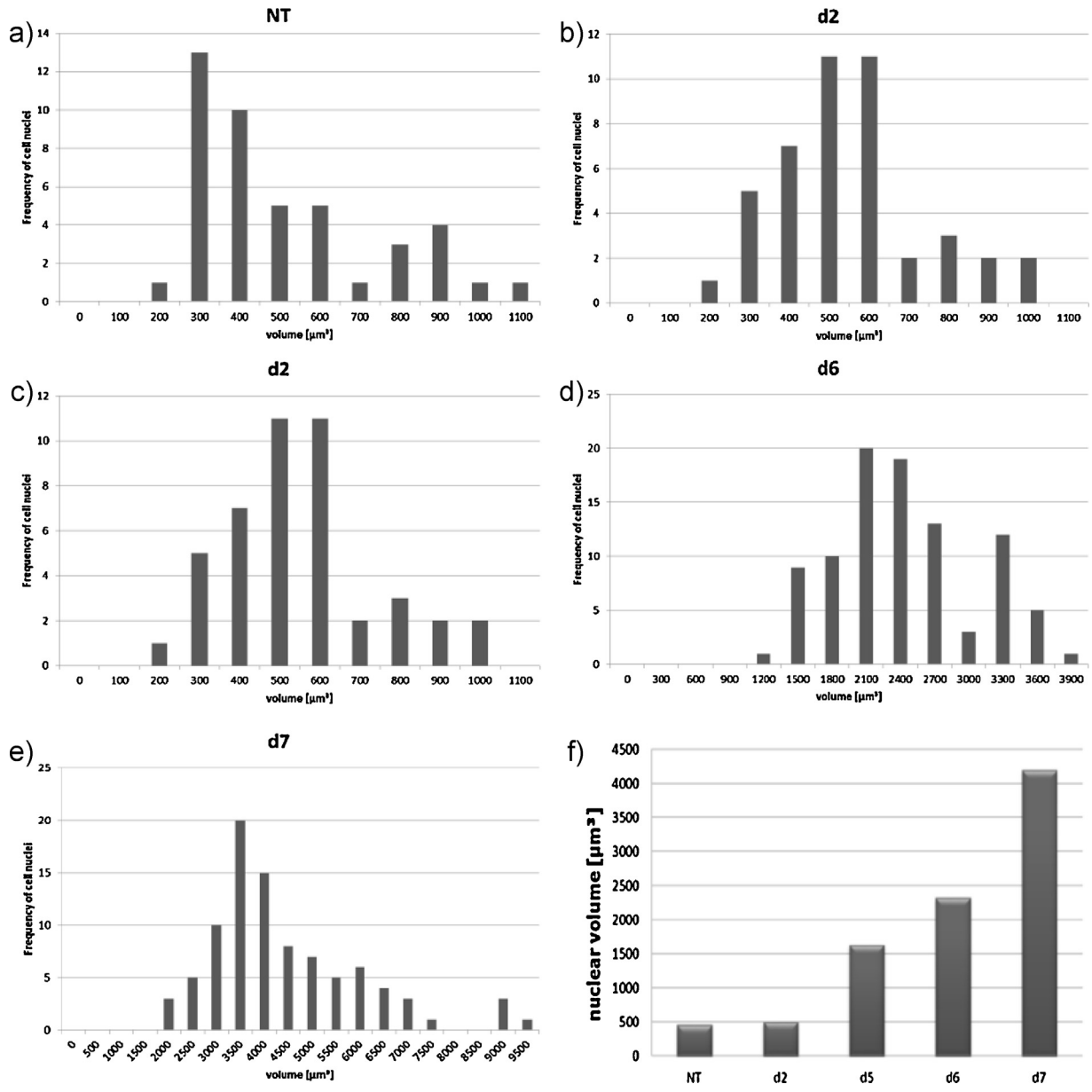

Fig. 5. Frequency histograms of nuclear volumes for NT (a), d2 (b), d5 (c), d6 (d), d7 (e). The columns represent volume values in steps of 100 μm^3 (a and b), 300 μm^3 (c and d), and 500 μm^3 (e). (f) Average volumes of cell nuclei obtained from the values of a–e. Note: the nuclear volumes on d7 refer only to the large nuclei detected. The modal values of nuclear volumes increase 3- to 5-fold on day 5.

- Chromosome #12: the frequency distribution curves of the pCTs showed shifts similar to those of the corresponding curves of chromosome #1 and #4. The distance frequency distributions of d5, d6, and d7 significantly differed from the distance frequency distribution of NT ($p = 0.0001$). In contrast to the pCTs the distance frequency distributions of the cCTs were not statistically different from those of NT.

4. Discussion

Recent investigations of the nuclear architecture and the positions of chromosome territories have demonstrated non-randomness and dynamic functionally correlated changes [24–32]. Here, dynamic features of the nuclear and chromosome architecture in p53-deficient, polyploidizing HeLa cell nuclei during 7 days following high dose (10 Gy) X-ray radiation exposure have been studied for the first time. It should be noted that only mononuclear endopolyploid cells or single sub-nuclei of multi-nucleated cells were investigated. In general, the data suggested that irradiation-induced endopolyploidization is accompanied by 3D intra-nuclear chromosome re-positioning in p53-deficient tumour cells.

Although high dose ionizing radiation causes massive DNA damage, a significant change in the numbers of chromosome territories was not observed in individual nuclei. This may be explained by DNA damage-induced re-replication during the polyploidization phase, which involves the maintenance of interchromosomal interactions (e.g. diplochromosomes) and gross chromosome territorial re-organization, and by multi-nucleation of most cells through a-cytotomic mitoses as well.

In contrast to territory numbers, significant increases of nuclear and territory volumes were found in the specimens d5, d6, and d7. Day 5 was the last day when endoreduplication cycles occurred and DNA repair took place, followed by a wave of de-polyploidizing mitoses [11]. Thus, this sharp increase in chromosome territory

Please cite this article in press as: J. Schwarz-Finsterle, et al., Volume increase and spatial shifts of chromosome territories in nuclei of radiation-induced polyploidizing tumour cells, Mutat. Res.: Genet. Toxicol. Environ. Mutagen. (2013), http://dx.doi.org/10.1016/j.mrgentox.2013.05.004

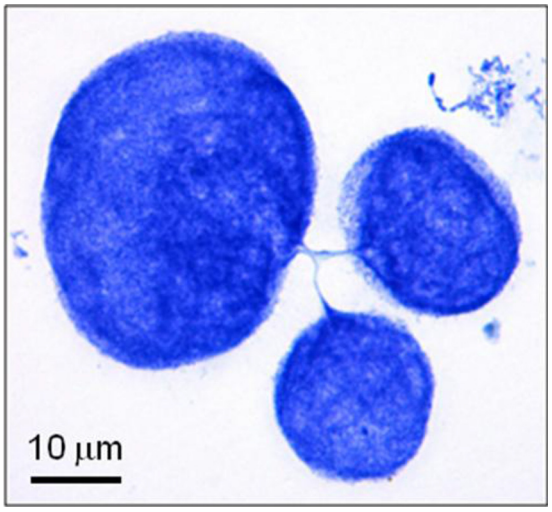

Fig. 6. Example of cell nuclei after DNA staining (blue) showing DNA bridges between the large and the two small cell nuclei indicating their origin from the larger mother nucleus.

Table 1
Kolmogorov–Smirnov significance levels for two cumulative frequency distributions of bary centre distances to the nuclear edge for CTs #1, #4, and #12. The numbers represent the significance level of two compared distributions (NT, d2, d5, d6, d7) being statistically different. Values for cCT above diagonal (indicated by '-'), for pCT below diagonal.

#1	NT	d2	d5	d6	d7
NT	"-"	0.000	0.000	0.000	0.000
d2	0.154	"-"	0.000	0.072	0.015
d5	0.000	0.013	"-"	2.567	5.552
d6	11.710	3.455	0.004	"-"	>50
d7	2.714	23.524	1.480	26.634	"-"

#4	NT	d2	d5	d6	d7
NT	"-"	0.001	0.000	0.002	26.032
d2	0.000	"-"	1.366	0.867	0.002
d5	0.000	31.789	"-"	7.633	0.000
d6	>50	0.000	0.004	"-"	0.042
d7	10.999	0.000	0.000	>50	"-"

#12	NT	d2	d5	d6	d7
NT	"-"	0.205	0.000	0.000	0.000
d2	5.722	"-"	0.006	0.098	0.401
d5	3.192	>50	"-"	17.784	44.757
d6	25.315	>50	17.784	"-"	>50
d7	4.677	0.140	0.027	0.317	"-"

volumes may be due to the particular changes of the nuclear chromatin preparing through DNA endoreplication/repair [23] and epigenetic changes of the interphase chromosomes for the upcoming divisions. In support, the activation of stem cell transcription factors in radiation induced polyploid tumour cells persisting in secondary descendents was observed. Irradiation of tumour cells was shown to induce stemness transcription profiles only in the endopolyploidy fraction [45]. Such a response has recently been confirmed on irradiated clinical material from breast cancer [46]. Polyploidy as such characterized by considerable change of the transcription profile [47] and the presence of chromosomes and molecular networks in duplicates may favour this phenotypic switch for escape of DNA damage resistant cells. On the other hand,

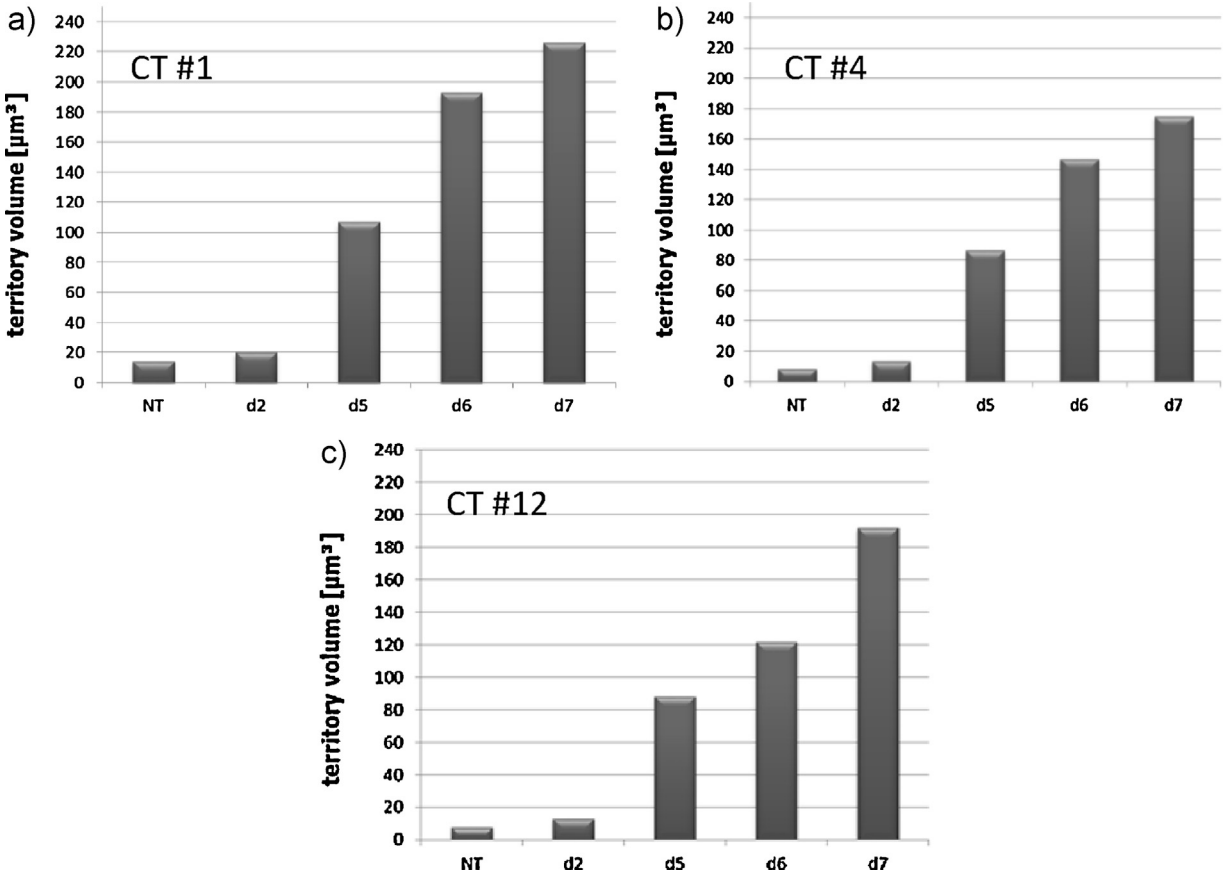

Fig. 7. Average volumes of CTs #1 (a), CTs #4 (b), and CTs #12 (c) for NT, d2, d5, d6, and d7. On day 5 an increase (12- to 25-fold) of the average chromosome territories volumes is observed.

Please cite this article in press as: J. Schwarz-Finsterle, et al., Volume increase and spatial shifts of chromosome territories in nuclei of radiation-induced polyploidizing tumour cells, Mutat. Res.: Genet. Toxicol. Environ. Mutagen. (2013), http://dx.doi.org/10.1016/j.mrgentox.2013.05.004

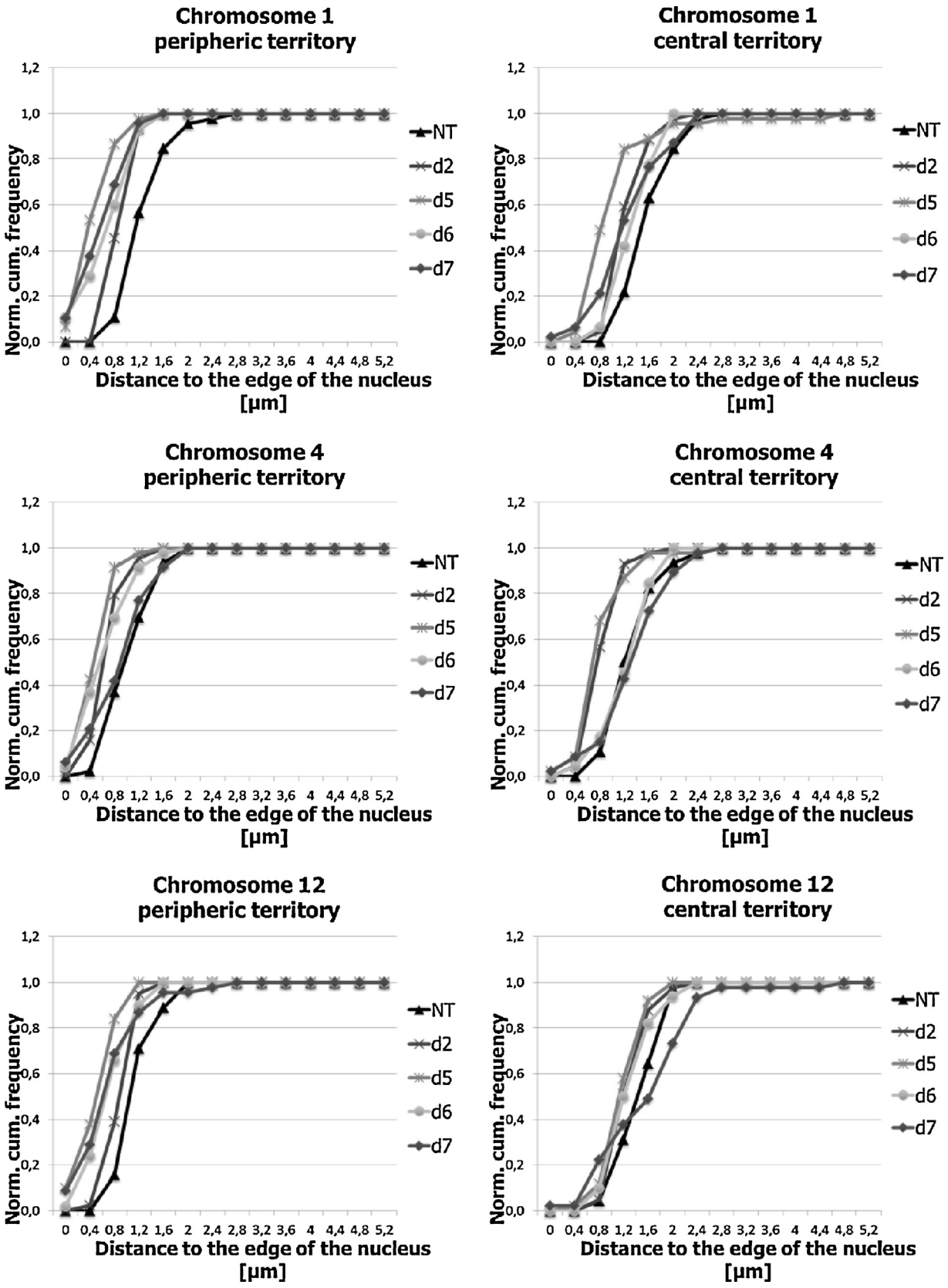

Fig. 8. Normalized cumulative frequency histograms of the measured distances in µm of the CT bary centre to the nuclear border. The positioning of fixed FISH-labelled CTs #1, #4, and #12 in HeLa clone 3 cells before and after 10 Gy γ-radiation exposure was measured. For the analysis, the most peripherally (pCT) and the most centrally (cCT) located chromosome territories were compared over the time course. Left column: distributions of the pCTs #1, #4, and #12. Right column: distributions of the cCTs #1, #4, and #12.

Please cite this article in press as: J. Schwarz-Finsterle, et al., Volume increase and spatial shifts of chromosome territories in nuclei of radiation-induced polyploidizing tumour cells, Mutat. Res.: Genet. Toxicol. Environ. Mutagen. (2013), http://dx.doi.org/10.1016/j.mrgentox.2013.05.004

de-compacted chromatin states may reflect a stem cell-like nuclear organization that may contribute to enhanced DNA repair capabilities. It may also be a cause of the chromosome territory volume enlargement in reprogrammed HeLa ETCs observed in our study. The increase of the analysed territory volumes was much stronger than the simultaneous increase of nuclear volumes. Under the assumption that this would also be the case for all other chromosomes, a stronger intermingling would be expected. In complement with the observed chromosome territory contour jaggedness especially on day 5 and 6, these three most important changes of the chromosome parameters (increase of volumes, partial sharing of the territories and fringy contours) should be attributed to endopolyploidization as such. On day 6 and day 7 several cell nuclei continued to increase their volumes; however, many cell nuclei also became flattened, changing the ratio of *x* and *y* diameter to *z* diameter presumptively due to senescence [48].

Chromosomes in the interphase nucleus of normal human cells occupy specific 3D positions in correlation to their gene density and size, with the gene-rich and small chromosomes being located more centrally than gene-poor and larger chromosomes [26–28]. Radiation treatment as well as exposure to DNA strand breaking chemicals leads to chromosomal aberrations and to movements of the chromatin, changing the nuclear architecture [17,18]. Over a period of 2 h after low dose irradiation, chromosome domains were found to join together and subsequently drift apart from each other [49–51]. In the investigation presented here, the generation of large polyploid cell nuclei with increased chromosome territories and nuclear volumes were associated with a considerable change in the genome architecture. This was correlated to a movement of the positions of chromosome territories #1 and #4 to the nuclear periphery until 5 days after irradiation. In d6 and d7 most chromosome territories showed a repositioning towards the nuclear centre, a position that was comparable to the one in non-irradiated cells (NT). This effect was less pronounced for chromosome territories #12 that were always located peripherally. Those territories, being positioned around the nuclear centre prior to ionizing radiation exposure, seemed to show stronger repositioning processes during the post radiation phase. The change of the nuclear architecture back to the mode of non-irradiated cells may reflect that the cells exit endopolyploidization and approach metaphase.

In conclusion, our results using high dose ionizing radiation exposure together with 3D image analysis of chromosome positions and architecture in HeLa cells undergoing endoreduplication provided quantitative data showing that interphase chromosomes in polyploidizing cells undergo enlargement of the territories and chromosome specific spatial repositioning during the post radiation period. This correlates with the previously observed upregulation of proteins and factors of cellular DNA repair and survival. Further investigations should elucidate the relationship between the observed chromosomal movements as well as volume changes and de-polyploidization and the production of viable para-diploid daughter cells.

Funding

Anda Huna: European Social Fund within the project "Support for Doctoral Studies at University of Latvia". Jekaterina Erenpreisa: Latvian Scientific Council grant 341/012. Michael Hausmann: Bundesministerium für Umwelt, Naturschutz und Reaktor Sicherheit (Federal Ministry of Enviroment, Nature Protection and Reactor Safety) – permission for publication has been given.

Conflict of interest statement

None.

Acknowledgements

The authors thank the Nikon Imaging Centre, Heidelberg, for access to the spinning disc microscope. The financial support of the BMU (German Federal Ministry of Environment, Nature Protection and Reactor Safety) is gratefully acknowledged. Furthermore the authors thank Kristine Salmina (Latvian Biomedical Centre) for fruitful discussions of the manuscript, and C.C. Seegler-Sandbanck (European Institute of Feasibility Studies, Strasburg) for finding a way through cryptography to clarify the subject.

References

[1] S. Haupt, M. Berger, Z. Goldberg, Y. Haupt, Apoptosis – the p53 network, J. Cell Sci. 116 (2003) 4077–4085.
[2] L. Yi, C. Lu, W. Hu, Y. Sun, A.J. Levine, Multiple roles of p53 related pathways in somatic cell programming and stem cell differentiation, Cancer Res. 72 (2012) 5635–5645.
[3] X.-P. Zhang, F. Liu, W. Wang, Two-phase dynamics of p53 in DNA damage response, Proc. Natl. Acad. Sci U.S.A. 108 (2011) 8990–8995.
[4] J. Erenpreisa, M.S. Cragg, MOS, aneuploidy and the ploidy cycle of cancer cells, Oncogene 29 (2010) 5447–5451.
[5] T.M. Illidge, M.S. Cragg, B. Fringes, P. Olive, J. Erenpreisa, Polyploid giant cells provide a survival mechanism for p53 mutant cells after DNA damage, Cell Biol. Int. 24 (2000) 621–633.
[6] M. Castedo, J.L. Perfettini, T. Roumier, K. Andreau, R. Medema, G. Kroemer, Cell death by mitotic catastrophe: a molecular definition, Oncogene 23 (2004) 2825–2837.
[7] J. Erenpreisa, M.S. Cragg, Mitotic death: a mechanism of survival? A review, Cancer Cell Int. 1 (2001) 1–7.
[8] P.E. Puig, M.N. Guilly, A. Bouchot, N. Droin, D. Cathelin, F. Bouyer, L. Favier, F. Ghiringhelli, G. Kroemer, E. Solari, F. Martin, B. Chauffert, Tumour cells can escape DNA-damaging cisplatin through DNA endoreduplication and reversible polyploidy, Cell Biol. Int. 32 (2008) 1031–1043.
[9] J. Erenpreisa, M. Kalejs, F. Ianzini, E.A. Kosmacek, M.A. Machey, D. Emzinsh, M.S. Cragg, A. Ivanov, T.M. Illidge, Segregation of genomes in polyploidy tumor cells following mitotic catastrophe, Cell Biol. Int. 29 (2005) 1005–1011.
[10] J. Erenpreisa, A. Ivanov, S.P. Wheatley, E.A. Kosmacek, F. Ianzini, A.P. Anisimov, M. Mackey, P.J. Plakhins, T.M. Illidge, Endoploryploidy in irradiated p53-deficient tumour cell lines: persistence of cell division activity in giant cells expressing Aurora-B kinase, Cell Biol. Int. 32 (2008) 1044–1056.
[11] J. Erenpreisa, K. Salmina, A. Huna, E.A. Kosmacek, M.S. Cragg, F. Ianzini, A.P. Anisimov, Polyploid tumour cells elicit paradiploid progeny through depolyploidizating divisions and regulated autophagic degradation, Cell Biol. Int. 35 (2011) 687–695.
[12] S. Hauf, A. Biswas, M. Langgegger, S.A. Kawashima, T. Tsukahara, Y-Watanabe, Aurora controls sister kinetochore mono-orientationand homolog bi-orientation in meiosis-I, EMBO J. 26 (2007) 4475–4486.
[13] S. Kaitna, P. Pasierbek, M. Jantsch, J. Loidl, M. Glotzer, The Aurora B kinase AIR-2 regulates kinotochores during mitosis and is required for separation of homologous chromosomes during meiosis, Curr. Biol. 12 (2002) 798–812.
[14] J. Erenpreisa, M.S. Cragg, K. Salmina, M. Hausmann, H. Scherthan, The role of meiotic cohesion REC8 in chromosome segregation in γ irradiation-induced endopolyploid tumour cells, Exp. Cell Res. 315 (2009) 2593–2603.
[15] F. Ianzini, E.A. Kosmacek, E.S. Nelson, E. Napoli, E. Erenpreisa, M. Kalejs, M.A. Mackey, Activation of meiosis-specific genes is associated with depolyploidization of human tumor cells following radiation-induced mitotic catastrophe, Cancer Res. 69 (2009) 2296–2304.
[16] A.E. Visser, R. Eils, A. Jauch, G. Little, P.J. Bakker, T. Cremer, J.A. Aten, Spatial distributions of early and late replicating chromatin in interphase chromosome territories, Exp. Cell Res. 243 (1998) 398–407.
[17] S. Monajembashi, A. Rapp, E. Schmitt, H. Dittmar, K.O. Greulich, M. Hausmann, Spatial association of homologous pericentric regions in human lymphocyte nuclei during repair, Biophys. J. 88 (2005) 2309–2322.
[18] H.I. Abdel-Halim, S.A. Imam, F.M. Badr, A.T. Natarajan, H.F. Mullenders, J.J.W.A. Boei, Ionizing radiation-induced instant pairing of heterochromatin of homologous chromosomes in human cells, Cytogenet. Genome Res. 1004 (2004) 193–199.
[19] J. Boei, J. Fomina, F. Darroudi, N. Nagelkerke, L. Mullender, Interphase chromosome positioning affects the spectrum of radiation-induced chromosomal aberrations, Radiat. Res. 166 (2006) 319–326.
[20] S. Bekker-Jensen, C. Lukas, R. Kitagawa, F. Melander, M.B. Kastan, J. Bartek, J. Lukas, Spatial organization of the mammalian genome surveillance machinery in response to DNA strand breaks, J. Cell Biol. 173 (2006) 195–206.
[21] M. Falk, E. Lukasova, S. Kozubek, Higher-order chromatin structure in DB induction, repair and misrepair, Mutat. Res. 704 (2010) 88–100.
[22] P.J. Johnston, P.L. Olive, P.E. Bryant, Higher-order chromatin structure-dependent repair of DNA double-strand breaks: modelling the elution of DNA from nucleotids, Radiat. Res. 148 (1997) 561–567.
[23] A. Ivanov, M.S. Cragg, J. Erenpreisa, D. Emzinsh, H. Lukman, T.M. Illidge, Endopolyploid cells produced after severe genotoxic damage have the potential to repair DNA double strand breaks, J. Cell Sci. 116 (2003) 4095–4106.

Please cite this article in press as: J. Schwarz-Finsterle, et al., Volume increase and spatial shifts of chromosome territories in nuclei of radiation-induced polyploidizing tumour cells, Mutat. Res.: Genet. Toxicol. Environ. Mutagen. (2013), http://dx.doi.org/10.1016/j.mrgentox.2013.05.004

[24] H. Scherthan, R. Eils, E. Trelles-Sticken, S. Dietzel, T. Cremer, H. Walt, A. Jauch, Aspects of three-dimensional chromosome reorganization during the onset of human male meiotic prophase, J. Cell Sci. 111 (1998) 2337–2351.
[25] T. Cremer, M. Cremer, S. Dietzel, S. Muller, I. Solovei, S. Fakan, Chromosome territories – a functional nuclear landscape, Curr. Opin. Cell Biol. 18 (2006) 307–316.
[26] S. Boyle, S. Gilchrist, J.M. Bridger, N.L. Mahy, J.A. Ellis, W. Bickmore, The spatial organization of human chromosomes within the nuclei of normal and emerin-mutant cells, Hum. Mol. Genet. 10 (2001) 211–219.
[27] A. Bolzer, G. Kreth, I. Solovei, D. Koehler, K. Saracoglu, C. Fauth, S. Mueller, R. Eils, C. Cremer, M.R. Speicher, T. Cremer, Three-Dimensional maps of all chromosomes in human male fibroblast nuclei and prometaphase rosettes, PloS Biol. 3 (2005) 826–843.
[28] C. Lanctôt, T. Cheutin, M. Cremer, G. Cavalli, T. Cremer, Dynamic genome architecture in the nuclear space: regulation of gene expression in three dimension, Nat. Rev. Genet. 8 (2007) 104–115.
[29] K. Küpper, A. Kölbl, D. Biener, S. Dittrich, J. Von Hase, T. Thormeyer, H. Fiegler, N.P. Carter, M.R. Speicher, T. Cremer, M. Cremer, Radial chromatin positioning is shaped by local gene density, not by gene expression, Chromosoma 116 (2007) 285–306.
[30] T. Wiech, S. Timme, F. Riede, S. Stein, M. Schuricke, C. Cremer, M. Werner, M. Hausmann, A. Walch, Archival tissues provide a valuable source for the analysis of spatial genome organisation, Histochem. Cell Biol. 123 (2005) 229–238.
[31] H. Albiez, M. Cremer, C. Tiberi, L. Vecchio, L. Schermelleh, S. Dittrich, K. Küpper, B. Joffe, T. Thormeyer, J. Von Hase, S. Yang, K. Rohr, H. Leonhardt, I. Solovei, C. Cremer, S. Fakan, T. Cremer, Chromatin domains and the interchromatin compartment form structurally defined and functionally interacting nuclear networks, Chromosome Res. 14 (2006) 707–733.
[32] L.A. Parada, P.C. McQueen, P.J. Munson, T. Misteli, Conservation of relative chromosome positioning in normal and cancer cells, Curr. Biol. 12 (2002) 1692–1697.
[33] H. Neves, C. Ramos, M.G. da Silva, A. Parreira, L. Parreira, The nuclear topography of ABL, BCR, PML, and RARa genes: evidence for gene proximity in specific phases of the cell cycle and stages of hematopoietic differentiation, Blood 93 (1999) 1197–1207.
[34] J.J. Roix, P.G. McQueen, P.J. Munson, L.A. Parada, T. Misteli, Spatial proximity of translocation-prone gene loci in human lymphocytes, Nat. Genet. 34 (2003) 287–291.
[35] M. Falk, E. Lukasova, S. Kozubek, Chromatin structure influences the sensitivity of DNA to γ-radiation, Biochim. Biophys. Acta 1783 (2008) 2398–2414.
[36] H. Scherthan, L. Hieber, H. Braselmann, V. Meinecke, H. Zitzelsberger, Accumulation of DSBs in gamma-H2AX domains fuel chromosomal aberrations, Biochem. Biophys. Res. Commun. 371 (2008) 694–697.
[37] F. Ianzini, M.A. Mackey, Spontaneous premature chromosome condensation and mitotic catastrophe following irradiation of HeLa S3 cells, Int. J. Radiat. Biol. 72 (1997) 409–421.
[38] S. Knehr, R. Huber, H. Braselmann, H. Schraube, M. Bauchinger, Multicolour FISH painting for the analysis of chromosomal aberrations induced by 220 kV X-rays and fission neutrons, Int. J. Radiat. Biol. 75 (1999) 407–418.
[39] H. Scherthan, M. Abend, K. Muller, C. Beinke, H. Braselmann, H. Zitzelsberger, F.M. Kohn, H. Pillekamp, R. Schiener, O. Das, R.U. Peter, G. Herzog, A. Tzschach, H.D. Dorr, T.M. Fliedner, V. Meineke, Radiation-induced late effects in two affected individuals of the Lilo radiation accident, Radiat. Res. 167 (2007) 615–623.
[40] D.E. Knuth, The Art of Computer Programming, vol. 2, Addison-Wesley, Reading, MA, 1981, pp. 48–51.
[41] T. Gonzalez, S. Sahni, W.R. Franta, An efficient algorithm for the Kolmogorov–Smirnov and Lilliefors tests, ACM Transact. Mathem. Softw. 3 (1977) 61–64.
[42] I.T. Young, Proof without prejudice: use of the Kolmogorov–Smirnov test for the analysis of histograms from flow systems and other sources, J. Histochem. Cytoch. 25 (1977) 935–941.
[43] T. Wiech, S. Stein, V. Lachenmaier, E. Schmitt, J. Schwarz-Finsterle, E. Wiech, G. Hildenbrand, M. Werner, M. Hausmann, Spatial allelic imbalance of BCL2 genes and chromosome 18 territories in nonneoplastic and neoplastic cervical squamous epithelium, Eur. Biophys. J. 38 (2009) 793–806.
[44] S. Timme, E. Schmitt, S. Stein, J. Schwarz-Finsterle, J. Wagner, A. Walch, M. Werner, M. Hausmann, T. Wiech, Nuclear position and shape deformation of chromosome 8 territories in pancreatic ductal adenocarcinoma, Analyt. Cell. Pathol. 34 (2011) 21–33.
[45] K. Salmina, E. Jankevics, A. Huna, D. Perminov, I. Radovica, T. Klymenko, A. Ivanov, E. Jascenko, H. Scherthan, M. Cragg, J. Erenpreisa, Up-regulation of the embryonic self-renewal network through reversible polyploidy in irradiated p53-mutant tumour cells, Exp. Cell Res. 316 (2010) 2099–2112.
[46] C. Lagadec, E. vlashi, L. Delle Donna, C. Dekmezian, F. Pajonk, Radiation-induced reprogramming of breast cancer cells, Stem Cells 30 (2012) 833–844.
[47] O. Anatskaya, A.E. Vinogradov, Somatic polyploidy promotes cell function under stress and energy depletion: evidence from tissue-specific mammal transcriptome, Funct. Integr. Genomics 10 (2010) 433–446.
[48] A. Huna, K. Salmina, E. Jascenko, G. Duburs, I. Inashkina, J. Erenpreisa, Self-renewal signalling in pre-senescent tetraploid IMR90 cells, J. Aging Res. (2011), http://dx.doi.org/10.4061/2011/103253, Article ID 103253.
[49] J.-A. Dolling, D.R. Boreham, D.L. Brown, G.P. Raaphorst, R.E. Mitchel, Rearrangement of human cell homologous chromosome domains in response to ionizing radiation, Int. J. Radiat. Biol. 72 (1997) 303–311.
[50] M. Skalnikova, S. Kozubek, E. Lukasova, E. Bartova, P. Jirsova, A. Cafourkova, I. Koutna, M. Kozubek, Spatial arrangement of genes, centromeres and chromosomes in human blood cell nuclei and its changes during the cell cycle, differentiation and after irradiation, Chromosome Res. 8 (2000) 487–499.
[51] J.N. Lucas, E. Certvantes, Significant large-scale chromosome territory movement occurs as a result of mitosis, but not during interphase, Int. J. Radiat. Biol. 78 (2002) 449–455.

Please cite this article in press as: J. Schwarz-Finsterle, et al., Volume increase and spatial shifts of chromosome territories in nuclei of radiation-induced polyploidizing tumour cells, Mutat. Res.: Genet. Toxicol. Environ. Mutagen. (2013), http://dx.doi.org/10.1016/j.mrgentox.2013.05.004

3.6. Tumour cells after therapy can survive trough life-cycle-like process – Review paper I

The "virgin birth", polyploidy, and the origin of cancer

Jekaterina Erenpreisa[1], Kristine Salmina[1], Anda Huna[1], Thomas R. Jackson[2], Alejandro Vazquez-Martin[1] and Mark S. Cragg[3]

[1] Latvian Biomedical Research & Study Centre, Riga

[2] Faculty Institute for Cancer Sciences, University of Manchester, Manchester Academic Health Science Centre, UK

[3] Southampton University School of Medicine, Southampton, UK

Correspondence to: *Jekaterina Erenpreisa,* ***email***: *katrina@biomed.lu.lv*

Mark S. Cragg, ***email***: *m.s.cragg@soton.ac.uk*

Keywords: cancer, embryonality, polyploidy, accelerated senescence, parthenogenesis

Received: *November 16, 2014* ***Accepted***: *December 16, 2014* ***Published***: *December 17, 2014*

ABSTRACT

Recently, it has become clear that the complexity of cancer biology cannot fully be explained by somatic mutation and clonal selection. Meanwhile, data have accumulated on how cancer stem cells or stemloids bestow immortality on tumour cells and how reversible polyploidy is involved. Most recently, single polyploid tumour cells were shown capable of forming spheroids, releasing EMT-like descendents and inducing tumours *in vivo*. These data refocus attention on the centuries-old embryological theory of cancer. This review attempts to reconcile seemingly conflicting data by viewing cancer as a pre-programmed phylogenetic life-cycle-like process. This cycle is apparently initiated by a meiosis-like process and driven as an alternative to accelerated senescence at the DNA damage checkpoint, followed by an asexual syngamy event and endopolyploid-type embryonal cleavage to provide germ-cell-like (EMT) cells. This cycle is augmented by genotoxic treatments, explaining why chemotherapy is rarely curative and drives resistance. The logical outcome of this viewpoint is that alternative treatments may be more efficacious - either those that suppress the endopolyploidy-associated 'life cycle' or, those that cause reversion of embryonal malignant cells into benign counterparts. Targets for these opposing strategies are components of the same molecular pathways and interact with regulators of accelerated senescence.

"The aim of science is to seek the simplest explanations of complex facts. We are apt to fall into the error of thinking that the facts are simple because simplicity is the goal of our quest. The guiding motto in the life of every natural philosopher should be, 'Seek simplicity and distrust it"

(Alfred North Whitehead, The Concept of Nature, 1929)

After more than 40 years of the "war on cancer" progress in achieving long-lasting cures and treating advanced, late stage, disease is still unsatisfactory. This failure likely stems from our limited understanding of the true complexity of the disease [1]. Attempts to define the basis behind cancer are many and varied, dating back centuries. One particular concept, the embryological theory of cancer, has existed for more than 150 years and was developed during the 19th century by prominent scientists of that time [2, 3]. Amongst these, David von Hansemann, wrote in 1890 that normal somatic cells can undergo de-differentiation and transform into cancer cells, which acquire "egg-like" features [4].

The biological equivalency between embryos and tumours was experimentally established in 1964 by Leroy Stevens who showed that normal pluripotent embryonic stem cells from murine blastocysts, could develop into teratomas/teratocarcinomas if they were injected into an adult testis or into an embryo if injected back into a uterus [5]. The same year, Barry Pierce and colleagues demonstrated the ability of a single malignant teratocarcinoma cell to form a primitive embryoid body with the capacity to give rise to the three major germ-cell layers [6, 7], subsequently showing these embryonal

properties for other carcinomas [8]. It was also shown that teratocarcinoma-embryo chimeras can be produced if the malignant cells are placed into the environment of a normal blastocyst [9, 10]. Although these experiments were forgotten for many years, in modern times induced pluripotent stem cells (iPSC) have been tested for their ability to cause teratomas and teratocarcinomas. Given all of these observations, and the current frustrations in our ability to understand the complexity of cancer and establish effective cures, even with our sophisticated ability to unpick their underlying somatic mutations and clonal architecture, it may be time to revisit the half-forgotten embryological theory of cancer.

The currently popular cancer stem cell (CSC) theory of tumourogenesis assigns the property of immortality (self-renewal) to adult stem cells that due to genetic mutations, or epigenetic changes, de-differentiate to a state similar to very early embryonal (ESC-like) cells [11, 12]. However, although this concept explains how proliferation capacity is extended, it does not explain why immortality is supported in tumours again and again. The only known natural process capable of supporting immortality indefinitely is the life cycle, which transfers the germ-line through one generation to the next. Recognition of this basic biological law formulated by August Weismann more than a century ago lies at the core of the embryological theory of cancer and its many variants [13].

Through more than a decade of research in our and other labs, it has been seen that meiotic genes are activated in TP53 mutant tumours, enhanced by genotoxic treatments or spindle inactivation and associated with reversible polyploidy capable of recovering clonogenic diploid cells [14-16]. Earlier induction of c-Mos by paclitaxel in SKOV3 cells was shown by Ling et al., [17], while Gorgoulis et al.,[18] found it in primary small cell lung cancer. Similarly, data on the presence of the so-called cancer testes-associated antigens (CTA) in tumours, among them meiotic, embryonal and placental gene products, revealed a link between gametogenesis and cancer [19, 20]. These data tempted Lloyd Old to provocatively entitle one of his commentaries “Cancer is a somatic cell pregnancy” [21]. He wrote: “Because many of the cardinal features of cancer are also characteristic of gametogenesis/placentation, e.g. migration, invasion, immune subversion, apoptosis resistance, induction of angiogenesis, etc., it takes little imagination to think that cancer-testes gene products controlling these processes during gametogenesis confer these same capacities on the cancer cell”. This statement contains a frank recognition of the embryological theory of cancer.

The last decade has added yet more complexity. In addition to activation of the main meiotic kinase Mos and genes of meiotic prophase, certain division features characteristic for meiosis (cohesion of sisters and omission of one S-phase) were observed in genotoxically-treated cancer cells with the involvement of the meiotic cohesin REC8 and recombinase DMC1[22]. Mos activation was also found during endomitosis [23] or multi-polar mitosis of TP53-mutant tumours[16, 24].Our initial speculations on these data were that cancer is associated with a programmatic recapitulation of the ancient ploidy-cycles and asexual life-cycles of early protists [23, 25, 26]. Some researchers described somewhat similar changes, but did not associate them with meiosis. Formation of endo-tetraploid cells with diplochromosomes through cohesion of sisters as a consequence of DNA damage was substantiated by Davoli and Lange [27]. Walen described (in normal senescing or glutamine-deprived cells) a-spindled co-segregation in endotetraploid cells of entire (haploid) genome complements (2x2C1n) and suggested the significance of this process for carcinogenesis [28, 29]. However, further studies revealed that not only meiotic genes but also the key genes of early embryogenesis were induced by genotoxic treatments in various tumour cell lines, (both male and female), and associated with reversible polyploidy [30-32]. ESC-like gene signatures were also revealed in aggressive primary tumours [33-36] and it was shown that neoplastic non-stem cells could spontaneously convert into CSCs through epigenetic regulation [37-40].

Two important new aspects were subsequently added to our understanding: (1) as predicted by Blagosklonny (2007) differentiated tumour cells were shown to have the capacity to de-differentiate and become CSC (or “stemloids”) [41]; (2) induction of stemness by DNA or spindle damage was shown to be associated with the activation of meiotic genes coupled to reversible endopolyploidy (in TP53 function deficient cells). So, along with meiosis, life-cycle features were coupled to reversible polyploidy as evidenced by the ectopic ESC gene expression in somatic tumour cells. To unite these aspects, we proposed that cancer-related polyploidy appeared at the same point in macro-evolution at which multicellularity occurred (formed by reversible endopolyploidy) in unicellular organisms [42].The rationale for this was because this evolutionary period coincides with the diversification of somatic and gametic lineages, simultaneous with the emergence of sexual reproduction and gastrulation [43].

While reversible polyploidisation of tumour cells through aborted mitoses (“mitotic slippage”) is now established [44, 45] currently, it is unclear how the giant polyploid tumour cells de-polyploidise. Various proposals have been made including; meiosis-like reduction divisions [15, 22]; reduction through diplochromosomes and haploidy [28, 29]; multi-polar mitoses [16, 46, 47]; and “a-mitotic budding” of descendent sub-cells [48-51]. Recently, we attempted to unite and order most of these various events as a necessary sequence of steps in a prolonged process of specific rearrangements [31, 52]. However, the mechanisms associated with survival of resistant tumour cells after the emergence of reversible

polyploidy under genotoxic stresses remain hitherto ill-defined, at least in part because of the complexity, extension in time, and rarity of the process (as most cells die), and so the full picture remains obscure.

Furthermore, despite the substantial progress in understanding the crucial role of polyploidy in cancer, recently reviewed by Coward and Hardings [53], clearly, we are currently unable to answer many questions. For example: Is the meiosis-like response of TP53-mutant tumours to genotoxic treatments followed by any syngamy (fertilization-like) event(s)? If so, how and when do they take place?; Why is stemness induced in somatic tumour cells by DNA damage, and why is it associated with transient (reversible) polyploidy?;Why do the sub-nuclei of polyploid giants cells behave autonomously and undergo asymmetric divisions [31, 54, 55];How and why do multinucleated tumour cells sequestrate cytoplasm to their individual sub-nuclear descendants [31]?; How do they identify and sort the sub-nuclei containing viable or non-viable genetic material [31, 42, 55]?; Why does the extent of reversible polyploidisation have an apparent limit of ~32C which coincides with the cell number in the morula (blastulation) stage of embryogenesis [42] and are these somehow related?; Why is accelerated senescence coupled to induced stemness in these DNA damaged cells [52, 56-58]?; What explains the kinetics of MOS and REC8 activation during the polyploidisation and de-polyploidisation processes [14, 15]?

Most of these questions can potentially be addressed in terms of the parthenogenetic theory of cancer, which stemmed from the embryonal theory. We have occasionally seen visual evidence that could be interpreted in this way in our own studies; some examples of which are presented in Fig. 1.

Parthenogenesis *("virgin birth"* in Greek) is a special reproductive strategy widely used in the plant and animal kingdom, in which an unfertilized egg is reunited with a polar body, and undergoes embryogenesis to develop adult offspring. The parthenogenetic theory of cancer was first suggested by Beutner [60] (cited from Erenpreiss [2]) and updated more recently by Vladimir Vinnitsky [3, 61]. This link is also made more apparent with a series of recent studies reporting the spherogenicity and malignancy of endopolyploid tumour cells (ETC). In these experiments, polyploid giant cancer cells were sorted either manually [62], or chemically – using the hypoxia mimic $CoCl_2$ [50, 63] or by serial selections in etoposide [51]. These ETC displayed increased resistance to chemo-radiotherapy, expressed key ESC and germline factors (Oct4/Nanog, Sox2, SCF, c-kit), and surface markers (CD44, CD133) as well as an ESC-like microRNA profiles. These single ETC were shown capable of forming tumour spheroids which could undergo differentiation into the three germ layers and critically to form tumours in immunodeficient mice with high efficiency [50, 62]. In other words, the revelations of Barry Pierce and colleagues detailed earlier for single carcinoma cells have now been shown to be attributable to single ETC. These experiments were performed on tumour cell lines representing almost all cancer types (breast, ovarian, bladder, colon, glioblastoma, fibrosarcoma, osteosarcoma, retinoblastoma, lymphoma). Moreover, it was shown that these giant polyploid tumour cells possessing large subnuclei ultimately bud smaller cells [51] of fibroblastic shape and with markers of epithelial-mesenchymal transition (EMT) [50].The occurrence of asymmetric mitotic divisions in the late ETC which precede cellularisation and the release of rejuvenated sub-cells was also suggested by us previously [31]. Thus, through the generation and reversal of polyploidy coupled to this embryonal-type stemness induction, these tumour cells potentially elicit an "invasion" phenotype in their descendants. Theoretically and based on our cancer cell "life cycle" hypothesis wherein reversible polyploidy releases the germline [24-26] it means that the cells undergoing EMT with 'embryo-like" features are the biological equivalent of a germ cell, as also concluded by Zhang and colleagues [50].

These observations and conclusions largely fit the embryonal theory of cancer. Its oncogerminative variant is proposed by Vladimir Vinnitsky [3, 61] and illustrated in Fig.2. Within the scheme, three main tenets are outlined: reproduction of the oncogerminative cell by an embryonal cleavage-like process (with the parthenogenetic origin of the tumour initiating CSC); the equivalence between the tumour spheroid and the a-vascular blastocyst-stage of embryogenesis; and the invading potential of the germline (EMT) mimicking the biological properties of primordial germ cells (PGC) in normal embryogenesis. The similarity between PGC and migrating tumour cells was previously supposed by John Beard in 1902 [64], cited from Beckett [65] highlighting the embryological theory as a gateway to the cancer stem cell theory. Notably, cycles of MET- EMT epigenetic transitions interspersed by this embryonal life-cycle are proposed by Vinnitsky as the mechanism behind the observed ongoing cancer relapses.

Although Vinnitsky did not consider the polyploidisation of tumour cells as a participant in this embryological process, the very idea of parthenogenesis provides a place for the observed activation of meiotic genes and meiotic-like divisions in the DNA damaged tumour cells because parthenogenesis needs first formation and maturation of an oocyte. Moreover, the main driver of oogenesis, Mos-kinase, was shown to be induced by genotoxic treatments in tumour cells of various origins, as described above. Therefore, a somatic meiosis-like process* seems to be the first step in the DNA damage response. Mos can also arrest cells in a 'mitotic checkpoint" protecting them from apoptosis as an alternative to mitotic catastrophe [24]. Given the evidence outlined above relating to ETC, the polyploid giant cells appear to represent pathological analogs of the early embryo. Subsequently, a syngamic event is required

to occur between "meiosis" and "embryo cleavage". A hypothetical scheme of how these key events may occur in sequence is presented in Fig.3.

* *somatic meiosis does not necessarily need recombination between homologs, which may be substituted by recombination between sister chromatids* [66].

A polyploid giant cell leading to the formation of a tumour spheroid, when put into the context of the embryological process (coined a pseudo-morula and pseudo-blastocyst by Vinnitsky 2014), coincides with our previous notion that the development of a giant tumour cell (through endopolyploidisation) is equivalent to the embryonal cleavage (endo-)cycles that reach "a developmental checkpoint of totipotency" at 32C. This represents ~4 abortive mitoses, which occur by day 5, the point from which the reverse of polyploidy, ultimately ending in de-polyploidisation and release of mitotic descendants, is initiated [31, 55, 67]. This period of five days may represent a checkpoint of tumour cell endopolyploidisation of embryonal origin and is seen in several other models [32, 68]. Here, we should explain why tumour 'pseudo-blastomeres' are polyploid. During cleavage of the tumour pseudo-embryo the pseudo-blastomeres do not undergo full cytotomy until the blastula-equivalent stage, after which the giant cell sub-nuclei undergo cellularisation (sequestration of individual cytoplasm territories) preceding the 'budding' of daughter cells (described in [26, 31, 48, 50, 51]. This type of cleavage where a syncytial blastoderm is formed and shortly afterwards a cluster of germ cells is separated along with cellularisation is well-characterised in Drosophila, perhaps the best understood of all developmental systems [69]. Endopolyploidy, multi-nucleation with multiplication of pronuclei and/or polar bodies are seen in pathological human eggs (numerous examples are seen in the pictures from the Advanced Fertility Center of Chicago http://www.advancedfertility.com/abnormal-ivf-egg-pictures.htm). These pictures resemble those of multi-nucleated ("pregnant") giant tumour cells presented by Diaz-

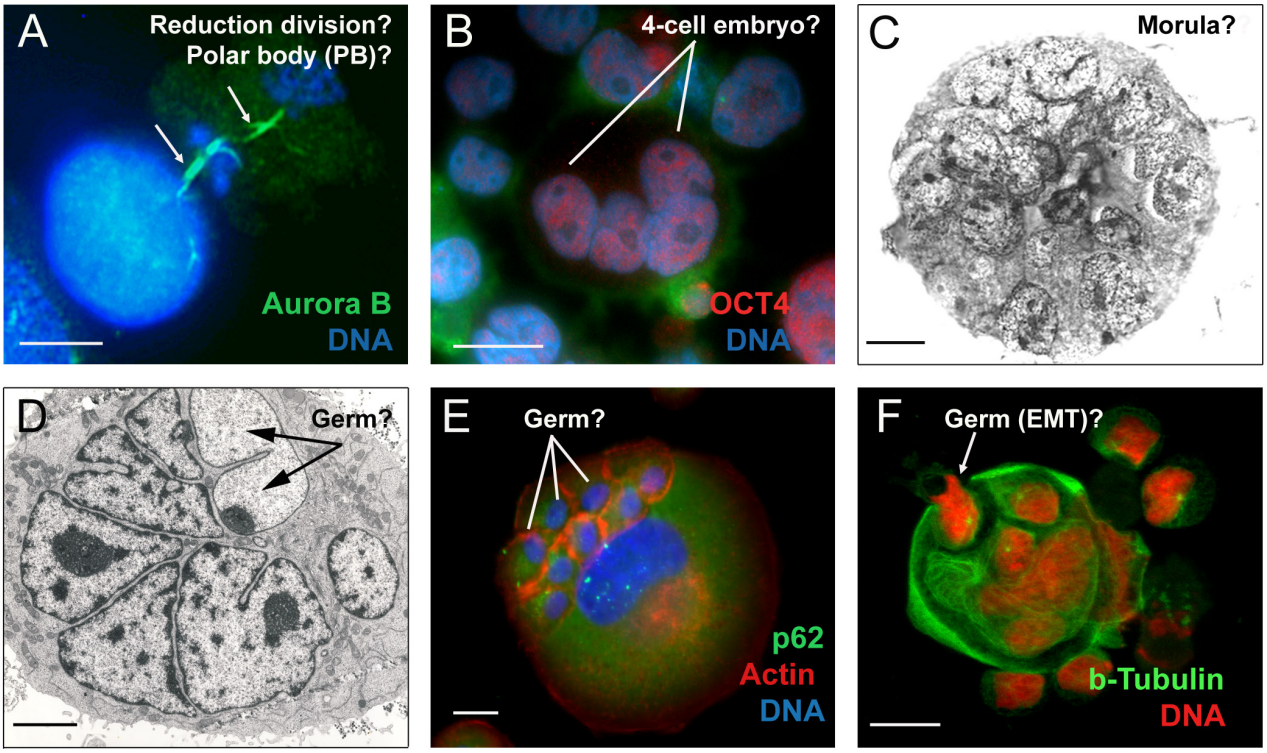

Fig.1: Embryonal features of endopolyploid tumour cells induced by DNA damage: A) Namalwa cells (44, X, -Y) (post 10 Gy irradiation). Two asymmetric reduction divisions are observed which resemble the formation and subsequent division of the first polar body (PB) in the maturing oocyte (2 hour treatment with lactocystin before fixation allowed the preservation of both mid-bodies, arrowed), republished from [54]; B) WI-L2-NS (47, XY) cells (post 10 Gy irradiation). The induced giant polyploid cell resembles a 4-cell embryo; C) HeLa S3 (68, XXX) cell line (post 10 Gy irradiation). A tumour-spheroid that resembles a morula is observed; (republished from [15] ; D) Namalwa cells 14 days post 10 Gy irradiation. Transmission EM of a giant polyploid tumour cell following aborted radial division. Two types of subnuclei are observed; one with a conventional structure and another with a juvenile-like structure (not present in non-treated controls, arrowed); E) A431MetforR (metformin-resistant) cells were selected as indicated [59], (72, XX). A giant cell showing mild autophagic activity and actin-enriched individual cytoplasmic regions around small sub-nuclei; F) Namalwa polyploid giant cell budding a cellularised descendant that has been sequestered from the parent's cytoplasm 13 days post 10 Gy irradiation, republished from [26]. Bars =10 μm.

Carballo, et al. [51] and Zhang, et al. [50]. Interesting changes are observed in giant tumour cells after reaching "the totipotency checkpoint". Radial divisions (incomplete cytotomy) described previously by us in late ETC occur which precede casting off the external layer of cytoplasm along with cellularisation and release of small descendants by 'budding' [31, 44, 67]. In some way, this process is associated with diversification (by asymmetric divisions) of the giant cell sub-nuclei into two types, larger (not individualizing cytoplasm) destined to degenerate, and smaller (proliferative, endowed by stemness factors and decompacted chromatin, acquiring their own cytoplasm and actin ring) for shedding with the aid autophagy (Fig. 1D-F). Radial cleavage furrows is a well-known feature of the animal cleavage pattern which situates the blastomeres in a doughnut pattern where they remain totipotent and bridged up to the 32 cell stage as reported in Volvox [70]. Curiously, fossils of early animals dated ca. 570- 620 Ma were found to show 32-cell blastula [71]. The genealogy of cancer may therefore be truly ancient!

However, there are two key points in the scheme of Vinnitsky that require further clarification. 1) How do settled MET cells return to the parthenogenetic life-cycle again, and what drives their entry/exit; 2) what is the role of the reversible accelerated senescence reported by multiple observers [58, 68, 72-75] which accompanies reversible polyploidy in this process and paradoxically can favour survival? The latest data demonstrate that tumour cells can shuttle between low and high malignant states according to their MET/EMT status through epigenetic changes of bi-stable chromatin [40]. This addresses the biochemical aspects of the phenomenon. Here, we would like to suggest that biologically the MET cells, previously produced from EMT, may undergo accelerated cellular senescence due to accumulation of ROS and DNA strand breaks. The accumulation of DNA damage is a hallmark of accelerated senescence [76]. However, DNA damage is also considered as a major cause for the evolution of DNA repair by recombination, which gave rise to meiosis through ploidy cycles [23, 66, 77]. Interestingly, a simple doubling in the amount of ROS is sufficient to induce the genes which initiate the facultative sexual reproduction cycle in Volvox *carteri* [78], indicating the ancestral role of sexual reproduction as an adaptive response to stress and ROS-induced DNA damage [77].

Markers of accelerated senescence and DNA damage were unexpectedly found to be linked to markers of stemness in senescing IMR-90 fibroblasts [56] and etoposide-or irradiation treated tumour cells arrested in G2-phase [57, 58]. The p21-dependent senescence related to stemness pathways (TGF-β and PI3K) was revealed in normal embryogenesis [79]. Moreover, senescence

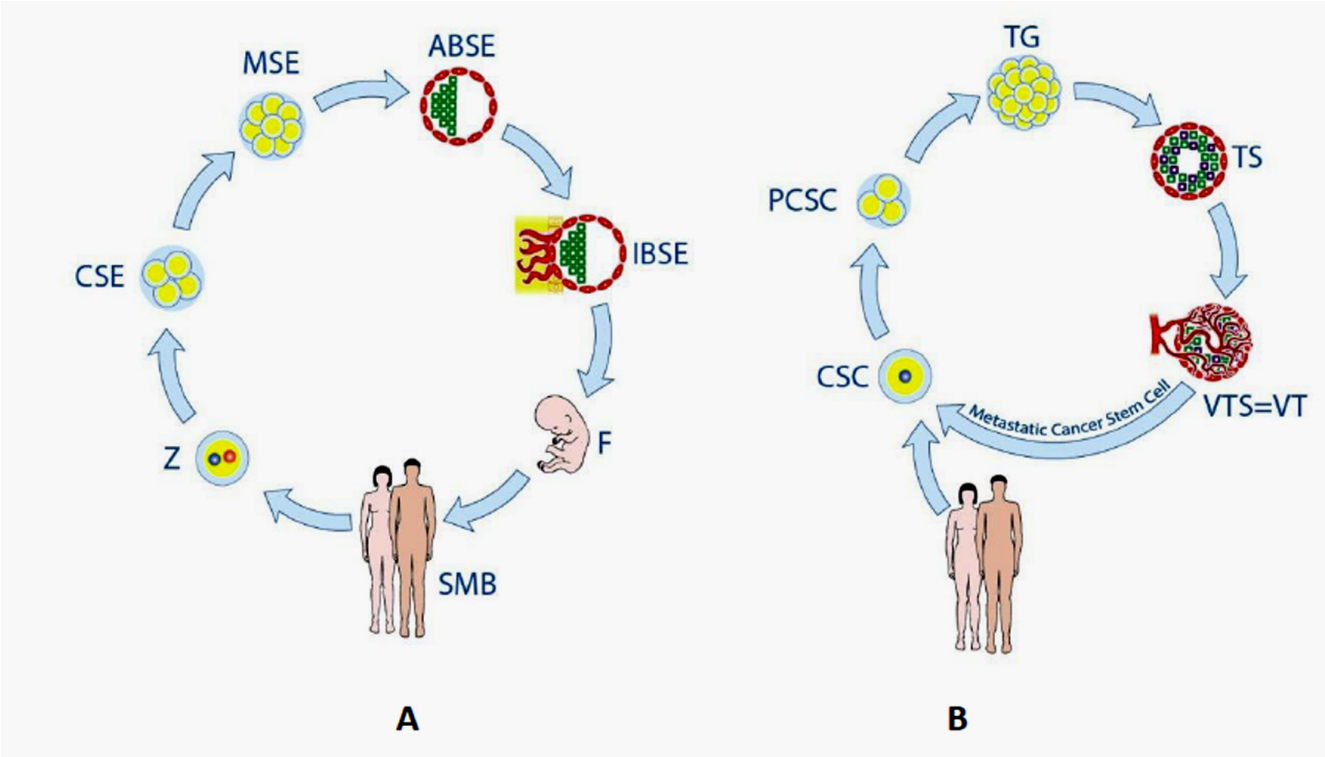

Fig.2: The figure and legend are reproduced from [3], with consent of Vladimir Vinnitsky. Stages of the life cycles of germline cells (A) and oncogerminative cells (B). (A) Z, zygote; CSE, cleavage stage embryo; MSE, morula stage embryo; ABSE, avascular blastocyst-stage embryo; IBSE, implanted blastocyst-stage embryo; F, fetus. SMB, sexually mature body. (B) CSC, cancer stem cell (i.e., oncogerminative cell); PCSC, parthenogenetic cancer stem cell (a pseudo-cleavage-stage embryo); TG, tumor germ (a morula-stage embryo-like structure); TS, tumor spheroid (an imitation avascular blastocyst-stage embryo); VTS/VT, vascularized tumor spheroid and/or vascularized tumor (an implanted blastocyst-stage embryo-like entity).

markers are predictors of poor prognosis in lung cancer patients after neo-adjuvant therapy [74]. All of this highlights the close link between accelerated senescence and stemness and their relationship to carcinogenesis [52].

The origin of sexual reproduction is a complex and much debated issue. DNA recombination by meiosis coupled with sex (i.e. the fusion of paternal gametes), although costly in energetic terms, apparently provides the optimal balance between DNA repair and genetic variation [80]. Polyploidy as such provides the advantage of masking deleterious mutations [66], resistance to toxicity and energy depletion [81] and therein better survival of polyploid tumour cells in unfavourable conditions [53]. Reversible polyploidy coupled with the generation of immortal germ cells therefore captures the advantages of both. We propose that mammalian cancer cells use exactly this phylogenetic program ensuring immortality (by a life-cycle) and genome plasticity and heterogeneity (by stemness) through epigenetic and genetic variation (and subsequent clonal selection) as a basis for developing resistance to treatments.

It can be suggested that accelerated senescence of genotoxically damaged tumour cells serves as a bridge and stochastic option for the initiation of the next (cancer) life-cycle, which is also accelerated (starting from meiotic- and syngamic-like events and ending with the blastula/spheroid through formation of the germ-like EMT tumour cells in a process akin to early embryogenesis carried out in approximately one-two weeks). Interestingly, our recent research on etoposide-treated embryonal carcinoma cells showed that a potential regulator and trigger for this switch is OCT4 (POU5F1), a carrier of life-cycle totipotency [82]; and induced in a TP53-dependent manner alongside p21CIP1. The choice between the two opposite cell fates (reinitiate cell divisions or undergo terminal senescence) in transiently bi-potential cells is undertaken in G2 arrest [57] and this barrier can become adapted to start polyploidy [56]. When the tetraploidy barrier is overcome, the TP53 tumour-suppressing function becomes surpassed [83], likely by methylation of its promoter [84], while mTOR linking to p21-mediated senescence becomes suppressed, thus allowing the reversal of senescence [58]. We suggest that the cancer cell 'life cycle' is therefore initiated by meiosis and locked by accelerated senescence with the opposing outcomes diverging from the same DNA damage checkpoint [52] supporting the earlier supposition that "Carcinogenesis always is started with immortalisation. That is a possibility to overcome senescence" [2, 85]. We therefore arrive at the same conclusion suggested by Rajaraman [49] that immortality of cancer cells is not perpetual but becomes cyclically renewed.

Intriguingly, an ~5 day period of 'stochastic' choice between senescence/MET and self-renewal/EMT, separated by a longer rate-limiting period of further determination of self-renewal has also been reported during the induction of pluripotent stem cells (iPSC) [86],

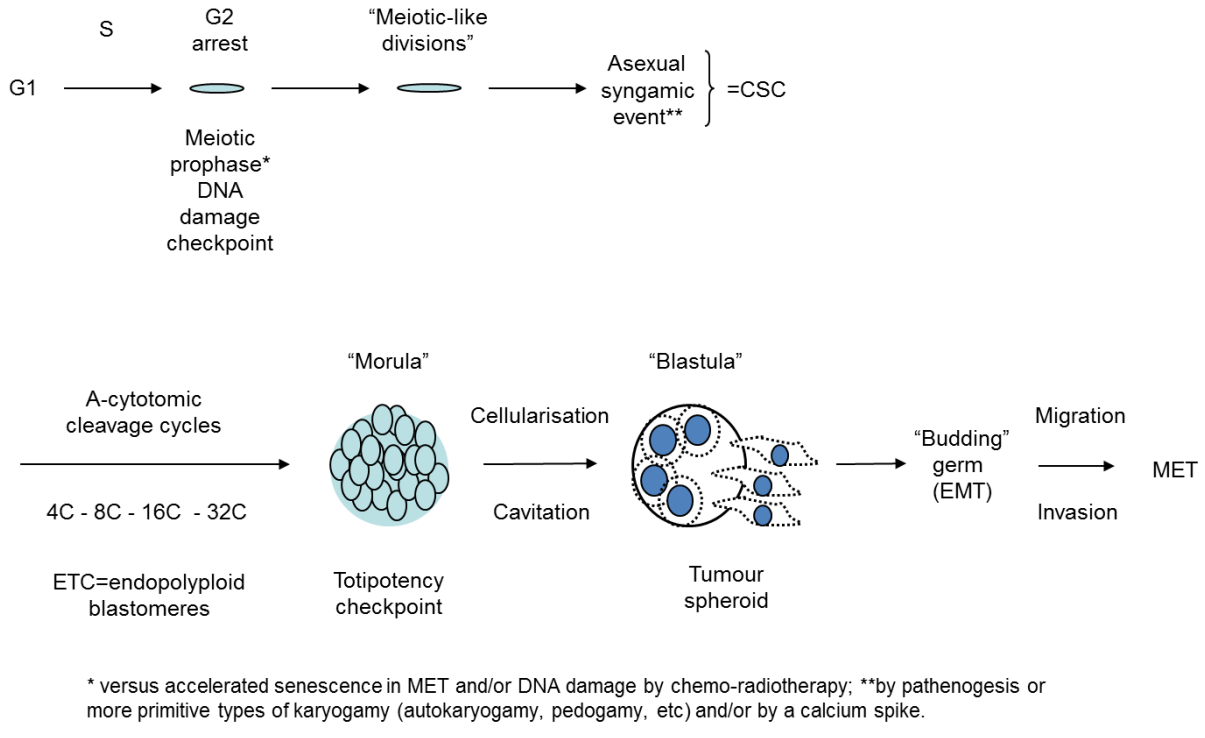

Fig.3: Hypothetical scheme of cancer cell 'life cycle' based on embryological concept and experimental observations of TP53 dysfunctional tumour cell lines after genotoxic treatments.

with the whole process taking ~30 days.

One further consideration of the parthenogenetic origin of cancer is that parthenogenesis is typically viewed as a female privilege. Although commonly believed, this is not quite true. Mammalian primordial germ cells (PGC) of either XX or XY karyotype are sexually dimorphic and have the potential to enter either spermatogenesis or oogenesis. In a female genital ridge, or in a non-gonadal environment *in vivo*, as well as autonomously in tissue culture both 46XX and 46XY PGCs develop as meiotic oocytes [87] and can therefore initiate parthenogenesis. Only male gonadal somatic cells, which differentiate, through SRY (sex determining gene on Y chromosome) instruction to SOX9, into Leydig and Sertoli cells producing and stabilizing testosterone inhibiting PGCs from entering oogenesis, are directed to a spermatogenic fate [88]. Therefore, it should be no surprise that male ECS cells can undergo development until the blastula stage as described by Hubner and Scholer[89] and that male lymphoblastoma cells, like WI-L2-NS, induce key drivers of oogenesis such as Mos[14],and OCT4 [30] and can develop after genotoxic damage into early embryo-like OCT4-positive giant cells (Fig.1B). Interestingly, there are reports of the frequent loss of Y chromosomes in male cancers, for example at initial diagnosis of myeloid malignancies, with restoration of the normal karyotype (46XY) at remission [90].

An additional facet to be considered relates to aneuploidy. Aneuploidy is a typical hallmark of cancer, accompanying polyploidy and is usually explained by the instability of the cancer genome losing or gaining chromosomes during proliferation [91, 92]. However, this approach does not explain the "aneuploidy paradox": given its inherent anti-proliferative potential, why is aneuploidy obstinately retained in proliferating tumours [93, 94]?.Why do many cancers keep to para-triploidy, which in childhood neuroblastoma is associated with less chromosomal aberration and more favourable outcome [95], while other tumours are para-haploid [28, 96]? This paradox may be also resolved within the parthenogenetic theory of cancer.

Animals use multiple mechanisms of parthenogenesis, most of which depend on polar bodies that do not degenerate. So, besides several variants of parthenogenetic fusions leading to restoration of 2n chromosome number, there are also other variants allowing triploid cells to form [97]. Notably, ESCs resulting from haploid mouse parthenogenesis can also acquire germline potency after diploidisation [98], which can thus lead to loss of heterozygosity and loss of tumour suppression. The essence of meiosis is genetic recombination, so that each meiotic division produces a distinct sibling. Embryos that retain their polar bodies during development thus have two or more different genomes enabling genetic variation a-sexually. If tumour cells are involved in a macroevolutionary predetermined life-cycle with parthenogenetic components, then segregation of haploid paternal genomes and their variable combinations during the parthenogenetic fusions may be nearly an inevitable component of this process recovering the immortal germ-line. In turn, losses and gains of separate chromosomes are only secondary acquisitions of tumour microevolution, driven by instability and stochastic events, which may be counterbalanced by the recombinative process of meiosis [24]. Interestingly, the "triploid bridge" has been established in plants as facilitating a shift from polyploid to diploid generations [99].

CONCLUSION

Accumulating data favours a change to the view of the phylo-ontogenetic origin of cancer as a pre-programmed life-cycle process. This view provides a conceptual framework within which to explain the origin of cancer cells, their immortality and resistance to genotoxic treatments, and allows resolution of much of the complexity behind cancer phenomenology. It furthermore allows us to place the current knowledge on CSC, the reversible polyploidy of giant polyploid tumour cells, and the ectopic induction of meiosis-like processes into a non-contradictory hypothesis.

Perspectives

Accepting this concept of cancer cell embryonality and its life-cycle-like process of immortality provides us with new ways of understanding and treating cancer. On one hand, the embryonal-type plasticity and heterogeneity allows tumour cells to bypass many targeted therapies by substituting them with alternatives and thereby allowing time to undergo genetic drift and clonal selection [100, 101]. Moreover, genotoxic treatments actually favour the embryonalisation of tumour cells, thus promoting resistance, relapse and metastases [102-105] causing them to become entrapped in the embryonal "cancer attractor' [106-108]. Therefore, truly targeted therapy should be designed to hit the ontogenetic root of the cancer life-cycle and maybe even its phylogenetic origin in early multicellularians [26, 42].

The view that the genes of cellular cooperation that evolved with multicellularity about a billion years ago are the same genes that malfunction to cause cancer is positioned as the atavistic theory of cancer, which is substantiated from both paleontology and genetics [109]. It is supposed that this program became suppressed in advanced Metazoans by newer genes, which are undoubtedly tumour suppressors. Multiple atavistic theories did not take into account the polyploidy component, however, we suggested previously and substantiated here that reversible polyploidy is an essential component of this evolutionary-originated cancer cell

"life-cycle" program. This consideration brings us to the c-myc protooncogene, whose overexpression uncouples DNA replication from mitosis, thus leading to endopolyploidy [110]. C-myc is one of the most ancient genes of early Metazoans [111], linked during evolution to the Warburg effect [112]. It is also the main oncogene imposing immortality to cancer cells and a master regulator of stemness [52]. Importantly, c-myc is a gene, whose suppression in *in vivo* models eliminates "oncogene addiction" and cures experimental cancer [113, 114]. Therefore, the targets for interrupting the cancer cell 'life-cycle' at its evolutionary root should likely focus around c-myc.

On the other hand, if a tumour cell can undergo an epigenetic embryonalisation, its epigenetic reverse to a differentiated cell should be also possible. This strategy - not to fight but to tame tumour cells- seems logical. Such studies have been undertaken since the beginning of the 20th century; (for rev. see [8, 115-117]. Recently, a very interesting experiment was performed showing that paclitaxel could induce both EMT and formation of benign fibroblasts in an ovarian cancer model [118]. The best known and widely applied example of this treatment strategy is the differentiation inducer all-trans-retinoic acid (RA). Intriguing this is an old Chinese medicine against cancer and capable of curing acute myeloid leukemia [119].

Tumours can be "normalized" by an embryonic morphogenetic field [120] or by putting them within a normal 3D stroma [121, 122]. The influence of a regenerative environment was seen by the insertion of sarcoma cells into a fractured rat tibia; the cartilage calus formation enslaved them and interrupted their invasive growth [123].

The most important thing is that while genotoxic treatments convert malignant tumour cells into even more malignant variants [105], the opposite strategy may convert a malignant tumour into a benign one and prevent metastases. The epigenetic reprogramming of tumor cells by inducing differentiation (f.ex. by cytokines) show that epigenetics wins over genetics [124]. This facet in principal confirms the notion that embryonalisation is the only essential biological feature of tumour cells [2, 42, 107].

The experiments with nuclear cloning of embryonal carcinoma cells revealed that both malignant and embryological potentials can co-exist [125]. Therefore although it may be impossible to obtain the irreversible normalization of genotypically altered tumour cells by epigenetic means [126], it should be possible to stop tumour progression [117].

However, the most exciting thing is that the potential targets for these opposing strategies, as well as the pathways for genotoxically induced resistance and accelerated senescence, all converge at the same molecular pathways, around c-myc. Suppression of Wnt/ β-catenin signalling (which up-regulates c-myc to promote cell proliferation), favours the RA-dependent differentiation of embryonal carcinoma [127]. Potential normalization targets in spontaneous TP53 mutant tumour revertants lead to, among others, presenilin1 activating Notch1 substrate ɤ-secretase, up-stream of c-myc stress signaling [117]. In turn, Notch1, which directly regulates c-myc is co-operating with Wnt in enhancing tumorigenesis [128] enriches mammospheres induced in breast cancer by irradiation [129]. In addition, it was also found that p21CIP1, involved in regulation of cellular senescence, functions as a negative transcriptional regulator of WNT4 downstream of Notch 1 [130] and that p21CIP1 potentially reorganizes the nucleus during tumour reversion [117]. So, at the molecular level, all roads meet. This provides the hope that a single key, unavoidable, pathway may be targeted to finally cure cancer.

ACKNOWLEDGMENTS

This study was supported by the Latvian Scientific Council grant Nr 341/2012.

Conflict of interests

The authors declare no conflict of interests.

REFERENCES

1. Weinberg RA. Coming Full Circle-From Endless Complexity to Simplicity and Back Again. Cell 2014;157:267-71.
2. Erenpreiss JO. Current concepts of malignant growth. Riga: Zinâtne Publ; 1993.
3. Vinnitsky VB. The development of a malignant tumor is due to a desperate asexual self-cloning process in which cancer stem cells develop the ability to mimic the genetic program of germline cells. Intrinsically Disordered Proteins 2014;2:1272-84.
4. Bignold LP, Coghlam B, Jersmann H. David Paul von Hansemann: Contributions to Oncology. 2007.
5. Stevens LC. Experimental Production of Testicular Teratomas in Mice. Proceedings of the National Academy of Sciences of the United States of America 1964;52:654-61.
6. Kleinsmith LJ, Pierce GB. Multipotentiality of Single Embryonal Carcinoma Cells. Cancer Research 1964;24:1544-51.
7. Pierce GB, Wallace C. Differentiation of Malignant to Benign Cells. Cancer Research 1971;31:127-34.
8. Pierce GB. Carcinoma Is to Embryology As Mutation Is to Genetics. American Zoologist 1985;25:707-12.
9. Illmensee K, Mintz B. Totipotency and Normal Differentiation of Single Teratocarcinoma Cells Cloned

by Injection Into Blastocysts. Proceedings of the National Academy of Sciences of the United States of America 1976;73:549-53.

10. Mintz B, Illmensee K. Normal Genetically Mosaic Mice Produced from Malignant Teratocarcinoma Cells. Proceedings of the National Academy of Sciences of the United States of America 1975;72:3585-9.
11. Reya T, Morrison SJ, Clarke MF, Weissman IL. Stem cells, cancer, and cancer stem cells. Nature 2001;414:105-11.
12. Dalerba P, Cho RW, Clarke MF. Cancer stem cells: Models and concepts. Annual Review of Medicine 2007;58:267-84.
13. Weismann A. Das Keimplasma: Eine Theorie Der Vererbung. 1892.
14. Kalejs M, Ivanov A, Plakhins G, Cragg MS, Emzinsh D, Illidge TM et al. Upregulation of meiosis-specific genes in lymphoma cell lines following genotoxic insult and induction of mitotic catastrophe. Bmc Cancer 2006;6.
15. Ianzini F, Kosmacek EA, Nelson ES, Napoli E, Erenpreisa J, Kalejs M et al. Activation of Meiosis-Specific Genes Is Associated with Depolyploidization of Human Tumor Cells following Radiation-induced Mitotic Catastrophe. Cancer Research 2009;69:2296-304.
16. Vitale I, Senovilla L, Jemaa M, Michaud M, Galluzzi L, Kepp O et al. Multipolar mitosis of tetraploid cells: inhibition by p53 and dependency on Mos. Embo Journal 2010;29:1272-84.
17. Ling YH, Yang YD, Tornos C, Singh BR, Perez-Soler R. Paclitaxel-induced apoptosis is associated with expression and activation of c-Mos gene product in human ovarian carcinoma SKOV3 cells. Cancer Research 1998;58:3633-40.
18. Gorgoulis VG, Zacharatos P, Mariatos G, Liloglou T, Kokotas S, Kastrinakis N et al. Deregulated expression of c-mos in non-small cell lung carcinomas: Relationship with p53 status, genomic instability, and tumor kinetics. Cancer Research 2001;61:538-49.
19. Old LJ. Cancer/testis (CT) antigens - a new link between gametogenesis and cancer. Cancer Immun 2001;1:1.
20. Kalejs M, Erenpreisa J. Cancer/testis antigens and gametogenesis: a review and „brain-storming“ session. Cancer Cell International 2005;5.
21. Old LJ. Cancer is a somatic cell pregnancy. Cancer Immun 2007;7:19.
22. Erenpreisa J, Cragg MS, Salmina K, Hausmann M, Scherthan H. The role of meiotic cohesin REC8 in chromosome segregation in gamma irradiation-induced endopolyploid tumour cells. Experimental Cell Research 2009;315:2593-603.
23. Erenpreisa J, Kalejs M, Cragg MS. Mitotic catastrophe and endomitosis in tumour cells: An evolutionary key to a molecular solution. Cell Biology International 2005;29:1012-8.
24. Erenpreisa J, Cragg MS. MOS, aneuploidy and the ploidy cycle of cancer cells. Oncogene 2010;29:5447-51.
25. Erenpreisa J, Cragg MS. Cancer: A matter of life cycle? Cell Biology International 2007;31:1507-10.
26. Erenpreisa J, Cragg. Life-cycle features of tumour cells. In: P.Pontarotti, editor. Evolutionary Biology from Concept to Application. Berlin-Heidelberg: Springer Verlag; 2008; p. 61-7.
27. Davoli T, de Lange T. The Causes and Consequences of Polyploidy in Normal Development and Cancer. Annual Review of Cell and Developmental Biology, Vol 27 2011;27:585-610.
28. Walen KH. Haploidization of Human Diploid Metaphase Cells: Is This Genome Reductive Mechanism Opperational in Near-Haploid Leukemia? Journal of Cancer Therapy 2014;4:101-14.
29. Walen KH. Spindle apparatus uncoupling in endo-tetraploid asymmetric division of stem and non-stem cells. Cell Cycle 2009;8:3234-7.
30. Salmina K, Jankevics E, Huna A, Perminov D, Radovica I, Klymenko T et al. Up-regulation of the embryonic self-renewal network through reversible polyploidy in irradiated p53-mutant tumour cells. Experimental Cell Research 2010;316:2099-112.
31. Erenpreisa J, Salmina K, Huna A, Kosmacek EA, Cragg MS, Ianzini F et al. Polyploid tumour cells elicit paradiploid progeny through depolyploidizing divisions and regulated autophagic degradation. Cell Biology International 2011;35:687-95.
32. Lagadec C, Vlashi E, Della Donna L, Dekmezian C, Pajonk F. Radiation-Induced Reprogramming of Breast Cancer Cells. Stem Cells 2012;30:833-44.
33. Ben-Porath I, Thomson MW, Carey VJ, Ge R, Bell GW, Regev A et al. An embryonic stem cell-like gene expression signature in poorly differentiated aggressive human tumors. Nature Genetics 2008;40:499-507.
34. Saigusa S, Tanaka K, Toiyama Y, Yokoe T, Okugawa Y, Ioue Y et al. Correlation of CD133, OCT4, and SOX2 in Rectal Cancer and Their Association with Distant Recurrence After Chemoradiotherapy. Annals of Surgical Oncology 2009;16:3488-98.
35. Ge N, Lin HX, Xiao XS, Guo L, Xu HM, Wang X et al. Prognostic significance of Oct4 and Sox2 expression in hypopharyngeal squamous cell carcinoma. Journal of Translational Medicine 2010;8.
36. Shen LF, Huang XQ, Xie XX, Su J, Yuan J, Chen X. High Expression of SOX2 and OCT4 Indicates Radiation Resistance and an Independent Negative Prognosis in Cervical Squamous Cell Carcinoma. Journal of Histochemistry & Cytochemistry 2014;62:499-509.
37. Roesch A, Fukunaga-Kalabis M, Schmidt EC, Zabierowski SE, Brafford PA, Vultur A et al. A Temporarily Distinct Subpopulation of Slow-Cycling Melanoma Cells Is Required for Continuous Tumor Growth. Cell 2010;141:583-94.
38. Gupta PB, Fillmore CM, Jiang GZ, Shapira SD, Tao K,

Kuperwasser C et al. Stochastic State Transitions Give Rise to Phenotypic Equilibrium in Populations of Cancer Cells. Cell 2011;146:633-44.

39. Chaffer CL, Brueckmann I, Scheel C, Kaestli AJ, Wiggins PA, Rodrigues LO et al. Normal and neoplastic nonstem cells can spontaneously convert to a stem-like state. Proceedings of the National Academy of Sciences of the United States of America 2011;108:7950-5.
40. Chaffer CL, Marjanovic ND, Lee T, Bell G, Kleer CG, Reinhardt F et al. Poised Chromatin at the ZEB1 Promoter Enables Breast Cancer Cell Plasticity and Enhances Tumorigenicity. Cell 2013;154:61-74.
41. Blagosklonny MV. Cancer stem cell and cancer stemloids. Cancer Biology & Therapy 2007;6:1684-90.
42 Erenpreisa J, Cragg MS, Anisimov AP, Illidge TM. Tumor cell embryonality and the ploidy number 32n Is it a developmental checkpoint? Cell Cycle 2011;10:1873-4.
43. Bell G. The origin and early evolution of germ cells as illustrated by the Volvocales. In. The origin and evolution of sex; 1985; p. 221-56.
44. Erenpreisa J, Kalejs M, Ianzini F, Kosmacek EA, Mackey MA, Emzinsh D et al. Segregation of genomes in polyploid tumour cells following mitotic catastrophe. Cell Biology International 2005;29:1005-11.
45. Vakifahmetoglu H, Olsson M, Zhivotovsky B. Death through a tragedy: mitotic catastrophe. Cell Death and Differentiation 2008;15:1153-62.
46. Gisselsson D, Hakanson U, Stoller P, Marti D, Jin Y, Rosengren AH et al. When the Genome Plays Dice: Circumvention of the Spindle Assembly Checkpoint and Near-Random Chromosome Segregation in Multipolar Cancer Cell Mitoses. Plos One 2008;3.
47. Vitale I, Galluzzi L, Senovilla L, Criollo A, Jemaa M, Castedo M et al. Illicit survival of cancer cells during polyploidization and depolyploidization. Cell Death and Differentiation 2011;18:1403-13.
48. Sundaram M, Guernsey DL, Rajaraman MM, Rajaraman R. Neosis - A novel type of cell division in cancer. Cancer Biology & Therapy 2004;3:207-18.
49. Rajaraman R, Guernsey DL, Rajaraman MM, Rajaraman SR. Stem cells, senescence, neosis and self-renewal in cancer. Cancer Cell International 2006;6.
50. Zhang S, Mercado-Uribe I, Xing Z, Sun B, Kuang J, Liu J. Generation of cancer stem-like cells through the formation of polyploid giant cancer cells. Oncogene 2014;33:116-28.
51. Diaz-Carballo D, Gustmann S, Jastrow H, Acikelli AH, Dammann P, Klein J et al. Atypical cell populations associated with acquired resistance to cytostatics and cancer stem cell features: the role of mitochondria in nuclear encapsulation. DNA Cell Biol 2014;33:749-74.
52. Erenpreisa J, Cragg MS. Three steps to the immortality of cancer cells: senescence, polyploidy and self-renewal. Cancer Cell International 2013;13.
53. Coward J, Harding A. Size Does Matter: Why Polyploid Tumor Cells are Critical Drug Targets in the War on Cancer. Front Oncol 2014;4:123.
54. Erenpreisa J, Ivanov A, Wheatley SP, Kosmacek EA, Ianzini F, Anisimov AP et al. Endopolyploidy in irradiated p53-deficient tumour cell lines: persistence of cell division activity in giant cells expressing Aurora-B kinase. Cell Biol Int 2008;32:1044-56.
55. Erenpreisa JA, Cragg MS, Fringes B, Sharakhov I, Illidge TM. Release of mitotic descendants by giant cells from irradiated Burkitt's lymphoma cell lines. Cell Biology International 2000;24:635-48.
56. Huna A, Salmina K, Jascenko E, Duburs G, Inashkina I, Erenpreisa J. Self-Renewal Signalling in Presenescent Tetraploid IMR90 Cells. J Aging Res 2011;2011:103253.
57. Jackson TR, Salmina K, Huna A, Inashkina I, Jankevics E, Riekstina U et al. DNA damage causes TP53-dependent coupling of self-renewal and senescence pathways in embryonal carcinoma cells. Cell Cycle 2013;12:430-41.
58. Chitikova ZV, Gordeev SA, Bykova TV, Zubova SG, Pospelov VA, Pospelova TV. Sustained activation of DNA damage response in irradiated apoptosis-resistant cells induces reversible senescence associated with mTOR downregulation and expression of stem cell markers. Cell Cycle 2014;13:1424-39.
59. Menendez JA, Cufi S, Oliveras-Ferraros C, Martin-Castillo B, Joven J, Vellon L et al. Metformin and the ATM DNA damage response (DDR): Accelerating the onset of stress-induced senescence to boost protection against cancer. Aging-Us 2011;3:1063-77.
60. Beutner R. Über die Ursache der Neoplasie. J Cancer Res Oncol 1926;24:99-116.
61. Vinnitsky VB. Oncogerminative Hypothesis of Tumor-Formation. Medical Hypotheses 1993;40:19-27.
62. Weihua Z, Lin Q, Ramoth AJ, Fan D, Fidler IJ. Formation of solid tumors by a single multinucleated cancer cell. Cancer 2011;117:4092-9.
63. Lopez-Sanchez LM, Jimenez C, Valverde A, Hernandez V, Penarando J, Martinez A et al. CoCl2, a Mimic of Hypoxia, Induces Formation of Polyploid Giant Cells with Stem Characteristics in Colon Cancer. Plos One 2014;9.
64. Beard J. Hereditary and the Epicycle of the Germ-Cells. Biologisches Centralblatt 1902;22:321-408.
65. Beckett A. Embryological aspects and etiology of carcinoma: Gateway to the cancer stem cell theory. 2006. 11-11-2014. Ref Type: Online Source
66. Kondrashov AS. The Asexual Ploidy Cycle and the Origin of Sex. Nature 1994;370:213-6.
67. Illidge TM, Cragg MS, Fringes B, Olive P, Erenpreisa JA. Polyploid giant cells provide a survival mechanism for p53 mutant cells after DNA damage. Cell Biology International 2000;24:621-33.
68. Puig PE, Guilly MN, Bouchot A, Droin N, Cathelin D, Bouyer F et al. Tumor cells can escape DNA-damaging cisplatin through DNA endoreduplication and reversible

polyploidy. Cell Biology International 2008;32:1031-43.

69. Wolpert L, Beddington R, Jessel T, Lawrence P, Meyerowitz E, Smith J. Principles of development. Oxford: Oxford University Press; 2002.
70. Green KJ, Viamontes GI, Kirk DL. Mechanism of Formation, Ultrastructure, and Function of the Cytoplasmic Bridge System During Morphogenesis in Volvox. Journal of Cell Biology 1981;91:756-69.
71. Xiao SH, Knoll AH. Phosphatized animal embryos from the Neoproterozoic Doushantuo Formation at Weng'An, Guizhou, South China. Journal of Paleontology 2000;74:767-88.
72. Sliwinska MA, Mosieniak G, Wolanin K, Babik A, Piwocka K, Magalska A et al. Induction of senescence with doxorubicin leads to increased genomic instability of HCT116 cells. Mech Ageing Dev 2009;130:24-32.
73. Sabisz M, Skladanowski A. Cancer stem cells and escape from drug-induced premature senescence in human lung tumor cells Implications for drug resistance and *in vitro* drug screening models. Cell Cycle 2009;8:3208-17.
74. Wang Q, Wu PC, Dong DZ, Ivanova I, Chu E, Zeliadt S et al. Polyploidy road to therapy-induced cellular senescence and escape. International Journal of Cancer 2013;132:1505-15.
75. Sikora E. Rejuvenation of senescent cells-The road to postponing human aging and age-related disease? Experimental Gerontology 2013;48:661-6.
76. di Fagagna FD. Living on a break: cellular senescence as a DNA-damage response. Nature Reviews Cancer 2008;8:512-22.
77. Bernstein H, Byerly H, Hopf F, Michod RE. DNA repair and complementation: The major factors in the origin and maintenance of sex. In. The origin and evolution of sex; 1985; p. 29-45.
78. Nedelcu AM, Marcu O, Michod RE. Sex as a response to oxidative stress: a twofold increase in cellular reactive oxygen species activates sex genes. Proceedings of the Royal Society B-Biological Sciences 2004;271:1591-6.
79. Munoz-Espin D, Canamero M, Maraver A, Gomez-Lopez G, Contreras J, Murillo-Cuesta S et al. Programmed Cell Senescence during Mammalian Embryonic Development. Cell 2013;155:1104-18.
80. Otto SP. The Evolutionary Enigma of Sex. American Naturalist 2009;174:S1-S14.
81. Anatskaya OV, Vinogradov AE. Somatic polyploidy promotes cell function under stress and energy depletion: evidence from tissue-specific mammal transcriptome. Functional & Integrative Genomics 2010;10:433-46.
82. Yeom YI, Fuhrmann G, Ovitt CE, Brehm A, Ohbo K, Gross M et al. Germline regulatory element of Oct-4 specific for the totipotent cycle of embryonal cells. Development 1996;122:881-94.
83. Park SU, Choi ES, Jang YS, Hong SH, Kim IH, Chang DK. [Effects of chromosomal polyploidy on survival of colon cancer cells]. Korean J Gastroenterol 2011;57:150-7.
84. Zheng L, Dai HF, Zhou MA, Li XJ, Liu CW, Guo ZG et al. Polyploid cells rewire DNA damage response networks to overcome replication stress-induced barriers for tumour progression. Nature Communications 2012;3.
85. Erenpreiss JG. Gametogenesis as a molecular model of cancerogenesis: A current view of the embryological theory of cancer. Proc Latv Acad Sci Part B 1992;3:55-63.
86. Buganim Y, Faddah DA, Jaenisch R. Mechanisms and models of somatic cell reprogramming. Nature Reviews Genetics 2013;14:427-39.
87. Chuma S, Nakatsuji N. Autonomous transition into meiosis of mouse fetal germ cells *in vitro* and its inhibition by gp130-mediated signaling. Developmental Biology 2001;229:468-79.
88. Adams IR, McLaren A. Sexually dimorphic development of mouse primordial germ cells: switching from oogenesis to spermatogenesis. Development 2002;129:1155-64.
89. Hubner K, Fuhrmann G, Christenson LK, Kehler J, Reinbold R, De La Fuente R et al. Derivation of oocytes from mouse embryonic stem cells. Science 2003;300:1251-6.
90. Zhang LJ, Shin ES, Yu ZX, Li SB. Molecular genetic evidence of Y chromosome loss in male patients with hematological disorders. Chinese Medical Journal 2007;120:2002-5.
91. Duesberg P, Li R, Fabarius A, Hehlmann R. Aneuploidy and cancer: from correlation to causation. Contrib Microbiol 2006;13:16-44.
92. Gordon DJ, Resio B, Pellman D. Causes and consequences of aneuploidy in cancer. Nature Reviews Genetics 2012;13:189-203.
93. Tang YC, Williams BR, Siegel JJ, Amon A. Identification of Aneuploidy-Selective Antiproliferation Compounds. Cell 2011;144:499-512.
94. Holland AJ, Cleveland DW. Losing balance: the origin and impact of aneuploidy in cancer. Embo Reports 2012;13:501-14.
95. Spitz R, Betts DR, Simon T, Boensch M, Oestreich J, Niggli FK et al. Favorable outcome of triploid neuroblastomas: a contribution to the special oncogenesis of neuroblastoma. Cancer Genet Cytogenet 2006;167:51-6.
96. Safavi S, Forestier E, Golovleva I, Barbany G, Nord KH, Moorman AV et al. Loss of chromosomes is the primary event in near-haploid and low-hypodiploid acute lymphoblastic leukemia. Leukemia 2013;27:248-50.
97. Schmerler S, Wessel GM. Polar Bodies-More a Lack of Understanding Than a Lack of Respect. Molecular Reproduction and Development 2011;78:3-8.
98. Leeb M, Walker R, Mansfield B, Nichols J, Smith A, Wutz A. Germline potential of parthenogenetic haploid mouse embryonic stem cells. Development 2012;139:3301-5.
99. Comai L. The advantages and disadvantages of being polyploid. Nature Reviews Genetics 2005;6:836-46.

100. Gillies RJ, Verduzco D, Gatenby RA. Evolutionary dynamics of carcinogenesis and why targeted therapy does not work. Nature Reviews Cancer 2012;12:487-93.

101. Yap TA, Gerlinger M, Futreal PA, Pusztai L, Swanton C. Intratumor Heterogeneity: Seeing the Wood for the Trees. Science Translational Medicine 2012;4.

102. Lagadec C, Pajonk F. Catch-22: does breast cancer radiotherapy have negative impacts too? Future Oncology 2012;8:643-5.

103. Vlashi E, Pajonk F. Cancer stem cells, cancer cell plasticity and radiation therapy. Semin Cancer Biol 2014.

104. Huang S. The war on cancer: lessons from the war on terror. Front Oncol 2014;4:293.

105. Hanahan D. Rethinking the war on cancer. Lancet 2014;383:558-63.

106. Huang S, Ernberg I, Kauffman S. Cancer attractors: A systems view of tumors from a gene network dynamics and developmental perspective. Seminars in Cell & Developmental Biology 2009;20:869-76.

107. Huang S. On the intrinsic inevitability of cancer: From foetal to fatal attraction. Seminars in Cancer Biology 2011;21:183-99.

108. Zhang Yue. Cancer Embryonic Stem Cell-like Attractors alongside Deficiency of Regulatory Restraints of Cell-Division and Cell-Cycle . J Genet Syndr Gene Ther 2013;4.

109. Davies PCW, Lineweaver CH. Cancer tumors as Metazoa 1.0: tapping genes of ancient ancestors. Physical Biology 2011;8.

110. Li Q, Dang CV. c-Myc overexpression uncouples DNA replication from mitosis. Molecular and Cellular Biology 1999;19:5339-51.

111. Hartl M, Mitterstiller AM, Valovka T, Breuker K, Hobmayer B, Bister K. Stem cell-specific activation of an ancestral myc protooncogene with conserved basic functions in the early metazoan Hydra. Proceedings of the National Academy of Sciences of the United States of America 2010;107:4051-6.

112. Vincent M. Cancer: A de-repression of a default survival program common to all cells? Bioessays 2012;34:72-82.

113. Soucek L, Whitfield J, Martins CP, Finch AJ, Murphy DJ, Sodir NM et al. Modelling Myc inhibition as a cancer therapy. Nature 2008;455:679-83.

114. Felsher DW. MYC Inactivation Elicits Oncogene Addiction through Both Tumor Cell-Intrinsic and Host-Dependent Mechanisms. Genes Cancer 2010;1:597-604.

115. Lipkin G. Plasticity of the cancer cell: Implications for epigenetic control of melanoma and other malignancies. Journal of Investigative Dermatology 2008;128:2152-5.

116. Baylin SB, Jones PA. A decade of exploring the cancer epigenome - biological and translational implications. Nature Reviews Cancer 2011;11:726-34.

117. Telerman A, Amson R. The molecular programme of tumour reversion: the steps beyond malignant transformation. Nature Reviews Cancer 2009;9:206-15.

118. Jia LZ, Zhang SW, Ye YF, Li X, Mercado-Uribe I, Bast RC et al. Paclitaxel inhibits ovarian tumor growth by inducing epithelial cancer cells to benign fibroblast-like cells. Cancer Letters 2012;326:176-82.

119. Sachs L. Control of normal cell differentiation and the phenotypic reversion of malignancy in myeloid leukaemia. Nature 1978;274:535-9.

120. Bizzarri M, Cucina A, Biava PM, Proietti S, D'Anselmi F, Dinicola S et al. Embryonic Morphogenetic Field Induces Phenotypic Reversion in Cancer Cells. Review Article. Current Pharmaceutical Biotechnology 2011;12:243-53.

121. Weaver VM, Petersen OW, Wang F, Larabell CA, Briand P, Damsky C et al. Reversion of the malignant phenotype of human breast cells in three-dimensional culture and *in vivo* by integrin blocking antibodies. Journal of Cell Biology 1997;137:231-45.

122. Kirshner J, Chen CJ, Liu PF, Huang J, Shively JE. CEACAM1-4S, a cell-cell adhesion molecule, mediates apoptosis and reverts mammary carcinoma cells to a normal morphogenic phenotype in a 3D culture. Proceedings of the National Academy of Sciences of the United States of America 2003;100:521-6.

123. ERENPREIS J. Tumour growth in the zone of bone regeneration. Acta Unio Int Contra Cancrum 1964;20:1560.

124. Lotem J, Sachs L. Epigenetics wins over genetics: induction of differentiation in tumor cells. Seminars in Cancer Biology 2002;12:339-46.

125. Blelloch RH, Hochedlinger K, Yamada Y, Brennan C, Kim MJ, Mintz B et al. Nuclear cloning of embryonal carcinoma cells. Proceedings of the National Academy of Sciences of the United States of America 2004;101:13985-90.

126. Loeb LA. A mutator phenotype in cancer. Cancer Res 2001;61:3230-9.

127. Zhang S, Li Y, Wu YL, Shi K, Bing LJ, Hao J. Wnt/beta-Catenin Signaling Pathway Upregulates c-Myc Expression to Promote Cell Proliferation of P19 Teratocarcinoma Cells. Anatomical Record-Advances in Integrative Anatomy and Evolutionary Biology 2012;295:2104-13.

128. Palomero T, Lim WK, Odom DT, Sulis ML, Real PJ, Margolin A et al. NOTCH1 directly regulates c-MYC and activates a feed-forward-loop transcriptional network promoting leukemic cell growth. Proceedings of the National Academy of Sciences of the United States of America 2006;103:18261-6.

129. Lagadec C, Vlashi E, Alhiyari Y, Phillips TM, Dratver MB, Pajonk F. Radiation-Induced Notch Signaling in Breast Cancer Stem Cells. International Journal of Radiation Oncology Biology Physics 2013;87:609-18.

130. Devgan V, Mammucari C, Millar SE, Brisken C, Dotto GP. p21WAF1/Cip1 is a negative transcriptional regulator of Wnt4 expression downstream of Notch1 activation. Genes Dev 2005;19:1485-95.

4. Discussion

In recent years studies have revealed there are two contrary phenomena in tumour cell response to the dosages of conventional genotoxic therapy applied for treatment of cancer patients: on one hand, cessation of growth by induction of cellular senescence and, on the other hand, induction of resistance and propagation of cancer stem cells. It turned out, that induction of polyploidy may unite these two opposites. Collaborative studies in our laboratory revealed that induced in TP53 mutant tumour cells polyploidy is reversible (Illidge *et al.,* 2000) and moreover, that induction of reversible polyploidy is associated with activation of embryonal stem cell key transcription cassette (Salmina *et al.,* 2010). This data were confirmed and extended by other researchers, who showed that induced polyploid cells can grow as spheroids, give tumours at xenotransplantation, even ofone giant cell, and produce epithelial-mesenchymal transition (EMT) descendants by de-polyploidisation (Weihua *et al.,* 2011; Ghisolfi *et al.,* 2012; Lagadec and Pajonk 2012; Zhang *et al.,* 2013c). However, the relationship between stemness and senescence, which also turned out to be reversible and associated with polyploidy (Puig *et al.,* 2008; Mosieniak *et al.,* 2012; Wang *et al.,* 2013), as well as the role of the main constituent of senescence, autophagy (Capparelli *et al.,* 2012; Mosieniak *et al.,* 2012; Young *et al.,* 2009) for resistant tumour growth is remaining entangled and unclear. Gaining a better understanding of the relationship of these complex phenomenon is the subject of the current study (original paper 1) we used *in vitro* senescence of normal human fibroblasts IMR90 as our first model. Surprisingly, we found the co-expression of embryonal self renewal transcription factor NANOP and senescence markers p21CIP1 and P16INK4a in the same pre-senesent cells signalling DNA damage by γ-H2AX. In particular, we found that this co-expression of opposites was associated with overcoming the G2/M barrier of tetraploidy. It was for the first time that self- renewal signaling has been revealed in normal senescing cells in association with G2 DNA damage checkpoint and its adaptation for polyploidy. When gradualy entering deeper senescence most IMR90 cells loose NANOG from cell nuclei; rare giant cells still continue to express it in paralel with senescence markers. NANOG, an activator, and P16INK4a, inhibitor of cyclin kinase complex cyclin D/cdk4,6 have adverse roles in initiation of the cell cycle (Neganova and Lako 2008). NANOG was also shown to suppress promoter of TP53 (Lin *et al.,* 2005), which is the main protector from polyploidy and aneuploidy (Aylon and Oren 2011), while polyploidy, in turn, causes inactivation of TP53 (Park *et al.,* 2011) (Zheng *et al.,* 2012). Therefore, the expression of NANOG in normal pre-senescent cells carrying DNA damage shows potential of compromising natural senescence barrier to malignant growth (Collado and Serrano 2010; Erenpreisa and Cragg 2013)**.** Notably, this transition of wt TP53 normal cells occurs through adaptation of G2 damage checkpoint, likewise shift to stemness and resistance

of genotoxically damaged TP53-mutant tumour cells (Salmina *et al.*, 2010) and both are united by emerging polyploidy (Figure 1).

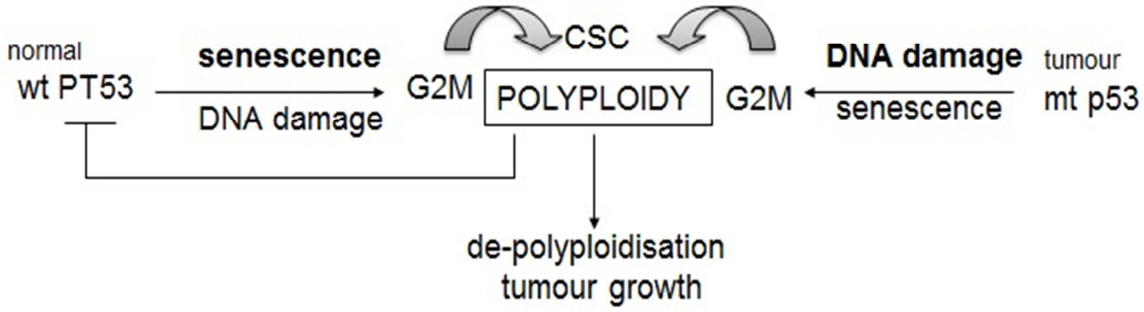

Figure 1. The left part of the scheme shows the tumorigenesis through senescence of normal cells, and theright part of the scheme shows the resistance of tumour cells to genotoxic therapy through senescence and polyploidy. DNA damage is a leading cause, while polyploidisation is associated with acquisition of CSC phenotype.

Next, we took the model of cancer stem cells with functional TP53, embryonal carcinoma PA1 andtreated it with inhibitor of topoisomerase II etoposide (original paper 2). After DNA-damage induced by etoposide, self-renewal transcription factor OCT4A and growth arrest/senescence regulator P21CIP1 were found highly increased in the same cells.

Silencing of mRNA TP53 in this model prevented the upregulation of P21CIP1 and, suprisingly, of stemness factor OCT4A as well, returning its levels back to control. This drove us to conclusion that activation of OCT4 by DNA damage in embryonal carcinoma cells is P53 dependent. That goes together with discovery by others, that OCT4 may have role in stress response (Bártová *et al.*, 2011). TP53 silencing also led cells to increased DNA damage and polyploidy. Premature exit of G2 arrest, mitosis, micronucleation and senescence (marked by sa-β-galactosidase) were all enhanced after TP53 silencing. Induction of senescence was confirmed by upregulation of CDKN2A/P16INK4A. Mitoses enhanced by TP53 silencing were shown to be multicentrosomal and multi-polar, containing fragmented and highly deranged chromosomes, indicating loss of genome stability, which otherwise was supported by TP53-dependent balance between two factors of opposite cell fates.

In further research on this model (original paper 3) we studied interactions between OCT4A and P21CIP1. Via silencing experiments, we found that OCT4A suppresses P21CIP1 but P21CIP1 does not directly influence OCT4A. Withdrawal of OCT4A led cells to irreversible

senescence and significally increased polyploidy and cancelled mitotic regrowth, although also showed decreased apoptosis. The latter effect can be caused byantiapoptotic effects of P21CIP1 (Shim *et al.,* 1996; Suzuki *et al.,* 1998).

It follows that the role of P53-dependant OCT4A is to keep a cell resisting terminal senescence by tempering P21CIP1. Down-regulation of P21CIP1 by OCT4A inducing methylation of its promoter was shown earlier (Lee *et al.,* 2010). So, this is a real mechanism of resistance of embryonal and cancer stem cells, which equip them with advantage, by giving more time for DNA repair, in comparison with normal cells where this mechanism is absent. If both - P53 and OCT4A can keep the DNA damaged cells in G2-arrest, then when removed, the cells with still persisting DNA damage can overcome this barrier and move into malignant aneupolyploidy. Therefore, this mechanism has a role in guarding stemness from the genome instability.

Next the question arose - what determines the limit of this capability, if P21CIP1 does not suppress OCT4? Our studies on this model with application of autophagy inhibitor Bafilomycin A1 showed that the limit is the capacity of autophagy to support cell by providing energy and metabolites. Suppression of autophagy abolished recovery of clonogenic growth after etoposide treatment (original paper 3).

Moreover, we revealed a novel mechanism of sequestration and digestion of P16INK4a in cytoplasm by functional autophagy, thus postponing onset of terminal senescence (original paper 3). This finding is in accord with the data that inhibition of autophagy leads to accumulation of P16INK4a and other markers of irreversible senescence (Kang *et al.*, 2011). As autophagy is the main constituent of cellular senescence ensuring metabolic activity of growth arrested cells, we conclude that autophagy is a key to the fate decision of DNA damaged tumour cells. This conclusion fits well with the data on the role of mTOR, the inhibitor of autophagy and AMPK, its activator and cell energy sensor (Galluzzi *et al.,* 2014; Sui *et al.,* 2013). In particular, after etoposide treatment, inhibition of pAMPK in G2-arrested hepatoma cells triggers apoptosis through suppression of autophagy (Xie *et al.,* 2011). Therefore our discovery of the pAMPKthr172 activation and its coordination with OCT4A expression, in the PA1-Etoposide model was very notable and in line (original paper 3). The link between OCT4A and pAMPK may be explained by the role as regulator of pAMPK in the DNA damage response (Sanli *et al.,* 2014) and in stabilisation of activated P53 (Bungard *et al.,* 2010).

We found another facet of autophagy associated with reversible polyploidy induced by genotoxic treatment (irradiation or etoposide) of tumour cells in the earlier study (original paper 4) – autophagic digestion and extrusion of sub-nuclei leaving behind the subnuclei, which accumulated stemness markers (OCT4A and NANOG). The latter were able to restart mitosis and were released from giant mothers as free subcells.

Hitherto, nucleophagy has been also observed in a small percentage of non-treated cells (Park *et al.,* 2009). It may be due to release of small portions of extrachromosomal DNA of telomeric origin found in senescing cells (Kunisada *et al.,* 1985; Gaubatz 1990); extrusion of small patches heterochromatic DNA from senescing cells was also found by Adams and colleagues (Ivanov *et al.,* 2013).

However, in our research sorting of the whole sub-nuclei from multi-nucleated tumour cells were found and they were preceded by multi-polar a-cytotomic mitosis. It was suggested that polyploid cells are able to re-assort and selectively remove more damaged sub-nuclei by autophagy and/or use this material for re-utilisation by neighbour sub-nuclei recovered as descending cells. Thus, much discussed paradoxical nature of autophagy in tumours (both pro-senescing and pro-survival) (Hanahan and Weinberg 2011) and their tendency to promote aneu-polyploidy in spite of its anti-proliferative effect may be explained by each other.

So, our findings of new facets of the role of autophagy in both TP53 wild type and mutant cancer cells indicate to its paramount role in genotoxic resistance provided by collaboration between senescence, polyploidy, and stemness. It follows that autophagy should be a key target for preventing resistance of cancer cells to genotoxic therapies, a supposition supported by others (Sui *et al.,* 2013; Dörr *et al.,* 2013).

The genotoxically treated tumour cells acquire stemness features through polyploidy and we have possibly revealed a structural aspect of it. We found significant (up to five-fold) expansion of chromosome territories in induced endopolyploid cells reaching maximum on day 5 (original paper 5) on the model of irradiated HeLa cells using the whole chromosome *in situ* fluorescent painting probes. Such rewiring should change function of the whole genome (Giuliani 2014). This data characterises the conformation of the chromatin in polyploid cells as highly open (unfolded), which fits well with the observed activation of embryonal stemness found earlier in this model (Salmina *et al.,* 2010) and results described here (original paper 5). The bivalent and open conformation of the chromatin in embryonal stem cells (Bernstein *et al.,* 2006) was shown to keep transcription of most genes initiated (Guenther *et al.,* 2007). Loose chromatin conformation is likely induced by activated c-Myc, which both favours endopolyploidy (Li and Dang 1999) and acetylation of core nucleosome histones (Martinato *et al.,* 2008). This epigenetic chromatin feature of the embryonal stemness provides these cells with plasticity to easily adapt transcription development programs and to stress conditions, including genotoxic and proteoxic stress of anticancer treatments.

Furthermore, the dual response of PA1 embryonal carcinoma cells to etoposide eventually determining two opposite cell fates, termination or survival, revealed high heterogeneity of expression in individual cells of eto-treated population (original paper 3) in our experiments and

this should be discussed. Detection of the DNA damage-P53-dependant OCT4A and P21CIP1 shows the apparently bi-potential state where the space spanned by OCT4A and P21CIP1 covers (on day 5) all the spectrum of relationships, while later cells separate for survivors and those which die. It indicates the disadaptation caused by high DNA damage (Gorban *et al.,* 2010; Giuliani *et al.,* 1998), and to the involvement of chaotic regulations. The traectory of individual cell in this state of instable bi-potential state between two opposites preceding bifurcation might be near-random (Huang 2004) and highly susceptible to intrinsic and extrinsic factors. The thermodynamics of instable self-organising systems developed by the Nobel Prize laureate (1977) Ilya Prigogine highlights an advantage of coherating fluctuations emerging in such self-organising systems, which due to positive feed-back loops may involve cell population to one or another equilibrium attractor of cell fate. Cell-to cell variability, due to ergodic theorem, corresponds temporal variability (Brock *et al.,* 2009). Indeed, OCT4A (Sustáčková *et al.,* 2012) and activator of both – OCT4A and P21CIP1, P53 (Purvis *et al.,* 2012) have been shown to fluctuate after DNA damage. Apparently, this chaotic regulation may be critical for the plasticity (adaptability) of the stem cell-like phenotype in the control of linear choice (Huang 2009; Brock *et al.,* 2009; Chang *et al.,* 2008) So, it appears that chaotic regulation, assigned together with epigenetic plasticity to tumour cells by stemness phenotype, is used for their escape from genotoxic treatments.

This raises the question, which evolutionary traits gave the origin to the biology of tumour cells and its resistance to genotoxic damage, characterized in this study by induced cellular senescence, polyploidy, and embryonal type stemness and acting as a whole? This conundrum was analyzed in the review paper included in this study (review paper 1). The apparent driver of this evolution is DNA damage repair relation to the origin of sex (Kondrashov 1994; Bernstein *et al.,* 1985). Therefore, molecularly, all three phenomena converge to DNA damage G2 checkpoint (Erenpreisa and Cragg 2013). The capability of induced polyploidy tumour cells to express the meiotic and early embryo genes (Ianzini *et al.,* 2009; Erenpreisa and Cragg 2010) and capability to grow as spheroids (Weihua *et al.,* 2011; Lagadec *et al.,* 2012; Zhang *et al.,* 2013) giving rise to differentiated tissues (Zhang *et al.,* 2013a; Zhang *et al.,* 2013b) drives us back to the roots - embryological theory of cancer (Cohnheim 1880, after Erenpreiss 1993). This, in turn, puts the possibility ofusing these embryonal properties of malignant tumours for epigenetic reverse to benign condition applying differentiating inducers back on the agenda (Pierce and Wallace 1971).

Accumulating data favours a change of current paradigm of the origin of cancer from purely stochastic (mutation-driven) to an evolutionary pre-programmed life-cycle-like process as discussed in our review (review paper 1).

5. Conclusions

- Coupling of the expression of embryonal self renewal transcription factor NANOG with senescence regulators P21CIP1 and P16INK4a in pre-senescent human fibroblasts coincide with DNA damage and overcoming the G2/M barrier of polyploidy.

- Activation and coupling of self renewal and senescence regulators OCT4A and P21CIP1 revealed in the cells of etoposide-treated teratocarcinoma PA1 is P53 dependant.

- The heterogenous pattern of the dual activation of the opposing regulators OCT4A and P21CIP1 after DNA damage indicates to metastable bi-potentiality as a mechanism of non-linear regulations in stress response of cells with properties of embryonal stemness.

- The role of P53-dependant OCT4A induced by DNA damage in PA1 cells is partial suppression of P21CIP1 preventing terminal senescence and genome destabilisation.

- P53-dependant OCT4A induced by DNA damage in PA1 cells is co-expressed and co-ordinated with activated AMPK thr172 - a master sensor of energy deficit, regulator of cellular metabolism and activator of autophagy. Dependance on P53 and co-operation with pAMPK indicates to a novel stress function of OCT4A in DNA-damaged cancer stem cells.

- Functional autophagy supports vitality of DNA-damaged cells, sequestrates the inducer of terminal senescence P16INK4a in cytoplasm. Irreversible senescence of DNA damaged tumour cells counterbalanced by stemness is mainly triggered by failure of autophagy.

- Selective chromatin degradation by autophagy in polyploid tumour cells favours their de-polyploidisation and resistant re-growth .

- Chromosome territory expansion in DNA damage induced poyploidy indicates nuclear architecture switch towards stem-like plasticity.

- Accumulating data favour the view on cancer as the phylogenetically pre-programmed life-cycle-like process.

6. Main thesis of defence

- Simultaneous activation of self renewal and accelerated senescence occurs in normal presenescent human fibroblasts in G2 damage checkpoint accompanied by overcoming the barrier to tetraploidy.

- Simultanous P53 dependent activation of self-renewal OCT4A and senescence P21CIP1 proteins in etoposide treated teratocarcinoma PA1, the model of damaged cancer stem cells, indicates the generality of coupling between senescence and stemness programs ocuring in DNA damage response.

- Stress activated P53-dependent OCT4A of eto-treated teratocarcinoma PA1 cells restricts expression of P21CIP1 and is coordinated with metabolic stress sensor and autophagy activator pAMPK, thus is acting as a DNA stress-responser.

- Adaptation to genotoxic stress is regulated through enormous heterogeneity in dual expression by individual cells of OCT4A and P21CIP1. This phenomenon reflects the features of population regulation by self-organisation principles.

- Autophagy is part of accelerated senescence, however prevents terminal senescence, while its failure overcomes resistance of tumour cells. Therefore, autophagy should be a key target for preventing resistance of cancer stem cells to genotoxic therapies.

Acknowledgements

This study was supported by:
ESF within the project «Support for Doctoral Studies at University of Latvia».
ESF project 2013/0023/1DP/1.1.1.2.0/13/APIA/VIAA/037
LZP project LZP341/2012
L'Oreal, UNESCO Latvian National Commission and Latvian Academy of Sciences Scholarship for Women in Science.

I am grateful to:
My supervisor
Jekaterina Ērenpreisa;
.
my colleagues

from Latvian Biomedical Research and Study Centre:
Kristīne Salmiņa, Bogdan Geraschenko, Jēkabs Krīgerts, Ēriks Jankevics, Inna Iņaškina, Zane Kalniņa, Alejandro Vazquez-Martin;

from University of Latvia:
Una Riekstina;

from the Latvian Institute of Organic Synthesis:
Elina Sokolova, Gunars Duburs;

and international collaborators:
Thomas Jackson, Mark Cragg, Andre Ivanov, Paul Townsend, Michael Hausmann , Jutta Schwarz-Finsterle, Harry Scherthan, Paula González, Patrick Mueller, Eberhard Schmitt, Elizabeth Kosmacek, Fiorenza Ianzini and Alim P. Anisimov;

et al.

I also would like to thank my friends and family for supporting me in many ways.

References

Acosta, J. C., Gil, J. (2012). Senescence: A new weapon for cancer therapy. *Trends in Cell Biology*, 22 (4), 211–219.

Anatskaya, O. V., Vinogradov, A. E. (2007). Genome multiplication as adaptation to tissue survival: evidence from gene expression in mammalian heart and liver. *Genomics*, 89 (1), 70–80.

Anatskaya, O. V., Vinogradov, A. E. (2010). Somatic polyploidy promotes cell function under stress and energy depletion: evidence from tissue-specific mammal transcriptome. *Functional & Integrative Genomics*, 10 (4), 433–446.

Atlasi, Y., Mowla, S. J., Ziaee, S. A., Gokhale, P. J., Andrews, P. W. (2008). OCT4 spliced variants are differentially expressed in human pluripotent and nonpluripotent cells. *Stem Cells (Dayton, Ohio)*, 26 (12), 3068–3074.

Atsumi, Y., Fujimori, H., Fukuda, H., Inase, A., Shinohe, K. *et al.* (2011). Onset of quiescence following p53 mediated down-regulation of H2AX in normal cells. *PloS One*, 6 (8), e23432.

Aylon, Y., Oren, M. (2011). P53: Guardian of ploidy. *Molecular Oncology*, 5 (4), 315–323.

Bartkova, J., Rezaei, N., Liontos, M., Karakaidos, P., Kletsas, D. *et al.* (2006). Oncogene-induced senescence is part of the tumorigenesis barrier imposed by DNA damage checkpoints. *Nature*, 444 (7119), 633–637.

Bártová, E., Šustáčková, G., Stixová, L., Kozubek, S., Legartová, S. *et al.* (2011). Recruitment of Oct4 protein to UV-damaged chromatin in embryonic stem cells. *PLoS ONE*, 6 (12), e27281.

Beauséjour, C. M., Krtolica, A., Galimi, F., Narita, M., Lowe, S. W. *et al.* (2003). Reversal of human cellular senescence: roles of the p53 and p16 pathways. *EMBO Journal*, 22 (16), 4212–4222.

Beck, B., Blanpain, C. (2013). Unravelling cancer stem cell potential. *Nature Reviews. Cancer*, 13 (10), 727–738.

Bernstein, B. E., Mikkelsen, T. S., Xie, X., Kamal, M., Huebert, D. J. *et al* (2006). A bivalent chromatin structure marks key developmental genes in embryonic stem cells. *Cell*, 125 (2), 315–326.

Bernstein, H., Byerly, H. C., Hopf, F. A., Michod, R. E. (1985). DNA repair and complementation: the major factors in the origin and maintenance of sex. *DNA Repair and Complementation: The Major Factors in the Origin and Maintenance of Sex*, 29–45.

Blagosklonny, M. V. (2007). Cancer stem cell and cancer stemloids: from biology to therapy. *Cancer Biology & Therapy*, 6 (11), 1684–1690.

Bond, J. A., Wyllie, F. S., Wynford-Thomas, D. (1994). Escape from senescence in human diploid fibroblasts induced directly by mutant p53. *Oncogene*, 9 (7), 1885–1889.

Boumahdi, S., Driessens, G., Lapouge, G., Rorive, S., Nassar, D. *et al.* (2014). SOX2 controls tumour initiation and cancer stem-cell functions in squamous-cell carcinoma. *Nature*, 511 (7508), 246-250.

Boyer, L.A., Lee, T.I., Cole, M.F., Johnstone, S.E., Levine, S.S. (2005). Core transcriptional regulatory circuitry in human embryonic stem cells. *Cell*, 122 (6), 947–956.

Brock, A., Chang, H., Huang, S. (2009). Non-genetic heterogeneity--a mutation-independent driving force for the somatic evolution of tumours. *Nature Reviews. Genetics*, 10 (5), 336–342.

Bungard, D., Fuerth, B. J., Zeng, P., Faubert, B., Maas, N. L. *et al.* (2010). Signaling kinase AMPK activates stress-promoted transcription via histone H2B phosphorylation. *Science (New York, N.Y.)*, 329 (5996), 1201–1205.

Cabrera, M. C., Hollingsworth, R. E., Hurt, E. M. (2015). Cancer stem cell plasticity and tumor hierarchy. *The World Journal of Stem Cells*, 7 (1), 27–36.

Campisi, J. (2001). Cellular senescence as a tumor-suppressor mechanism. *Trends in Cell Biology*, 11 (11), 27-31.

Campisi, J. (2005). Senescent cells, tumor suppression, and organismal aging: good citizens, bad neighbors. *Cell*, 120 (4), 513–522.

Campisi, J., d'Adda di Fagagna, F. (2007). Cellular senescence: when bad things happen to good cells. *Nature Reviews. Molecular Cell Biology*, 8 (9), 729–740.

Cantz, T., Key, G., Bleidiβel, M., Gentile L. (2008). Absence of OCT4 expression in somatic tumor cell lines. *Stem Clls*, 26 (3), 692–697.

Capparelli, C., Chiavarina, B., Whitaker-Menezes, D., Pestell, T. G., Pestell, R. G. *et al.* (2012). CDK inhibitors (p16/p19/p21) induce senescence and autophagy in cancer-associated fibroblasts, "fueling" tumor growth via paracrine interactions, without an increase in neo-angiogenesis. *Cell Cycle*, 11 (19), 3599–3610.

Castedo, M., Vitale, I., Kroemer, G. (2010). A novel source of tetraploid cancer cell precursors: telomere insufficiency links aging to oncogenesis. *Oncogene*, 29 (44), 5869–5872.

Celton-Morizur, S., Merlen, G., Couton, D., Desdouets, C. (2010). Polyploidy and liver proliferation central role of insulin signaling. *Cell Cycle*, 9 (3), 460-466.

Chambers, I., Smith, A. (2004). Self-renewal of teratocarcinoma and embryonic stem cells. *Oncogene*, 23 (43), 7150–7160.

Chang, H. H., Hemberg, M., Barahona, M., Ingber, D. E., Huang, S. (2008). Transcriptome-wide noise controls lineage choice in mammalian progenitor cells. *Nature*, 453 (7194), 544–547.

Chin, J., Shiwaku, H., Goda, O., Komuro, A., Okazawa, H. (2009). Neural stem cells express Oct-3/4. *Biochemical and Biophysical Research Communications*, 388 (2), 247–251.

Cho, R. W., Clarke, M.F. (2008). Recent advances in cancer stem cells. *Current Opinion in Genetics and Development*, 18 (1), 48–53.

Collado, M. and Serrano, M. (2010). Senescence in tumours: evidence from mice and humans. *Nature Reviews. Cancer*, 10 (1), 51–57.

Comai, L. (2005). The advantages and disadvantages of being polyploid. *Nature Reviews. Genetics*, 6 (11), 836–846.

Conant, G. C., Wolfe, K. H. (2007). Increased glycolytic flux as an outcome of whole-genome duplication in yeast. *Molecular Systems Biology*, 3 (1), 129.

Coward, J., Harding, A. (2014). Size does matter: why polyploid tumor cells are critical drug targets in the war on cancer. *Frontiers in Oncology*, 4 , 123.

Csermely, P., Hódsági, J., Korcsmáros, T., Módos, D., Perez-Lopez, A. R. *et al.* (2014). Cancer stem cells display extremely large evolvability: alternating plastic and rigid networks as a

potential mechanism: network models, novel therapeutic target strategies, and the contributions of hypoxia, inflammation and cellular senescence. *Seminars in Cancer Biolog*, 30, 42–51.

Cuervo, A. M., Bergamini, E., Brunk, U. T., Dröge, W., Ffrench, M. *et al.* (2005). Autophagy and aging: the importance of maintaining "clean" cells. *Autophagy*, 1(3), 131-140.

d'Adda di Fagagna, F. (2008). Living on a break: cellular senescence as a DNA-damage response. *Nature Reviews. Cancer*, 8 (7), 512–522.

d'Adda di Fagagna, F., Reaper, P. M., Clay-Farrace, L., Fiegler, H., Carr, P. *et al.* (2003). A DNA damage checkpoint response in telomere-initiated senescence. *Nature*, 426 (6963), 194-198.

Davoli, T., de Lange, T. (2011). The causes and consequences of polyploidy in normal development and cancer. *Annual Review of Cell and Developmental Biology*, 27, 585–610.

Davoli, T., Denchi, E. L., de Lange, T. (2011). Persistent telomere damage induces by-pass of mitosis and tetraploidy. *Cell*, 141 (1), 81–93.

Dewhurst, S. M., McGranahan, N., Burrell, R. A., Rowan, A. J., Grönroos, E. *et al.* (2014). Tolerance of whole-genome doubling propagates chromosomal instability and accelerates cancer genome evolution. *Cancer Discovery*, 4 (2), 175-185.

Dörr, J. R., Yu, Y., Milanovic, M., Beuster, G., Zasada, C. *et al.* (2013). Synthetic lethal metabolic targeting of cellular senescence in cancer therapy. *Nature*, 501, 421-425.

Duesbery, N.S., Vande Woude, G. F. (2002). Developmental biology: An arresting activity. *Nature*, 416 (6883), 804–805.

Duncan, A. W., Taylor, M. H., Hickey, R. D., Newell, A. E. H., Lenzi, M. L. *et al.* (2010). The ploidy conveyor of mature hepatocytes as a source of genetic variation. *Nature*, 467 (7316), 707–710.

Elledge, S. J. (1996). Cell cycle checkpoints: preventing an identity crisis. *Science (New York, N.Y.)*, 274 (5293): 1664–1672.

Elsir, T., Edqvist, P., Carlson, J., Ribom, D., Bergqvist, M., *et al.* (2014). A study of embryonic stem cell-related proteins in human astrocytomas: identification of Nanog as a predictor of survival. *International Journal of Cancer. Journal International Du Cancer*, 134 (5), 1123–1131.

Erenpreisa, J., Cragg, M. S. (2010). MOS, aneuploidy and the ploidy cycle of cancer cells. *Oncogene*, 29 (40), 5447–51.

Erenpreisa, J., Cragg, M. S. (2013). Three steps to the immortality of cancer cells: senescence, polyploidy and self-renewal. *Cancer Cell International*, 13 (1), 92.

Erenpreisa, J., Cragg, M. S., Fringes, B., Sharakhov, I., Illidge, T. M. (2000). Release of mitotic descendants by giant cells from irradiated burkitt's lymphoma cell line. *Cell Biology International*, 24 (9), 635-648.

Erenpreisa, J., Cragg, M. S., Salmina, K., Hausmann, M., Scherthan, H. (2009). The role of meiotic cohesin REC8 in chromosome segregation in gamma irradiation-induced endopolyploid tumour cells. *Experimental cell research*, 315 (15), 2593–2603.

Erenpreisa, J., Freivalds, T. (1979). Anisotropic staining of apurinic acid with toluidine blue. *Histochemistry*, 60 (3), 321–325.

Erenpreisa, J., Ivanov, A., Wheatley, S. P., Kosmacek, E. A, Ianzini, F. *et al.* (2008). Endopolyploidy in irradiated p53-deficient tumour cell lines : persistence of cell division activity in giant cells expressing Aurora-B kinase. *Cell Biology International*, 32 (9), 1044–1056.

Erenpreisa, J., Kalejs, M., Ianzini, F., Kosmacek, E. A., Mackey, M. A. *et al.* (2005). Segregation of genomes in polyploid tumour cells following mitotic catastrophe. *Cell biology international*, 29 (12), 1005–1011.

Erenpreiss, J. (1993). Current Concepts of Malignant growth.Part A. From a Normal Cell to Cancer. Riga: Zvaigzne Publishers, 191 pp.

Funayama, R., Saito, M., Tanobe, H., Ishikawa, F. (2006). Loss of linker histone H1 in cellular senescence. *The Journal of Cell Biology*, 175 (6), 869–880.

Futreal, P. A., Coin, L., Marshall, M., Down, T., Hubbard, T. *et al.* (2004). A census of human cancer genes. *Nature Reviews. Cancer*, 4 (3), 177–183.

Gallardo, M. H., Bickham, J. W., Honeycutt, R. L., Ojeda, R. A., Köhler, N. (1999). Discovery of tetraploidy in a mammal. *Nature*, 401 (6751), 341.

Galluzzi, L., Pietrocola, F., Levine, B., Kroemer, G. (2014). Metabolic control of autophagy. *Cell*, 159 (6), 1263–1276.

Ganem, N. J., Storchova, Z., Pellman, D. (2007). Tetraploidy, aneuploidy and cancer. *Current Opinion in Genetics and Development*, 17 (2), 157-162.

Gao, C., Miyazaki, M., Li, J. W., Tsuji, T., Inoue, Y. *et al.* (1999). Cytogenetic characteristics and p53 gene status of human teratocarcinoma PA-1 cells in 407-445 passages. *International Journal of Molecular Medicine*, 4 (6), 597–600.

Gaubatz, J. W. (1990). Extrachromosomal circular DNAs and genomic sequence plasticity in eukaryotic cells. *Mutation Research*, 237 (5-6), 271–292.

Geigl, J. B., Obenauf, A. C., Schwarzbraun, T., Speicher, M. R. (2008). Defining ‘chromosomal instability’. *Trends in Genetics : TIG*, 24 (2), 64–69.

Gewirtz, D. A., Holt, S. E., Elmore, L. W. (2008). Accelerated senescence: an emerging role in tumor cell response to chemotherapy and radiation. *Biochemical* Pharmacology, 76 (8), 947–957.

Gewirtz, D. A. (2013). Autophagy and senescence: a partnership in search of definition. *Autophagy*, 9 (5), 808–812.

Gey, C., Seeger, K. (2013). Metabolic changes during cellular senescence investigated by proton NMR-spectroscopy. *Mechanisms of Ageing and Development*, 134 (3-4), 130–138.

Ghisolfi, L., Keates A. C., Hu, X., Lee, D., Li, C. J. (2012). Ionizing radiation induces stemness in cancer cells. *PloS One*, 7 (8), e43628.

Gisselsson, D., Björk, J., Höglund, M., Martens, F., Dal Cin, P., Akerman, M. *et al.* (2001). Abnormal nuclear shape in solid tumors reflects mitotic instability. *The American Journal of Pathology*, 158 (1), 199-206.

Gisselsson, D., Pettersson, L., Höglund, M., Heidenblad, M., Gorunova, L. *et al.* (2000). Chromosomal breakage-fusion-bridge events cause genetic intratumor heterogeneity. *Proceedings of the National Academy of Sciences of the United States of America*, 97 (10), 5357–5362.

Giuliani, A. (2014). Networks as a privileged way to develop mesoscopic level approaches in systems biology. *Systems*, 2 (2), 237-242.

Giuliani, A., Colosimo, A., Benigni, R., Zbilut, J. P. (1998). On the constructive role of noise in spatial systems. *Physics Letters A.*, 247 (1-2), 47-52.

Gorban, A. N., Smirnova, E. V, Tyukina, T. A. (2010). Correlations, risk and crisis: from physiology to finance. *Physica A: Statistical Mechanics and Its Applications*, 389 (16), 3193–3217.

Gordon, D. J., Resio, B., Pellman, D. (2012). Causes and consequences of aneuploidy in cancer. *Nature Reviews. Genetics*, 13 (3), 189–203.

Gorgoulis, V. G., Halazonetis, T. D. (2010). Oncogene-induced senescence: the bright and dark side of the response. *Current Opinion in Cell Biology*, 22 (6), 816–827.

Guenther, M. G., Levine, S. S., Boyer, L. A., Jaenisch, R., Young, R. A. (2007). A chromatin landmark and transcription initiation at most promoters in human cells. *Cell*, 130 (1), 77–88.

Haber, A. H., Rothstein, B. E. (1969). Radiosensitivity and Rate of Cell Division: "Law of Bergonié and Tribondeau". *Science (New York, N.Y.)*, 163 (3873), 1338–1339.

Hanahan, D. (2014). Rethinking the war on cancer. *The Lancet*, 383 (9916), 558–563.

Hanahan, D., Weinberg, R. A. (2011). Hallmarks of cancer: the next generation. *Cell*, 144 (5), 646–674.

Harley, C. B., Futcher, A. B., Greider, C. W. (1990). Telomeres shorten during ageing of human fibroblasts. *Nature*, 345 (6274), 458–460.

Haroske, G., Baak J. P., Danielsen, H., Giroud, F., Gschwendtner, A. (2001). Fourth updated ESACP consensus report on diagnostic DNA image cytometry. In *Analytical Cellular Pathology : The Journal of the European Society for Analytical Cellular Pathology*, 23 (2), 89–95.

Hayat, M. A. (2013). Tumor Dormancy, Quiescence, and Senescence, Volume 1. Dordrecht: Springer Netherlands. 316pp doi:10.1007/978-94-007-5958-9.

Hayflick, L. (1965). The limited *in vitro* lifetime of human diploid cell strains. *Experimental Cell Research*, 37 (3), 614–636.

Hemberger, M., Dean, W., Reik, W. (2009). Epigenetic dynamics of stem cells and cell lineage commitment: digging waddington's canal. *Nature Reviews. Molecular Cell Biology*, 10 (8), 526–537.

Herbig, U., Jobling, W. A., Chen, B. P., Chen, D. J., Sedivy, J. M. (2004). Telomere shortening triggers senescence of human cells through a pathway involving ATM, p53, and p21(CIP1), but not p16(INK4a). *Molecular Cell*, 14 (4), 501–513.

Hixon, M. L., Gualberto, A. (2003). Vascular smooth muscle polyploidization--from mitotic checkpoints to hypertension. *Cell Cycle (Georgetown, Tex.)*, 2 (2), 105-110.

Hu, J., Locasale, J. W., Bielas, J. H., O'Sullivan, J., Sheahan, K. *et al.* (2013). Heterogeneity of tumor-induced gene expression changes in the human metabolic network. *Nat Biotechnology*, 31 (6), 522-529.

Huang, S. (2004). Back to the biology in systems biology: what can we learn from biomolecular networks? *Briefings in Functional Genomics and Proteomics*, 2 (4): 279–297.

Huang, S. (2009). Reprogramming cell fates: reconciling rarity with robustness. *BioEssays : News and Reviews in Molecular, Cellular and Developmental Biology*, 31 (5), 546–560.

Hurley, J. H., Schulman, B. A. (2014). Atomistic Autophagy: The structures of cellular self-digestion. *Cell*, 157 (2), 300–311.

Ianzini, F., Kosmacek, E. A., Nelson, E. S., Napoli, E., Erenpreisa, J. *et al.* (2009). Activation of meiosis-specific genes is associated with depolyploidization of human tumor cells following radiation-induced mitotic catastrophe. *Cancer Research*, 69 (6), 2296–2304.

Illidge, T. M., Cragg, M. S., Fringes, B., Olive, P., Erenpreisa, J. (2000). Polyploid giant cells provide a survival mechanism for p53 mutant cells after DNA damage. *Cell biology international*, 24 (9), 621–33.

Ivanov, A., Pawlikowski, J., Manoharan, I., van Tuyn, J., Nelson, D. M. *et al.* (2013). Lysosome-mediated processing of chromatin in senescence. *The Journal of Cell Biology*, 202 (1), 129–143.

Ivanov, A., Cragg, M. S., Erenpreisa, J., Emzinsh, D., Lukman, H. *et al.* (2003). Endopolyploid cells produced after severe genotoxic damage have the potential to repair DNA double strand breaks. *Journal of Cell Science*, 116 (Pt 20), 4095–4106.

Kang, H. T., Lee, K. B., Kim, S. Y., Choi, H. R., Park, S. C. (2011). Autophagy impairment induces premature senescence in primary human fibroblasts. *PloS One*, 6 (8), e23367.

Kastan, M. B., Bartek, J. (2004). Cell-cycle checkpoints and cancer. *Nature*, 432 (7015), 316–323.

Kastan, M. B. (2007). Wild-type p53: tumors can't stand it. *Cell*, 128 (5), 837-840.

Kaufman, M. H. (1991). New insights into triploidy and tetraploidy, from an analysis of model systems for these conditions. *Human Reproduction (Oxford, England)*, 6 (1), 8–16.

Kim, J., Woo, A. J., Chu, J., Snow, J. W., Fujiwara, Y. *et al.* (2010). A Myc network accounts for similarities between embryonic stem and cancer cell transcription programs. *Cell*, 143 (2), 313–324.

Kim, J. W., Dang, C. V. (2006). Cancer's molecular sweet tooth and the Warburg effect. *Cancer Research*, 66 (18), 8927-8930.

Kimmelman, A. C. (2011). The dynamic nature of autophagy in cancer. *Genes & Development*, 25 (19), 1999–2010.

Kinzler, K. W., Vogelstein, B. (1997). Cancer-susceptibility genes. Gatekeepers and caretakers. *Nature*, 386 (6627), 761, 763.

Kondrashov, A. S. (1994). The asexual ploidy cycle and the origin of sex. *Nature*, 370 (6486), 213–216.

Kops, G. J., Weaver, B. A., Cleveland, D. W. (2005). On the road to cancer: aneuploidy and the mitotic checkpoint. *Nature Reviews. Cancer*, 5 (10), 773–785.

Krämer, A., Neben, K., Ho, A. D. (2002). Centrosome replication , genomic instability and cancer. *Leukemia*, 16 (5), 767–775.

Kuma, A., Mizushima, N. (2010). Physiological role of autophagy as an intracellular recycling system: with an emphasis on nutrient metabolism. *Seminars in Cell and Developmental Biology*, 21 (7), 683-690.

Kunisada, T., Yamagishi, H., Ogita, Z., Kirakawa, T., Mitsui, Y. (1985). Appearance of extrachromosomal circular DNAs during *in vivo* and *in vitro* ageing of mammalian cells. *Mechanisms of Ageing and Development*, 29 (1), 89–99.

Jordan, C.T., Guzman, M. L., Noble, M. (2006). Cancer stem cells. *The New England Journal of Medicine*, 355 (12), 1253–1261.

Lagadec, C., Pajonk, F. (2012). Catch-22: Does breast cancer radiotherapy have negative impacts too? *Future Oncology*, 8 (6), 643–645.

Lagadec, C., Vlashi, E., Della Donna, L., Dekmezian, C., Pajonk, F. (2012). Radiation-induced reprogramming of breast cancer cells. *Stem Cells*, 30 (5), 833–844.

Lee, H. O., Davidson, J. M., Duronio, R. J. (2009). Endoreplication: polyploidy with purpose. *Genes & Development*, 23 (21), 2461–2477.

Lee, J., Paull, T. T. (2007). Activation and regulation of ATM kinase activity in response to DNA double-strand breaks. *Oncogene*, 26, 7741-7748.

Lee, J., Go, J., Kang, I., Han, Y., Kim, J. (2010). Oct-4 controls cell-cycle progression of embryonic stem cells. *The Biochemical Journal*, 426 (2), 171–181.

Lee, S. H., Oh, S., Do, S. I., Lee, H. J., Kang, H. J. *et al.* (2014). SOX2 regulates self-renewal and tumorigenicity of stem-like cells of head and neck squamous cell carcinoma. *British Journal of Cancer*, 111 (11), 2122–2130.

Leis, O., Eguiara, A., Lopez-Arribillaga, E., Alberdi, M. J., Hernandez-Garcia, S. *et al.* (2012). Sox2 expression in breast tumours and activation in breast cancer stem cells. *Oncogene*, 31 (11), 1354–1365.

Li, Q., Dang, C. V. (1999). c-Myc overexpression uncouples DNA replication from mitosis. *Molecular and Cellular Biology*, 19 (8), 5339–5351.

Liang, Y., Zhong, Z., Huang, Y., Deng, W., Cao, J. *et al.* (2010). Stem-like cancer cells are inducible by increasing genomic instability in cancer cells. *The Journal of Biological Chemistry*, 285 (7), 4931–4940.

Lin, T., Chao, C., Saito, S., Mazur, S. J., Murphy, M. E. *et al.* (2005). p53 induces differentiation of mouse embryonic stem cells by suppressing nanog expression. *Nature Cell Biology*, 7 (2), 165–171.

Lu, E., Wolfe, J. (2001). Lysosomal enzymes in the macronucleus of Tetrahymena during its apoptosis-like degradation. *Cell Death and Differentiation*, 8 (3), 289–297.

Lu, X., Mazur, S. J., Lin, T., Appella, E., Xu, Y. (2014). The pluripotency factor nanog promotes breast cancer tumorigenesis and metastasis. *Oncogene*, 33 (20), 2655–2664.

Magee, J. A., Piskounova, E., Morrison, S. J. (2012). Cancer stem cells: impact, heterogeneity, and uncertainty. *Cancer Cell*, 21 (3), 283–296.

Mantel, C., Guo, Y., Lee, M. R., Kim, M-K., Han, M. *et al.* (2008). Checkpoint-apoptosis uncoupling in human and mouse embryonic stem cells : a source of karyotpic instability. *Blood*, 109 (10), 4518–4527.

Marjanovic, N. D., Weinberg, R. A., Chaffer, C. L. (2013). Cell plasticity and heterogeneity in cancer. *Clinical Chemistry*, 59 (1), 168-179.

Martinato, F., Cesaroni, C., Amati, B., Guccione, E. (2008). Analysis of Myc-induced histone modifications on target chromatin. *PLoS ONE*, 3 (11), e3650.

McClintock, B. (1942). The fusion of broken ends of chromosomes following nuclear fusion. *Proceedings of the National Academy of Sciences of the United States of America*, 28 (11), 458–463.

Mosieniak, G., Adamowicz, M., Alster, O., Jaskowiak, H., Szczepankiewicz, A. A. *et al.* (2012). Curcumin induces permanent growth arrest of human colon cancer cells: link between senescence and autophagy. *Mechanisms of Ageing and Development*, 133 (6), 444–455.

Muñoz-Espín, D., Cañamero, M., Maraver, A., Gómez-López, G., Contreras, J. *et al.* (2013). Programmed cell senescence during mammalian embryonic development. *Cell*, 155 (5), 1104-1118.

Nagata, Y., Jones, M. R., Nguyen, H. G., McCrann, D. J., St. Hilaire, C. *et al.* (2005). Vascular smooth muscle cell polyploidization involves changes in chromosome passenger proteins and an endomitotic cell cycle. *Experimental Cell Research*, 305 (2), 277–291.

Nagl, W. (1978). Endopolyploidy and polyteny in differentiation and evolution. Holland: North-Holland Publishing Company, 283 pp.

Narita, M.,Nũnez, S., Heard, E., Narita, M., Lin, A. W. *et al.* (2003). Rb-mediated heterochromatin formation and silencing of E2F target genes during cellular senescence. *Cell*, 113 (6), 703–716.

Neganova, I., Lako, M. (2008). G1 to S phase cell cycle transition in somatic and embryonic stem cells. *J Anat*, 213 (1), 30–44.

Nelson, G., Wordsworth, J., Wang, C., Jurk, D., Lawless, C. *et al.* (2012). A senescent cell bystander effect: senescence-induced senescence. *Aging Cell*, 11 (2), 345–349.

Nowak, M. A., Komarova, N. L., Sengupta, A., Jallepalli, P. V., Shih, I. *et al.* (2002). The role of chromosomal instability in tumor initiation. *Proceedings of the National Academy of Sciences of the United States of America*, 99 (25), 16226–16231.

Nowell, P. C. (1976). The clonal evolution of tumor cell populations. *Science*, 194 (4260), 23-28.

Okamoto, K. (2014). Organellophagy: Eliminating cellular building blocks via selective autophagy. *Journal of Cell Biology*, 205 (4), 435-445.

Park, S. U., Choi, E. S., Jang, Y. S., Hong, S., Kim, I. *et al.* (2011). Effects of chromosomal polyploidy on survival of colon cancer cells. *The Korean Journal of Gastroenterology*, 57 (3), 150-157.

Park, Y. E., Hayashi, Y. K., Bonne, G., Arimura, T., Noguchi, S. *et al.* (2009). Autophagic degradation of nuclear components in mammalian cells. *Autophagy*, 5 (6), 795–804.

Peng, S., Maihle, N. J., Huang, Y. (2010). Pluripotency factors Lin28 and Oct4 identify a sub-population of stem cell-like cells in ovarian cancer. *Oncogene*, 29 (14), 2153–2159.

Phillips, T. M., McBride, W. H., Pajonk, F. (2006). The response of CD24-/low/CD44+ breast cancer-initiating cells to radiation. *Journal of the National Cancer Institute*, 98 (24), 1777–1785.

Pierce, G. B., Wallace, C. (1971). Differentiation of malignant to benign cells. *Cancer Research*, 31 (2), 127–134.

Piva, M., Domenici, G., Iriondo, O., Rábano, M., Simões, B. M. *et al.* (2014). Sox2 promotes tamoxifen resistance in breast cancer cells. *EMBO Molecular Medicine*, 6 (1), 66–79.

te Poele, R. H., Okorokov, A. L., Jardine, L., Cummings, J., Joel, S. P. (2002). DNA damage is able to induce senescence in tumor cells *in vitro* and *in vivo*. *Cancer* Research, 62 (6): 1876–1883.

Puig, P., Guilly, M., Bouchot, A., Droin, N., Cathelin, D. *et al.* (2008). Tumor cells can escape DNA-damaging cisplatin through DNA endoreduplication and reversible polyploidy. *Cell Biology International*, 32 (9), 1031–1043.

Purvis, J. E., Karhohs, K. W., Mock, C., Batchelor, E., Loewer, A. *et. al.* (2012). p53 dynamics control cell fate. *Science (New York, N.Y.)*, 336 (6087), 1440–1444.

de Resende, M. F., Chinen, L. T.,Vieira, S., Jampietro, J., da Fonseca, F. P. *et al.* (2013). Prognostication of OCT4 isoform expression in prostate cancer. *Tumour Biology : The Journal of the International Society for Oncodevelopmental Biology and Medicine*, 34 (5), 2665–2673.

Roberson, R. S., Kussick, S. J., Vallieres, E., Chen, S., Wu, D. Y. (2005). Escape from therapy-induced accelerated cellular senescence in p53-null lung cancer cells and in human lung cancers. *Cancer Research*, 65 (7), 2795–2803.

Rodda, D. J., Chew, J. L., Lim, L. H., Loh, Y. H, Wang, B. *et al.* (2005). Transcriptional regulation of nanog by OCT4 and SOX2. *Journal of Biological Chemistry*, 280 (26), 24731–24737.

Roninson, I. B., Broude, E. V., Chang, B. D. (2001). If not apoptosis, then what? Treatment-induced senescence and mitotic catastrophe in tumor cells. *Drug Resistance Updates : Reviews and Commentaries in Antimicrobial and Anticancer Chemotherapy*, 4 (5), 303–313.

Rosenfeldt, M. T., Ryan, K. M. (2011). The multiple roles of autophagy in cancer. *Carcinogenesis*, 32 (7), 955-963.

Rothenberg, M. E., Clarke, M. F., Diehn, M. (2010). The Myc connection: ES cells and cancer. *Cell*, 143 (2), 184–186.

Rozen, S., Skaletsky, H. (2000). Primer3 on the WWW for general users and for biologist programmers. *Methods in Molecular Biology*, 132, 365–386.

Salmina, K., Jankevics, E., Huna, A., Perminov, D., Radovica, I. *et al.* (2010). Up-regulation of the embryonic self-renewal network through reversible polyploidy in irradiated p53-mutant tumour cells. *Experimental Cell Research*, 316 (13), 2099–2112.

Sanli, T., Steinberg, G. R., Singh, G., Tsakiridis, T. (2014). AMP-activated protein kinase (AMPK) beyond metabolism: a novel genomic stress sensor participating in the DNA damage response pathway. *Cancer Biology and Therapy*, 15 (2), 156-169.

Schmitt, C. A. (2007). Cellular senescence and cancer treatment. *Biochimica et Biophysica Acta*, 1775 (1), 5–20.

Schmitt, C. A., Fridman, J. S., Yang, M., Lee, S., Baranov, E. (2002). A senescence program controlled by p53 and p16 INK4a contributes to the outcome of cancer therapy. *Cell*, 109 (3), 335–346.

Serrano, M., Blasco, M. A. (2007). Cancer and ageing: convergent and divergent mechanisms. *Nature Reviews. Molecular Cell Biology*, 8 (9), 715–722.

Serrano, M., Lin, A. W., McCurrach, M. E., Beach, D., Lowe, S.W. (1997). Oncogenic ras provokes premature cell senescence associated with accumulation of p53 and p16(INK4a). *Cell*, 88 (5), 593–602.

Seviour, E. G., Lin, S. Y. (2010). The DNA damage response: Balancing the scale between cancer and ageing. *Aging*, 2 (12), 900-907.

Sharpless, N. E., DePinho, R. A. (2005). Cancer: Crime and punishment. *Nature*, 436, 636–637.

Shay, J. W., Roninson, I. B. (2004). Hallmarks of senescence in carcinogenesis and cancer therapy. *Oncogene*, 23 (16), 2919–2933.

Shekhani, M. T, Jayanthy, A., Maddodi, N., Setaluri, V. (2013). Cancer stem cells and tumor transdifferentiation : implications for novel therapeutic strategies. *American Journal of Stem Cells*, 2 (1), 52–61.

Shim, J., Lee. H., Park, P., Kim, H., Choi,E. J. (1996). A non-enzymatic p21 protein inhibitor of stress-activated protein kinases. *Nature*, 381 (6585), 804–806.

Shoji, J. Y., Kikuma, T., Arioka, M., Kitamoto, K. (2010). Macroautophagy-mediated degradation of whole nuclei in the filamentous fungus Aspergillus oryzae. *PLoS ONE*, 5 (12), e15650.

Silva, J., Nichols, J., Theunissen, T. W., Guo, G., van Oosten, A. L. *et al.* 2009. Nanog is the gateway to the pluripotent ground state. *Cell*, 138 (4), 722–737.

Singh, A., Settleman, J. (2010). EMT, cancer stem cells and drug resistance: an emerging axis of evil in the war on cancer. *Oncogene*, 29 (34), 4741–4751.

Singh, S. K., Hawkins, C., Clarke, I. D., Squire, J. A., Bayani, J. *et al.* (2004). Identification of human brain tumour initiating cells. *Nature Cell Biology*, 432 (7015), 396–401.

Smith, J., Tho, L. M., Xu, N., Gillespie, D. A. (2010). The ATM-Chk2 and ATR-Chk1 Pathways in DNA Damage Signaling and Cancer. *Advances in Cancer Research*, 108, 73-112.

Soto, A. M., Sonnenschein, C. (2014). One hundred years of somatic mutation theory of carcinogenesis: Is it time to switch? *BioEssays*, 36 (1), 118–120.

Storchova, Z., Kuffer, C. (2008). The consequences of tetraploidy and aneuploidy. *Journal of Cell Science*, 121 (Pt 23), 3859–3866.

Sui, X., Chen, R., Wang, Z., Huang, Z., Kong, N., *et al.* (2013). Autophagy and chemotherapy resistance: a promising therapeutic target for cancer treatment. *Cell Death & Disease*, 4 (10), e838.

Sustáčková, G., Legartová,S., Kozubek, S., Stixová, L., Pacherník, J. *et al.* (2012). Differentiation-independent fluctuation of pluripotency-related transcription factors and other epigenetic markers in embryonic stem cell colonies. *Stem Cells and Development*, 21 (5), 710–720.

Suzuki, A., Tsutomi, Y., Akahane, K., Araki, T., Miura, M. (1998). Resistance to Fas-mediated apoptosis: activation of caspase 3 is regulated by cell cycle regulator p21WAF1 and IAP gene family ILP. *Oncogene*, 17 (8), 931–939.

Tam, W. L., Ng, H. H. (2014). Sox2: masterminding the root of cancer. *Cancer Cell*, 26 (1), 3–5.

Tu, S. (2013). Cancer: a “stem-cell” disease? *Cancer Cell International*, 13 (1), 40.

Vigneron, A., Vousden, K. H. (2010). p53, ROS and senescence in the control of aging. *Aging*, 2 (8), 471-474.

Vitale, I., Galluzzi, L., Senovilla, L., Criollo, A., Jemaà, M. *et al.* (2011). Illicit survival of cancer cells during polyploidization and depolyploidization. *Cell Death and Differentiation*, 18 (9), 1403–1413.

Vitale, I., Senovilla, L., Jemaà, M., Michaud, M., Galluzzi, L., *et al.* (2010). Multipolar mitosis of tetraploid cells: inhibition by p53 and dependency on Mos. *The EMBO Journal*, 29 (7), 1272–1284.

Walen, K.H. (2013). Senescence Arrest of Endopolyploid Cells Renders Senescence into One Mechanism for Positive Tumorigenesis. In:Dormancy, Quiescence, and Senescence, Volume 1, 215-226.

Walen, K. H. (2008). Genetic stability of senescence reverted cells: genome reduction division of polyploidy cells, aneuploidy and neoplasia. *Cell Cycle*, 7 (11), 1623–1629.

Wang, Q., Wu, P. C., Dong, D. Z, Ivanova, I., Chu, E. *et al.* (2013). Polyploidy road to therapy-induced cellular senescence and escape. *International Journal of Cancer*, 132 (7), 1505–1515.

Wang, Q., Wu, P. C., Roberson, R. S. Luk, B. V., Ivanova, I. *et al.* (2011). Survivin and escaping in therapy-induced cellular senescence. *International Journal of Cancer. Journal International Du Cancer*, 128 (7), 1546–1558.

Wang, Y., Armstrong, S. A. (2008). Cancer: inappropriate expression of stem cell programs?" *Cell Stem Cell*, 2 (4), 297–299.

Ward, P. S., Thompson, C. B. (2012). Metabolic reprogramming: a cancer hallmark even warburg did not anticipate. *Cancer Cell*, 21 (3), 297–308.

Weaver, B. A. A., Cleveland, D. W. (2007). Aneuploidy: instigator and inhibitor of tumorigenesis. *Cancer Research*, 67 (21), 10103–10105.

Weihua, Z., Lin, Q., Ramoth, A.J., Fan, D., Fidler, I. J. (2011). Formation of solid tumors by a single multinucleated cancer cell. *Cancer*, 117 (17), 4092–4099.

Weinberg, R. A. (2014). Coming full circle-from endless complexity to simplicity and back again. *Cell*, 157 (1), 267–271.

Wen, K., Fu, Z., Wu, X., Feng, J., Chen, W. *et al.* (2013). Oct-4 is required for an antiapoptotic behavior of chemoresistant colorectal cancer cells enriched for cancer stem cells: effects associated with STAT3/Survivin. *Cancer Letters*, 333 (1), 56–65.

Wong, D. J., Segal, E., Chang, H. Y. (2008). Stemness, cancer and cancer stem cells. *Cell Cycle*, 7 (23), 3622–3624.

Wu, P. C., Wang, Q., Grobman, L., Chu, E., Wu, D. Y. (2012). Accelerated cellular senescence in solid tumor therapy. *Experimental Oncology*, 34 (3), 298–305.

Xie, B. S., Zhao, H. C., Yao, S. K., Zhuo, D. X., Jin, B. *et al.* (2011). Autophagy inhibition enhances etoposide-induced cell death in human hepatoma G2 cells. *International Journal of Molecular Medicine*, 27 (4), 599–606.

Xue, W., Zender, L., Miething, C., Dickins,R. A., Hernando, E. *et al.* (2007). Senescence and tumour clearance is triggered by p53 restoration in murine liver carcinomas. *Nature*, 445 (7128), 656–660.

Ye, C. J., Stevens, J. B., Liu, G., Bremer, S. W., Jaiswal, A. S. *et al.* (2009). Genome based cell population heterogeneity promotes tumorigenicity: the evolutionary mechanism of cancer. *J Cell Physiol*, 219 (2), 288–300.

Yoshioka, K., Atsumi, Y., Fukuda, H., Masutani, M., Teraoka, H. (2012). The quiescent cellular state is Arf/p53-dependent and associated with H2AX downregulation and genome stability. *International Journal of Molecular Sciences*, 13 (5), 6492–6506.

Young, A. R., Narita, M., Ferreira, M., Kirschner, K., Sadaie, M. *et al.* (2009). Autophagy mediates the mitotic senescence transition. *Genes & Development*, 23 (7), 798–803.

Young, A. R., Narita, M. (2010). Connecting autophagy to senescence in pathophysiology. *Current Opinion in Cell Biology*, 22 (2), 234-240.

Zapperi, S., La Porta, C. A. M. (2012). Do cancer cells undergo phenotypic switching? The case for imperfect cancer stem cell markers. *Scientific Reports*, 2, 441.

Zeuthen, J., Nørgaard, J. O. R., Avner, P., Fellous, M., Wartiovaara, J. *et al.* (1980). Characterization of a human ovarian teratocarcinoma-derived cell line. *International Journal of Cancer. Journal International Du Cancer*, 25 (1), 19–32.

Zhang, J., Espinoza, L. A., Kinders, R. J., Lawrence, S. M., Pfister, T. D. *et al.* (2013). NANOG modulates stemness in human colorectal cancer. *Oncogene*, 32 (37), 4397–4405.

Zhang, S., Mercado-Uribe, I., Xing, Z., Sun, B., Kuang, J. *et al.* (2013). Generation of cancer stem-like cells through the formation of polyploid giant cancer cells. *Oncogene*, 33 (1), 116–128.

Zhang, S., Mercado-Uribe, I., Liu, J. (2013a). Generation of erythroid cells from fibroblasts and cancer cells *in vitro* and *in vivo*. *Cancer Letters*, 333 (2), 205–212.

Zhang, S., Mercado-Uribe, I., Liu, J. (2013b). Tumor stroma and differentiated cancer cells can be originated directly from polyploid giant cancer cells induced by paclitaxel. *International Journal of Cancer. Journal International Du Cancer*, 134 (3), 508-518.

Zheng, L., Dai, H., Zhou, M., Li, X., Liu, C., (2012). Polyploid cells rewire DNA damage response networks to overcome replication stress-induced barriers for tumour progression. *Nature Communications*, 3, 815.

Zhou, D., Wu, D., Li, Z., Qian, M., Zhang, M. Q. (2013). Population dynamics of cancer cells with cell state conversions. *Quantitative Biology*, 1 (3), 201–208.

Supplement

Primary antibody table

Antibody against	Description	Product nr and Manufacturer	Use*
AURORA B	Rabbit polyclonal	ab2254, Abcam	IF 1:300
bromodeoxyuridine (BdU)	Mouse monoclonal	A21300, Invitrogen	IF 1:200
b-TUBULIN	Mouse monoclonal	Neomarkers; clone DM1B	IF 1:100
CATHEPSIN B	Rabbit polyclonal	ab30443, Abcam	IF 1:100
CDKN2A/p16INK4a	Rabbit polyclonal	ab7962, Abcam	IF 1:100
CHK2 (phospho T68)	Rabbit polyclonal	ab38461, Abcam	IF 1:100, W 1:500
GAPDH	Mouse monoclonal, clone 6C5	ab8245, Abcam	W 1:500
LAMIN B1	Rabbit polyclonal	ab16048, Abcam	IF 1:300
LAMP-2	Mouse monoclonal	ab25631, Abcam	IF 1:500
LC3A/B	Rabbit polyclonal	PA1-16930, Pierce	IF 1:100
LC3B	Rabbit polyclonal	ab63817, Abcam	IF 1:100
NANOG	Mouse monoclonal, clone NNG-811	N3038, Sigma	IF 1:50
NANOG (23D2-3C6)	Mouse monoclonal	MA-1-017, Pierce	IF 1:50
NANOG H-155	Rabbit polyclonal	sc-33759, Santa Cruz	IF 1:50
OCT3/4	Mouse monoclonal	sc-5279, Santa Cruz	IF 1:50, F 1:100
OCT3/4	Goat polyclonal	sc-8630X, Santa Cruz	IF 1:200
OCT4	Rabbit polyclonal, ChIP Grade	ab19857, Abcam	IF 1:200-400
p21	Rabbit polyclonal	sc-397, Santa Cruz	IF 1:50
p21 Waf1/cip1	Rabbit monoclonal	MA5-14949, Pierce	IF 1:100 F 1:100
p-AMPKα1/2 (Thr183/172)	Rabbit polyclonal	sc-101630, Santa Cruz	IF 1:100
PL2-6	Mouse monoclonal	A kind gift from Olins	IF 1:100
PML	Mouse monoclonal	sc-966, Santa Cruz	IF 1:150
RAD51	Mouse monoclonal	ab213, Abcam	IF 1:100
RAD52	Goat polyclonal	sc-7674, Santa Cruz	IF 1:400
SOX2	Mouse monoclonal	MA1-014, Pierce	IF 1:50
SOX2	Rabbit polyclonal	sc-20088x, Santa Cruz	IF 1:50
SQSTM1 (p62)	Rabbit polyclonal	sc-25575, Santa Cruz	IF 1:200
TERT	Mouse monoclonal	ab5181, Abcam	IF 1:100
β-ACTIN	Rabbit polyclonal	ab8227, Abcam	W 1:200
γ TUBULIN	Mouse monoclonal	ab11316, Abcam	IF 1:2000
γ-H2AX	Rabbit polyclonal	4411-PC-100, Trevigen	IF 1:200

*W, western; IF, immunofluorescent staining; F, flow cytometry

Secondary antibody table

Antibody	Conjugate	Product nr and Manufacturer	Use *
Goat anti-mouse IgG	Alexa Fluor 488	A31619, Invitrogen	IF 1:300-400
Goat anti-mouse IgG	Alexa Fluor 594	A31623, Invitrogen	IF 1:300-400
Goat anti-rabbit IgG	Alexa Fluor 488	A31627, Invitrogen	IF 1:300-400
Goat anti-rabbit IgG	Alexa Fluor 594	A31631, Invitrogen	IF 1:300-400
Rabbit anti-goat IgG	Cy3	C2821, Sigma	IF 1:500
Donkey anti-goat IgG	Alexa Fluor 594	A-11058, Invitrogen	IF 1:300-400
Chicken anti-rabbit IgG	Alexa Fluor 488	A-21441, Invitrogen	IF 1:300-400
Donkey anti goat IgG	Alexa Fluor 488	A11055, Invitrogen	IF 1:300-400
Chicken anti-rabbit IgG	Alexa Fluor 594	A-21442, Invitrogen	IF 1:300-400
Chicken anti-mouse IgG	FITC	sc-2989, Santa Cruz	IF 1:200
sheep anti-human IgG	FITC		IF 1:100
Rabbit anti-mouse IgG	HRP	61-6520, Invitrogen	W 1:500
Goat anti-rabbit IgG	HRP	32460,Thermo Fisher Scientific	W 1:500
Goat anti-mouse IgG	Biotin	Vector Labs, UK	IF 1:100
Streptavidin	FITC	Vector Labs, UK	IF 1:150

*W, western; IF, immunofluorescent staining; F, flow cytometry